ENTROPY GENERATION IN JEFFREY FLUID FLOW THROUGH CHANNEL WITH INCLINED MAGNETIC EFFECT

A Thesis Submitted to
NATIONAL INSTITUTE OF TECHNOLOGY, WARANGAL (A.P.)
for the award of the degree of

DOCTOR OF PHILOSOPHY
IN
MATHEMATICS

BY

RAVI MAHLA
(ROLL NO: 21MAFJ151)

UNDER THE SUPERVISION OF

Prof. K. KALADHAR

DEPARTMENT OF MATHEMATICS
NATIONAL INSTITUTE OF TECHNOLOGY
WARANGAL - 506004 (TELANGANA)

JULY 2024

CERTIFICATE

This is to certify that the thesis entitled **"ENTROPY GENERATION IN JEFFREY FLUID FLOW THROUGH CHANNEL WITH INCLINED MAGNETIC EFFECT"**, submitted to the Department of Mathematics, National Institute of Technology, Warangal, is a record of bonafide research work carried out by **Mr. RAVI MAHLA**, Roll No. 21MAFJ151, for the award of Degree of Doctor of Philosophy in Mathematics under my supervision. The contents of the thesis have not been submitted for any other degree or diploma elsewhere.

Date:

Prof. K. Kaladhar
(Supervisor)
Assistant Professor
Department of Mathematics
National Institute of Technology, Warangal
Telangana State - 506004
India.

DECLARATION

This is to certify that the work presented in the thesis entitled **"ENTROPY GENERATION IN JEFFREY FLUID FLOW THROUGH CHANNEL WITH INCLINED MAGNETIC EFFECT"**, is a bonafide work done by me under the supervision of **Prof. K. Kaladhar**, Assistant Professor, Department of Mathematics, National Institute of Technology, Warangal and has not been submitted elsewhere for the award of any degree or diploma.

I declare that this written submission represents my ideas in my own words and where others' ideas or words have been included, I have adequately cited and referenced the original sources. I also declare that I have adhered to all principles of academic honesty and integrity and have not misrepresented or fabricated or falsified any idea / data / fact /source in my submission. I understand that any violation of the above will be a cause for disciplinary action by the Institute and can also evoke penal action from the sources which have thus not been properly cited or from whom proper permission has not been taken when needed.

Ravi Mahla

Roll No. 21MAFJ151

Date:_____

Dedicated

to

My beloved parents

Shri. Sajjan Kumar and Smt. Kavita

&

My Teachers

Who made me what i am today.

Acknowledgements

I express my sincere thanks to the National Institute of Technology, Warangal (NITW) in particular Department of Mathematics, for giving me an opportunity to pursue my Ph.D and supporting me during my research tenure in the Institute.

I would like to take this opportunity to express my utmost gratitude to my beloved supervisor Prof. K. Kaladhar, who has always been a source of inspiration for me. Words are inadequate to express my thankfulness for his regular support, guidance and encouragement throughout my research work. His thought provoking comments, suggestions and friendly guidance enabled me in enhancing my research skills. Without his generous help and support it would not be possible for me to complete this work. I shall ever remain indebted to him.

I express my sincere thanks to Prof. Bidyadhar Subudhi, Director, National Institute of Technology, Warangal for his kind support and encouragement at every stage of this endeavor.

I am grateful to Prof. A. Benerji Babu, Head, Department of Mathematics for his support. I am greatly indebted to the dynamic personality Prof. D. Srinivasacharya for his affectionate support, encouragement and for sparing his valuable time as a DSC Chairman.

I thank the members of the Doctoral Scrutiny Committee Prof. Ch. RamReddy, Prof. Satyanarayana Engu, Department of Mathematics, for their inspiring lectures and Prof. S. Srinath, Department of chemical engineering for his valuable suggestions, moral support and encouragement while my work was in progress.

I am grateful to Prof. J. V. Ramana Murthy, Prof. Kasi Viswanadham K N S, Prof. Debashis Dutta, and all other faculty members of the Department of Mathematics for their help and support throughout my research period. Also, I thank the office staff.

I would like to express my gratitude to my seniors scholars, my senior Khushbu, my friend Subham Jangid, and all my fellow research scholars for their friendship and companionship.

I owe special thanks to my parents and family members for their constant source of encouragement and tremendous care.

I would also like to thank my college friends and Dr. Amit sir for their motivation and support.

I wish to thank all people who helped me in one way or the other towards my success in research endeavors.

- Ravi Mahla

Abstract

Predicting the characteristics of heat and mass transfer in natural or mixed convection is crucial due to its practical engineering applications. Numerous studies have been conducted on combined heat and mass transfer in Newtonian fluids. However, it is widely recognized that many fluids used in chemical and related processing do not adhere to Newton's classical law and are classified as non-Newtonian fluids. Various mathematical models have been developed to describe the rheological behavior of these non-Newtonian fluids. No single fluid model accurately captures all the properties of real fluids. As a result, over the past century, several fluid models have been proposed to characterize the behavior of real fluids. Among these, Jeffrey fluids introduced by George Barker Jeffrey which is capable of describing the stress relaxation property of non-Newtonian fluids. The Jeffrey fluid displays an extrinsic correlation between stress and strain rate. The Jeffrey fluid explains the concepts of retardation and relaxation time. The aim of this thesis is to study about entropy generation analysis in free and mixed convection heat and mass transfer in Jeffrey fluid in the presence of inclined magnetic, radiation, chemical reaction, and Soret effects. The problems considered deal with vertical parallel plates and inclined parallel plates.

The thesis is divided into four parts and six chapters. **Part-I** includes a single introductory chapter (chapter 1), which presents the basic equations for the flow, heat, and mass transfers of Jeffrey fluids and a review of relevant literature. **Part-II** contains two chapters (i.e. chapters 2 and 3) and deal with inclined magnetic, chemical reaction, and radiation effects on entropy generation of Jeffrey fluid flow between vertical parallel plates. **Part-III** contains two chapters (chapters 4 and 5) investigates the impact of Soret number, chemical reaction, and angled magnetic field on entropy generation of Jeffrey fluid flow between inclined parallel plates.

In all the above chapters, using similarity transformations, the nonlinear governing equations along with boundary conditions are first transformed into a non-dimensional form. The spectral quasi-linearization approach is used to solve the resulting system of equations. The impact of Jeffrey fluid parameter and some other parameters on entropy, velocity of fluid, temperature, and concentration are presented graphically.

Part-IV consists of a single chapter (chapter 6), which presents the summary of the thesis with main conclusions and point out various problems which are yet to be solved in this area of research.

Contents

[1] Case(a):Published in "**Special Topics and Reviews in Porous Media**", (2024). DOI: 10.1615/SpecialTopicsRevPorousMedia.2024048949

Case(b): Published in "**Special Topics and Reviews in Porous Media**", (2024). DOI: 10.1615/SpecialTopicsRevPorousMedia.2024048872

[2]Case(a): Published in "**The European Physical Journal Plus**", 138, 1-14, (2023).
Case(b):Published in "**Proc IMechE Part E: J Process Mechanical Engineering**", 1-12, (2023). DOI:https://doi.org/10.1177/09544089231218977

[3]Case(a): Accepted for publication in "**Journal of Thermal Analysis and Calorimetry**"
Case(b): Accepted for publication in "**Thermophysics and Aeromechanics**"

[4]Case(a): Published in "**East Asian Journal of Applied Mathematics**", (2024). DOI:https://10.4208/eajam.2023-227.221023
Case(b):Published in "**Journal of Applied Mathematics and Mechanics (ZAMM)**", 104, e202300700 (1-15), (2024).

NOMENCLATURE

A_1	Dimensionless temperature difference
B_0	External magnetic field
B_1	Dimensionless concentration difference
Be	Bejan number
Br	Brinkman number
C	Concentration.
C_f	Dimensionless shear stress
c_p	Specific heat
D	Mass diffusivity
Da	Darcy number
g^*	gravitational acceleration.
Gr	Grashof number
Gr_T, Gr_C	Thermal, and Solutal Grashof numbers respectively
Ha	Magnetic parameter
k	Permeability porous medium
k_1	Rate of chemical reaction.
k_f	Thermal conductivity
K_T	Thermal diffusion ratio.
m	Hall parameter
N	Buoyancy ratio
Nu	Nusselt number
Ns	Dimensionless entropy generation
p	Pressure
Pr	Prandtl number
Q	Chemical reaction parameter
q_r	Radiation heat flux
Rd	Radiation parameter
Re	Reynolds number
Sc	Schmidt number
Sr	Soret number
S_{gen}	Volumetric entropy generation
Sh	Sherwood number
T	Temperature.
T_m	Mean fluid temperature.
u, v, w	Velocity components in the direction of x, y and z.
α	Inclination angle
β_C	Coefficient of Solutal expansion
β_T	Coefficient of thermal expansion
ϵ	Dimensionless constant parameter
γ	Channel angle of inclination
$\dot{\Gamma}$	Shear rate
$\ddot{\Gamma}$	Derivative of shear rate with respect to time.
λ_1	Jeffrey fluid parameter
μ	Coefficient of viscosity
ρ	Density
σ	Electrical conductivity

Part I

Introduction

Chapter 1

Introduction

Introduction

Fluid Dynamics is a scientific field that examines the motion of fluids and the interaction between solid bodies and fluids. It has extensive implementation across various disciplines, including Atmospheric science, Astrophysics, Geophysics, Biophysics, Oceanography, and Meteorology. Beyond it's relevance to basic sciences, Fluid Dynamics is also crucial in numerous engineering fields. In Mechanical and Nuclear engineering, it aids in the design of turbines, heat exchangers, pumps, cooling systems, compressors, fluid couplings, and electro-chemical devices. In Aerospace engineering, it is essential for designing airplanes with low resistance and high lift to support their weight. In Civil engineering, it is used for designing dams, water supply systems, and irrigation canals. In Chemical and Petroleum engineering, it helps in creating efficient devices for mixing and filtering industrial chemicals, petroleum, and oils.

Newtonian fluids follow Newton's law, which relates shear stress and shear rate to a simple material property known as viscosity. This property is independent of flow factors like shear rate and time, but it depends on fundamental thermodynamic variables like temperature and pressure. However, most fluids used in engineering

and industrial applications do not meet the assumptions of a Newtonian fluid. These fluids include industrial coatings, architectural paints, drilling muds, hydrogels, lubricants, detergents, shampoos, food industry, and more. Because no fluid model can exhibit all of the properties of these non-Newtonian fluids, several fluid models (visco-elastic fluids, power-law fluids, dusty fluids, Micropolar fluids, Oldroyd fluids, etc.) have been proposed. One of the models is the Jeffrey fluid, which was introduced by George Barker Jeffery. This type of viscoelastic fluid model is used to describe the behavior of certain non-Newtonian fluids. It extends the Newtonian fluid model by incorporating both viscous and elastic effects, making it suitable for modeling fluids that exhibit both solid-like and liquid-like behavior under different conditions. The Jeffrey fluid displays an extrinsic correlation between stress and strain rate and explains the concepts of retardation and relaxation time.

The study of fluid flows with the Jeffrey fluid has garnered significant interest due to its extensive range in application of different fields. This includes fiber suspensions and pulps, paints, paper pulp, toothpaste, simulate the flow of magma, and the act of swallowing food through the esophagus and animal blood.

1.1 Jeffrey fluid

The Jeffrey fluid model is used to describe viscoelastic fluids that exhibit both viscous (fluid-like) and elastic (solid-like) properties. It is particularly useful for materials that have both relaxation (delayed return to original shape after deformation) and retardation (delayed response to applied stress) characteristics. The Jeffrey fluid displays an extrinsic correlation between stress and strain rate. The Jeffrey fluid explains the concepts of retardation and relaxation time. It reduces to the Newtonian fluid model, which has a linear relationship between stress and strain rate.

This model is extensively utilized due to its considerable mathematical simplic-

ity relative to other models. Recently, it has garnered significant interest from researchers as it offers more accurate approximations for most physiological fluids. For example, Ellahi et al. [1] investigated mathematical models of nanoparticles with Jeffrey fluid model in arteries with a tapered shape. Other important fields where this fluid have applications are Bio-fluid mechanics, blood flow, polymer processing, paints, toothpaste, material design, paper pulp, and cosmetics. The field equations of Jeffrey fluid dynamics [2] are:

$$T = -pI + S$$

$$S = \frac{\mu}{1 + \lambda_1}(\dot{\Gamma} + \lambda_2 \ddot{\Gamma})$$

where T denotes Cauchy stress tensor, p represents pressure, S denotes extra stress tensor, λ_1 represents relaxation to retardation ratio, λ_2 represents the retardation time, $\dot{\Gamma}$ denotes the shear rate, and $\ddot{\Gamma}$ represents the derivative of shear rate with respect to time.

1.2 Magnetohydrodynamics (MHD)

Magnetohydrodynamics (MHD) is the study of the dynamics of electrically conducting fluids, which combines principles from both magnetism and fluid dynamics. This field examines how magnetic fields interact with and influence the behavior of conducting fluids like plasmas, liquid metals, and saltwater. The foundational idea of MHD is that the motion of the conducting fluid can induce electric currents, which in turn generate magnetic fields. These magnetic fields can interact with the fluid flow, leading to complex behaviors and phenomena.

The governing equations of MHD merge the Maxwell's equations from electromagnetism and Navier-Stokes equations from fluid dynamics, adapted to account

for the conductive properties of the fluid. One of the critical effects in MHD is the Lorentz force, which is the force experienced by the conducting fluid due to the magnetic field and the electric currents. This force can alter the motion of the fluid, leading to phenomena such as magnetic damping or magnetic confinement.

Thus, the behavior of an incompressible, electrically conductive fluid influenced by a magnetic field is described by the MHD equation.

The governing equation of MHD Jeffrey fluid will have the form

$$\rho\left[\frac{\partial\vec{q}}{\partial t}+(\vec{q}\cdot\nabla)\vec{q}\right]=-\frac{\mu}{1+\lambda_1}(\nabla\times(\nabla\times q))+\bar{J}\times\bar{B}-\nabla P \tag{1.1}$$

When an electric current flows through a conductor situated in a magnetic field, the moving charge carriers encounter a transverse force, causing them to be pushed to one side of the conductor. This leads to a charge buildup on the sides of the conductor, which counteracts the magnetic influence. Consequently, a measurable voltage is established between the two sides of the conductor, a phenomenon known as the Hall effect, discovered by E. H. Hall in 1879. Understanding magnetohydrodynamic flows with Hall currents is important in engineering for applications like magnetohydrodynamic generators, flight magnetohydrodynamics, as well as in Hall accelerators.

If we assume that the frequency of electron-atom collisions is relatively high, then we cannot ignore the Hall effect. In this scenario, Sutton's [3] generalized Ohm's law describes the current density $\bar{J}$ as

$$\bar{J}=\sigma\{\bar{E}+\vec{q}\times\bar{B}-\eta(\bar{J}\times\bar{B})\} \tag{1.2}$$

where η denotes the Hall factor and $\bar{E}$ is the total electric field current which is neglected due to the assumption that the induced magnetic field is very small.

There are many technical and scientific applications of MHD flow, such as in

devices like tokamaks and stellarators, magnetic confinement of high-temperature plasmas, understanding and controlling plasma behavior, devices that convert thermal and kinetic energy from a conducting fluid into electrical power using magnetic fields, measure the flow rate of blood and other conducting fluids in medical applications, lubricants, used in plasma-enhanced chemical vapor deposition and other plasma processes for the manufacturing of semiconductors and thin films etc.

1.3 Heat and Mass Transfer

Heat and mass transfer are fundamental concepts in the study of thermodynamics and fluid dynamics. Heat transfer occurs when thermal energy moves from one area to another due to temperature differences. This process happens through three primary mechanisms: convection, conduction, and radiation. Convection involves the transfer of heat between a solid surface and a moving fluid (liquid or gas). Convection can be natural (due to buoyancy effects) or forced (due to an external force). Conduction is the process by which thermal energy is transferred through a material because of microscopic collisions and interactions between molecules and atoms. Radiation is a mode of heat transfer that occurs through the emission of electromagnetic waves. Radiation does not required medium to transfer the heat. Convective heat transfer is the process of transferring thermal energy between a moving fluid and a solid surface. It combines the effects of conduction and convection. Convective heat transfer is divided in 3 distinct scenario: Forced convection, Natural convection and Mixed convection. Forced convection is a mechanism in which fluid motion is generated by an external force. Natural convection, on the other hand, is driven by buoyancy forces caused by density differnces in the fluid. In mixed convection, the fluid motion is influenced by both external forces and buoyancy forces resulting from temperature differences in the fluid.

In order to determine how heat is transferred within a medium, we must first

establish its temperature distribution or temperature field by solving the heat equation, which is a statement of first law of thermodynamics. When dealing with Jeffrey fluids, the local equilibrium model can be applied to derive the appropriate energy equation, which yields the appropriate equation.

$$\rho c_p \left[\frac{\partial T}{\partial t} + (\vec{q}\cdot\nabla)T\right] = k_f \nabla^2 T + \frac{\mu}{1+\lambda_1}[(\nabla\vec{q}) : (\nabla\vec{q})^T + (\nabla\vec{q}) : (\nabla\vec{q})] \\ +4\eta[(\nabla\bar{\omega}) : (\nabla\bar{\omega})^T] + 4\eta'[(\nabla\bar{\omega}) : (\nabla\bar{\omega})] \tag{1.3}$$

where k_f denotes the thermal conductivity, T is the temperature, and $\bar{\omega}$ represents the angular velocity.

The process by which a component in a mixture travels from an area of higher concentration to an area of lower concentration due to their random thermal motion is called mass transfer. Mass transfer occurs via two different mechanisms: convection and diffusion. Convection mass transfer happens between an exposed solid surface and a moving mixture of fluid species. Mass transfer processes are often described using differential equations that account for the conservation of mass. This equation provides the mass conservation.

$$\frac{\partial C}{\partial t} + (\vec{q}\cdot\nabla)C = \nabla\cdot(D\nabla C) \tag{1.4}$$

where C represents the concentration and D is the solutal diffusivity.

1.4 Soret Effect

The Soret effect, also known as thermal diffusion is a phenomenon in fluid mixtures where different species of particles migrate along a temperature gradient [4]. In the majority of studies involving heat and mass transfer processes, the Soret effect is often overlooked because it is generally considered to be less significant compared

to the effects described by Fourier's and Fick's laws. Fourier's law. This effect have significant application in microfluidic devices, where precise control over particle and molecule movement is crucial, in separating and sorting biological molecules, such as proteins and nucleic acids, in biomedical research and diagnostics, in isotope separation processes and in enhancing oil recovery, etc. In these applications, controlling species movement through temperature gradients enhances efficiency and precision, highlighting the practical importance of the Soret effect in various scientific and industrial fields.

With Soret effect (see Nield and Bejan [5]), the modified concentration equation in steady state can be written as

$$\vec{q} \cdot \nabla C = \nabla \cdot (D\nabla C + D_{CT}\nabla T) \tag{1.5}$$

where D represents the mass diffusivity and D_{CT}/D is considered as Soret coefficient (number) of the medium.

1.5 Chemical Reaction

Chemical reactions play a important role in heat and mass transfer processes. In various materials processing systems, chemical reactions can play a crucial role, such as production of elemental bromine electrochemically in porous electrode systems [6], glass melt flows with sodium oxide and silicon dioxide [7], and the process of creating intumescent paints for use in fire safety [8]. Furthermore, investigating combined heat and mass transfer alongside chemical reactions and thermophoresis effects find critical applications in various fields such as combustion, chemical engineering, industrial and environmental science. In combustion processes, the intricate interplay between heat release from chemical reactions and mass transfer of reactants and products determines efficiency and emission profiles. In chemical engineering,

reactors often rely on precise control of heat and mass transfer to optimize reaction rates and yield, with thermophoresis (the movement of particles due to temperature gradients) playing a significant role in particle deposition and catalyst efficiency. In the energy sector, they are crucial for processes like combustion in power plants and internal combustion engines, where chemical energy from fuels is converted into mechanical or electrical energy. Environmental applications include atmospheric chemistry, where pollutants undergo complex chemical reactions influenced by heat and mass transfer, while thermophoresis affects the distribution and deposition of aerosols, impacting air quality and climate models.

Numerous researchers have explored the impact of chemical reactions on heat and mass transfer in various scenarios, including channels, past vertical plates, and within concentric cylinders.

The concentration equation in a steady state for chemical reaction can be expressed as

$$\vec{q} \cdot \nabla C = \nabla \cdot (D \nabla C) - k_1 (C - C_0) \tag{1.6}$$

where k_1 represents the rate of chemical reaction.

1.6 Entropy Generation

Entropy generation is a concept from thermodynamics that refers to the increase in entropy that occurs within a system during a process. In thermodynamics, it quantifies the increase in entropy resulting from irreversible processes such as friction, heat transfer across finite temperature differences, and fluid flow through dissipative channels, that lead to an increase in entropy. This increase in entropy is often unavoidable and is a fundamental aspect of the second law of thermodynamics, which says that the entropy of the system tends to grow over time.

The importance of entropy generation lies in various engineering and scientific

applications because it plays a role in the efficiency and performance of many systems. In heat-exchanger design, the goal is to maximize fluid flow and heat transfer with minimal entropy generation in order to achieve high overall efficiency of the system. In thermal power plants, improvement in efficiency of energy conversion processes reduces fuel consumption and emission of greenhouse gases as a consequence of reduced entropy generation. One of the goals in developing an understanding of entropy generation is to optimize chemical and separation processes so they can be performed with minimal energy expenditure and maximal product yield. For refrigeration and air conditioning systems, a decrease in the entropy generation aids in achieving enhanced cooling. Furthermore, in renewable energy production, minimization of entropy generation maximizes energy capture and efficiency in conversion. Overall, controlling entropy generation is fundamental to designing sustainable and high-performance systems across various industries.

1.7 Spectral Quasi-linearization Method

Non-linearity is a crucial aspect of applied mathematics, as most of the real-world problems are non-linear in nature. Lately, much attention has been paid to finding more efficient and effective solution methods for both analytical and numerical approximations of non-linear models. Obtaining exact or approximate solutions for these equations is important and interesting, but it's also a challenging task. Despite the availability of high-performance supercomputers and quality computation software such as Mathematica and Maple, it's still difficult to obtain numerical approximations for solutions of non-linear ordinary differential equations. The spectral quasi-linearization method (SQLM) is a commonly-used approach to obtain numerical approximations of non-linear problems. Srinivasacharya et al. [9] applied a numerical method for solving nonlinear problems using SQLM. This method provides a computationally efficient and accurate solution by employing a rapidly convergent

series. The SQLM is a versatile method that can solve various types of nonlinear equations, including coupled, decoupled, homogeneous, and non-homogeneous. Scientists have applied this method to solve engineering problems.

In contrast to all other known numerical techniques, including the Adomian's decomposition method, the Runge-Kutta method, and the Finite Difference Method, the SQLM has the following advantages:

- By exploiting the spectral properties of the linearized system, SQLM can achieve fast convergence, especially for stiff or highly nonlinear problems.
- The method can provide accurate solutions even for challenging ODEs where traditional techniques may struggle.
- SQLM is relatively robust and can handle a wide range of nonlinearities and stiffness properties.
- SQLM often exhibits good numerical stability properties, which are crucial for maintaining accuracy and reliability during the solution process.

Later Kaladhar et al. [10], Reddy et al. [11], and Zare et al. [12] employed the spectral quasi-linearization method (SQLM) to address nonlinear fluid-related problems in fluid dynamics.

1.8 Literature Survey

The study of natural convection heat and mass transfer and fluid flows in vertical channels has been extensively researched for many decades because of their broad range of applications in heat exchange processes. This includes solar collectors, passive solar heating, electronic cooling, room heating radiators, and heat removal in nuclear technology. Elenbaas [13] conducted experimental and theoretical analysis on natural convection between isothermal parallel plates in 1942, proposing a

optimisation of heat transfer. The study conducted by Cohen and Rohsenow [14] examined the ideal thermal distance for natural convection flow between two vertical parallel plates. Hajizadeh et al. [15] investigated the unforced convective flow of a nanofluid between vertically aligned parallel plates. Tanveer et al. [16] explored the free convection flows of nanofluids by taking the generalized fractional thermal flux into account. Ali et al. [17] investigated the influence of magnetic field and heat transfer on the phenomenon of free convection in MHD Casson fluid flow occurring between parallel plates. Bako and Ajibade [18] explored the impacts of g-jitter on free convection Couette flow within a vertical channel.

Heat and mass transfer in mixed convection flow in a vertical channel has attracted attention over the years due to its diverse applications, such as in thermal Comfort in buildings, spacecraft thermal control and in chemical reactors. Numerous researchers have investigated the problem of heat transfer and fluid flow in mixed convection between vertical parallel plates, using both analytical and primarily numerical methods. The research by Cheng et al. [19] dealt with the phenomenon of heat transmission and flow reversal in mixed convection through a vertical channel. Azizi et al. [20] investigated the buoyancy impact on mixed convection laminar flow in a vertical channel. The researchers looked at both uphill and downward motion. Heat transport in a partially heated vertical duct under mixed convection was examined by Celik et al. [21]. Xu [22] examined the combined convective motion of a hybrid nanofluid within an inclined channel. The top wall of the channel exhibits slip behavior due to a patterned surface, while the heat flux remains constant along the walls. Ullah and Alkinidri [23] investigated the influence of viscosity fluctuations in mixed convective flow along a sloping heated plate is explored in the context of reduced gravity conditions.

Porous media flow research is a multi-disciplinary scientific discipline that includes hydrogeology, fluid mechanics, environmental engineering, petroleum engi-

neering, and many others. This science area describes the movement of fluids through materials whose structure contains interconnecting voids. This illustrates the relevance of porous media in the practical solutions of problems related to water management, energy production, protection of the environment, and many other engineering disciplines. Yang et al. [24] established a model to describe the flow of water through a channel embedded with a polymer gel, which is considered an elastic and deformable porous medium. Hayat and Abbas [25] studied second-grade MHD fluid flow through a porous medium. Ellahi and Afzal [26] examined the third-grade fluid flow through a pipe in porous medium. Fiza et al. [27] examined the magnetohydrodynamic nanofluid flow with porous medium between parallel plates. Abou et al. [28] researched the hall current effect on nanofluid flow between two parallel plates in a porous media. Sudarmozhi et al. [29] analyzed the MHD Maxwell fluid flow over a flat, porous surface, considering the effect of radiation and heat generation.

In recent years, various elementary flow problems related to classical hydrodynamics have garnered renewed interest within the broader framework of magnetohydrodynamics (MHD). Following the groundbreaking research by Hartman and Lazarus [30] on the effect of magnetic fields on the laminar flow of viscous fluids between parallel plates, numerous researchers have expanded upon existing hydrodynamic solutions in various flow geometries to incorporate the impact of magnetic fields, particularly in cases where the fluid exhibits electrical conductivity. Many researchers have studied the MHD flow and heat transfer of different types of non-Newtonian fluids (Axford [31], Jahanshah and Vireshwar [32], Chamkha [33], Kurtcebe and Erim [34]). In most MHD flow problems, the Hall term in Ohm's law is neglected. But in the event of a strong magnetic field, the effect of Hall current becomes important and can't be neglected. Elshehabey et al. [35] examined natural convection in a curved L-shaped enclosure containing copper/water nanofluids

operating on a differentially heated wall under the influence of an angled magnetic field. Bondareva et al. [36] examined the impact of an angled magnetic field and a local heater on melting and natural convection heat transfer in a cubical chamber filled with pure gallium. Convection study of radiative nanofluid flow with an angled magnetic field through porous media over a stretching surface was studied by Hussian and Sheremet [37].

The study of problems involving the Soret effect with various surface geometries has garnered significant attention from researchers across different fields. These studies are crucial for understanding heat and mass transfer phenomena in diverse engineering applications. Dursunkaya and Worek [38] investigated thermal-diffusion and diffusion-thermo impacts in steady and transient natural convection from a vertical surface. The Soret effect was examined by Sheri and Raju [39] on an unsteady MHD convective flow via a semi-infinite vertical plate, taking into account the viscous dissipation. Mandal et al [40] conducted a study using an inclined stretching plate with different surface conditions to explore the characteristics of the Soret effect and magnetohydrodynamics. Mishra and Panda [41] investigated the effect of Soret on the hydromagnetically mixed convective flow passing through the center of infinite vertical plates. Durojaye et al. [42] employed a numerical method called method of lines to examine the impact of Dufour and Soret effects on heat and mass transfer in a naturally convecting MHD Couette flow.

Heat transfer is a common occurrence in various biological processes, and it usually happens through conduction, convection, or radiation. Unfortunately, such processes can lead to energy losses, which may result in disorder. To prevent this from happening, researchers have been using entropy generation analysis as a powerful tool for reducing energy waste or maximizing energy utilization to improve system performance. Recently, there is a growing interest in reducing energy waste in thermal processes. Tasnim et al. [43] focused on how efficiently energy is used

within a fluid flowing through a porous channel when a magnetic field is present. They utilized the concept of generation of entropy to carry out the analysis. Odat et al. [44] examined the impact of a magnetic field on the formation of entropy in fluid flow across a horizontal plate. The method of entropy generation minimization was used by Ibanez et al. [45] to optimize the MHD flow with finite electrical conductivity between two endless parallel walls. Jery et al. [46] examined the influence of external magnetic field on entropy due to free convection. Abbas et al. [47] examined the entropy production in MHD viscous fluid flow with radiation immersed in a vertical permeable channel. Jayaprakash and Patil [48] demonstrated the concept of irreversibility analysis for mixed convective Casson fluid flow in a vertical microchannel with radiation effect. Iftikhar et al. [49] conferred the entropy production to MHD mixed convection in a saturated fluid in a square cavity.

A number of studies have been reported in the literature focusing on the problem of combined heat and mass transfer with chemical reaction effect. Exothermic reaction effect on fully developed mixed convection flow in a vertical channel was studied by Pop et al. [50]. Dash et al. [51] explored the effect of chemical reaction in MHD flow of micropolar fluid with heat source/sink between two parallel plates. The study is aimed at understanding the influence of chemical reactions on micropolar fluid behavior under the impact of magnetic fields in varying thermal conditions. Mondal and Bharti [52] presented SQLM solution of boundary layer flow of MHD nanofluid with chemical reaction. Awais and Salahuddin [54] investigated thermophysical properties of MHD fluid model with the influence of chemical reaction and energy dissipation.

1.9 Aim and Scope

Motivated by previous research and recognizing the importance of the applications in this thesis, the authors aim to study the entropy generation linked to

convective heat and mass transfer of Jeffrey fluid. This investigation includes considerations such as the Hall effect, inclined magnetic effect, chemical reaction effect, and Soret effect. The problems under consideration involve both vertical parallel plates and inclined parallel plates. The problems were solved utilizing the spectral quasi-linearization method. Subsequently, graphical solutions for these problems were presented.

1.10 Outline of the Thesis

This thesis divided into four parts and ten chapters.

Part-I consists of a single **Chapter-1** which gives an introduction, providing the motivation for the investigations conducted in the thesis. A thorough review of the relevant literature is provided to highlight the importance of the issues being examined. Additionally, the fundamental equations that describe the fluid flow of Jeffrey fluid are presented.

Part-II deals with the irreversibility analysis in natural/mixed convection flow of Jeffrey fluid through a channel with chemical reaction, angled magnetic field, radiation, and Hall effects. This consists of two chapters (chapter 2, and 3). In each of these chapters, the similarity transformations are first introduced to convert the nonlinear governing equations into dimensionless form. In the sequel, the transformed equations are solved using the approach of Spectral Quasi-linearization Method (SQLM).

In **Chapter-2**, we investigate the Hall and radiation effects on entropy generation of steady convective Jeffrey fluid flow in a vertical channel under angled magnetic field in porous medium. The non-dimensional profiles of velocities, temperature, concentration, and entropy are graphically presented for various values of hall current, magnetic parameter, Jeffrey fluid parameter, radiation parameter, and Soret parameter.

In **Chapter-3**, we discuss the generation of entropy of steady convective Jeffrey fluid flow between two vertical parallel plates under navier-slip condition. The effects of Hall parameter, Jeffrey fluid parameter, and magnetic parameter on the dimensionaless entropy, velocities, temperature, and concentration are discussed.

In the above chapters, two types (cases) of problems are considered. The first type is of natural convection and the second type is of mixed convection flow.

Part-III deals with the entropy generation of steady, incompressible free/mixed convection flow of Jeffrey fluid through an inclined channel with an angled magnetic field, Hall current, radiation, Soret, and chemical reaction effects. This consists of two chapters (**chapters 4 and 5**). In these two chapters, the similarity transformations are first introduced to convert the nonlinear governing equations into dimensionless form. In the sequel, the transformed equations are solved using the approach of SQLM, as done earlier.

In **Chapter-4**, we investigate the generation of entropy in steady convective Jeffrey fluid flow in porous medium between two inclined parallel plates. The graphical display of the acquired results demonstrates the impact of the magnetic parameter, Soret number, Jeffrey parameter, and radiation parameter on the dimensionless velocity, temperature, concentration, and entropy.

In **Chapter-5**, we discuss the entropy generation of steady convective heat and mass transfer between inclined parallel plates saturated with Jeffrey fluid under navier-slip condition. The effect of magnetic parameter, Hall current, Soret number, and Jeffrey fluid parameters on the non-dimensional velocities, temperature, concentration, and entropy are discussed.

In the above mentioned chapters 4 and 5 in part-III, two types (cases) of problems are considered. The first type is of natural convection and the second type is of mixed convection flow.

Part-IV has only one chapter (**Chapter - 6**), which sums up the important

findings out of the earlier chapters and provides suggestions for future research directions.

Part II

Entropy Generation in Jeffrey Fluid Flow between vertical parallel plates.

Chapter 2

Irreversibility Analysis of Jeffrey fluid flow between two vertical plates with porous medium under the effect of angled magnetic field [1]

2.1 Introduction

The study of natural and mixed convection flow between two parallel plates has garnered significant theoretical and practical attention. Heat and mass transfer in Jeffrey fluid plays a crucial role in various fields such as industrial manufacturing processes, aerospace engineering, and chemical engineering. The study of mixed and natural convection in vertical channel is relevant to many heat transfer applications. These include processes in polymer manufacturing like extrusion and injection molding, as well as drug delivery systems, reactor design, and even nuclear reactors.

[1] Case(a):Published in "**Special Topics and Reviews in Porous Media**", (2024). DOI: 10.1615/SpecialTopicsRevPorousMedia.2024048949
Case(b): Published in "**Special Topics and Reviews in Porous Media**", (2024). DOI: 10.1615/SpecialTopicsRevPorousMedia.2024048872

Several researchers have discussed the importance and advancements of heat and mass transfer [55, 56]. Bakar et al. [57] studied the mixed convection effect in a lid-driven cavity with an angled magnetic field. Kumar and Premachandran [58] examined the transition phenomena occurring in a natural convection flow within a tilted parallel plate channel. A vertical porous channel was used to study how hall and ion slip affected mixed convection of Jeffrey nanofluid by Channappa et al. [59].

In this chapter, we examine the entropy generation in the flow of Jeffrey fluid between two vertical parallel plates, influenced by Hall current, heat radiation, and angled magnetic field. The resulting flow equations are solved using SQLM. The impact of various relevant flow parameters on entropy, velocity, temperature, and concentration is examined.

2.2 Mathematical formulation

The physical configuration of this chapter (figure 2.1) involves two infinitely extended parallel plates. It exhibits that the plates are separated with a distance of $2d$. C_1, T_1, C_2, T_2 are the concentrations and temperatures at both plates respectively. An external magnetic field B_0 is acting on plates in an inclined direction, which makes α angle with the base. Further, it is assumed that the considered Jeffrey fluid flow is steady, incompressible, and laminar. Since the limits are infinitely extended along the $x-$ axis, the flow parameters are presumed to be solely dependent on y. Except for density changes in the buoyancy force term, fluid parameters are assumed to be constant. Therefore, these conventions are naturally genuine and practically applicable.

For this version, the governing equations are derived as follows:

$$\frac{dv}{dy} = 0 \Rightarrow v = v_0 = constant \tag{2.1}$$

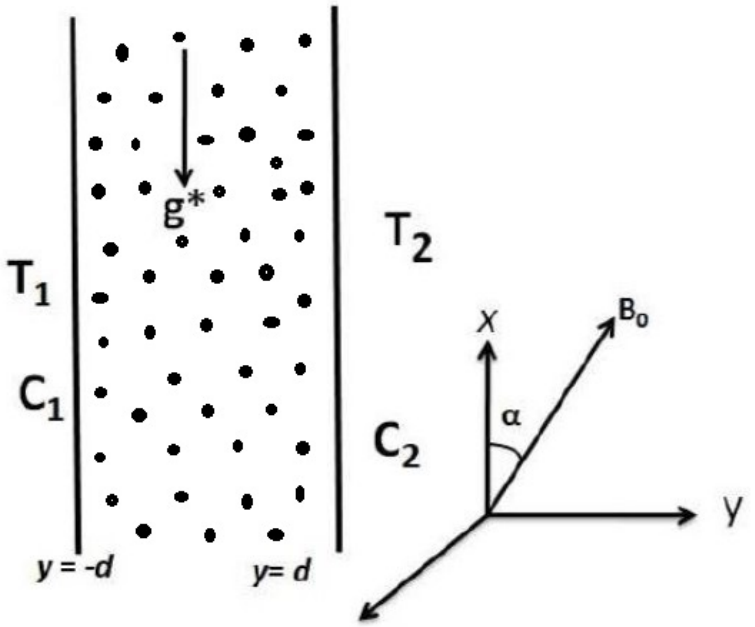

Figure 2.1: Diagrammatic representation of the fluid flow.

$$\rho v_0 \frac{du}{dy} = \frac{\mu}{1+\lambda_1}\frac{d^2u}{dy^2} - \frac{\sigma B_0^2 cos\alpha}{1+m^2cos^2\alpha}\left(ucos\alpha - v_0 sin\alpha + mwcos^2\alpha\right) \\ -\frac{dp}{dx} + \rho g^*\beta_T(T-T_1) + \rho g^*\beta_C(C-C_1) - \frac{\mu u}{(1+\lambda_1)k} \tag{2.2}$$

$$\rho v_0 \frac{dw}{dy} = \frac{\mu}{1+\lambda_1}\frac{d^2w}{dy^2} + \frac{\sigma B_0^2 cos^2\alpha}{1+m^2cos^2\alpha}\left(mucos\alpha - w - mv_0 sin\alpha\right) - \frac{\mu w}{(1+\lambda_1)k} \tag{2.3}$$

$$\rho c_p v_0 \frac{dT}{dy} = k_f \frac{d^2T}{dy^2} - \frac{dq_r}{dy} + \frac{\mu}{1+\lambda_1}\left(\left(\frac{du}{dy}\right)^2 + \left(\frac{dw}{dy}\right)^2\right) \tag{2.4}$$

$$v_0 \frac{dC}{dy} = D\frac{d^2C}{dy^2} - k_1(C-C_1) + \frac{DK_T}{T_m}\frac{d^2T}{dy^2} \tag{2.5}$$

where c_p represents specific heat, g^* represents the gravitational acceleration, k_f denotes thermal conductivity, k is permeability parameter, ρ is the density, $m = \eta\,\sigma$ B_0 is the Hall parameter, σ is the electric conductivity, k_1 denotes chemical reaction, μ represent the viscosity, β_T and β_C denote the thermal and solutal expansion, T_m is the mean fluid temperature, D denote the diffusivity of mass, K_T represent the ratio of thermal diffusion and the radiation heat flow is denoted by q_r.

The boundary conditions for this problem are given by

$$\begin{aligned} u = w = T - T_1 = C - C_1 = 0, \quad when\ y = -d \\ u = w = T - T_2 = C - C_2 = 0, \quad when\ y = d. \end{aligned} \tag{2.6}$$

In this chapter, two types (cases) of problems of (a) natural convection and (b) mixed convection are considered.

2.2.1 Case (a): Natural convection

Natural convection flow is due to buoyancy forces, with the assumption that there is no external pressure gradient ($\frac{\partial p}{\partial x} = 0$).

similarity transformations for this given problem is given as

$$\eta = \frac{y}{d}, \quad u = \frac{\gamma Gr}{d} f, \quad w = \frac{\gamma Gr}{d} g, \quad \theta = \frac{T - T_1}{T_2 - T_1}, \quad \phi = \frac{C - C_1}{C_2 - C_1} \tag{2.7}$$

In equations (2.2) - (2.5), Non-dimensional equations are obtained as

$$\begin{aligned} & f'' - Re(1+\lambda_1) f' + (1+\lambda_1)(\theta + \phi) \\ & - \frac{Ha^2 cos\alpha (1+\lambda_1)}{1 + m^2 cos^2\alpha} \left(f cos\alpha - \lambda sin\alpha + mg cos^2\alpha \right) - \frac{f}{Da} = 0 \end{aligned} \tag{2.8}$$

$$g'' - Re(1+\lambda_1) g' + \frac{Ha^2 cos^2\alpha (1+\lambda_1)}{1 + m^2 cos^2\alpha} \left(mf cos\alpha - g - m\lambda sin\alpha \right) - \frac{f}{Da} = 0 \tag{2.9}$$

$$\left(1 + \frac{4}{3} Rd\right) \theta'' - RePr\theta' + \frac{BrGr^2}{(1+\lambda_1)} f'^2 + \frac{BrGr^2}{(1+\lambda_1)} g'^2 = 0 \tag{2.10}$$

$$ScSr\theta'' + \phi'' - ReSc\phi' - QSc\phi = 0 \tag{2.11}$$

with

$$\begin{aligned} f = g = \theta = \phi = 0, \quad when\ \eta = -1 \\ f = g = 0, \quad \theta = \phi = 1, \quad when\ \eta = 1 \end{aligned} \tag{2.12}$$

where $Da = \frac{k}{d^2}$ represents the Darcy number, $Re = \frac{\rho v_0 d}{\mu}$ represents Reynolds number, $Sr = \frac{DK_T(T_2 - T_1)}{\nu T_m(C_2 - C_1)}$ is the parameter of thermo diffusion, $Pr = \frac{\mu c_p}{k_f}$ is Prandtl number, $Gr = \frac{g\beta(T_2 - T_1)d^3}{v^2}$ is thermal Grashof number, $Br = \frac{\mu v^2}{k_f d^2(T_2 - T_1)}$ denotes Brinkman number, $Ha = dB_0\sqrt{\frac{\sigma}{\mu}}$ is the magnetic parameter, $\lambda = \frac{Re}{Gr}$, $Sc = \frac{\nu}{D}$ is the Schmidt number, $Rd = \frac{4\sigma T_0^3}{k_f k^*}$ denote the Radiation parameter, and $Q = \frac{k_1 d}{v_0}$ is the chemical reaction parameter.

The shearing stress, as well as the heat and mass fluxes can be calculated from

$$\tau_w = \mu\frac{du}{dy}\mid_{y=\pm d};\quad q_w = \left[-k_f\frac{dT}{dy} + q_r\right]\mid_{y=\pm d};\quad q_m = -D\frac{dC}{dy}\mid_{y=\pm d}$$

The dimensionless shear stress $C_f = \frac{\tau_w}{\rho u_0^2}$ is given by $ReC_{f_{1,2}} = f'(\eta)\mid_{\eta=-1,1}$.
The Sherwood number $Sh = q_m d/D(C_2 - C_1)$ and Nusselt number $Nu = q_w d/k_f(T_2 - T_1)$ for this problem are given by

$$Sh_{1,2} = -\left[\phi'(\eta)\right]\mid_{\eta=-1,1};\quad Nu_{1,2} = -\left[1 + \frac{4}{3}Rd\right]\theta'(\eta)\mid_{\eta=-1,1}.$$

Solution of the problem using SQLM

The set of coupled non-linear equations (2.8) - (2.11) is numerically solved with boundary conditions (2.12) using the Spectral Quasi-Linearization Method (SQLM) [60]. This method uses Taylor series expansion to linearize the differential equation and build the iteration scheme.

Next applying the SQLM to solve the equations (2.8) - (2.11) by assuming the approximate solution as f_r, g_r, $\theta_r$and ϕ_r. Then the improved solutions are f_{r+1},

g_{r+1}, $\theta_{r+1}$and ϕ_{r+1}. The following describes an iterative model based on SQLM:

$$f''_{k+1} - Re(1+\lambda_1)f'_{k+1} + (1+\lambda_1)(\theta_{r+1}+\phi_{r+1}) + a_1 f_{k+1} + a_2 g_{k+1} - \frac{1}{Da} f_{k+1} = a_3 \quad (2.13)$$

$$g''_{k+1} - Re(1+\lambda_1)g'_{k+1} + a_4 f_{k+1} + a_5 g_{k+1} - \frac{1}{Da} g_{k+1} = a_6 \quad (2.14)$$

$$a_7\theta''_{r+1} - RePr\theta'_{r+1} + a_8 f'_{k+1} + a_9 g'_{k+1} = a_{10} \quad (2.15)$$

$$\phi''_{r+1} - ReSc\phi'_{r+1} - QSc\phi_{r+1} + ScSr\theta''_{r+1} = 0 \quad (2.16)$$

where

$$a_1 = -\frac{Ha^2(1+\lambda_1)cos^2\alpha}{1+m^2cos^2\alpha}, \quad a_2 = -\frac{mHa^2(1+\lambda_1)cos^3\alpha}{1+m^2cos^2\alpha},$$
$$a_3 = -\frac{\lambda Ha^2(1+\lambda_1)cos\alpha sin\alpha}{1+m^2cos^2\alpha}, \quad a_4 = \frac{mHa^2cos^3(1+\lambda_1)}{1+m^2cos^2},$$
$$a_5 = -\frac{Ha^2(1+\lambda_1)cos^2\alpha}{1+m^2cos^2\alpha}, \quad a_6 = \frac{\lambda mHa^2cos^2\alpha sin\alpha(1+\lambda_1)}{1+m^2cos^2\alpha}$$
$$a_7 = \left(1+\frac{4}{3}\right)Rd, \quad a_8 = \frac{2BrGr^2}{1+\lambda_1}f'_k, \quad a_9 = \frac{2BrGr^2}{1+\lambda_1}g'_k, \quad a_{10} = \frac{BrGr^2}{(1+\lambda_1)}\left(f'^2_k + g'^2_k\right)$$

The preceding system (2.13) - (2.16) is an iterative system of linear differential equations which solved for $r = 1, 2, 3, ...$ The quasi-linearization scheme in this study was solved using the Chebyshev pseudo-spectral method. The iteration procedures $((2.13) - (2.16))$ can be solved step by step for $\mathbf{F}_{r+1}$, $\mathbf{G}_{r+1}$, Θ_{r+1} and Φ_{r+1} by taking the values of r as 1, 2, ... with starting approximations $f_0, g_0, \theta_0, \phi_0$ respectively. To solve equations (2.13) - (2.16), we discretize them and utilize the Chebyshev spectral collocation method. This method employs a differential matrix, denoted as D,

by introducing the collocation points.

$$\eta_j = cos\frac{j\pi}{N_x}, \qquad (j = 0, 1, 2, 3...N_x)$$

Now SQLM makes the entire system in matrix form as

$$\mathbf{A}_r\mathbf{X}_{r+1} = \mathbf{B}_r$$

where

$$\mathbf{A}_r = \begin{bmatrix} A_{11} & A_{12} & A_{13} & A_{14} \\ A_{21} & A_{22} & A_{23} & A_{24} \\ A_{31} & A_{32} & A_{33} & A_{34} \\ A_{41} & A_{42} & A_{43} & A_{44} \end{bmatrix}$$

$$\mathbf{X}_{r+1} = \begin{bmatrix} \mathbf{F}_{k+1} & \mathbf{G}_{k+1} & \mathbf{\Theta}_{k+1} & \mathbf{\Phi}_{k+1} \end{bmatrix}^T$$

$$\mathbf{B}_r = \begin{bmatrix} \mathbf{M}_1 & \mathbf{M}_2 & \mathbf{M}_3 & \mathbf{M}_4 \end{bmatrix}^T$$

where

$$A_{11} = D^2 - Re(1+\lambda_1)D + a_1 - \frac{1}{Da},\ A_{12} = a_2,\ A_{13} = (1+\lambda_1) * I,\ A_{14} = (1+\lambda_1) * I,$$

$$A_{21} = a_4,\quad A_{22} = D^2 - Re(1+\lambda_1)D + a_5 - \frac{1}{Da},\quad A_{23} = O,\quad A_{24} = O,$$

$$A_{31} = a_8 D,\quad A_{32} = a_9 D,\quad A_{33} = a_7 D^2 - RePrD,\quad A_{34} = O,$$

$$A_{41} = O,\quad A_{42} = O,\quad A_{43} = ScSrD^2,\quad A_{44} = D^2 - ReScD - QSc.$$

$$\mathbf{F}_{k+1} = \begin{bmatrix} f_{r+1}(\xi_0) \\ f_{r+1}(\xi_1) \\ \vdots \\ f_{r+1}(\xi_{N_x}) \end{bmatrix}, \mathbf{G}_{k+1} = \begin{bmatrix} g_{r+1}(\xi_0) \\ g_{r+1}(\xi_1) \\ \vdots \\ g_{r+1}(\xi_{N_x}) \end{bmatrix}, \mathbf{\Theta}_{k+1} = \begin{bmatrix} \theta_{r+1}(\xi_0) \\ \theta_{r+1}(\xi_1) \\ \vdots \\ \theta_{r+1}(\xi_{N_x}) \end{bmatrix}, \mathbf{\Phi}_{k+1} = \begin{bmatrix} \phi_{r+1}(\xi_0) \\ \phi_{r+1}(\xi_1) \\ \vdots \\ \phi_{r+1}(\xi_{N_x}) \end{bmatrix}$$

$$\mathbf{M}_1 = \begin{bmatrix} a_3(\xi_0) \\ a_3(\xi_1) \\ \vdots \\ a_3(\xi_{N_x}) \end{bmatrix}, \mathbf{M}_2 = \begin{bmatrix} a_6(\xi_0) \\ a_6(\xi_1) \\ \vdots \\ a_6(\xi_{N_x}) \end{bmatrix}, \mathbf{M}_3 = \begin{bmatrix} a_{10}(\xi_0) \\ a_{10}(\xi_1) \\ \vdots \\ a_{10}(\xi_{N_x}) \end{bmatrix}, \mathbf{M}_4 = O.$$

Here O and I are the zero and identity matrices of order $(N_x + 1)$.

The numerical solutions using SQLM is obtained as

$$\mathbf{X}_{r+1} = \mathbf{A}_r^{-1}\mathbf{B}_r$$

Entropy generation

Entropy generation analysis is crucial for designing efficient thermal devices. Because entropy minimization helps to maximizing the efficiency of ongoing thermal processes. Thermodynamics tells us that when heat transfer occurs in a system, the effects are believed to be thermodynamic reversibility and entropy generation. Since the transfer of heat in flowing fluids is not a purely reversible process, irreversibility must be considered when such systems undergo an analysis in thermodynamics. The 2^{nd} law of thermodynamics provides a framework for calculating the local rate of entropy generation [61, 62], which is calculated as follows:

$$S_{gen} = \frac{k_f}{T_0^2}\left[1 + \frac{16\sigma T_0^3}{3k_f k^*}\right]\left[\frac{dT}{dy}\right]^2 + \frac{\mu}{T_0(1+\lambda_1)}\left[\left(\frac{du}{dy}\right)^2 + \left(\frac{dw}{dy}\right)^2\right] + \frac{RD}{C_0}\left(\frac{dC}{dy}\right)^2 + \frac{RD}{T_0}\left(\frac{dT}{dy}\right)\left(\frac{dC}{dy}\right) + \frac{\mu}{kT_0}(u^2 + w^2) + \frac{\sigma B_0^2}{T_0}\left[w^2 + (ucos\alpha - v_0 sin\alpha)^2\right] \tag{2.17}$$

The first term in the right hand side of equation (2.17) is due to heat transfer, the second term because of energy dissipation due to fluid viscosity, the third and fourth are because of mass transfer, the fifth one due to porosity, and the magnetic field

is responsible for the sixth. The expression for rate of entropy generation $(S_{gen})_0$ is determined by

$$(S_{gen})_0 = \frac{k_f(T_2 - T_1)^2}{T_0^2 d^2} \tag{2.18}$$

By using equations (2.17) and (2.18), the creation of non-dimensional entropy can be expressed in the following manner:

$$N_s = \frac{S_{gen}}{(S_{gen})_0}$$

$$N_s = \left[1 + \frac{4}{3}Rd\right](\theta')^2 + \frac{BrGr^2}{(1+\lambda_1)A_1}(f'^2 + g'^2) + \frac{\varepsilon B_1^2}{A_1^2}(\phi')^2 + \frac{\varepsilon B_1}{A_1}\theta'\phi' + \frac{BrGr^2}{DaA_1}(f^2 + g^2) + \frac{BrGr^2 Ha^2}{A_1}\left(g^2 + (fcos\alpha - \lambda sin\alpha)^2\right)$$

where A_1, Br, B_1, Gr, Rd, ε, Ha and Da are dimensionless temperature difference, Brinkman number, dimensionless concentration difference, Grashof number, thermal radiation parameter, dimensionless constant parameter, magnetic parameter, Darcy number, respectively, which are given by

$$Rd = \frac{4\sigma T_0^3}{k_f k^*}, \quad Br = \frac{\mu v^2}{k_f d^2 (T_2 - T_1)}, \quad Gr = \frac{g\beta(T_2 - T_1)d^3}{v^2}, \quad \varepsilon = \frac{RDC_0}{k_f},$$
$$A_1 = \frac{T_2 - T_1}{T_0}, \quad B_1 = \frac{C_2 - C_1}{C_0}, \quad Ha = dB_0\sqrt{\frac{\sigma}{\mu}}, \quad Da = \frac{k}{d^2}$$

Results and discussion

The analytical solutions for equations (2.8), (2.10), and (2.11), along with their boundary conditions (2.12), were derived without considering the brinkman number (Br), magnetic parameter (Ha), chemical reaction parameter (Q), and Jeffrey fluid parameter (λ_1), along with inclination angle at $\alpha = 60°$. A comparison was made between these analytical solutions and the solutions obtained using SQLM, which are presented in Table 2.1. The results of comparisons show a high level of agreement.

As a result, the SQLM code can be utilized with assurance to investigate the topic addressed in this research.

Figures 2.2 - 2.7 depict how these parameters affect the aforementioned variables, with Q, Re, Pr, Sc, Gr, Da by fixing their value at 2, 2, 0.71, 0.22, 10, and 2, respectively.

Figure 2.2 illustrates the impact of Ha on velocities, temperature, concentration, and entropy generation when $Sr = 10$, $\alpha = \pi/3$, m =2, Rd =0.2, λ_1=0.5, Br = 0.5. It is seen from figures 2.2(a) and 2.2(b) that the velocities magnify as Ha magnifies. The magnetic field is inclined at an angle $\alpha > 0$, which implies that the drag force cannot be produced in the flow and cross-flow directions. Figure 2.2(c) illustrates that as Ha increases, the fluid temperature also rises. It is observed from figures 2.2(d) and 2.2(e) that as Ha increases, the concentration of fluid and entropy generation increase.

The influence of m on velocities, temperature, concentration, and entropy generation can be seen in figure 2.3 at $Sr = 10$, α=$\pi/3$, Ha =2, Rd =0.1, λ_1=0.1 and $Br = 0.5$. Figures 2.3(a), 2.3(b) and 2.3(d) reveals that the flow velocity, cross-flow velocity, and concentration decreases as m increase. This is because the magnetic field is inclined at an angle of $\alpha = \pi/3$, which causes the hall effect to generate charge in the direction of inclined plates, thereby making it unable to act as a drag on the fluid. Figures 2.3(c) and 2.3(e) show that as m increases, the fluid temperature and entropy generation also increases. The hall current plays a crucial role in magnetohydrodynamic flows, as it introduces additional complexity in fluid motion and magnetic field distribution.

The influence of Rd on velocities, temperature, concentration, and entropy generation can be noticed in figure 2.4 at α=$\pi/3$, $Sr = 3$, Ha =2, m =2, λ_1=0.5 and $Br = 1$. It is noted from figures 2.4(a) and 2.4(b) reveals that as Rd increases, the flow velocity rises while the cross-flow velocity falls. Figures 2.4(c) and 2.4(d) shows

that the temperature of the fluid goes up and concentration goes down as the value of Rd increases. Figure 2.4(e) reveals that entropy generation fall as the radiation parameter increase.

The effect on α on velocities, temperature, concentration, and entropy generation can be observed in figure 2.5 by fixing the other parameter at Sr=10, Ha=2, λ_1=0.1, m=2, Rd=0.5 and Br=1. Figures 2.5(a) and 2.5(b) reveals that as α increase, the flow velocity increase while the cross-flow velocity decrease. Figures 2.5(c) and 2.5(d) shows that increasing in α leads to a fall in dimensionless temperature but a rise in concentration. This behavior occurs because raising the inclination angle of the applied magnetic field reduces the drag force, which enhances the net flow in the fluid. Figure 2.5(e) shows that the entropy generation increase as α increase. An inclined magnetic field is used in magneto-hydrodynamics generators to convert the kinetic energy of hot, electrically conducting fluid into electrical energy.

The effect on λ_1 on velocities, temperature, concentration, and entropy generation can be noted in figure 2.6 by fixing the other parameter at Rd=0.1, $Sr = 10$, Ha =1, m =2, α= $\pi/3$ and $Br = 0.5$. Figures 2.6(a) and 2.6(b) indicates that as λ_1 increases, the flow and cross-flow velocity both fall. Figures 2.6(c), 2.6(d) and 2.6(e) shows that a rise in λ_1 leads to a fall in fluid temperature but rise in concentration and entropy generation.

Figure 2.7 demonstrates how the parameter Sr affects velocity, temperature, concentration, and entropy generation when other parameters are fixed at $\alpha = \pi/3$, $m = 2$, $Ha = 2$, $\lambda_1 = 0.5$, Rd=0.2 and $Br = 2$. Figures 2.7(a) and 2.7(b) demonstrate that increasing m causes the flow and cross-flow velocity both decrease. Figures 2.7(c) and 2.7(d) reveal that the fluid temperature decrease while the concentration increase as Sr increase. Figure 2.7(e) reveals that as Sr increase, entropy generation increase but decrease near the plate $y = d$. The soret parameter plays a role in mass transfer in multi-component fluid systems and can significantly impact

flow behavior, particularly in situations involving heat and mass transfer.

Table 2.2 examines how the coefficient of skin friction, heat transfer rate, and mass transfer rate change under the influence of various parameters. These parameters include the Hall current (m), inclination angle (α), magnetic parameter (Ha), Soret effect (Sr), radiation parameter (Rd), and Jeffrey fluid parameter (λ_1), while keeping other values at Q=2, Re=2, Pr=0.71, Br=0.5, Sc=0.22, Gr=10 and Da=2. As the values of the magnetic parameter, inclination angle, and Jeffrey fluid parameter increase, the skin friction coefficient increases at first but lowers towards the final plate. However, a reverse tendency is seen as m increases. The friction factor decreases at both plates as Sr and Rd increases. The finding shows that when Sr, α, m and λ_1 increase, the heat transfer rate rises at $y = -d$ plate and falls at $y = d$ plate, whereas the opposite tendency is seen as Ha increase. The rate of heat transfer decrease at both plates as Rd increase. As for the mass transfer rate, the table shows that it rises at both walls as Sr, α, and λ_1 increase, whereas the opposite tendency is observed as Rd increases. The rate of mass transfer rise at the starting plate but fall at the terminal plate as m increase whereas the reverse tendency is observed with a rise in magnetic parameter.

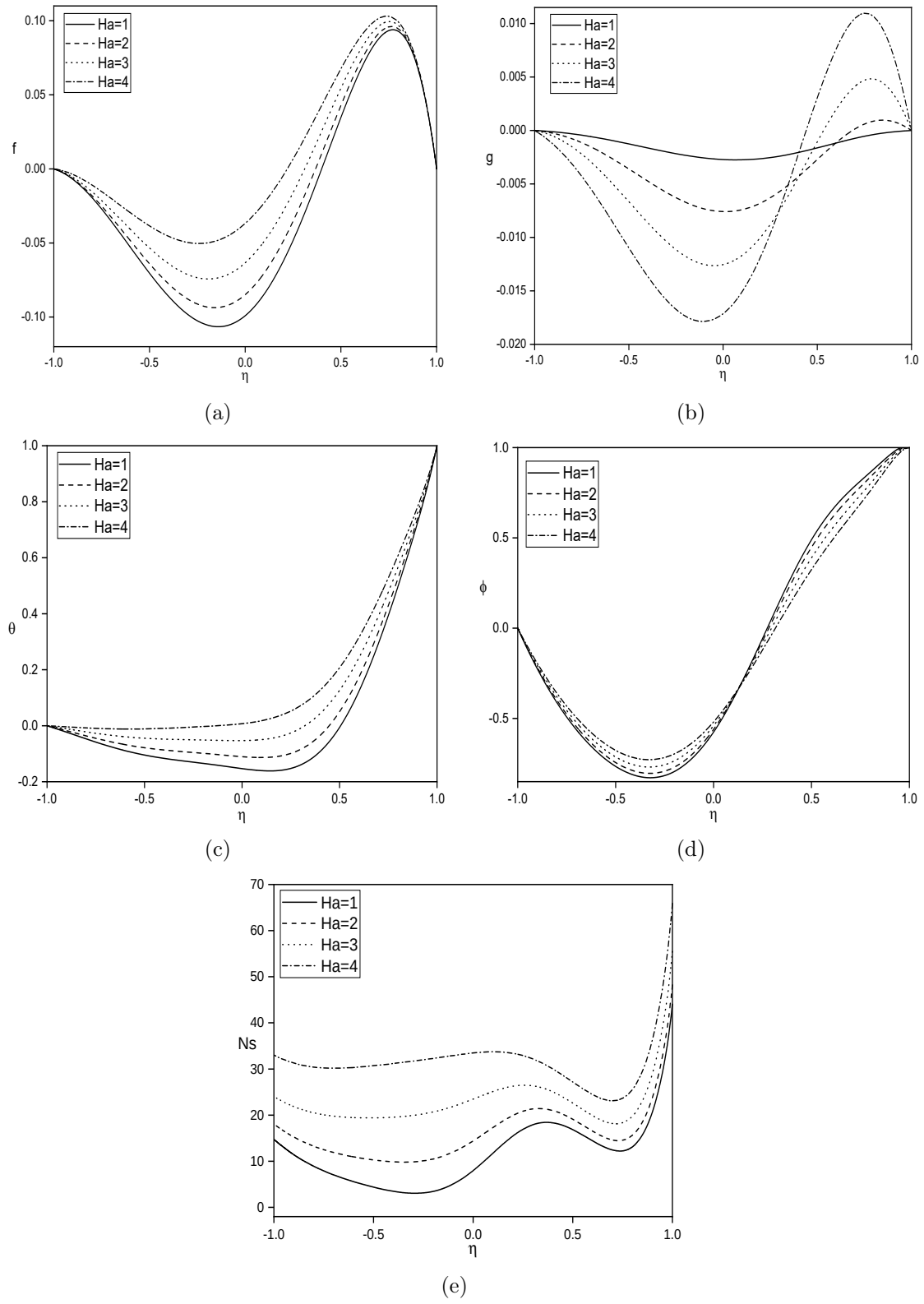

Figure 2.2: Impact of magnetic parameter (Ha) on (a) $f(\eta)$, (b) $g(\eta)$, (c) $\theta(\eta)$ (d) $\phi(\eta)$, and (e) Ns.

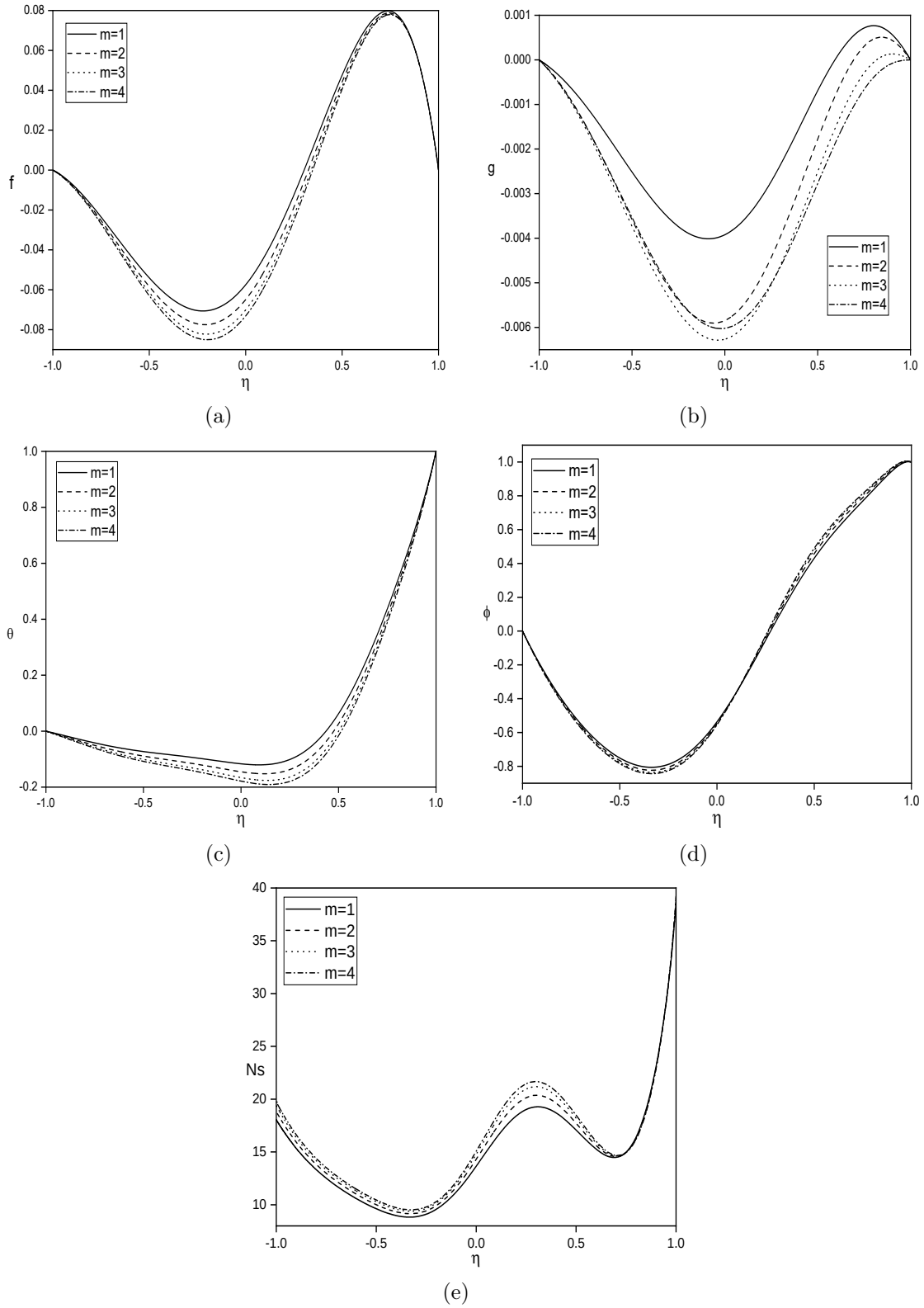

Figure 2.3: Impact of hall current (m) on (a) $f(\eta)$, (b) $g(\eta)$, (c) $\theta(\eta)$ (d) $\phi(\eta)$, and (e) Ns.

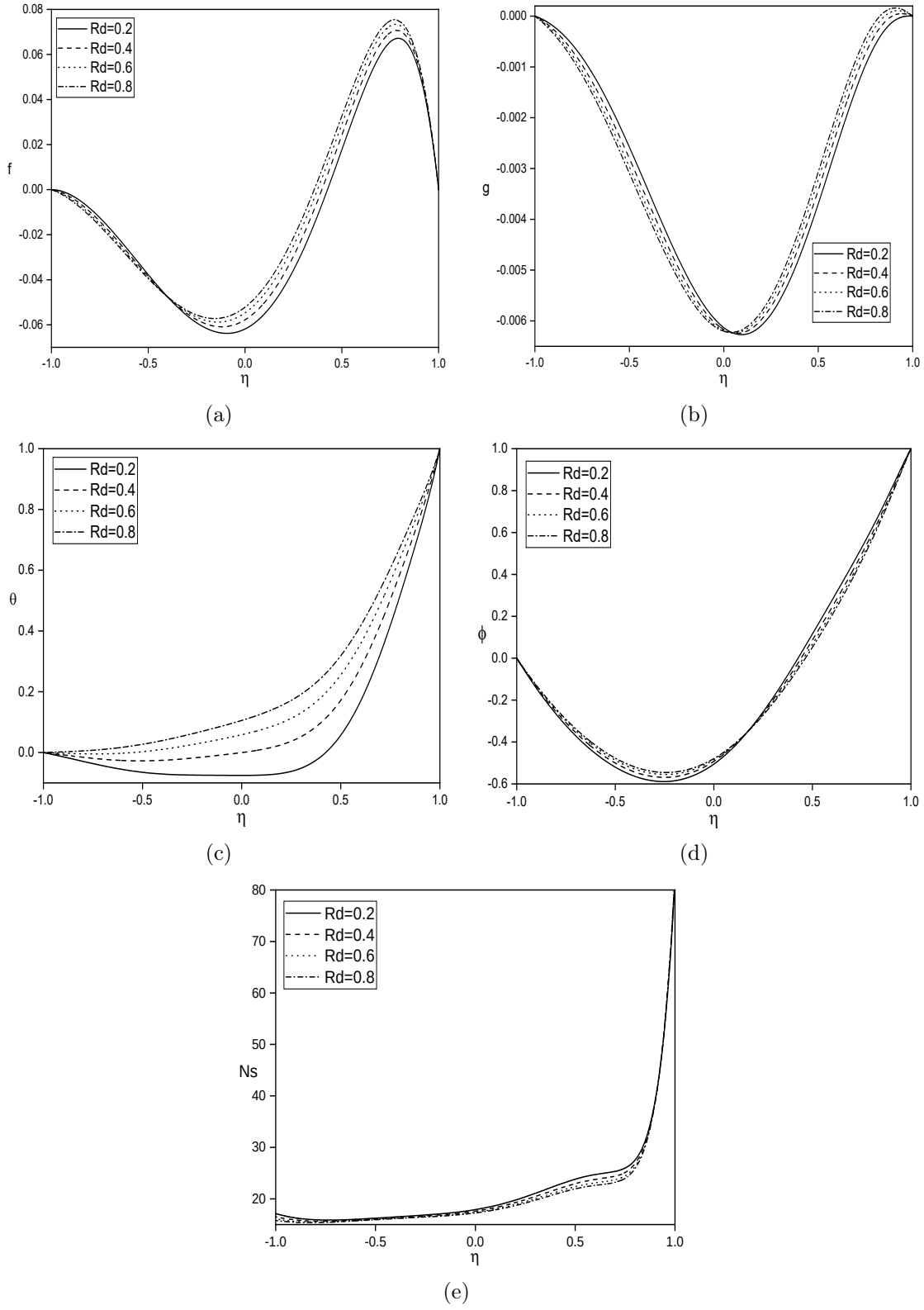

Figure 2.4: Impact of radiation parameter (Rd) on (a) $f(\eta)$, (b) $g(\eta)$, (c) $\theta(\eta)$ (d) $\phi(\eta)$, and (e) Ns.

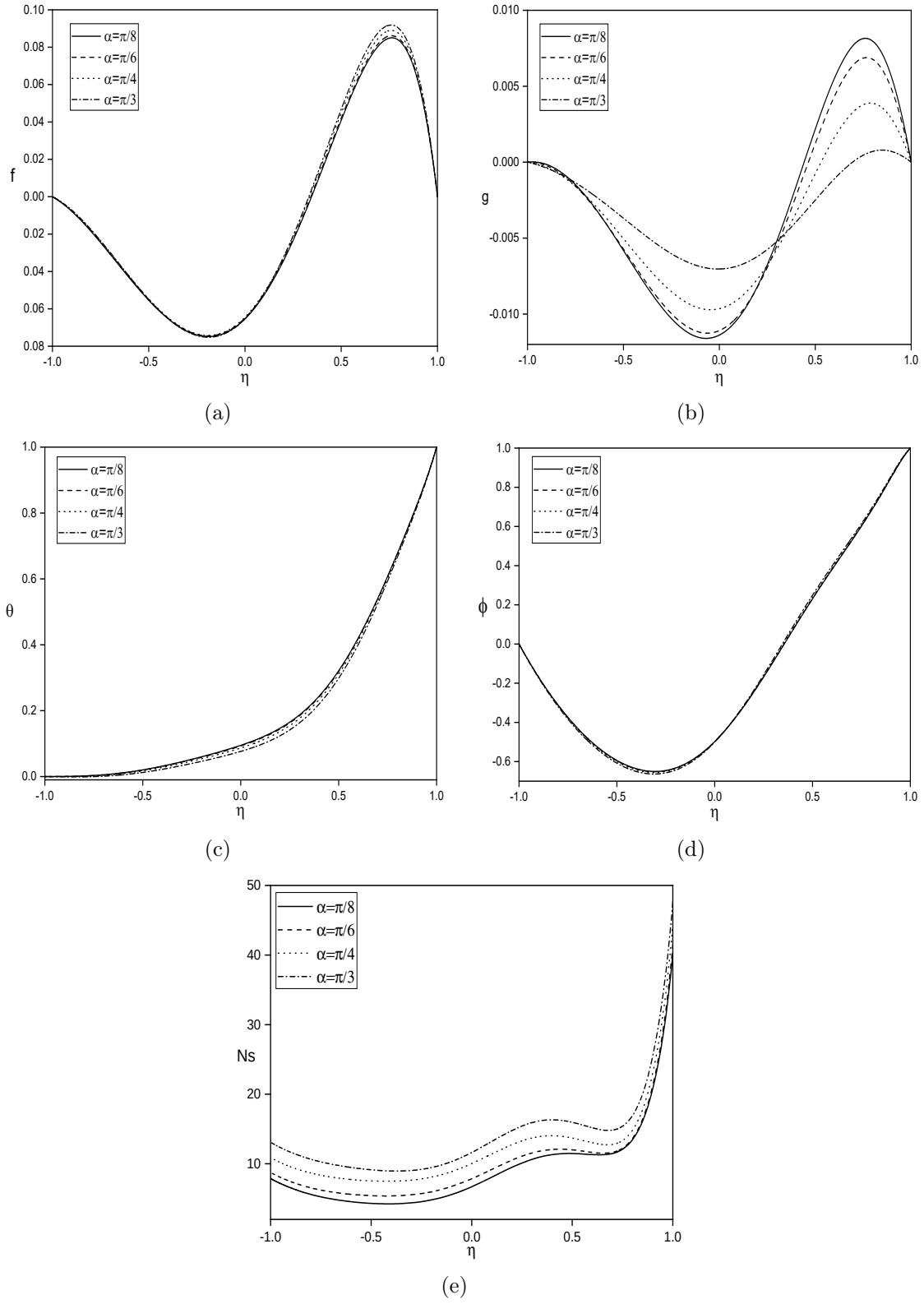

Figure 2.5: Impact of inclination angle (α) on (a) $f(\eta)$, (b) $g(\eta)$, (c) $\theta(\eta)$ (d) $\phi(\eta)$, and (e) Ns.

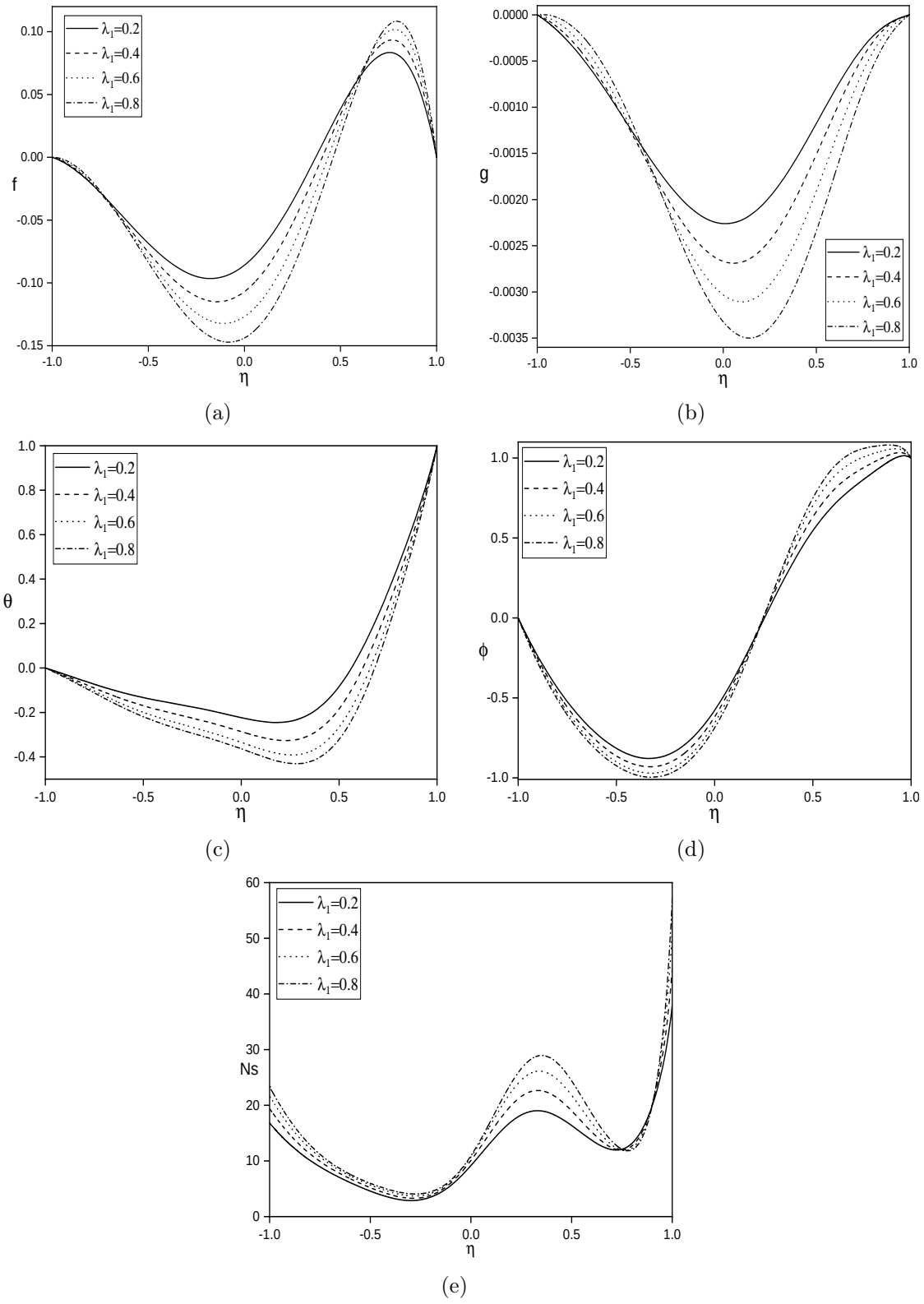

Figure 2.6: Impact of Jeffrey fluid parameter (λ_1) on (a) $f(\eta)$, (b) $g(\eta)$, (c) $\theta(\eta)$ (d) $\phi(\eta)$, and (e) Ns.

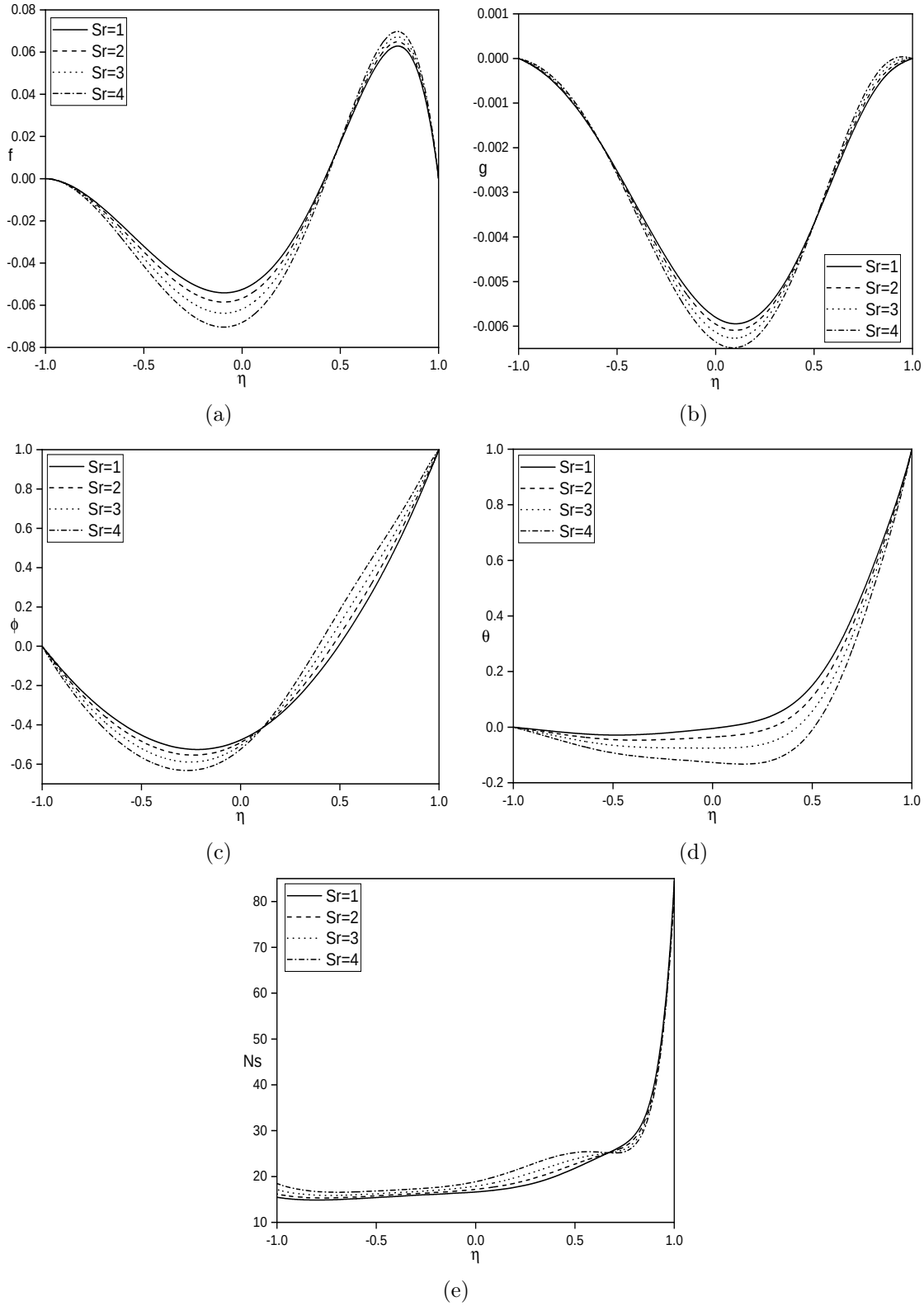

Figure 2.7: Impact of Soret number (Sr) on (a) $f(\eta)$, (b) $g(\eta)$, (c) $\theta(\eta)$ (d) $\phi(\eta)$, and (e) Ns.

Table 2.1: Comparison between exact solution and SQLM solution for the case when λ_1=0, Br=0, Sr=0, $Q = 0$, $Da = 1$ and Ha=0.

η	f		θ		ϕ	
	Exact	SQLM	Exact	SQLM	Exact	SQLM
-1	0	$-1.05 \times 10^{-}15$	0	0	0	$-1.5 \times 10^{-}15$
-0.5	0.090302	0.090311	0.179046	0.179112	0.2188	0.2185
0	0.21928	0.21921	0.404374	0.404381	0.478833	0.478921
0.5	0.288324	0.288332	0.678804	0.678910	0.752541	0.752539
1	0	$-4.4 \times 10^{-}15$	1	1	1	1

Table 2.2: Overview of the effect of different values of Ha, Sr, α, m, Rd and λ_1 on skin friction ($Cf_{1,2}$), rate of heat transfer ($Nu_{1,2}$) and mass transfer ($Sh_{1,2}$).

Ha	Sr	α	m	Rd	λ_1	Cf_1	Cf_2	Nu_1	Nu_2	Sh_1	Sh_2
1	2	$\pi/3$	2	2	0.1	-0.07168	-0.58981	-0.94398	-3.64116	1.20990	-2.66705
2	2	$\pi/3$	2	2	0.1	-0.06525	-0.59959	-0.96546	-3.62203	1.20937	-2.66627
3	2	$\pi/3$	2	2	0.1	-0.05345	-0.61476	-0.99681	-3.59422	1.20843	-2.66496
2	1	$\pi/3$	2	2	0.1	-0.06449	-0.59713	-0.97008	-3.60976	1.19435	-2.70768
2	2	$\pi/3$	2	2	0.1	-0.06525	-0.59959	-0.96546	-3.62203	1.20937	-2.66627
2	3	$\pi/3$	2	2	0.1	-0.06602	-0.60209	-0.96070	-3.63462	1.22472	-2.62422
2	2	0	2	2	0.1	-0.07255	-0.56061	-0.97172	-3.53308	1.20696	-2.67382
2	2	$\pi/4$	2	2	0.1	-0.06687	-0.58792	-0.97060	-3.58747	1.20844	-2.66888
2	2	$\pi/3$	2	2	0.1	-0.06525	-0.59959	-0.96546	-3.62203	1.20937	-2.66627
2	2	$\pi/3$	1	2	0.1	-0.05952	-0.60763	-0.98161	-3.60942	1.20900	-2.66550
2	2	$\pi/3$	2	2	0.1	-0.06525	-0.5995	-0.96546	-3.62203	1.20937	-2.66627
2	2	$\pi/3$	3	2	0.1	-0.06872	-0.59454	-0.95439	-3.63157	1.20963	-2.66669
2	2	$\pi/3$	2	1	0.1	-0.05610	-0.59357	-0.38486	-3.02132	1.23559	-2.59998
2	2	$\pi/3$	2	2	0.1	-0.06525	-0.59959	-0.96546	-3.62203	1.20937	-2.66627
2	2	$\pi/3$	2	3	0.1	-0.06959	-0.60192	-1.59039	-4.25469	1.19907	-2.69249
2	2	$\pi/3$	2	2	0.1	-0.06525	-0.59959	-0.96546	-3.62203	1.20937	-2.66627
2	2	$\pi/3$	2	2	0.2	-0.06476	-0.65782	-0.95927	-3.68532	1.21077	-2.66082
2	2	$\pi/3$	2	2	0.3	-0.06386	-0.71619	-0.95468	-3.74393	1.21202	-2.65559

2.2.2 Case (b): Mixed convection

Consider a mixed convection flow occurring under the influence of buoyancy forces and external pressure gradient.

similarity transformations for this case is given as

$$\eta = \frac{y}{d},\ \ u = u_0 f,\ \ w = u_0 g,\ \ \theta = \frac{T - T_1}{T_2 - T_1},\ \ \phi = \frac{C - C_1}{C_2 - C_1} \tag{2.19}$$

In equations (2.2) - (2.5), Non-dimensional equations are obtained as

$$\begin{aligned} f'' - Re(1+\lambda_1)f' + (1+\lambda_1)\frac{Gr_T}{Re}\theta + (1+\lambda_1)\frac{Gr_C}{Re}\phi - \frac{f}{Da} \\ -\frac{Ha^2 cos\alpha(1+\lambda_1)}{1+m^2cos^2\alpha}\left(fcos\alpha - \lambda sin\alpha + mgcos^2\alpha\right) - (1+\lambda_1)A = 0 \end{aligned} \tag{2.20}$$

$$g'' - Re(1+\lambda_1)g' + \frac{Ha^2cos^2\alpha(1+\lambda_1)}{1+m^2cos^2\alpha}\left(mfcos\alpha - g - m\lambda sin\alpha\right) - \frac{g}{Da} = 0 \tag{2.21}$$

$$\left(1 + \frac{4}{3}Rd\right)\theta'' - RePr\theta' + \frac{Br}{(1+\lambda_1)}f'^2 + \frac{Br}{(1+\lambda_1)}g'^2 = 0 \tag{2.22}$$

$$ScSr\theta'' + \phi'' - ReSc\phi' - QSc\phi = 0 \tag{2.23}$$

with

$$\begin{aligned} f = g = \theta = \phi = 0, \quad when\ \eta = -1 \\ f = g = 0, \quad \theta = \phi = 1, \quad when\ \eta = 1 \end{aligned} \tag{2.24}$$

where $Sc = \nu/D$ is the Schmidt number, $Re = \rho v_0 d/\mu$ represents Reynolds number, $Pr = \mu c_p/k_f$ is Prandtl number, $Ha = dB_0\sqrt{\sigma/\mu}$ is the magnetic parameter, $Gr_T = g^*\beta_T(T_2 - T_1)d^3/v^2$ and $Gr_C = g^*\beta_C(T_2 - T_1)d^3/v^2$ represent thermal and Solutal Grashof number, $Br = \mu v^2/k_f d^2(T_2 - T_1)$ denotes Brinkman number, $Rd = 4\sigma T_0^3/k_f k^*$ denotes the Radiation parameter, $Q = k_1 d/v_0$ is the rate of chemical reaction, $\lambda = Re/Gr$, $Sr = DK_T(T_2 - T_1)/\nu T_m(C_2 - C_1)$ is the parameter of thermo diffusion, and $Da = k/d^2$ represents the Darcy number.

The expressions for shear stress, heat flux, and mass flux are given by:

$$\tau_w = \left[\mu \frac{du}{dy}\right] |_{y=\pm d}; \quad q_w = \left[-k_f \frac{dT}{dy} + q_r\right] |_{y=\pm d}; \quad q_m = -D\frac{dC}{dy} |_{y=\pm d}$$

The dimensionless shear stress $C_f = \tau_w/\rho u_0^2$ is given by $ReC_{f_{1,2}} = f'(\eta) |_{\eta=-1,1}$. The Sherwood number defined as $Sh = q_m d/D(C_2 - C_1)$ and Nusselt number defined as $Nu = q_w d/k_f(T_2 - T_1)$ for this problem are given by

$$Sh_{1,2} = -\left[\phi'(\eta)\right] |_{\eta=-1,1}; \quad Nu_{1,2} = -\left[1 + \frac{4}{3}Rd\right] \theta'(\eta) |_{\eta=-1,1} .$$

Entropy Generation

The expression for local volumetric rate of entropy generation (as explained in earlier case) is given by

$$S_{gen} = \frac{k_f}{T_0^2}\left[1 + \frac{16\sigma T_0^3}{3k_f k^*}\right]\left[\frac{dT}{dy}\right]^2 + \frac{\mu}{T_0(1+\lambda_1)}\left[\left(\frac{du}{dy}\right)^2 + \left(\frac{dw}{dy}\right)^2\right] + \frac{RD}{C_0}\left(\frac{dC}{dy}\right)^2 + \frac{RD}{T_0}\left(\frac{dT}{dy}\right)\left(\frac{dC}{dy}\right) + \frac{\mu}{kT_0}(u^2 + w^2) + \frac{\sigma B_0^2}{T_0}\left[w^2 + (ucos\alpha - v_0 sin\alpha)^2\right] \tag{2.25}$$

The first term in the right-hand side of equation (2.25) is caused by heat transfer, the second term because of energy dissipation by fluid viscosity, the third and fourth by mass transfer, the fifth by porosity, and the sixth by the applied magnetic field. The expression for rate of entropy production $(S_{gen})_0$ is given by

$$(S_{gen})_0 = \frac{k_f(T_2 - T_1)^2}{T_0^2 d^2} \tag{2.26}$$

By using equations (2.25) - (2.26), the creation of non-dimensional entropy can be expressed as follows:

$$N_s = \frac{S_{gen}}{(S_{gen})_0}$$

$$N_s = \left[1 + \frac{4}{3}Rd\right](\theta')^2 + \frac{BrGr^2}{(1+\lambda_1)A_1}(f'^2 + g'^2) + \frac{\varepsilon B_1^2}{A_1^2}(\phi')^2 + \frac{\varepsilon B_1}{A_1}\theta'\phi' + \frac{BrGr^2}{DaA_1}(f^2 + g^2) + \frac{BrGr^2Ha^2}{A_1}\left(g^2 + (fcos\alpha - \lambda sin\alpha)^2\right)$$

where A_1, Br, B_1, Gr, Rd, ε, Ha and Da are dimensionless temperature difference, Brinkman number, dimensionless constant parameter, Grashof number, radiation parameter, dimensionless concentration difference, magnetic parameter, Darcy number, respectively, which are given by

$$Rd = \frac{4\sigma T_0^3}{k_f k^*}, \quad Br = \frac{\mu v^2}{k_f d^2(T_2 - T_1)}, \quad Gr = \frac{g\beta(T_2 - T_1)d^3}{v^2}, \quad \varepsilon = \frac{RDC_0}{k_f},$$
$$A_1 = \frac{T_2 - T_1}{T_0}, \quad B_1 = \frac{C_2 - C_1}{C_0}, \quad Ha = dB_0\sqrt{\frac{\sigma}{\mu}}, \quad Da = \frac{k}{d^2}$$

Results and discussion

The analytical solutions for equations (2.20), (2.22), and (2.23), along with their boundary conditions (2.24), were derived without considering the brinkman number (Br), $A = 0$, magnetic parameter (Ha), chemical reaction parameter (Q), and Jeffrey fluid parameter (λ_1), along with inclination angle at $\alpha = 60°$. A comparison was made between these analytical solutions and the solutions obtained using SQLM (as explained in earlier case), which are presented in Table 2.3. The results of comparisons show a high level of agreement. As a result, the SQLM code can be utilized with assurance to investigate the topic addressed in this research.

Figures 2.8 - 2.13 illustrate the impact of parameters such as Ha, m, Rd, α, λ_1, and Sr on flow and cross flow velocities, temperature, concentration, and entropy.

These effects are analyzed with a fixed value of Q, Re, Pr, Sc, at 2, 2, 0.71 and 0.22, respectively.

Figure 2.8 indicates the influence of magnetic parameter (Ha) on velocities, temperature, concentration, and entropy whilst Br=0.5, $\alpha = \pi/3$, Sr=10, m=2, λ_1=0.5, A=1, Gr_T=20, Gr_C=20, and Da=0.2. It is determined from Figs. 2.8(a) - 2.8(b) that there's a rise in flow velocity and fall in cross-flow velocity as Ha enhances. Because, the inclined magnetic field, the drag cannot be generated. It could be visible from Fig. 2.8(c) that temperature (θ) decreases as Hartman number increases. As Ha grows, the fluid's concentration (ϕ) increases as shown in Fig. 2.8(d). It is noted from Fig. 2.8(e) show that entropy generation increase near $\eta = -1$ and decrease near $\eta = 1$.

Figure 2.9 demonstrates the effect of Rd on velocities, temperature, concentration, and entropy at $\alpha = \pi/3$, $Sr = 10$, $Ha = 2$, $m = 2$, $\lambda_1 = 0.5$, $Br = 0.5$, $A = 1$, $Da = 3$, $Gr_T = 20$, and $Gr_C = 20$. As seen in Figures 2.9(a), 2.9(b) and 2.9(c), velocities and fluid temperature magnifies with an rise in Rd. Concentration of the fluid as shown in Fig. 2.9(d) fall as radiation parameter enhance. Figure 2.9(e) shows that entropy generation decrease as Rd increase.

Figure 2.10 demonstrate how m affects velocities, temperature, concentration, and entropy at $\alpha = \pi/3$, $Sr = 20$, $Ha = 3$, $Rd = 0.2$, $\lambda_1 = 0.5$, $Br = 0.5$, $A = 1$, $Gr_T = 10$, $Gr_C = 10$, and $Da = 0.2$. As illustrated in Figures 2.10(a) and 2.10(b), we can see that as the value of the parameter m increases, there's also an increase in both the flow velocity and the cross-flow velocity. The fluid temperature drops as m rise, as shown in fig. 2.10(c). From fig. 2.10(d), the fluid concentration rise as m increase. This phenomenon is attributed to the inclined magnetic field with an angle of $\alpha = \pi/3$, which results in the Hall effect producing charge in the direction of inclined plates, thereby making it unable to act as a flagon velocity. As mentioned earlier, the Hall current produces additional charge, which leads to a decrease in the

temperature of the fluid. It is observed from 2.10(e) that the entropy generation rise as m rise.

In Figure 2.11, the behavior of velocities, temperature, concentration, and entropy is depicted as a function of α at fixed values of Rd=2, Sr=20, Ha=2, m=2, λ_1=0.5, Br=0.8, A=1, Da=0.2, Gr_T=20, and Gr_C=20. It can seen from figures 2.11(a) and 2.11(b) that the flow velocity magnifies and cross-flow velocity diminishes as α magnifies. Figure 2.11(c) show that the fluid temperature diminishes as α magnifies. It can predict from Fig. 2.11(d) that the concentration gains with rising values of α. The reason for this behavior is that an increase in the inclination angle of the applied magnetic field leads to a reduction in the drag force, which enhances the net flow in the fluid. Figure 2.11(e) show that entropy generation increase as α increase.

The influence of λ_1 on velocities, temperature, concentration, and entropy can be seen in Fig. 2.12 while keeping other parameters fixed at $Rd = 2$, $Sr = 20$, $Ha = 1$, $m = 2$, $\alpha = \pi/3$, $Br = 0.5$, $A = 1$, $Da = 0.2$, $Gr_T = 20$, and $Gr_C = 20$. Figures 2.12(a) and 2.12(b) show that the velocities (f, g) enhances as λ_1 enhance. Figure 2.12(c) shows that the fluid temperature drops as λ_1 rise. It is found in figure 2.12(d) that the concentration enhance as λ_1 enhances. Figure 2.12(e) demonstrate that as λ_1 magnify, entropy generation also magnify.

Figure 2.13 illustrates the behavior of velocities, temperature, concentration, and entropy under varying values of Sr, with Rd=0.1, Ha=2, m=2, α=$\pi/3$, λ_1=0.5, Br=0.5, A=1, Gr_T=10, Gr_C=10, and Da=0.2 held constant. As shown in figures 2.13(a) and 2.13(b), the velocities (f, g) enhance as the value of Sr increase. Figure 2.13(c) reveals that the fluid temperature drop as Sr rise. The fluid concentration increases as depicted in Fig. 2.13(d) when Sr increases. It is seen from Fig. 2.13(e) that entropy generation magnify as Sr magnify.

Table 2.4 displays how different factors, including Hall number (m), Soret effect

(Sr), magnetic parameter (Ha), radiation parameter (Rd), angle of inclination (α), and Jeffrey fluid parameter (λ_1), impact various aspects of the system while holding other variables at Q=2, Re=2, Pr=0.71, Br=0.5, Sc=0.22, Gr_T=20, Gr_C=20, A=1 and Da=0.2. Table show that when Rd increase, the skin friction coefficient subside at starting plate and rise at terminal plate, whereas the opposite tendency is seen as λ_1 rise. The friction factor decreases at both the walls as Sr, α, and m increase, while the opposite trend is observed with an rise in Ha. Furthermore, the table indicates that rate of heat transfer subside at the left plate and rise at right plate with an rise in Sr, α, m, and λ_1, while the opposite tendency is noted with an rise in Ha. The heat transfer rate decreases at both the walls as Rd increases. As for the mass transfer rate, the table shows that it rises at both walls as Sr, α, m, and λ_1 rise, while the opposite trend is observed as magnetic parameter rise. Rate of mass transfer subside at one wall and rise at the other wall as Rd rise.

2.3 Conclusions

This chapter investigates the entropy generation in Jeffrey fluid flow between vertical parallel plates with a porous medium, influenced by an angled magnetic field, chemical reactions, and heat radiation. The original complex equations describing the system are changed into dimensionless equations using similarity transformations. SQLM is used to solve these dimensionless equations. The flow characteristics are thoroughly analyzed and discussed through graphical representations.

From this study (both case(a) and case(b)), we can conclude that entropy generation increases with the inclination angle (α), Hall parameter (m), Jeffrey fluid parameter (λ_1), and Soret parameter (Sr). A rise in the radiation parameter, Jeffrey fluid parameter, and Soret parameter also causes the flow direction's velocity to increase. Conversely, as the magnetic parameter, inclination angle, Jeffrey fluid parameter, and Soret parameter increase, the cross-flow velocity decreases. Addi-

tionally, an increase in Jeffrey fluid parameter and Soret number leads to a fall in fluid temperature and a rise in concentration. In contrast, with increasing radiation parameter, we observe the opposite trend.

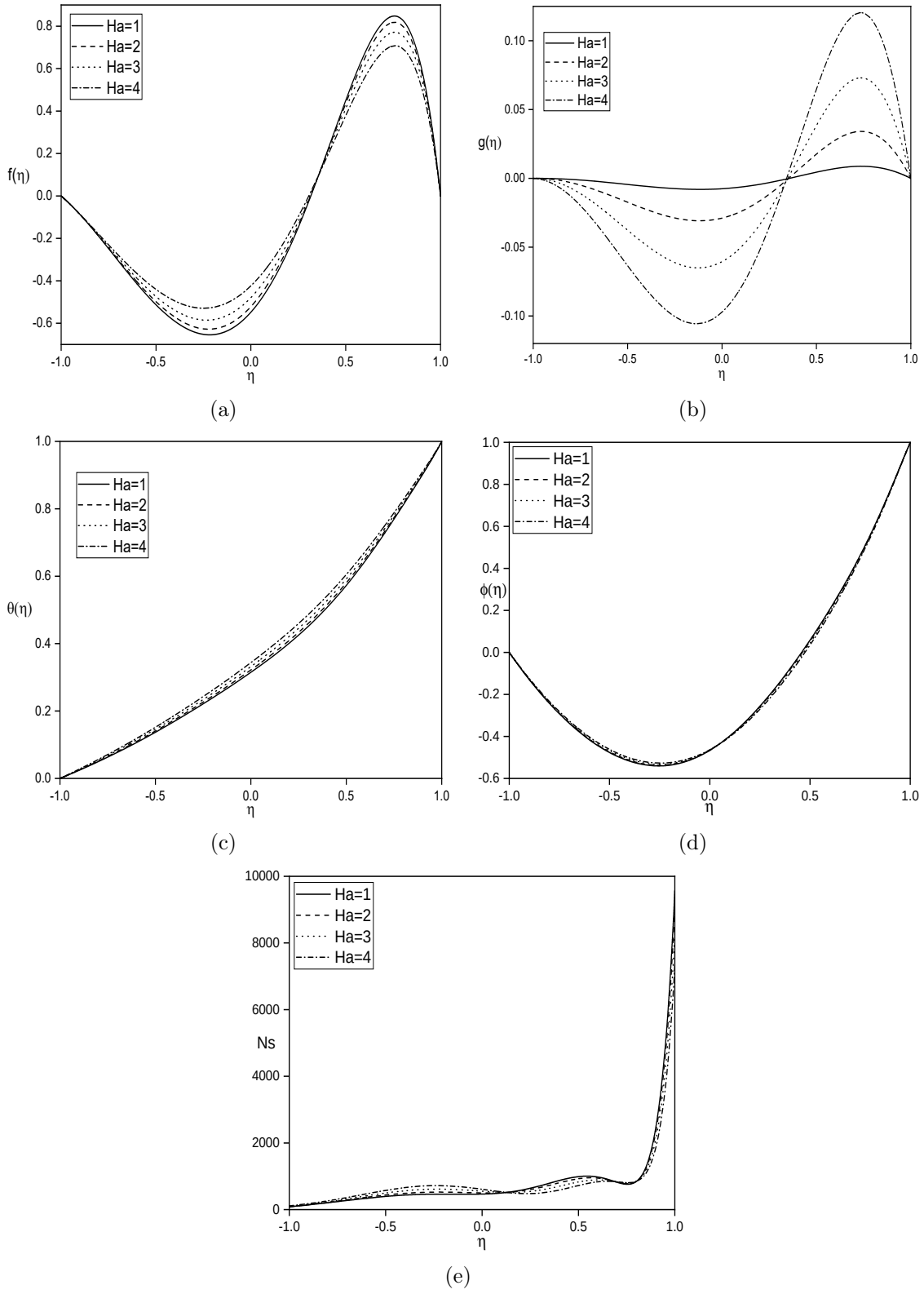

Figure 2.8: Influence of magnetic parameter (Ha) on (a) $f(\eta)$, (b) $g(\eta)$, (c) $\theta(\eta)$ (d) $\phi(\eta)$, and (e) Ns.

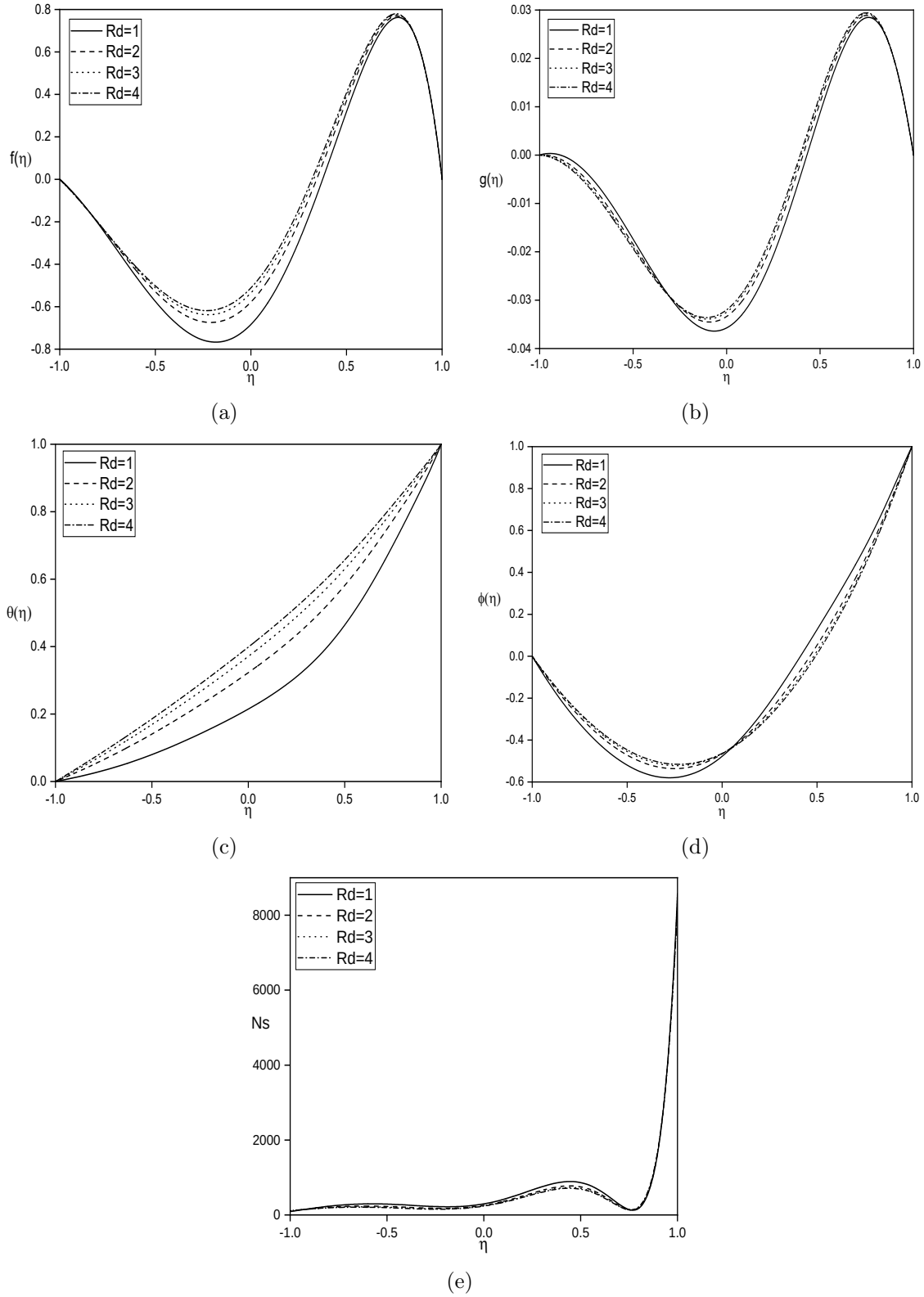

Figure 2.9: Influence of radiation parameter (Rd) on (a) $f(\eta)$, (b) $g(\eta)$, (c) $\theta(\eta)$ (d) $\phi(\eta)$, and (e) Ns.

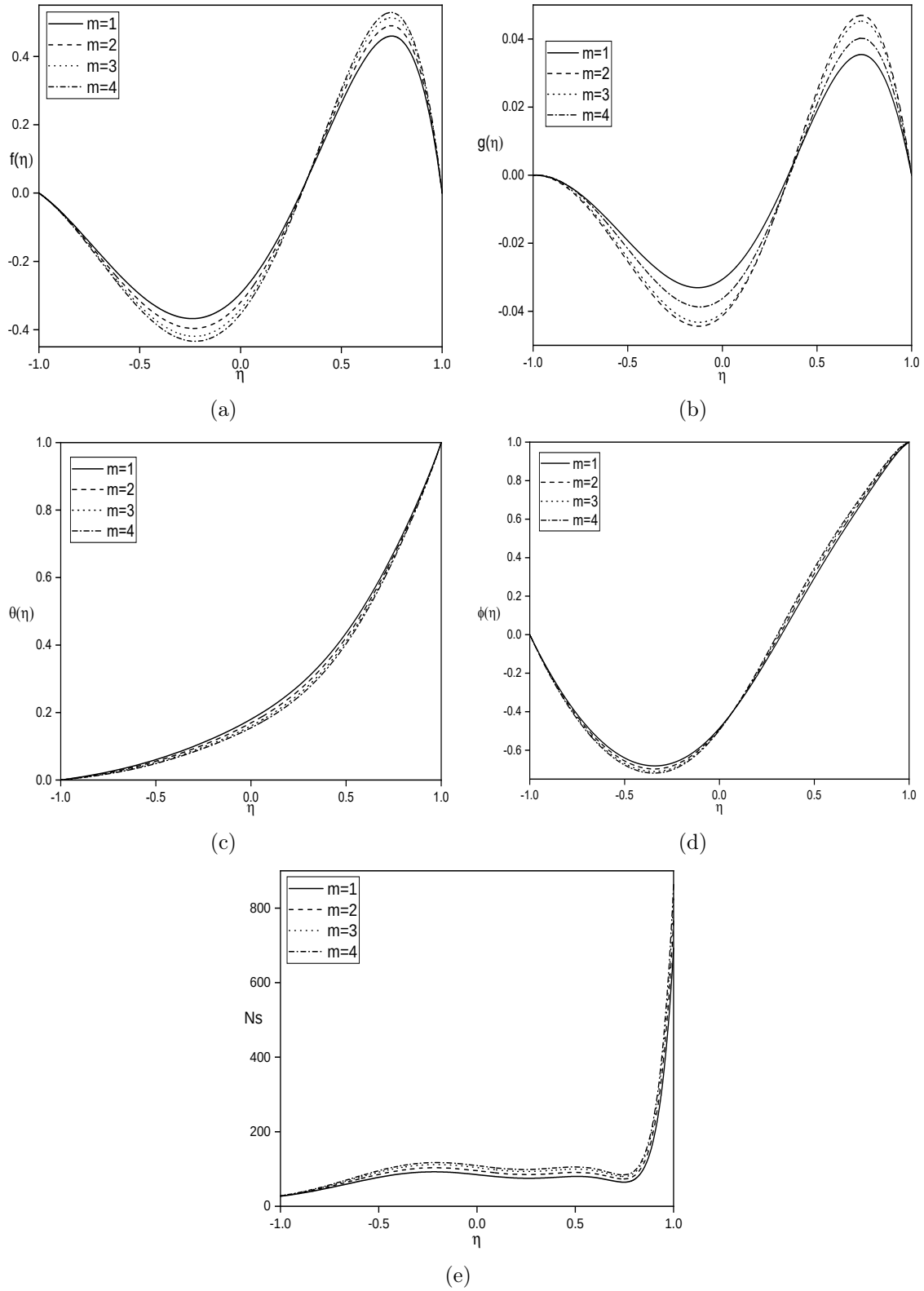

Figure 2.10: Influence of hall current (m) on (a) $f(\eta)$, (b) $g(\eta)$, (c) $\theta(\eta)$ (d) $\phi(\eta)$, and (e) Ns.

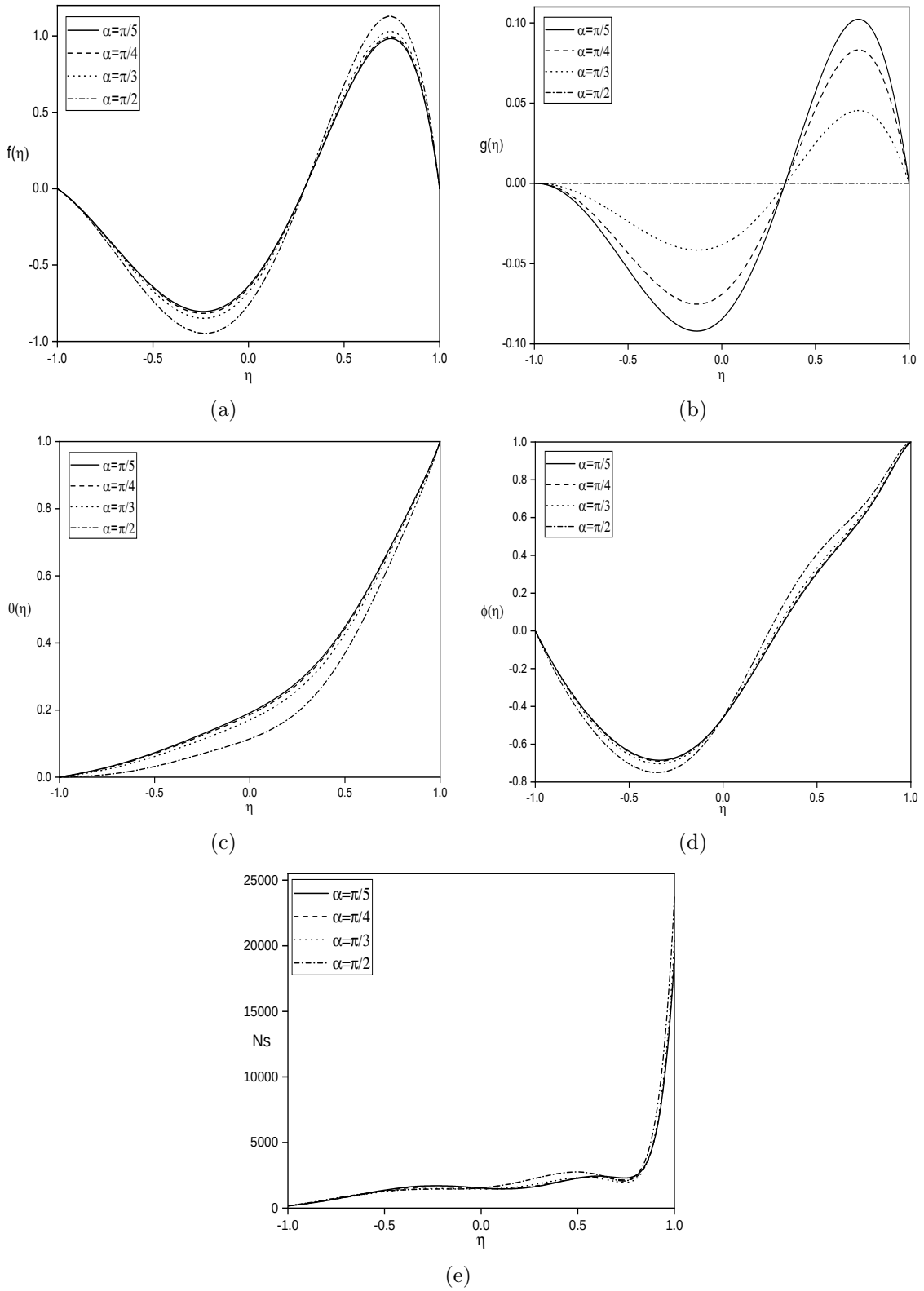

Figure 2.11: Influence of inclination angle (α) on (a) $f(\eta)$, (b) $g(\eta)$, (c) $\theta(\eta)$ (d) $\phi(\eta)$, and (e) Ns.

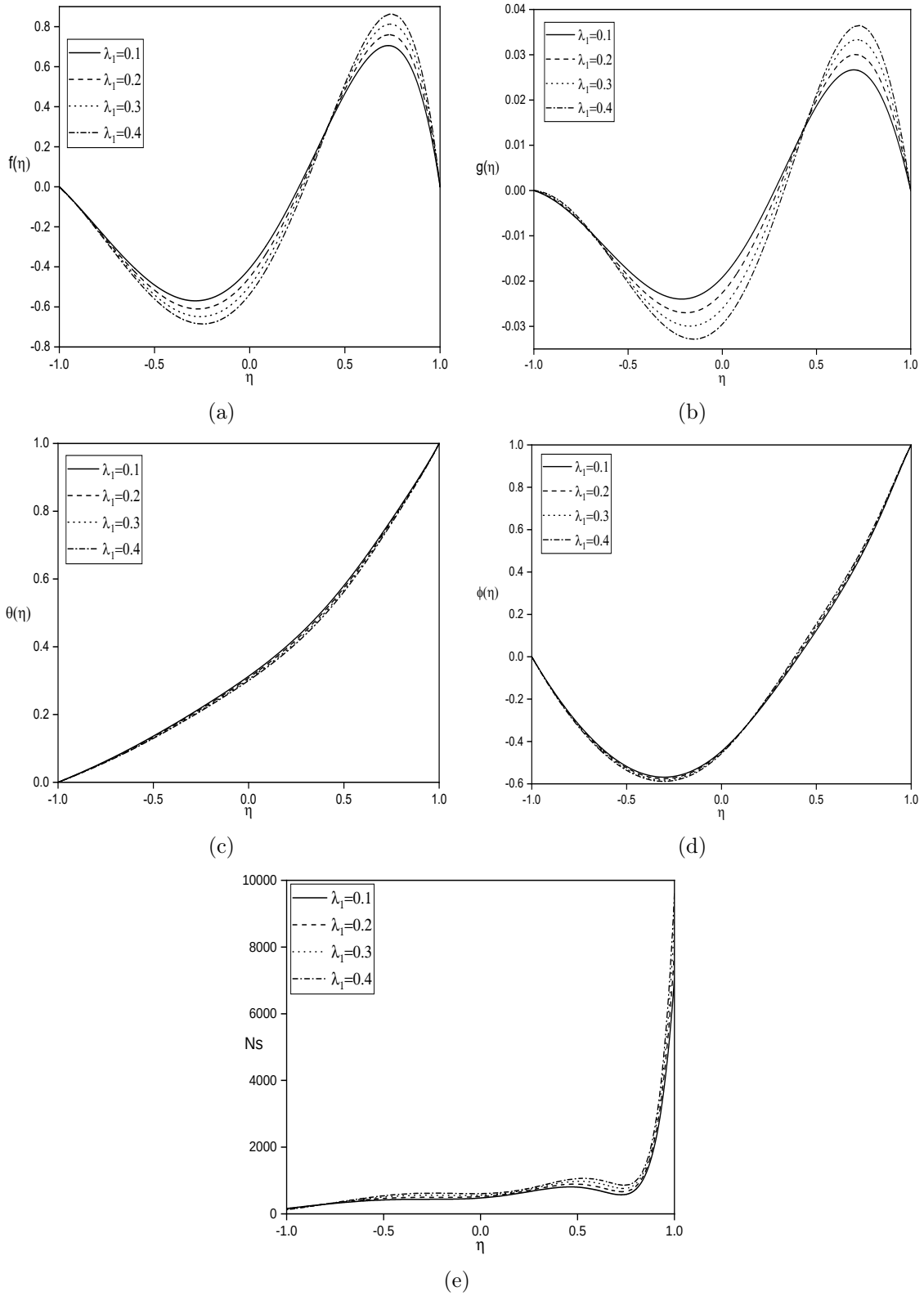

Figure 2.12: Influence of Jeffrey fluid parameter (λ_1) on (a) $f(\eta)$, (b) $g(\eta)$, (c) $\theta(\eta)$ (d) $\phi(\eta)$, and (e) Ns.

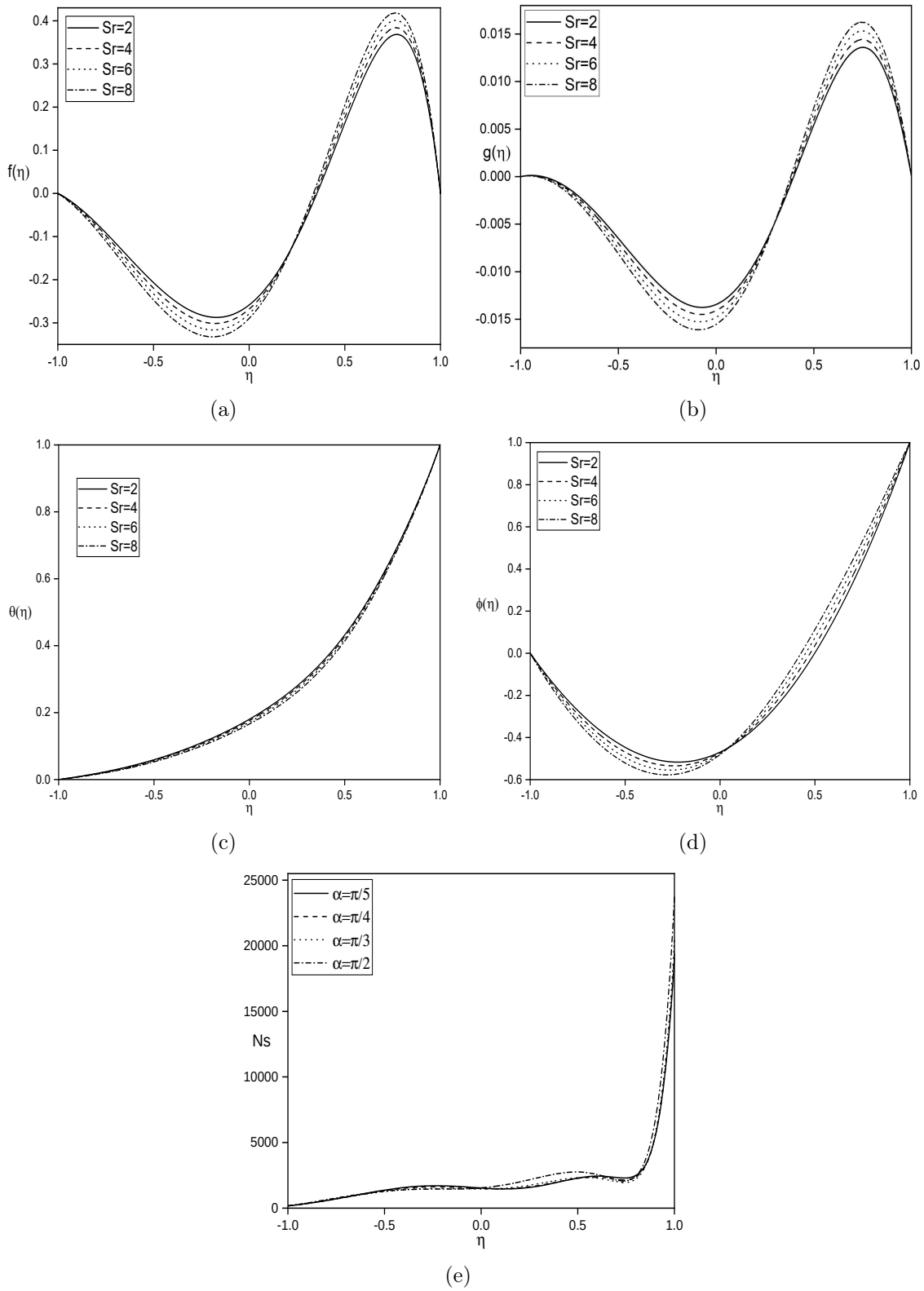

Figure 2.13: Influence of Soret number (Sr) on (a) $f(\eta)$, (b) $g(\eta)$, (c) $\theta(\eta)$ (d) $\phi(\eta)$, and (e) Ns.

Table 2.3: Comparison between exact solution and SQLM solution for the case when λ_1=0, Br=0, Sr=0, $Q = 0$, $Da = 1$, Gr_T=20, Gr_C=20, and Ha=0.

η	f		θ		ϕ	
	Exact	SQLM	Exact	SQLM	Exact	SQLM
-1	0	$-1 \times 10^{-}14$	0	0	0	$-1.5 \times 10^{-}15$
-0.5	0.90302	0.90314	0.179046	0.179112	0.2188	0.2185
0	2.1928	2.1932	0.404374	0.404381	0.478833	0.478921
0.5	2.88324	2.88331	0.678804	0.678910	0.752541	0.752539
1	0	$-4.4 \times 10^{-}14$	1	1	1	1

Table 2.4: Overview of the effect of different values of Ha, Sr, α, m, Rd and λ_1 on skin friction ($Cf_{1,2}$), rate of heat transfer ($Nu_{1,2}$) and mass transfer ($Sh_{1,2}$).

Ha	Sr	α	m	Rd	λ_1	Cf_1	Cf_2	Nu_1	Nu_2	Sh_1	Sh_2
1	2	$\pi/3$	2	2	0.1	-5.79148	-0.74670	-3.62339	-0.94007	-2.66897	1.20942
2	2	$\pi/3$	2	2	0.1	-5.67373	-0.74586	-3.57079	-0.95550	-2.67204	1.20799
3	2	$\pi/3$	2	2	0.1	-5.47857	-0.74317	-3.48971	-0.97916	-2.67680	1.20580
2	1	$\pi/3$	2	2	0.1	-5.64872	-0.73873	-3.55898	-0.96007	-2.71055	1.19367
2	2	$\pi/3$	2	2	0.1	-5.67373	-0.74586	-3.57079	-0.95550	-2.67204	1.20799
2	3	$\pi/3$	2	2	0.1	-5.69921	-0.75312	-3.58291	-0.95078	-2.63292	1.22262
2	2	0	2	2	0.1	-5.53933	-0.74576	-3.52262	-0.96908	-2.67492	1.20668
2	2	$\pi/4$	2	2	0.1	-5.61163	-0.74565	-3.54633	-0.96251	-2.67348	1.20733
2	2	$\pi/3$	2	2	0.1	-5.67373	-0.74586	-3.57079	-0.95550	-2.67204	1.20799
2	2	$\pi/3$	1	2	0.1	-5.58941	-0.74463	-3.53285	-0.96668	-2.67425	1.20696
2	2	$\pi/3$	2	2	0.1	-5.67373	-0.74586	-3.57079	-0.95550	-2.67204	1.20799
2	2	$\pi/3$	3	2	0.1	-5.73157	-0.74641	-3.59682	-0.94784	-2.67052	1.20870
2	2	$\pi/3$	2	1	0.1	-5.70179	-0.62819	-2.98640	-0.37719	-2.60643	1.23420
2	2	$\pi/3$	2	2	0.1	-5.67373	-0.74586	-3.57079	-0.95550	-2.67204	1.20799
2	2	$\pi/3$	2	3	0.1	-5.65349	-0.80203	-4.19485	-1.57947	-2.69732	1.19787
2	2	$\pi/3$	2	2	0.1	-5.67373	-0.74586	-3.57079	-0.95550	-2.67204	1.20799
2	2	$\pi/3$	2	2	0.2	-6.21900	-0.74358	-3.62849	-0.94977	-2.66713	1.20932
2	2	$\pi/3$	2	2	0.3	-6.76376	-0.73727	-3.68146	-0.94565	-2.66244	1.21049

Chapter 3

Analysis of entropy generation in Jeffrey fluid flow between two parallel plates with Soret and angled magnetic effect under Navier-slip conditions [1]

3.1 Introduction

Various technologies, including surface polishing and slip flow in liquids at both micro and macro levels, play a significant role in fluid dynamics. In 1823, Navier introduced a slip boundary condition, stating that the slip velocity has a linear relation to shear stress. There is great evidence of the application and importance of slip flow given by many researchers [63, 64, 65]. Gie and Whitehead [66] described

[1] Case(a): Published in "**The European Physical Journal Plus**", 138, 1-14, (2023).
Case(b):Published in "**Proc IMechE Part E: J Process Mechanical Engineering**", 1-12, (2023). DOI:https://doi.org/10.1177/09544089231218977

how Navier-slip Rayleigh-Benard convection behaves when an ultimate state is absent. Zhang and He [67] created a technique that employs the least-squares domain method to simulate the interaction between particles and flow on the Navier slip boundary condition. Recently, Badday and Harfash [68] studied thermosolutal convection with a Navier-Stokes-Voigt fluid under the impact of Soret and slip boundary conditions. Most Recently, Housiadas and Tsangaris [69] examined the impact of navier slip for laminar flow with variable geometry using high-order lubrication theory.

The impact of magnetic fields plays a crucial role in various engineering applications. These applications include MHD generators, dampers and clutches, biomedical devices, astrophysics and space applications, cooling systems, geothermal energy extraction etc. Several researchers have been interested in magnetic fields having non-zero inclinations. Dogonchi et al. [70] studied the nanofluid flow through a porous channel with an angled magnetic field. Goswami et al. [71] investigated the unsteady magnetohydrodynamic flow with an angled magnetic field between two infinite parallel plates.

In this chapter, we examine the entropy generation on steady convective Jeffrey fluid flow through a channel with navier-slip condition. The resulting flow equations are solved using SQLM.

3.2 Mathematical Formulation

The flow under consideration is assumed to be a steady and incompressible Jeffrey fluid flow. The physical setup (refer to figure 3.1) consists of two parallel plates. The plates are positioned at a separation distance of $2d$. The concentrations and temperatures at the plates are denoted as C_1, T_1, C_2, and T_2 respectively are all discussed in Fig. 3.1. An external magnetic field denoted as B_0, positioned at an angle α about the base, exerts an impact on the plates. With the assumption that

the boundaries extend infinitely along the x-axis, the parameters governing the flow are treated as functions solely dependent on the y coordinate. The properties of fluid are taken as constant, except for the change in density that affects the term in the buoyancy force. As such, these assumptions align with natural principles and are relevant in practical applications.

The governing equations are derived as follows:

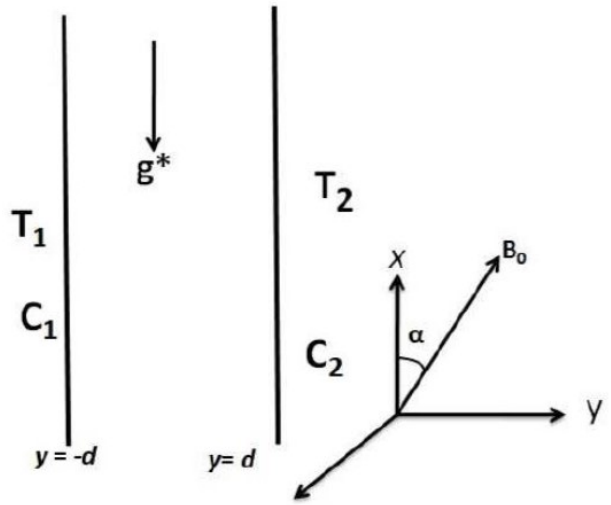

Figure 3.1: Diagrammatic representation of the fluid flow

$$\frac{dv}{dy} = 0 \Rightarrow v = v_0 = constant \tag{3.1}$$

$$\begin{aligned} \rho v_0 \frac{du}{dy} = \frac{\mu}{1+\lambda_1}\frac{d^2u}{dy^2} + \rho g^* \left(\beta_C (C - C_1) + \beta_T (T - T_1)\right) \\ -\frac{dp}{dx} - \frac{\sigma B_0^2 cos\alpha}{1 + m^2 cos^2\alpha}\left(ucos\alpha - v_0 sin\alpha + mwcos^2\alpha\right) \end{aligned} \tag{3.2}$$

$$\rho v_0 \frac{dw}{dy} = \frac{\mu}{1+\lambda_1}\frac{d^2w}{dy^2} + \frac{\sigma B_0^2 cos^2\alpha}{1 + m^2 cos^2\alpha}\left(mucos\alpha - w - mv_0 sin\alpha\right) \tag{3.3}$$

$$\rho c_p v_0 \frac{dT}{dy} = k_f \frac{d^2T}{dy^2} + \frac{\mu}{1+\lambda_1}\left((\frac{du}{dy})^2 + (\frac{dw}{dy})^2\right) \tag{3.4}$$

$$v_0 \frac{dC}{dy} = D\frac{d^2C}{dy^2} + \frac{DK_T}{T_m}\frac{d^2T}{dy^2} \tag{3.5}$$

where k_f represents the thermal conductivity, c_p denotes the specific heat, g^*

represents gravitational acceleration, ρ is the density, $m = \eta\ \sigma B_0$ denotes the Hall parameter, β_T and β_C denote the thermal and solutal expansion, σ represents the electrical conductivity, μ is the viscosity, D denotes the diffusivity of mass, T_m represents the mean fluid temperature and K_T represents the ratio of thermal diffusion.

Boundary conditions of given problem are given by

$$\begin{aligned} u &= \gamma_1 \frac{du}{dy},\ w = T - T_1 = C - C_1 = 0, \quad when\ y = -d \\ u &= \gamma_2 \frac{du}{dy},\ w = T - T_2 = C - C_2 = 0, \quad when\ y = d. \end{aligned} \tag{3.6}$$

3.2.1 Case (a): Natural convection

Natural convection flow is driven by buoyant forces. There is no external pressure gradient ($\frac{\partial p}{\partial x} = 0$).

similarity transformations for this given problem is given as

$$\eta = \frac{y}{d}, \quad u = \frac{\nu Gr}{d} f, \quad w = \frac{\nu Gr}{d} g, \quad \phi = \frac{C - C_1}{C_2 - C_1}, \quad \theta = \frac{T - T_1}{T_2 - T_1}, \tag{3.7}$$

In equations (3.2) - (3.5), Non-dimensional equations are obtained as

$$\begin{aligned} f'' - Re(1+\lambda_1) f' + (1+\lambda_1)\left(\theta + N\phi\right) \\ - \frac{Ha^2 cos\alpha (1+\lambda_1)}{1 + m^2 cos^2\alpha} \left(f cos\alpha - \lambda sin\alpha + mg cos^2\alpha\right) = 0 \end{aligned} \tag{3.8}$$

$$g'' - Re(1+\lambda_1) g' + \frac{Ha^2 cos^2\alpha (1+\lambda_1)}{1 + m^2 cos^2\alpha} \left(mf cos\alpha - g - m\lambda sin\alpha\right) = 0 \tag{3.9}$$

$$\theta'' - RePr\theta' + \frac{BrGr^2}{(1+\lambda_1)} \left(f'^2 + g'^2\right) = 0 \tag{3.10}$$

$$ScSr\theta'' + \phi'' - ReSc\phi' = 0 \tag{3.11}$$

where $Re = \rho v_0 d/\mu$ represents Reynolds number, $Sr = DK_T(T_2 - T_1)/\nu T_m(C_2 - C_1)$ represents the thermal diffusion parameter, $Br = \mu v^2/k_f d^2(T_2 - T_1)$ is Brinkman

number, $Gr = g^*\beta_T(T_2 - T_1)d^3/v^2$ denotes the Grashof number, $Pr = \mu c_p/k_f$ is Prandtl number, $\lambda = Re/Gr$, $Ha = dB_0\sqrt{\sigma/\mu}$ indicates the magnetic parameter, $Sc = \nu/D$ is the Schmidt number, $N = \beta_C(C_2 - C_1)/\beta_T(T_2 - T_1)$ indicates the buoyancy parameter, $\beta_1 = \gamma_1/d$ and $\beta_2 = \gamma_2/d$ are the slip parameters.

Boundary conditions (3.6) become

$$\begin{aligned} f &= \beta_1 f', \quad g = \theta = \phi = 0, \quad when\ \eta = -1 \\ f &= \beta_2 f', \quad g = 0, \quad \theta = \phi = 1, \quad when\ \eta = 1 \end{aligned} \tag{3.12}$$

The shear stress, heat, and mass flows are given by

$$\tau_w = \left[\mu\frac{du}{dy}\right] |_{y=\pm d}; \quad q_w = \left[-k_f\frac{dT}{dy}\right] |_{y=\pm d}; \quad q_m = \left[-D\frac{dC}{dy}\right] |_{y=\pm d}$$

The dimensionless shear stress $C_f = \tau_w/\rho u_0^2$ is given by $ReC_{f_{1,2}} = f'(\eta) |_{\eta=-1,1}$. The Sherwood number defined as $Sh = q_m d/D(C_2 - C_1)$ and the Nusselt number defined as $Nu = q_w d/k_f(T_2 - T_1)$ for this problem are given by

$$Sh_{1,2} = -\left[\phi'(\eta)\right] |_{\eta=-1,1}; \quad Nu_{1,2} = -\left[\theta'(\eta)\right] |_{\eta=-1,1}\ .$$

Entropy Generation

The expression for local volumetric entropy generation rate (as explained in eariler chapter) is given by

$$\begin{aligned} S_{gen} = &\frac{k_f}{T_0^2}\left[\frac{dT}{dy}\right]^2 + \frac{\mu}{T_0(1+\lambda_1)}\left[\left(\frac{du}{dy}\right)^2 + \left(\frac{dw}{dy}\right)^2\right] + \frac{RD}{C_0}\left(\frac{dC}{dy}\right)^2 \\ &+ \frac{RD}{T_0}\left(\frac{dT}{dy}\right)\left(\frac{dC}{dy}\right) + \frac{\sigma B_0^2}{T_0}\left[w^2 + (ucos\alpha - v_0 sin\alpha)^2\right] \end{aligned} \tag{3.13}$$

The first term in the right-hand side of equation (3.13) is caused by heat transfer, the second term because of energy dissipation by fluid viscosity, the third and fourth

by mass transfer, and the fifth term due to magnetic field. The expression for rate of entropy production is given as

$$(S_{gen})_0 = \frac{k_f(T_2 - T_1)^2}{T_0^2 d^2} \tag{3.14}$$

By using equations (3.13) and (3.14), the creation of non-dimensional entropy can be expressed as follows:

$$N_s = \frac{S_{gen}}{(S_{gen})_0}$$

$$N_s = (\theta')^2 + \frac{BrGr^2}{(1+\lambda_1)A_1}(f'^2 + g'^2) + \frac{\varepsilon B_1^2}{A_1^2}(\phi')^2 + \frac{\varepsilon B_1}{A_1}\theta'\phi' + \frac{BrGr^2Ha^2}{A_1}\left(g^2 + (fcos\alpha - \lambda sin\alpha)^2\right)$$

where A_1, Br, B_1, Gr, Ha, and ε, are dimensionless temperature difference, Brinkman number, dimensionless concentration difference, Grashof number, Magnetic parameter, dimensionless constant parameter, respectively, which are represented as

$$Br = \frac{\mu v^2}{k_f d^2(T_2 - T_1)}, \quad Gr = \frac{g\beta(T_2 - T_1)d^3}{v^2}, \quad \varepsilon = \frac{RDC_0}{k_f},$$
$$A_1 = \frac{T_2 - T_1}{T_0}, \quad B_1 = \frac{C_2 - C_1}{C_0}, \quad Ha = dB_0\sqrt{\frac{\sigma}{\mu}}$$

Results and discussion

The nonlinear and coupled flow eqns. (3.8) - (3.11) with respect to boundary conditions (3.12) are numerically solved by SQLM (as explained in earlier chapter). The velocities, temperature, concentration, and entropy generation are influenced by several parameters, including Ha, Sr, m, α, λ_1, β_1, and β_2. Figures 3.2 - 3.8 depict how these parameters affect the aforementioned variables, with Re, Pr, Sc, N, β_1, and β_2 being held constant at values of 2, 0.71, 0.22, 2, 0.1, and 0.1, respectively.

Figure 3.2 illustrate the influence of Ha on velocities, temperature, concentra-

tion, and entropy while keeping the other parameters fixed at $\alpha = \pi/4$, $Sr = 2$, $m = 2$, $\lambda_1 = 0.5$, $Br = 0.5$, and $Gr = 20$. A rise in flow and cross-flow velocity is observed as Ha increases, as shown in Figures 3.2(a) and 3.2(b). It is because the observed inclination angle of the applied magnetic field is $\alpha > 0$, meaning that no drag force can be produced. From figures 3.2(c) and 3.2(d), it can be noted that a rise in Ha causes the fluid's temperature to decrease and its concentration to increase. This is because a magnetic field produces resistive force, which causes the temperature to drop. Figure 3.2(e) shows that the rate of entropy generation in the system goes up with increasing values of Ha. The magnetic field can induce Lorentz forces on the charged particles in the fluid. These forces cause additional dissipation, which consequently leads to a higher rate of entropy generation.

Figure 3.3 show how the Soret number (Sr) affects velocity, temperature, concentration, and entropy generation when other parameters are held constant at $\alpha = \pi/4$, $Sr = 10$, $Ha = 1$, $m = 2$, $\lambda_1 = 0.2$, $Br = 0.5$, and $Gr = 2$. Figures 3.3(a) and 3.3(b) demonstrate that an enhancement in Sr leads to an enhancement in flow velocity and cross-flow velocity. Higher Soret parameter values cause a steeper temperature gradient within the fluid. This, in turn, leads to increased velocities. It could be visible from figure 3.3(c) that as Sr grows, the fluid's temperature falls. It is noted from figures 3.3(d) and 3.3(e) that as Sr increases, the concentration of fluid and entropy in the system increases. A higher Soret number amplifies the energy transfer driven by both the rate of mass diffusion and the concentration gradients, leading to a radical enhancement in the concentration profile and entropy generation.

Figure 3.4 demonstrates how the hall parameter (m) affects the velocity, temperature, concentration, and entropy generation when other parameters are fixed at $\alpha = \pi/4$, $Sr = 5$, $Ha = 1$, $\lambda_1 = 0.2$, $Br = 0.5$, and $Gr = 10$. Figures 3.4(a) and 3.4(b) show that the velocities decrease as hall parameter rise. This effect is due to the tilted magnetic field. A magnetic field is angled at $\alpha = \frac{\pi}{4}$ will produce

a Hall current that is perpendicular to both the direction and will act as a drag on velocities. As hall parameter enhance, the fluid temperature also enhance, and fluid concentration subside as shown in figures 3.4(c) and 3.4(d). The fluid temperature rises as a result of the extra charge produced by the hall current, as previously mentioned. There is a slight decrease in entropy generation as m increases as shown in figure 3.4(e).

Figure 3.5 shows how an inclination angle (α) affects velocity, temperature, concentration, and entropy generation when other parameters are held constant at Sr=5, Ha=2, m=2, λ_1=0.1, Br=0.5 and Gr=2. Figures 3.5(a) and 3.5(b) demonstrate that an increase in α results in a rise in flow velocity and a fall in cross-flow velocity. Figures 3.5(c), 3.5(d) and 3.5(e) shows that an increase in α leads to subside in dimensionless temperature but a rise in concentration and entropy generation.

The influence of Jeffrey fluid parameter (λ_1) on velocities, temperature, concentration, and entropy generation can be observed in figure 3.6 when other parameter are held constant at $Sr = 5$, $Ha = 2$, $m = 2$, $\alpha = \pi/4$, $Br = 0.5$, and $Gr = 2$. As depicted in figures 3.6(a) and 3.6(b), when λ_1 magnifies, the flow velocities also magnify. Figure 3.6(c) illustrates that decrease in dimensionless temperature as λ_1 increases. A higher Jeffrey fluid parameter (λ_1) leads to a greater concentration, as shown in Figure 3.6(d). Figure 3.6(e) shows that there is little increase in entropy generation near $\eta = 1$ as λ_1 increases. This is because the presence of viscoelasticity in the Jeffrey fluid affects the drag force experienced by the fluid. Higher values of λ_1 can lead to an increase in drag force due to the elastic nature of the fluid.

In figure 3.7, the variations in velocities, temperature, concentration, and entropy are displayed for different values of β_1, while Ha=2, m=2, α=$\pi/4$, λ_1=0.1, Br=0.5, Gr=2, and β_2=0.1 are held constant. It is noted from figures 3.7(a) and 3.7(b) that the velocities enhances as β_1 enhance. Figures 3.7(c) and 3.7(d) illustrate that as β_1 increases, both the temperature and concentration of the fluid decrease. Figure

3.7(e) indicates that the entropy generation decreases near $\eta = -1$ and increases near $\eta = 1$ as β_1 increases. This is because the fluid velocity within the channel and the fluid velocity close to the plates differ when the slip condition is present.

Figure 3.8 displays how velocity, temperature, concentration, and entropy generation behave for different values of β_2; while keeping Ha=2, m=2, α=$\pi/4$, λ_1=0.1, Br=0.5, Gr=2, and β_1=0.1 constant. As depicted in figures 3.8(a) and 3.8(b), as β_2 magnifies, the flow velocity and cross-flow velocity both fall. Figures 3.8(c) and 3.8(d) shows that a decrease in temperature and increase in concentration as β_2 increases. It is noted from figure 3.8(e) that the entropy of the system increases near $\eta = 1$ as β_2 increases. This is because the fluid velocity within the channel and the fluid velocity close to the plates differ when the slip condition is present.

Table 3.1 displays how different factors, including the angle of inclination (α), Hall number (m), Magnetic parameter (Ha), Soret effect (Sr), and Jeffrey fluid parameter (λ_1) impact various aspects of the system while holding other variables at M=2, Re=2, Pr=0.71, Br=0.5, Sc=0.22, Gr=2, β_1=0.1, and β_2=0.1. The results indicate that the skin friction diminishes at $\eta = -1$ plate and amplifies at $\eta = 1$ as Ha, Sr, and α enhance, while the opposite tendency is noticed with a rise in m. Moreover, as the Jeffrey fluid parameter λ_1 increases, the friction factor decreases at both walls. Additionally, the table shows that the heat transfer rate decreases at both walls as Ha, Sr, and α increase, while the reverse trend is noted as m magnifies. Furthermore, as λ_1 magnifies, the heat transfer rate fall at $\eta = -1$ plate and rises at $\eta = 1$ plate. From the table, it is observed that the mass transfer rate magnifies at both plates as Sr, Ha, and α magnifies, and falls as m magnifies. The table also shows that the mass transfer rate rises at $\eta = -1$ plate and falls at $\eta = 1$ plate with a rise of λ_1.

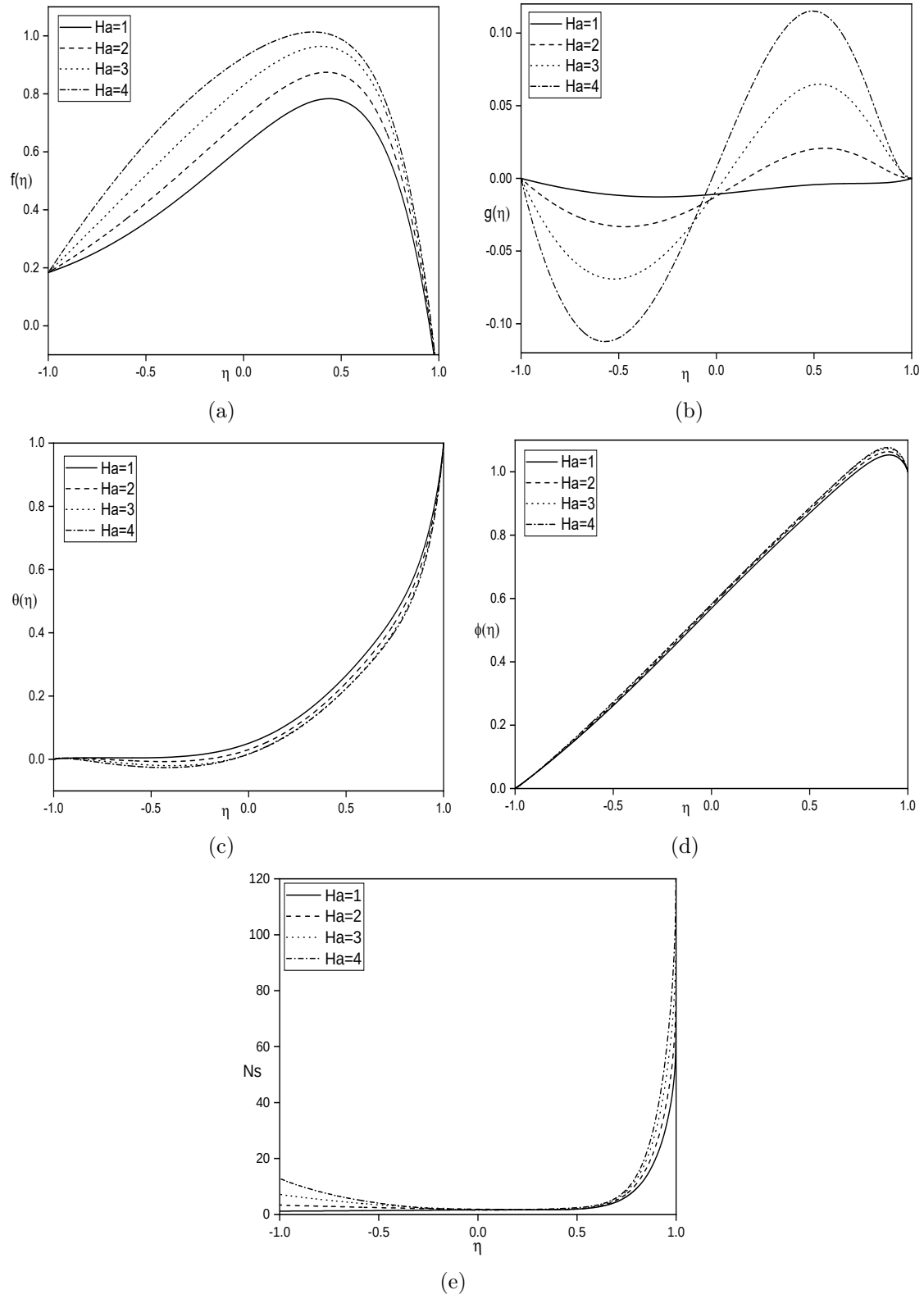

Figure 3.2: *Influence of magnetic parameter (Ha) on (a) $f(\eta)$, (b) $g(\eta)$, (c) $\theta(\eta)$ (d) $\phi(\eta)$, and (e) Ns.*

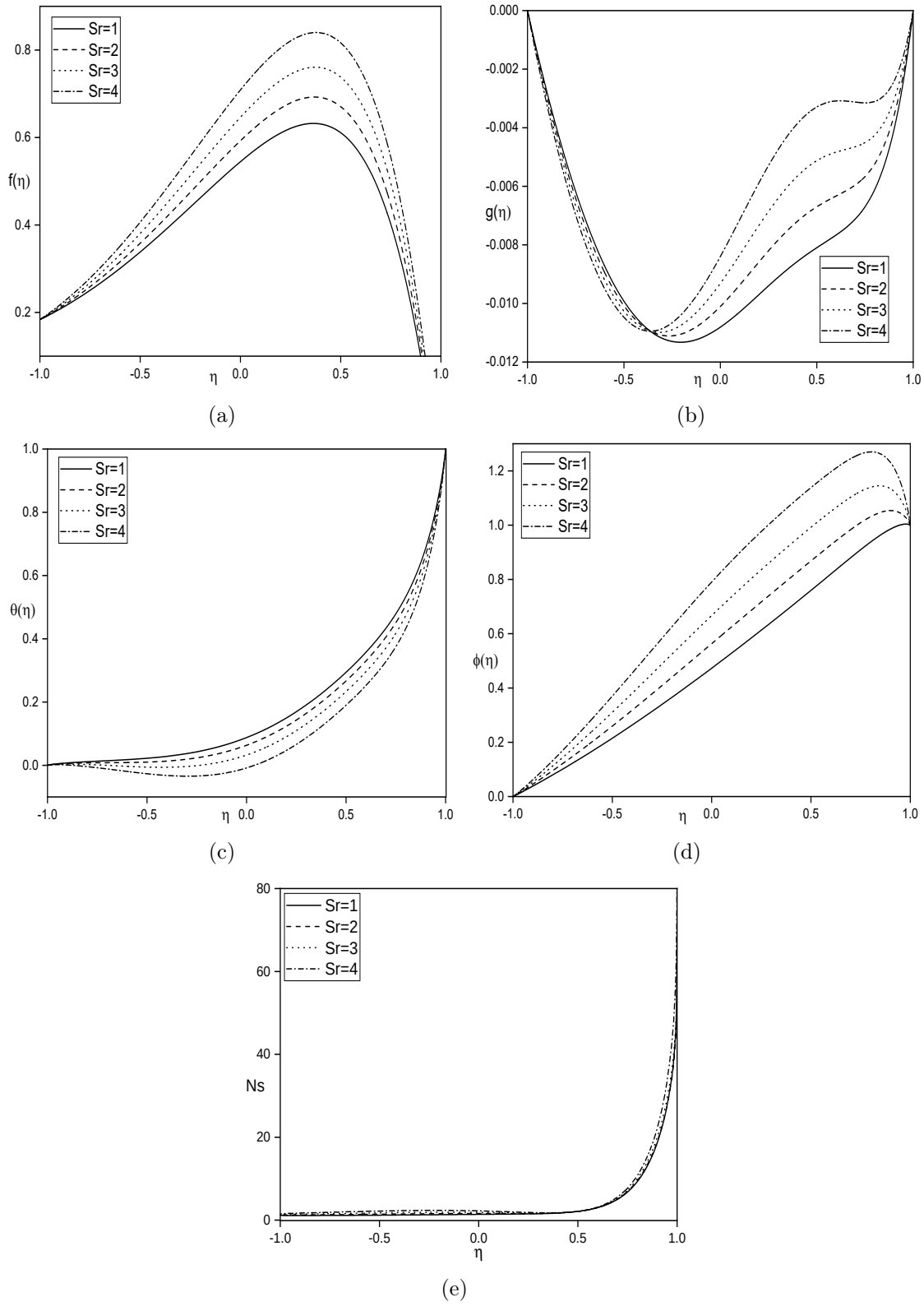

Figure 3.3: *Influence of Soret number (Sr) on (a) $f(\eta)$, (b) $g(\eta)$, (c) $\theta(\eta)$ (d) $\phi(\eta)$, and (e) Ns.*

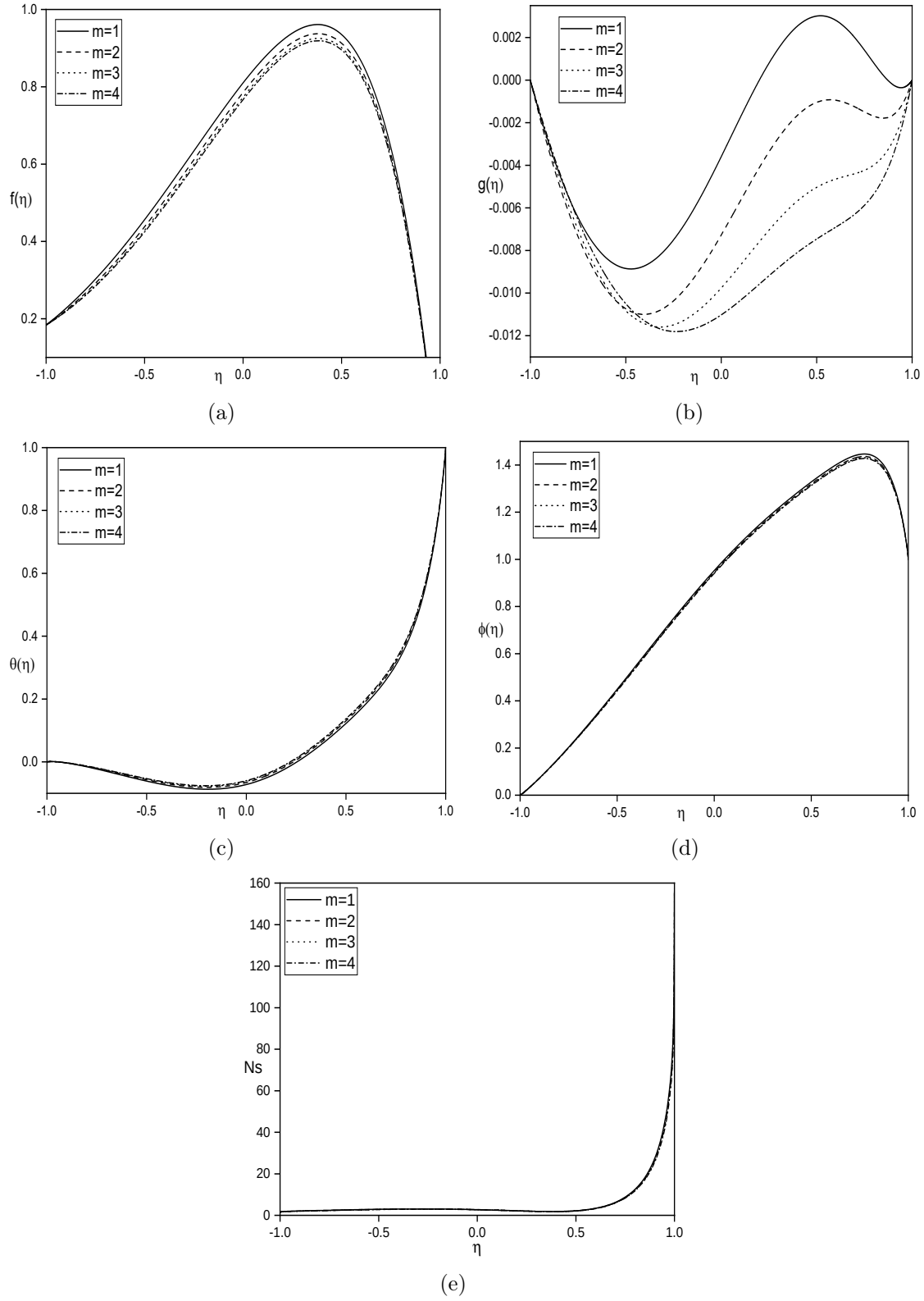

Figure 3.4: *Influence of hall current (m) on (a) $f(\eta)$, (b) $g(\eta)$, (c) $\theta(\eta)$ (d) $\phi(\eta)$, and (e) Ns.*

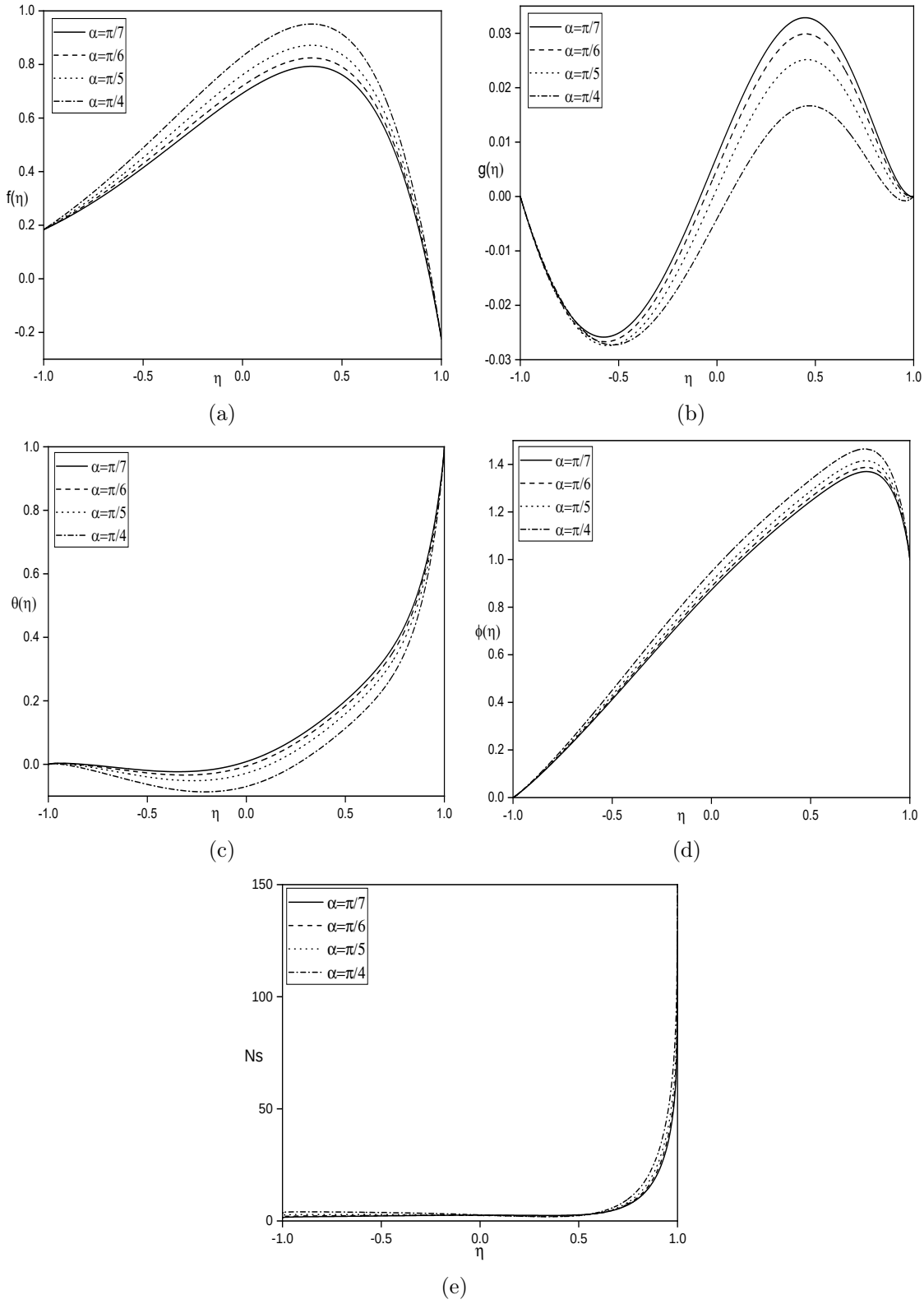

Figure 3.5: *Influence of inclination angle (α) on (a) $f(\eta)$, (b) $g(\eta)$, (c) $\theta(\eta)$ (d) $\phi(\eta)$, and (e) Ns.*

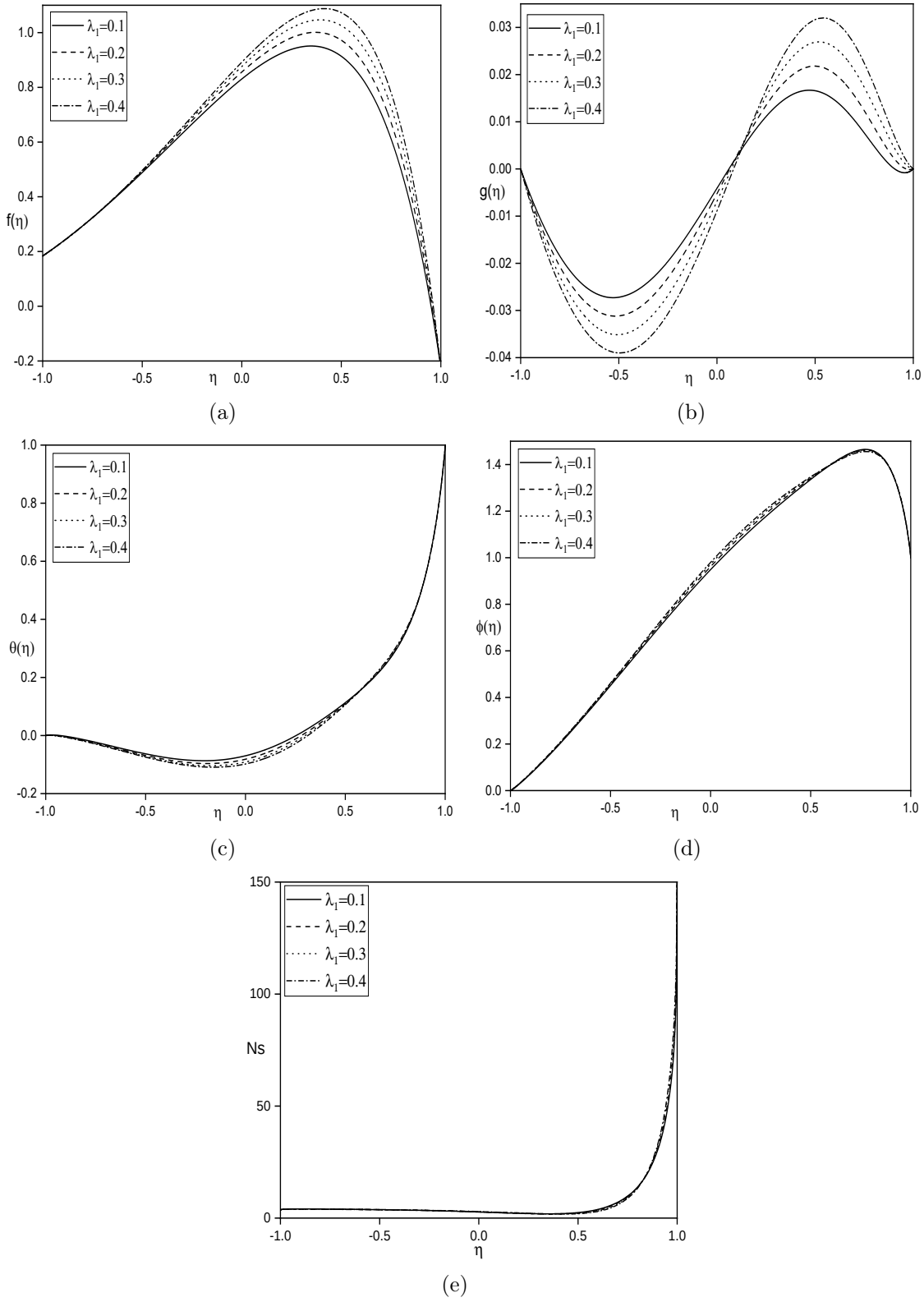

Figure 3.6: *Influence of Jeffrey fluid parameter (λ_1) on (a) $f(\eta)$, (b) $g(\eta)$, (c) $\theta(\eta)$ (d) $\phi(\eta)$, and (e) Ns.*

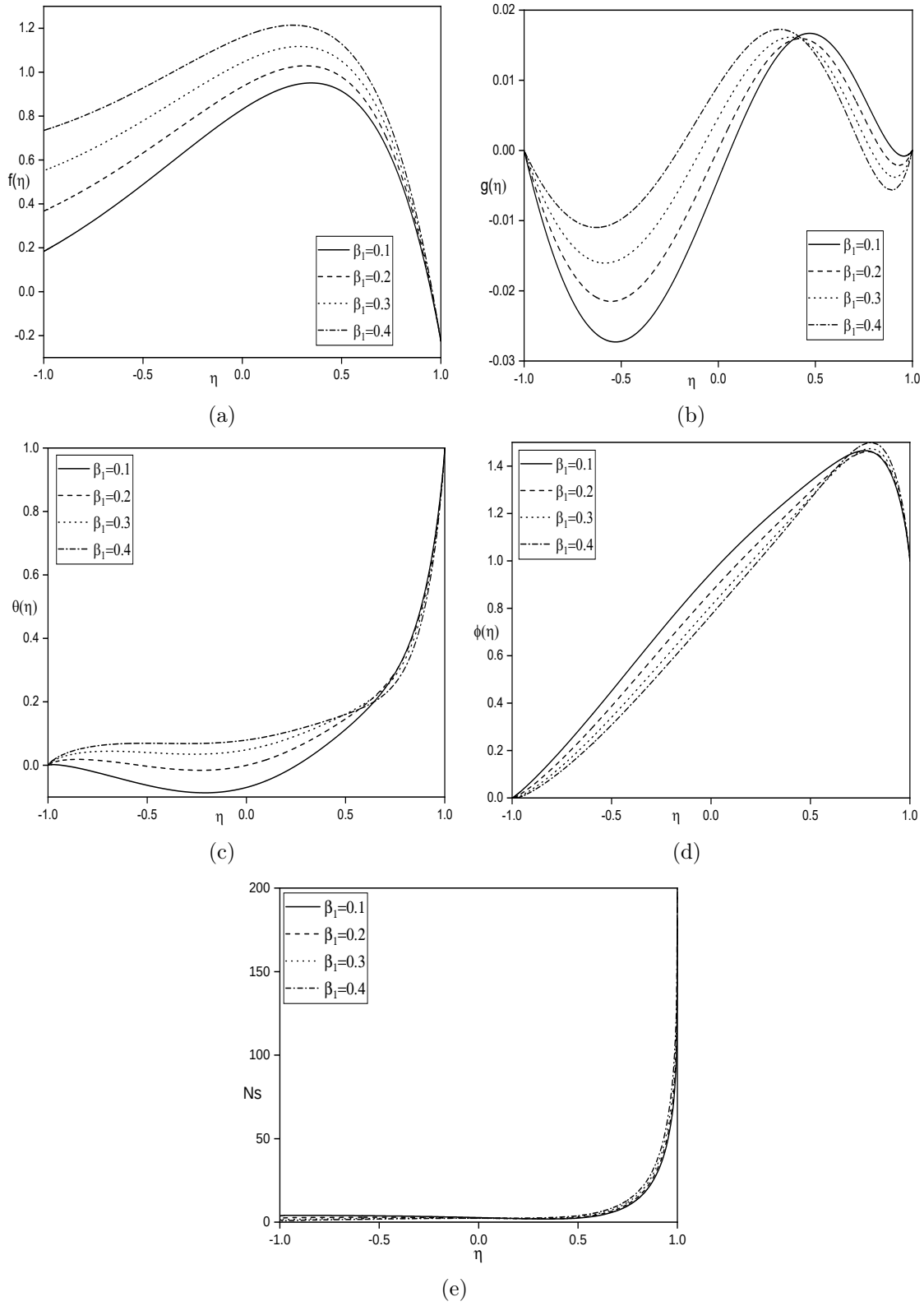

Figure 3.7: *Influence of slip condition β_1 on (a) $f(\eta)$, (b) $g(\eta)$, (c) $\theta(\eta)$ (d) $\phi(\eta)$, and (e) Ns.*

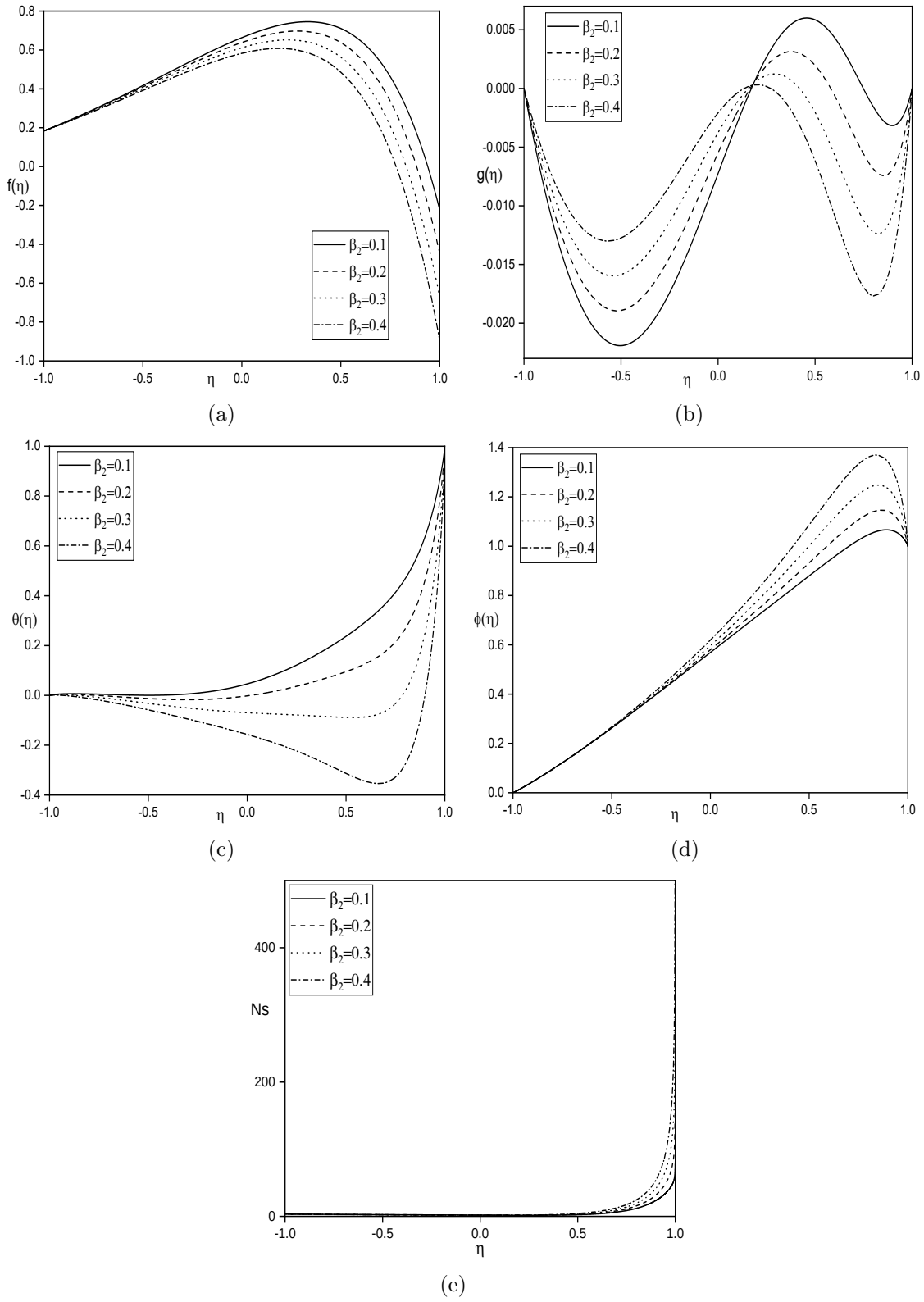

Figure 3.8: *Influence of slip condition β_2 on (a)$f(\eta)$, (b) $g(\eta)$, (c) $\theta(\eta)$ (d) $\phi(\eta)$, and (e) Ns.*

Table 3.1: Overview of the effect of various values of Ha, Sr, α, m, and λ_1 on skin friction ($Cf_{1,2}$), rate of heat transfer ($Nu_{1,2}$) and mass transfer ($Sh_{1,2}$).

Ha	Sr	α	m	λ_1	Cf_1	Cf_2	Nu_1	Nu_2	Sh_1	Sh_2
1	2	$\pi/4$	2	0.1	-3.70050	0.25323	-8.32613	-0.30603	2.74934	-0.33950
2	2	$\pi/4$	2	0.1	-4.09014	0.40460	-9.18599	-0.44047	3.13114	-0.27688
3	2	$\pi/4$	2	0.1	-4.54839	0.63393	-10.17744	-0.63682	3.57096	-0.18690
2	1	$\pi/4$	2	0.1	-3.87896	0.38031	-8.66233	-0.43409	1.07283	-0.29737
2	2	$\pi/4$	2	0.1	-4.09014	0.40460	-9.18599	-0.44047	3.13114	-0.27688
2	3	$\pi/4$	2	0.1	-4.32716	0.43156	-9.79034	-0.44444	5.47740	-0.25089
2	2	0	2	0.1	-3.06247	0.10509	-6.83102	-0.18312	2.08400	-0.40107
2	2	$\pi/4$	2	0.1	-4.09014	0.40460	-9.18599	-0.44047	3.13114	-0.27688
2	2	$\pi/3$	2	0.1	-4.50585	0.51287	-10.24809	-0.50843	3.60498	-0.24046
2	2	$\pi/4$	1	0.1	-4.47496	0.57739	-10.01889	-0.59156	3.50052	-0.20750
2	2	$\pi/4$	2	0.1	-4.09014	0.40460	-9.18599	-0.44047	3.13114	-0.27688
2	2	$\pi/4$	3	0.1	-3.87448	0.31701	-8.71268	-0.36256	2.92104	-0.31300
2	2	$\pi/4$	2	0.1	-4.09014	0.40460	-9.18599	-0.44047	3.13114	-0.27688
2	2	$\pi/4$	2	0.2	-4.46768	0.40345	-9.21909	-0.39841	3.14609	-0.29501
2	2	$\pi/4$	2	0.3	-4.84567	0.40090	-9.24625	-0.36222	3.15831	-0.31066

3.2.2 Case (b): Mixed Convection

Consider a mixed convection flow occurring under the influence of buoyancy forces and external pressure gradient.

similarity transformations for this given problem is given as

$$\eta = \frac{y}{d},\ u = u_0 f,\ w = u_0 g,\ \phi = \frac{C - C_1}{C_2 - C_1},\ \theta = \frac{T - T_1}{T_2 - T_1} \tag{3.15}$$

In equations (3.2) – (3.5), Non-dimensional equations are obtained as

$$\begin{aligned} &f'' - Re(1+\lambda_1)f' + \frac{Gr_T}{Re}(1+\lambda_1)\theta + \frac{Gr_C}{Re}(1+\lambda_1)\phi \\ &- \frac{Ha^2 cos\alpha(1+\lambda_1)}{1+m^2cos^2\alpha}\left(fcos\alpha - \lambda sin\alpha + mgcos^2\alpha\right) - A(1+\lambda_1) = 0 \end{aligned} \tag{3.16}$$

$$g'' - Re(1+\lambda_1)g' + \frac{Ha^2 cos^2\alpha(1+\lambda_1)}{1+m^2cos^2\alpha}\left(mfcos\alpha - g - m\lambda sin\alpha\right) = 0 \tag{3.17}$$

$$\frac{Br}{(1+\lambda_1)}\left(f'^2 + g'^2\right) + \theta'' - RePr\theta' = 0 \tag{3.18}$$

$$ScSr\theta'' + \phi'' - ReSc\phi' = 0 \tag{3.19}$$

with

$$\begin{aligned} &f = \beta_1 f',\ g = \theta = \phi = 0, \quad when\ \eta = -1 \\ &f = \beta_2 f', \quad g = 0, \quad \theta = \phi = 1, \quad when\ \eta = 1 \end{aligned} \tag{3.20}$$

where f, g, θ, and ϕ are the dimensionless forms of flow velocity, cross–flow velocity, temperature, and concentration; $Re = \rho v_0 d/\mu$ represents the Reynolds number, $Pr = \mu c_p/k_f$ is a Prandtl number, $Sc = \nu/D$ is the Schmidt number, $Ha = dB_0\sqrt{\sigma/\mu}$ indicates the magnetic parameter, $Br = \mu v^2/k_f d^2(T_2 - T_1)$ represents the brinkman number, $Sr = DK_T(T_2 - T_1)/\nu T_m(C_2 - C_1)$ represents the thermal diffusion parameter, $Gr_T = g^*\beta_T(T_2 - T_1)d^3/v^2$ and $Gr_C = g^*\beta_C(C_2 - C_1)d^3/v^2$ denotes the thermal and Solutal Grashof numbers, $\lambda = Re/Gr$, $\beta_1 = \gamma_1/d$ and $\beta_2 = \gamma_2/d$ represent

the slip parameters.

The shear stress, heat, and mass flows can obtained by

$$\tau_w = \left[\mu \frac{du}{dy}\right] |_{y=\pm d}; \quad q_w = \left[-k_f \frac{dT}{dy}\right] |_{y=\pm d}; \quad q_m = \left[-D \frac{dC}{dy}\right] |_{y=\pm d}$$

The dimensionless shear stress $C_f = \tau_w/\rho u_0^2$ is given by $ReC_{f_{1,2}} = f'(\eta) \mid_{\eta=-1,1}$. The Sherwood number defined as $Sh = q_m d/D(C_2 - C_1)$ and the Nusselt number defined as $Nu = q_w d/k_f(T_2 - T_1)$ for this problem are given by

$$Sh_{1,2} = [-\phi'(\eta)] \mid_{\eta=-1,1}; \quad Nu_{1,2} = [-\theta'(\eta)] \mid_{\eta=-1,1} .$$

Entropy Generation

The volumetric rate of entropy production (as explained in earlier chapter) is given as

$$\begin{aligned} S_{gen} = & \frac{k_f}{T_0^2}\left[\frac{dT}{dy}\right]^2 + \frac{\mu}{T_0(1+\lambda_1)}\left[\left(\frac{du}{dy}\right)^2 + \left(\frac{dw}{dy}\right)^2\right] + \frac{RD}{C_0}\left(\frac{dC}{dy}\right)^2 \\ & + \frac{RD}{T_0}\left(\frac{dT}{dy}\right)\left(\frac{dC}{dy}\right) + \frac{\sigma B_0^2}{T_0}\left[w^2 + (ucos\alpha - v_0 sin\alpha)^2\right] \end{aligned} \tag{3.21}$$

The first term of the right-hand side of equation (3.21) is associated with heat transfer; the second term due to energy dissipation by fluid viscosity; the third and fourth are caused by mass transfer; and the fifth term is because of magnetic field. The expression for rate of entropy generation $(S_{gen})_0$ [72] is determined by

$$(S_{gen})_0 = \frac{k_f(T_2 - T_1)^2}{T_0^2 d^2} \tag{3.22}$$

Bejan [73] defines the dimensionless entropy generation (N_s) as the capacity ratio between the local volumetric entropy generation and the characteristic rate of

entropy generation. Hence, the creation of dimensionless entropy is provided by

$$N_s = \frac{S_{gen}}{(S_{gen})_0}$$

$$N_s = (\theta')^2 + \frac{Br}{(1+\lambda_1)A_1}(f'^2 + g'^2) + \frac{\varepsilon B_1^2}{A_1^2}(\phi')^2 + \frac{\varepsilon B_1}{A_1}\theta'\phi' + \frac{BrHa^2}{A_1}\left(g^2 + (fcos\alpha - \lambda sin\alpha)^2\right)$$

where A_1, Br, B_1, Ha, ε, are dimensionless temperature difference, brinkman number, dimensionless concentration difference, magnetic parameter, dimensionless constant parameter, and respectively, which are represented as

$$Br = \frac{\mu v^2}{k_f d^2(T_2 - T_1)}, \quad \varepsilon = \frac{RDC_0}{k_f}, \quad Ha = dB_0\sqrt{\frac{\sigma}{\mu}}$$
$$A_1 = \frac{T_2 - T_1}{T_0}, \quad B_1 = \frac{C_2 - C_1}{C_0},$$

Results and discussion

The nonlinear and coupled flow eqns. (3.16) - (3.19) with respect to boundary conditions (3.20) are numerically solved by SQLM (as explained in earlier chapter). The velocities (f, g) of fluid, temperature (θ), concentration (ϕ), and entropy generation (Ns) of the system are influenced by several parameters, including Ha, Sr, m, α, λ_1, β_1, and β_2.

Figures 3.9 – 3.14 depict how these parameters affect the aforementioned variables, with Re, Br, Pr, Sc, β_1, β_2, Gr_T, Gr_C, Gr, and A being held constant at values of 2, 0.5, 0.71, 0.22, 0.1, 0.1, 2, 2, 2, and 1, respectively.

Figure 3.9 demonstrates the influence of Ha on velocities, temperature, concentration, and entropy generation when other parameters are fixed at $\alpha = \pi/3$, $Sr = 2$, $m = 2$, $\lambda_1 = 0.5$, and $Br = 0.5$. As depicted in figure 3.9(a), the fluid velocity magnifies as Ha magnifies. Figure 3.9(b) indicates that the cross-flow velocity also rises with a rise in Ha. The magnetic field is inclined at an angle $\alpha > 0$,

which implies that the drag force cannot be produced in the flow and cross–flow directions. Furthermore, figures 3.9(c) and 3.9(d) show that the fluid temperature decreases and concentration increases as Ha increases. Figure 3.9(e) reveals that entropy generation increases as Ha increases. This is because a magnetic field generates a resistive force perpendicular to the applied magnetic field direction, and the generated electric charges are not in the flow direction, which leads to a decrease in temperature.

Figure 3.10 shows how the soret number (Sr) affects velocity, temperature, concentration, and entropy generation when other parameters are held constant at $\alpha = \pi/4$, $Ha = 3$, $m = 2$, $\lambda_1 = 0.1$, and $Br = 0.5$. Figures 3.10(a) and 3.10(b) illustrate that as the parameter Sr increases, the flow and cross–flow velocity both exhibit an upward trend. A stronger Soret effect (higher Soret parameter) creates a larger temperature difference within the fluid, which in turn makes the fluid flow faster. The soret effect, in turn, leads to changes in the concentration distribution. Since buoyancy forces are linked to temperature variations, alterations in the temperature profile can modify the buoyancy–driven component of the flow. As shown in figures 3.10(c) and 3.10(d), the fluid gets colder (temperature falls) and increase in concentration when the Soret parameter is increased. Figure 3.10(e) shows that entropy generation increases on the left of $\eta = -1$ and decreases on the right of $\eta = 1$. The soret parameter plays a role in mass transfer in multicomponent fluid systems and can significantly impact flow behavior, particularly in situations involving heat and mass transfer.

Figure 3.11 demonstrates how the hall parameter (m) affects velocity, temperature, concentration, and entropy generation when other parameters are fixed at $\alpha = \pi/3$, $Sr = 10$, $Ha = 2$, $\lambda_1 = 0.5$, and $Br = 0.5$. Figures 3.11(a) and 3.11(b) show that the flow and cross–flow velocity both drop as m increases. On the other hand, figures 3.11(c) and 3.11(d) indicate that the fluid temperature increases and

the fluid concentration decreases as m increases. This is because the magnetic field is inclined at an angle of $\alpha = \pi/3$, which causes the hall effect to generate charge in the direction of inclined plates, thereby making it unable to act as a drag on the fluid. As mentioned earlier, the fluid's temperature drops as a result of the extra charge that the hall current generates. Entropy generation rises but falls at the end when η approaches 1 as m rises, as shown in figure 3.11(e). The hall current plays a crucial role in magnetohydrodynamic flows, as it introduces additional complexity in fluid motion and magnetic field distribution. Magnetohydrodynamics is relevant in plasma physics, astrophysics, and engineering applications like magnetohydrodynamics power generation and magnetohydrodynamics propulsion systems.

Figure 3.12 demonstrates the behavior of velocities, temperature, concentration, and entropy generation as a function of α while keeping Sr=10, Ha=2, m=2, λ_1=0.1, and Br=0.5 constant. Figures 3.12(a) and 3.12(b) show that increasing α leads to a rise in the main flow velocity, while the cross–flow velocity decreases. Figures 3.12(c) and 3.12(d) show that increasing α leads to a decrease in dimensionless temperature but an increase in concentration. This behavior is caused by an increase in the inclination angle of the applied magnetic field, which reduces drag force and hence increases net flow in the fluid. Figure 3.12(e) shows that as α increases, entropy of the system increases. An inclined magnetic field is used in magnetohydrodynamics generators to convert the kinetic energy of hot, electrically conducting fluid into electrical energy.

In figure 3.13, the variations in velocities, temperature, concentration, and entropy generation are displayed for different values of β_1, while Ha=2, m=2, α=$\pi/4$, λ_1=0.1, Br=0.5, and β_2=0.1 are held constant. Figures 3.13(a) and 3.13(b) show that with the increase in β_1, the main flow velocity and cross–flow velocity also increase. Figure 3.13(c) indicates that the fluid temperature decreases as β_1 increases. Additionally, figure 3.13(d) shows a rise in the concentration as β_1 rises. Figure

3.13(e) indicates that a rise in β_1 leads to a fall in entropy generation.

Figure 3.14 displays the behavior of velocities, temperature, concentration, and entropy generation for different values of β_2 while keeping Ha=2, m=2, α=$\pi/4$, λ_1=0.1, Br=0.5, Sr=2, and β_1=0.1 constant. As depicted in figures 3.14(a) and 3.14(b), a decrease in flow velocity and cross–flow velocity is observed as β_2 increases. Figures 3.14(c), 3.14(d), and 3.14(e) demonstrate that as β_2 increases, there is a subside in temperature and a rise in concentration and entropy generation. Slip conditions are commonly used when modeling fluid flow over surfaces with high slip characteristics, such as superhydrophobic surfaces.

Table 3.2 displays how different factors, including hall number (m), angle of inclination, soret effect (Sr), magnetic parameter (Ha), and Jeffrey fluid parameter (λ_1), impact various aspects of the system while holding other variables constant. According to table 3.2, when α, Ha, and Sr rise, the skin friction coefficient falls at the starting plate and rises at the terminal plate, whereas the opposite tendency is seen as m increases. Moreover, the friction factor decreases at both walls as λ_1 increases. Additionally, the table shows that the heat transfer rate decreases at both walls as α, Ha, and Sr increase, but the opposite tendency is seen as m and λ_1 increase. The table also shows that the mass transfer rate magnifies at both plates as Ha and α magnifies, while the opposite tendency is seen as m and λ_1 increases. A rising Soret effect (Sr) causes the mass transfer rate to increase at the initial plate but decrease at the terminal plate.

3.3 Conclusions

In this chapter, we explore the irreversibility of the system in fully developed flow of electrically conducting Jeffrey fluid. A fluid is considered to flow between two vertical parallel plates under Navier-slip condition. In order to reduce the governing equations to dimensionless form of equations, similarity transformation has been

used. In the current investigation, solutions are obtained using the SQLM technique. From our study, the analysis reveals that the entropy of the system goes up with higher values of the inclination angle (α), magnetic parameter (Ha), and β_2, while the reverse trend is notes for β_1. The fluid velocities increase as the slip parameters β_1 increase. Additionally, with an increase in the inclination angle (α), the temperature of the fluid decreases. Moreover, the presence of Jeffrey fluid leads to an increase in velocity and temperature but a decrease in concentration.

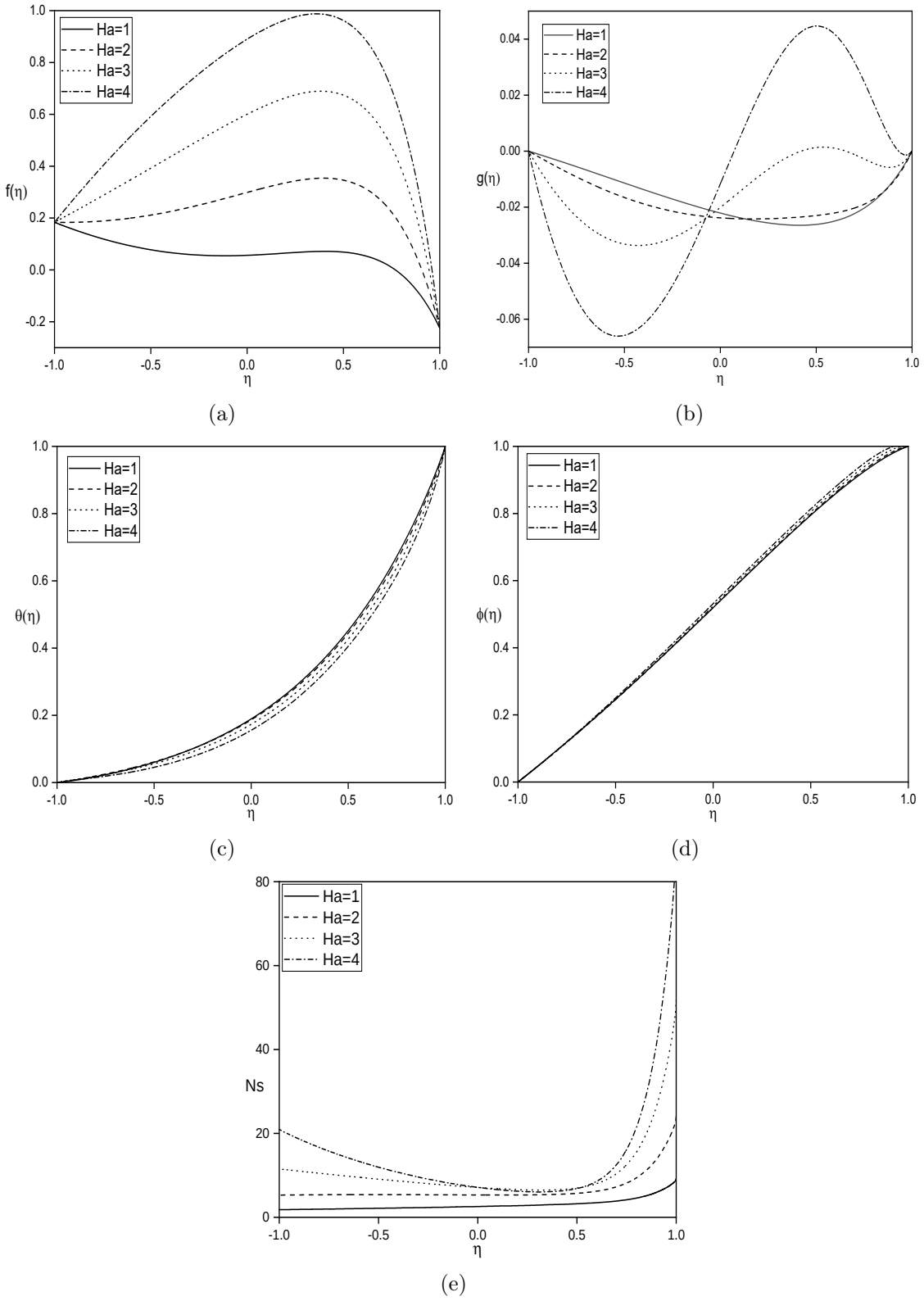

Figure 3.9: *Influence of magnetic parameter (Ha) on (a) $f(\eta)$, (b) $g(\eta)$, (c) $\theta(\eta)$, (d) $\phi(\eta)$, and (e) Ns.*

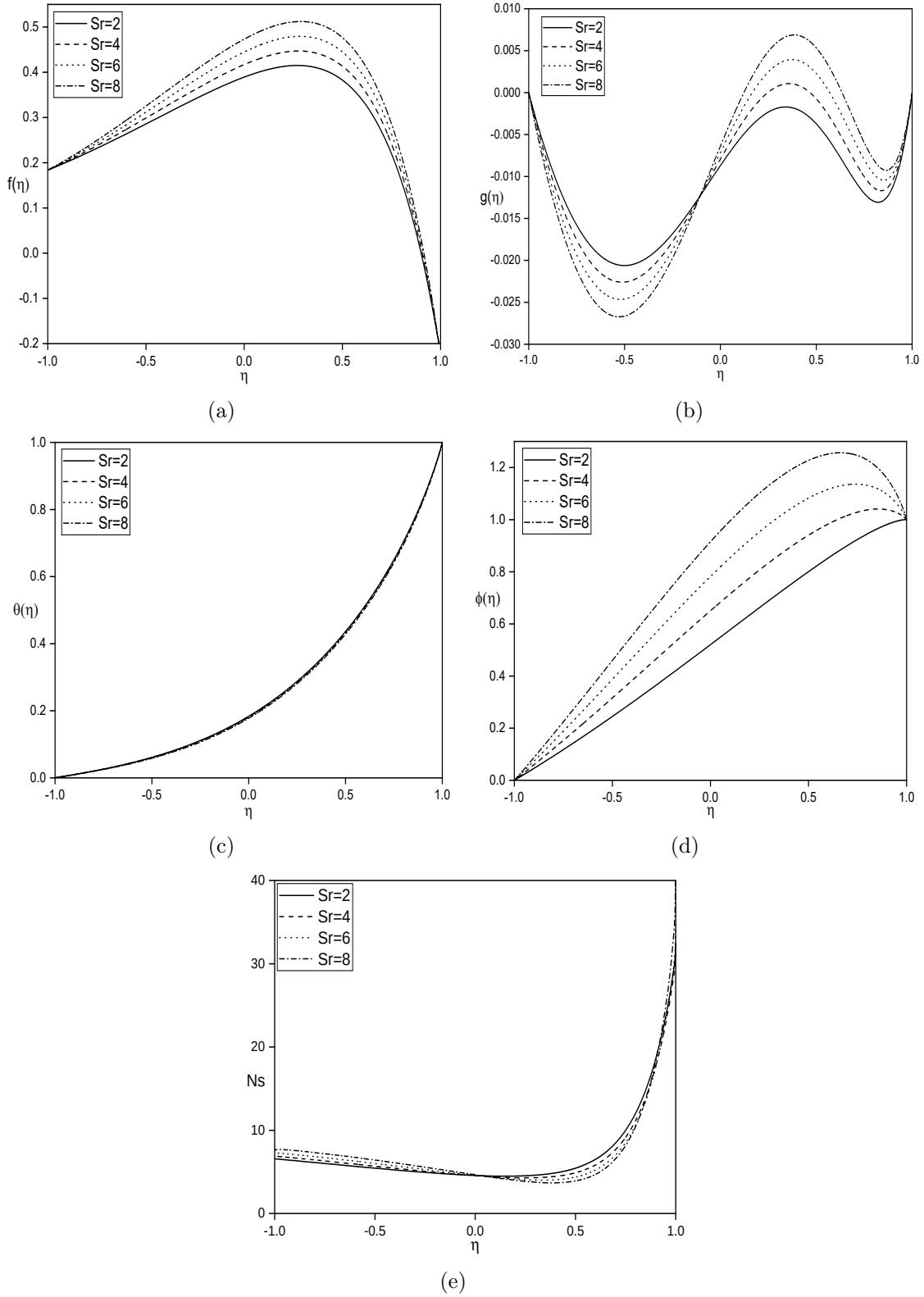

Figure 3.10: *Influence of Soret number (Sr) on (a) $f(\eta)$, (b) $g(\eta)$, (c) $\theta(\eta)$, (d) $\phi(\eta)$, and (e) Ns.*

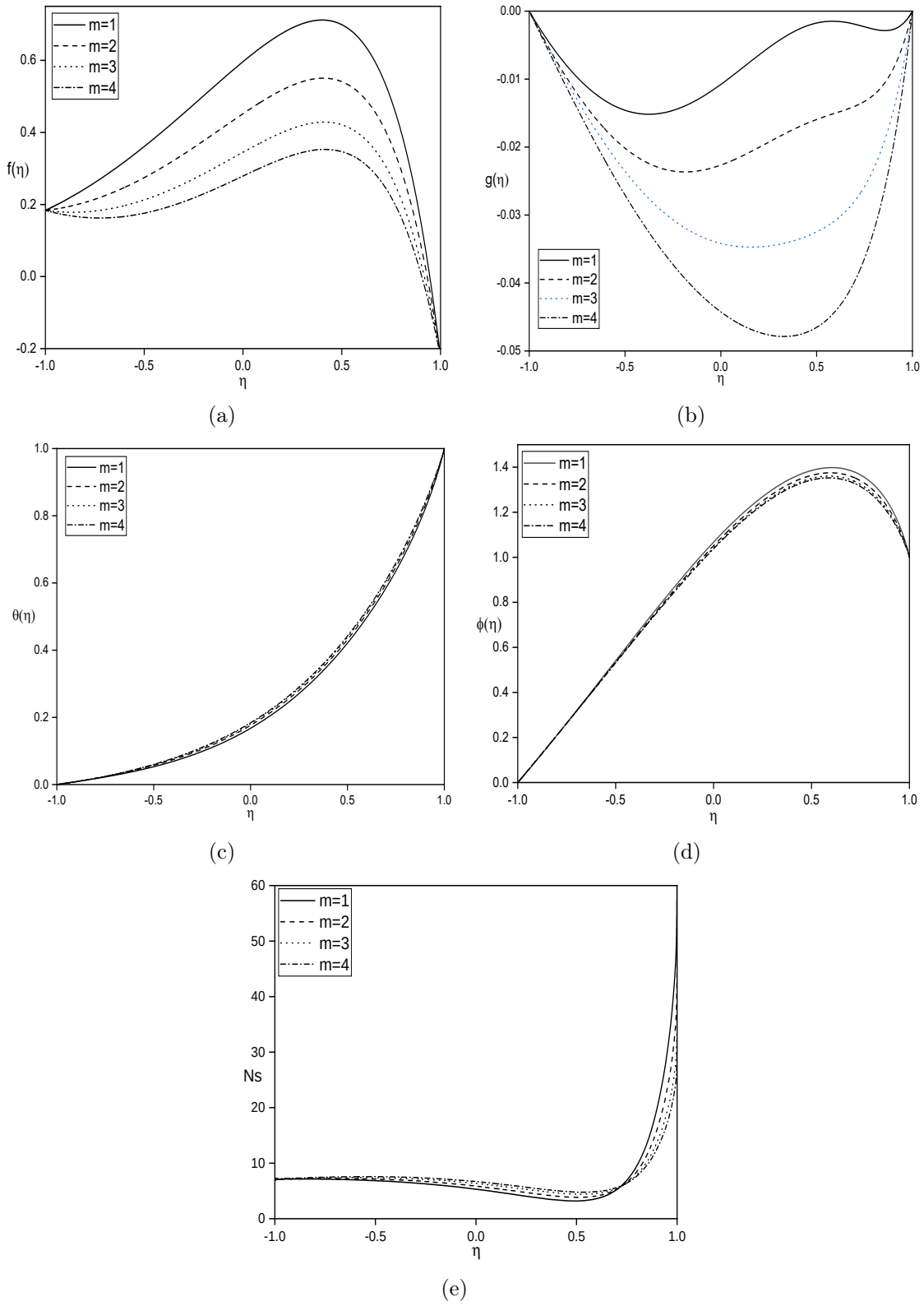

Figure 3.11: *Influence of hall current (m) on (a) $f(\eta)$, (b) $g(\eta)$, (c) $\theta(\eta)$, (d) $\phi(\eta)$, and (e) Ns.*

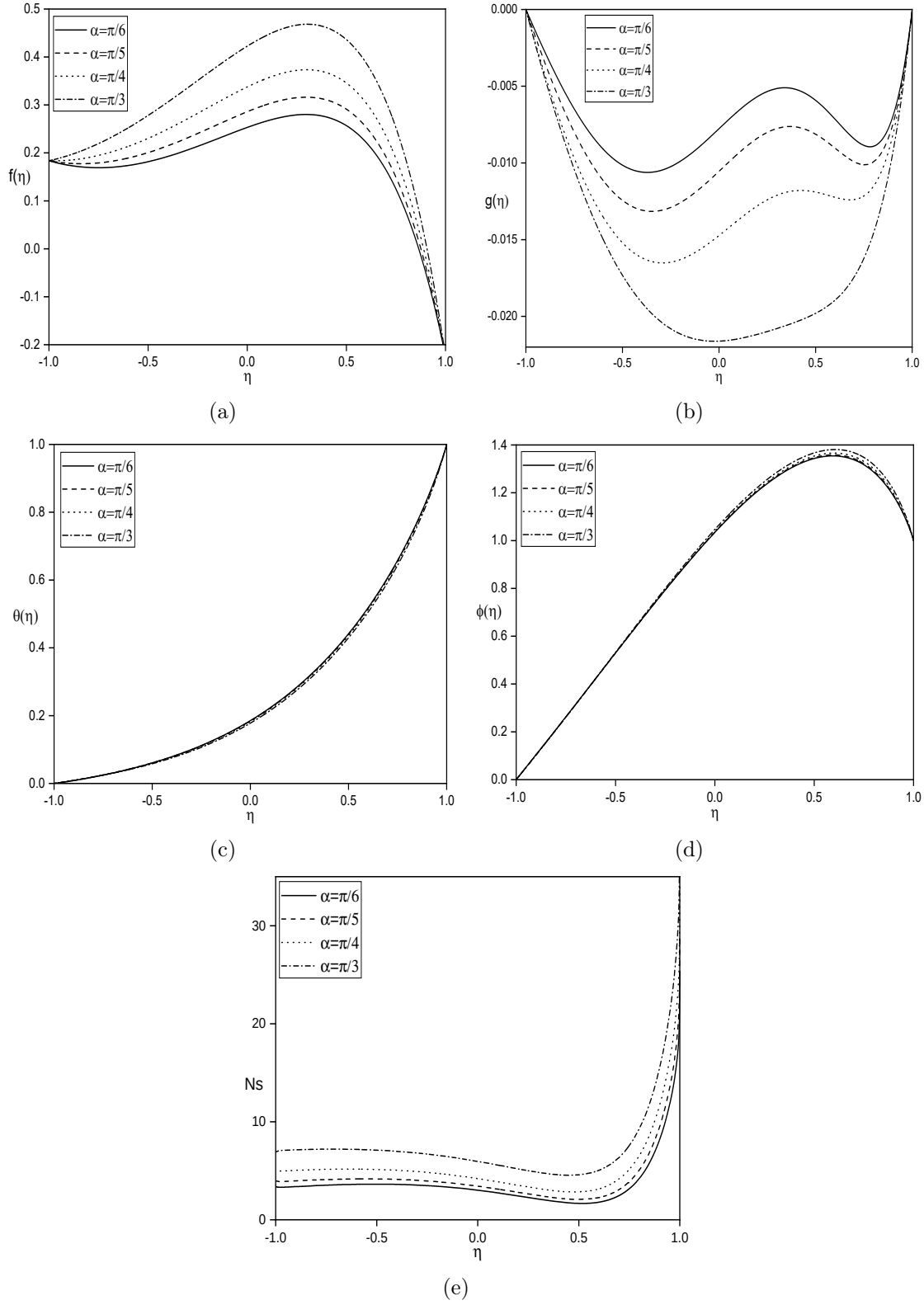

Figure 3.12: *Influence of inclination angle (α) on (a) $f(\eta)$, (b) $g(\eta)$, (c) $\theta(\eta)$, (d) $\phi(\eta)$, and (e) Ns.*

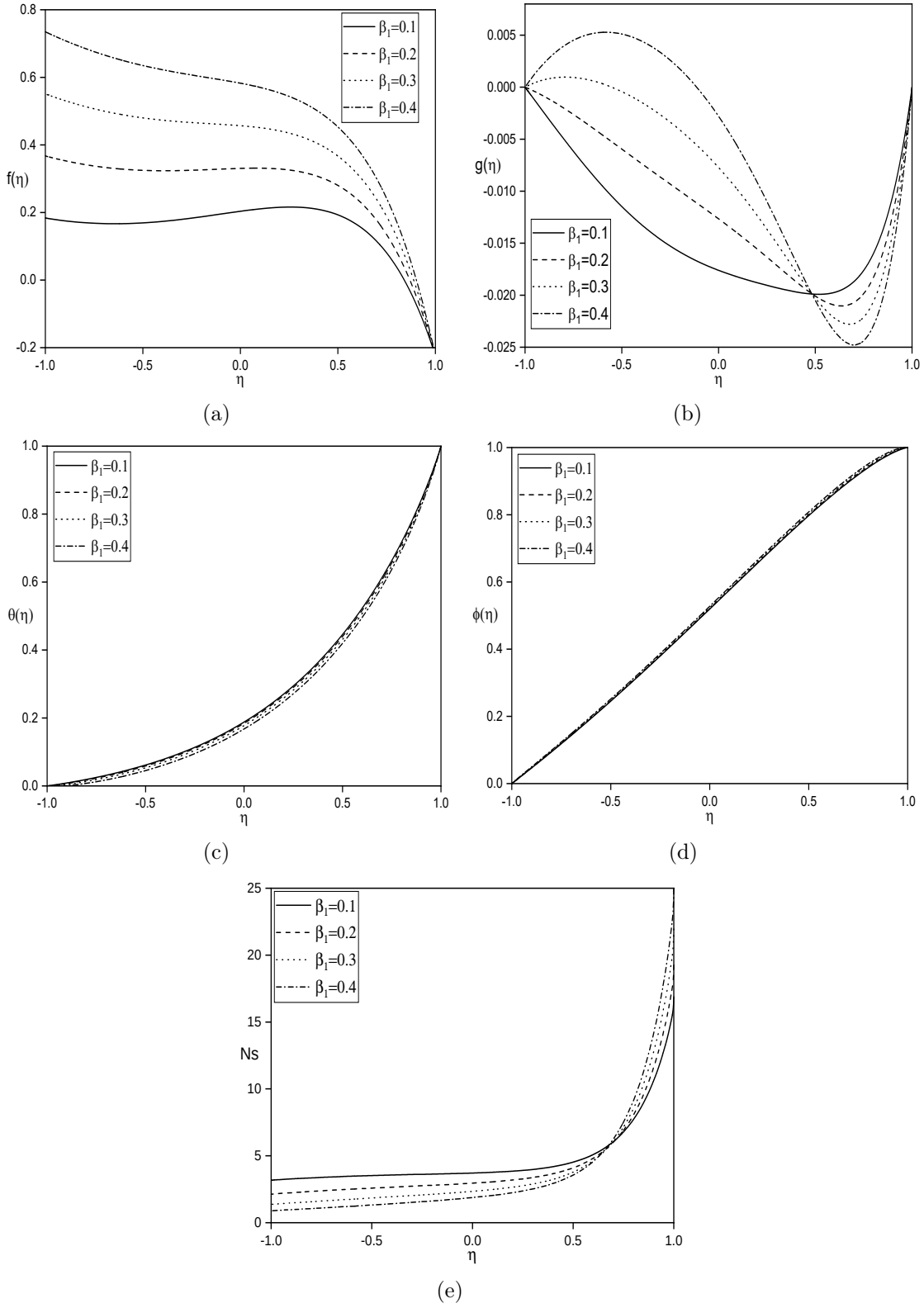

Figure 3.13: *Influence of slip parameter β_1 on (a) $f(\eta)$, (b) $g(\eta)$, (c) $\theta(\eta)$, (d) $\phi(\eta)$, and (e) Ns.*

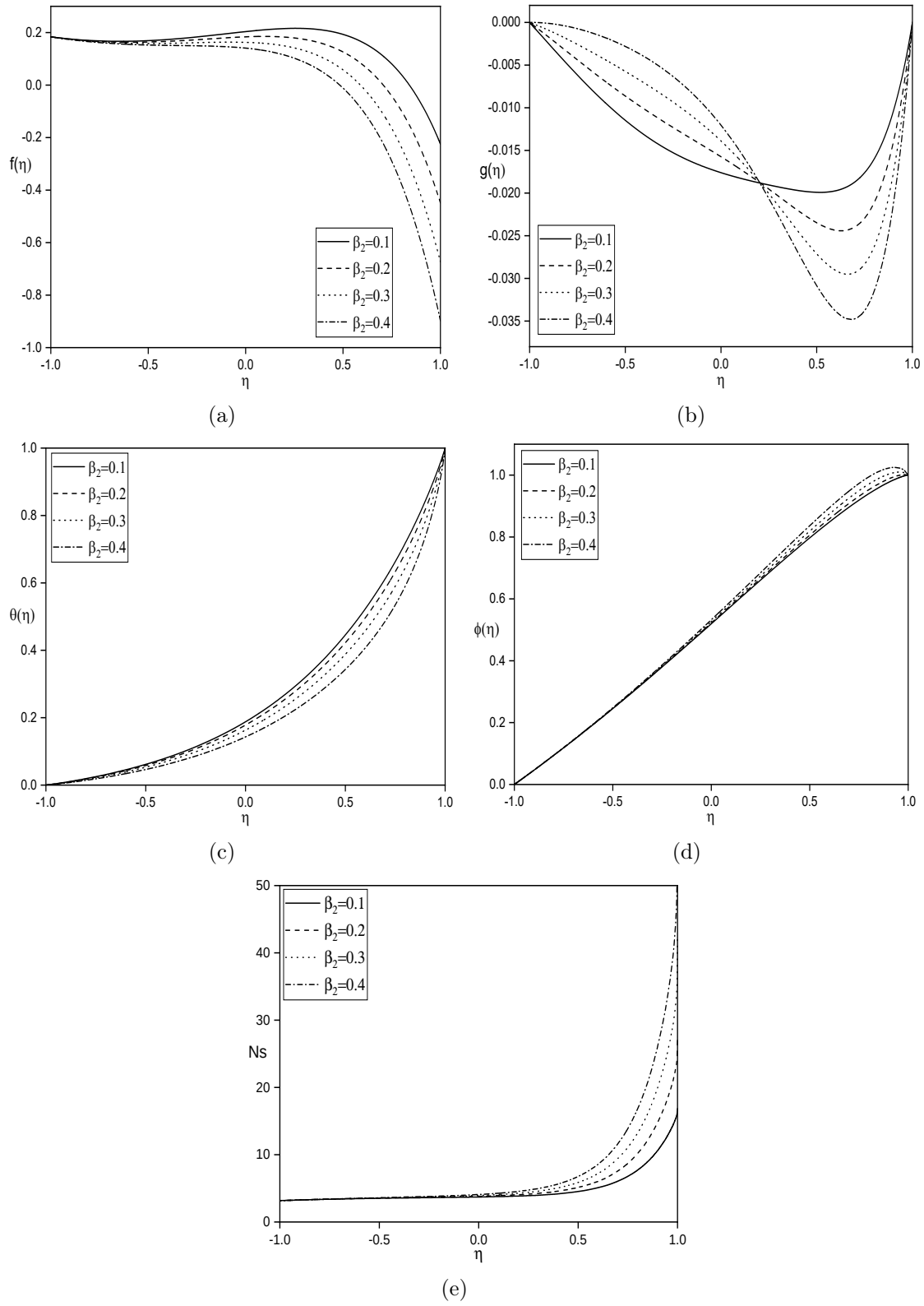

Figure 3.14: *Influence of slip parameter β_2 on (a) $f(\eta)$, (b) $g(\eta)$, (c) $\theta(\eta)$, (d) $\phi(\eta)$, and (e) Ns.*

Table 3.2: Overview of the effect of different values of α, Sr, Ha, m, and λ_1 on skin friction ($Cf_{1,2}$), rate of heat transfer ($Nu_{1,2}$) and mass transfer ($Sh_{1,2}$).

Ha	Sr	α	m	λ_1	Cf_1	Cf_2	Nu_1	Nu_2	Sh_1	Sh_2
1	2	$\pi/3$	2	0.1	-1.19075	-0.26466	-1.97449	-0.00354	-0.06325	-0.49047
2	2	$\pi/3$	2	0.1	-2.14802	0.00219	-2.39746	-0.08714	0.12318	-0.45335
3	2	$\pi/3$	2	0.1	-3.36617	0.39214	-3.01416	-0.18505	0.39636	-0.40843
2	1	$\pi/3$	2	0.1	-2.07307	-0.00861	-2.36041	-0.08409	-0.32253	-0.38333
2	2	$\pi/3$	2	0.1	-2.14802	0.00219	-2.39746	-0.08714	0.12318	-0.45335
2	3	$\pi/3$	2	0.1	-2.22336	0.01300	-2.43522	-0.09010	0.58578	-0.52199
2	2	0	2	0.1	-0.86804	-0.39545	-1.84351	0.04152	-0.12067	-0.51009
2	2	$\pi/4$	2	0.1	-1.82503	-0.09705	-2.24536	-0.05804	0.05600	-0.46642
2	2	$\pi/3$	2	0.1	-2.14802	0.00219	-2.39746	-0.08714	0.12318	-0.45335
2	2	$\pi/3$	1	0.1	-2.76699	0.19341	-2.70019	-0.13829	0.25713	-0.43010
2	2	$\pi/3$	2	0.1	-2.14802	0.00219	-2.39746	-0.08714	0.12318	-0.45335
2	2	$\pi/3$	3	0.1	-1.69543	-0.12912	-2.19090	-0.04794	0.03201	-0.47089
2	2	$\pi/3$	2	0.1	-2.14802	0.00219	-2.39746	-0.08714	0.12318	-0.45335
2	2	$\pi/3$	2	0.2	-2.33794	-0.00226	-2.39292	-0.08574	0.12114	-0.45400
2	2	$\pi/3$	2	0.3	-2.52795	-0.00704	-2.38879	-0.08445	0.11930	-0.45460

Part III

Entropy Generation in Jeffrey Fluid Flow through inclined channel

Chapter 4

Entropy-Based Investigation of Jeffrey Fluid Flow in a Sloping Channel with Hall Current, Thermal Radiation, and Inclined Magnetic Field Effects [1]

4.1 Introduction

Heat and mass transfer with chemical reactions is a science that involves understanding the simultaneous transfer of both heat and mass in processes where chemical reactions are taking place. This area is important for modeling many industrial and natural processes, including reactors, biological systems, combustion, and engineering for the environment. An important example is the creation of smog, which involves first-order chemical reactions. For example, when nitrogen dioxide (NO_2)

[1] Case(a): Accepted for publication in "**Journal of Thermal Analysis and Calorimetry**"
Case(b): Accepted for publication in "**Thermophysics and Aeromechanics**"

is released from vehicles and other sources, it chemically reacts and make formation of a layer of pollution known as photochemical smog. Biswas et al. [74] studied the impact of chemical reaction on the flow MHD micropolar fluid through a vertical plate. Iranian et al. [75] studied the influence of chemical reaction and heat generation on the flow of MHD Powell-Eyring fluid along a vertical surface.

The Soret effect, which involves a mass flux induced by a temperature difference, holds significant importance in numerous physical processes, including applications in geoscience and chemical engineering, among others. Rauf et al. [76] studied the impact of Dufour and Soret on Maxwell hybrid nanofluid flow. Das and Majumdar [77] explored the impact of Soret number and magnetic field on MHD flow of fluids on a vertical channel.

In this chapter, we inspect the entropy generation on steady natural/mixed convection Jeffrey fluid flow between two inclined parallel plates, considering the effect of soret number, chemical reaction, and heat radiation. The resulting flow equations of given problem are solved using SQLM. The impact of various parameters on entropy in the system, velocity, temperature, and concentration is analyzed through graphs.

4.2 Mathematical formulation

In this chapter, the physical setup (refer to figure 4.1) consists of two inclined parallel plates, forming an angle γ with the base. The plates are positioned at a separation distance of $2d$. The concentrations and temperatures at the plates are denoted as C_1, T_1, C_2, T_2 respectively. An external magnetic field B_0 acts on the plates at an inclined angle α with the base. The flow under consideration is assumed to be a steady and incompressible Jeffrey fluid flow. Since the flow extends infinitely along the x-axis, the flow parameters are assumed to be dependent solely on the y direction. The properties of fluid are taken as constant, except for the change

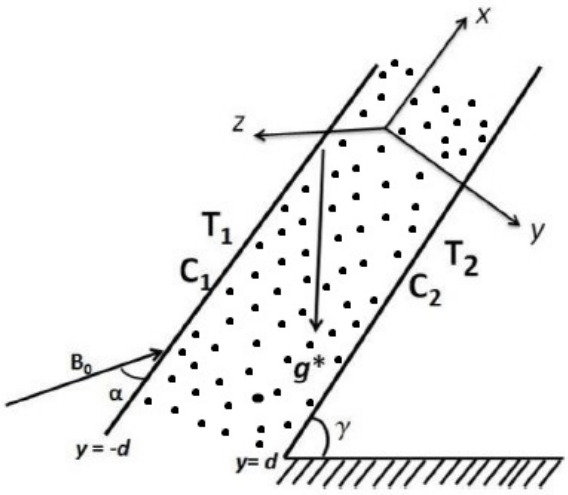

Figure 4.1: Physical Interpretation.

in density that affects the term in the buoyancy force. As such, these assumptions align with natural principles and are relevant in practical applications.

In this version, we can drive the governing equations as follows:

$$\frac{\partial v}{\partial y} = 0 \;\Rightarrow\; v = v_0 = constant \tag{4.1}$$

$$\begin{aligned} v_0\rho\frac{\partial u}{\partial y} = &-\frac{dp}{dx} + \frac{\mu}{(1+\lambda_1)}\frac{\partial^2 u}{\partial y^2} + \rho g^* sin\gamma(\beta_C(C-C_1) + \beta_T(T-T_1)) \\ &-\frac{\sigma B_0^2 \cos\alpha}{1+m^2\cos^2\alpha}\left(mw\cos^2\alpha + u\cos\alpha - v_0\sin\alpha\right) - \frac{\mu u}{(1+\lambda_1)k} \end{aligned} \tag{4.2}$$

$$\begin{aligned} v_0\rho\frac{\partial w}{\partial y} = &\frac{\mu}{(1+\lambda_1)}\frac{\partial^2 w}{\partial y^2} - \rho g^* cos\gamma(\beta_C(C-C_1) + \beta_T(T-T_1)) \\ &+\frac{\sigma B_0^2 \cos^2\alpha}{1+m^2\cos^2\alpha}\left(mu\cos\alpha - mv_0\sin\alpha - w\right) - \frac{\mu w}{(1+\lambda_1)k} \end{aligned} \tag{4.3}$$

$$\rho c_p v_0\frac{\partial T}{\partial y} = \frac{\mu}{(1+\lambda_1)}\left[\left(\frac{\partial u}{\partial y}\right)^2 + \left(\frac{\partial w}{\partial y}\right)^2\right] + k_f\frac{\partial^2 T}{\partial y^2} - \frac{\partial q_r}{\partial y} \tag{4.4}$$

$$v_0\frac{\partial C}{\partial y} = D\frac{\partial^2 C}{\partial y^2} - k_1(C-C_1) + \frac{DK_T}{T_m}\frac{\partial^2 T}{\partial y^2} \tag{4.5}$$

where k_f represents the thermal conductivity, g^* denotes the gravitational acceler-

ation, c_p represents specific heat, $m = \eta_1\ \sigma B_0$ denotes the Hall parameter, k is the permeability porous medium, thermal and solutal expansion are represent by β_T and β_C, k_1 is rate of chemical reaction, σ represent the electrical conduction, μ represent viscosity, D signifies the mass diffusivity, thermal diffusion ratio is represents by K_T, T_m designates the mean temperature, and the radiation heat flux is denoted by q_r.

The boundary conditions of given problem are given by

$$\begin{aligned} u = w = T - T_1 = C - C_1 = 0, \quad when\ y = -d \\ u = w = T - T_2 = C - C_2 = 0, \quad when\ y = d \end{aligned} \tag{4.6}$$

4.2.1 Case (a): Natural Convection

Natural convection flow is driven by buoyant forces. There is no external pressure gradient ($\frac{\partial p}{\partial x} = 0$).

similarity transformations for this given problem is given as

$$\eta = \frac{y}{d}, \quad u = \frac{\nu Grf}{d}, \quad w = \frac{\nu Grg}{d}, \quad \phi = \frac{C - C_1}{C_2 - C_1}, \quad \theta = \frac{T - T_1}{T_2 - T_1} \tag{4.7}$$

From equations (4.2) - (4.5), we get the governing eqns. as

$$\begin{aligned} f'' - Re(1+\lambda_1)f' + (1+\lambda_1)(\theta + N\phi)sin\gamma - \frac{f}{Da} \\ - \frac{Ha^2 cos\alpha(1+\lambda_1)}{1 + m^2 cos^2\alpha}\left(f cos\alpha - \lambda sin\alpha + mg cos^2\alpha\right) = 0 \end{aligned} \tag{4.8}$$

$$\begin{aligned} g'' - Re(1+\lambda_1)g' + (1+\lambda_1)(\theta + N\phi)cos\gamma - \frac{g}{Da} \\ + \frac{Ha^2 cos^2\alpha(1+\lambda_1)}{1 + m^2 cos^2\alpha}\left(mf cos\alpha - g - m\lambda sin\alpha\right) = 0 \end{aligned} \tag{4.9}$$

$$\frac{BrGr^2}{(1+\lambda_1)}\left(f'^2 + g'^2\right) + \left(1 + \frac{4Rd}{3}\right)\theta'' - RePr\theta' = 0 \tag{4.10}$$

$$ScSr\theta'' + \phi'' - ReSc\phi' - QSc\phi = 0 \tag{4.11}$$

where $Ha = dB_0\sqrt{\sigma/\mu}$ indicates the magnetic parameter, $Re = \rho v_0 d/\mu$ represents Reynolds number, $N = \beta_C(C_2 - C_1)/\beta_T(T_2 - T_1)$ indicates the buoyancy parameter, $Br = \mu v^2/k_f d^2(T_2 - T_1)$ is Brinkman number, $Pr = \mu c_p/k_f$ is Prandtl number, $Gr = g^*\beta_T(T_2 - T_1)d^3/v^2$ is grashof number, $\lambda = Re/Gr$, $Sc = \nu/D$ is the Schmidt number, $Rd = 4\sigma T_0^3/k_f k^*$ denotes the Radiation parameter, $Da = k/d^2$ represents the Darcy number, $Q = k_1 d/\nu$ represents the chemical reaction parameter, and $Sr = DK_T(T_2 - T_1)/\nu T_m(C_2 - C_1)$ represent the thermal diffusion parameter.

Boundary conditions (4.6) become

$$\begin{aligned} f = g = \theta = \phi = 0, \quad when\ \eta = -1 \\ f = g = 0, \quad \theta = \phi = 1, \quad when\ \eta = 1 \end{aligned} \tag{4.12}$$

The shear stress, heat flow, and mass flow can be deduced from.

$$\tau_w = \left[\mu \frac{du}{dy}\right] |_{y=\pm d}; \quad q_w = \left[-k_f \frac{dT}{dy} + q_r\right] |_{y=\pm d}; \quad q_m = \left[-D\frac{dC}{dy}\right] |_{y=\pm d}$$

The dimensionless shear stress $C_f = \tau_w/\rho u_0^2$ is given by $ReC_{f_{1,2}} = f'(\eta) |_{\eta=-1,1}$. The Sherwood number defined as $Sh = q_m d/D(C_2 - C_1)$ and Nusselt number defined as $Nu = q_w d/k_f(T_2 - T_1)$ for this problem are given by

$$Sh_{1,2} = -\left[\phi'(\eta)\right] |_{\eta=-1,1}; \quad Nu_{1,2} = -\left[1 + \frac{4}{3}Rd\right] \theta'(\eta) |_{\eta=-1,1}\ .$$

Entropy Generation

The entropy production denoted as S_{gen} is given by:

$$S_{gen} = \frac{k_f}{T_0^2}\left[1+\frac{16\sigma T_0^3}{3k_f k^*}\right]\left[\frac{dT}{dy}\right]^2 + \frac{\mu}{T_0(1+\lambda_1)}\left[\left(\frac{du}{dy}\right)^2+\left(\frac{dw}{dy}\right)^2\right] + \frac{RD}{C_0}\left(\frac{dC}{dy}\right)^2 + \frac{RD}{T_0}\left(\frac{dT}{dy}\right)\left(\frac{dC}{dy}\right) + \frac{\mu}{kT_0}(u^2+w^2) + \frac{\sigma B_0^2}{T_0}\left[w^2+(ucos\alpha - v_0 sin\alpha)^2\right] \tag{4.13}$$

The initial term in the right-hand side of equation (4.13) pertains to heat transfer, the second term because of viscous dissipation, the third and fourth terms account for mass transfer, the fifth term represents porosity effects, and the sixth term because of magnetic field. The definition of the characteristic entropy generation rate denoted by $(S_{gen})_0$ is given by

$$(S_{gen})_0 = \frac{k_f(T_2-T_1)^2}{T_0^2 d^2} \tag{4.14}$$

By using equations (4.13) and (4.14), the creation of non-dimensional entropy can be expressed in the following manner:

$$N_s = \frac{S_{gen}}{(S_{gen})_0}$$

$$N_s = \left[1+\frac{4}{3}Rd\right](\theta')^2 + \frac{BrGr^2}{(1+\lambda_1)A_1}(f'^2+g'^2) + \frac{\varepsilon B_1^2}{A_1^2}(\phi')^2 + \frac{\varepsilon B_1}{A_1}\theta'\phi' + \frac{BrGr^2}{DaA_1}(f^2+g^2) + \frac{BrGr^2Ha^2}{A_1}\left(g^2+(fcos\alpha-\lambda sin\alpha)^2\right)$$

where A_1, Rd, Br, B_1, Ha, Gr, Da, and ε are dimensionless temperature difference, radiation parameter, Brinkman number, dimensionless concentration difference, magnetic parameter, Grashof number, Darcy number, dimensionless constant

parameter, respectively, which are represented as

$$Br = \frac{\mu v^2}{k_f d^2(T_2 - T_1)}, \quad Gr = \frac{g^* \beta_T (T_2 - T_1) d^3}{v^2}, \quad Rd = \frac{4\sigma T_0^3}{k_f k^*}, \quad \varepsilon = \frac{RDC_0}{k_f},$$
$$Da = \frac{k}{d^2}, \quad A_1 = \frac{T_2 - T_1}{T_0}, \quad B_1 = \frac{C_2 - C_1}{C_0}, \quad Ha = dB_0\sqrt{\frac{\sigma}{\mu}}$$

Result and Discussion

The nonlinear and coupled flow equations (4.8)–(4.11) are numerically solved with boundary conditions (4.12) using SQLM as explained in chapter-2.

Figures 4.2 to 4.8 show the behavior of $f(\eta)$, $g(\eta)$, $\theta(\eta)$, $\phi(\eta)$, and Ns for distinct values of Ha, α, m, Rd, Sr, λ_1, and γ. These figures were generated with fixed values for the following parameters: $Pr = 0.71$, $N = 2$, $Da = 2$, $K = 2$, $Br = 0.5$, $Re = 2$, $Gr = 10$, and $Sc = 0.22$.

In figures 4.2, the variations in f, g, θ, ϕ, and Ns for different values of the magnetic parameter (Ha), while $Rd = 2$, $Sr = 12$, $\alpha = \pi/4$, $m = 2$, $\lambda_1 = 0.5$, and $\gamma = \pi/4$ are held constant. According to figures 4.2(a) and 4.2(b), there is an opposite effect on fluid velocities when the magnetic parameter (Ha) is increased. The main flow velocity decreases, while the cross-flow velocity increases. It's important to highlight that the magnetic field is inclined at an angle $\alpha > 0$. This configuration implies that the drag force typically associated with a magnetic field cannot be generated in this context. Concurrently, as depicted in figures 4.2(c) and 4.2(d), the fluid temperature tends to rise, whereas the concentration decreases with an increase in the Ha. It is seen in figure 4.2(e) that entropy magnifies as Ha magnify. This phenomenon arises because the magnetic field generates a resistive force that acts perpendicular to the direction of the applied magnetic field. Consequently, the resulting electric charges do not align with the flow direction, ultimately causing a increase in temperature.

Figures 4.3 displays the behavior of f, g, θ, ϕ, and Ns for different values of Soret

parameter (Sr), while keeping $Ha = 2$, $Rd = 2$, $m = 1$, $\lambda_1 = 0.1$, $\alpha = \pi/4$, and $\gamma = \pi/4$ constant. Flow velocity and cross-flow velocity magnify with a rise in Sr as shown in figures 4.3(a) and 4.3(b). Figure 4.3(c) shows that the temperature fall with a rise in Sr. This occurs because an increase in the Soret parameter results in a heightened temperature gradient, subsequently leading to increased velocities. The Soret effect, in turn, induces alterations in the concentration distribution. Given that buoyancy forces are directly related to temperature variations, changes in the temperature profile can thereby modify the buoyancy-driven component of the flow. Figures 4.3(d) and 4.3(e) clearly indicate that as the soret number (Sr) increases, both the concentration and entropy generation exhibit an increase. The Soret effect plays a pivotal role in mass transfer within multicomponent fluid systems and can exert a substantial influence on flow behavior, especially in scenarios involving concurrent heat and mass transfer.

Figure 4.4 presents an analysis of how the parameter m influences the functions f, g, θ, ϕ, and Ns, while keeping $\alpha = \pi/4$, $Sr = 12$, $Ha = 2$, $\lambda_1 = 0.5$, $\gamma = \pi/4$, and $Br = 0.5$ constant. Figures 4.4(a) and 4.4(b) show that the main flow velocity rise and cross-flow velocity drop as m rise. This is because the magnetic field is inclined at an angle of $\alpha = \pi/4$, which causes the Hall effect to generate charge in the direction of inclined plates, thereby making it unable to act as a drag on the fluid. Figures 4.4(c) and 4.4(d) show that fluid temperature decreases and concentration increases with increasing m. As mentioned earlier, the fluid's temperature drops as a result of the extra charge that the Hall current generates. Entropy generation increases as the parameter m rises, as illustrated in Figure 4.4(e).

Figures 4.5 shows the behavior of f, g, θ, ϕ, and Ns for distinct value of α when $Rd = 2$, $Sr = 10$, $Ha = 3$, $m = 2$, $\lambda_1 = 0.5$, and $\gamma = \pi/4$. Figure 4.5(a) reveals a rise in velocity, while figures 4.5(b) and 4.5(c) demonstrate a contrasting trend, where both cross-flow velocity and temperature decrease with an increase in α. This

behavior arises due to an increase in the inclination angle of magnetic field, which diminishes the drag force and consequently results in an augmentation of the net fluid flow. Figure 4.5(d) and 4.5(e) reveal that the concentration and entropy both rise with a rise in α.

Figure 4.6 provides an overview of how the parameter λ_1 impact the functions f, g, θ, ϕ, and Ns, while maintaining other parameters at $Sr = 10$, $Ha = 2$, $m = 2$, $\alpha = \pi/4$, $Rd = 2$, and $\gamma = \pi/4$. As evident in figures 4.6(a) and 4.6(b), an increase in λ_1 corresponds to an elevation in both the flow velocity and cross-flow velocity. Figure 4.6(c) depicts the reduction in temperature with an increasing value of λ_1. As shown in figures 4.6(d) and 4.6(e), increasing the parameter λ_1 leads to a rise in both concentration and entropy generation.

In Figure 4.7, we observe the variations in the functions f, g, θ, ϕ, and Ns for different values of the parameter Rd at $Ha = 2$, $m = 2$, $\alpha = \pi/4$, $\lambda_1 = 0.5$, $Sr = 10$, and $\gamma = \pi/4$. Figures 4.7(a) and 4.7(b) illustrates that as Rd increases, both the flow and cross-flow velocity decrease. The results in figure 4.7(c) indicate that the fluid temperature increase as Rd increase. Figures 4.7(d) and 4.7(e) indicate that a rise in Rd leads to a fall in concentration and entropy generation. Radiation parameter used in greenhouse gas analysis, aerospace engineering, medical imaging, nuclear engineering etc.

Figures 4.8 displays the behavior of f, g, θ, ϕ, and Ns for different values of γ, while keeping Ha=2, m=1, α=$\pi/4$, λ_1=0.1, Sr=10, and Rd=2 constant. As depicted in figure 4.8(a) and 4.8(b), an increase in flow and decrease in cross-flow velocity is observed as γ increases. Figure 4.8(c) reveals that the temperature of fluid rise with a rise in γ. Figures 4.8(d) and 4.8(e) demonstrate that as γ increases, there is subside in concentration and entropy generation.

Table 4.1 presents the variations in the magnetic parameter (Ha), radiation parameter (Rd), Hall current (m), Soret number (Sr), inclination angle (α), Jeffrey

fluid parameter (λ_1), and channel angle of inclination (γ) while keeping other parameters at $Q = 2$, Re=2, Gr=10, Pr=0.71, Br=0.5, Sc=0.22, $M = 2$, and Da=2. The table shows that the skin friction increases at the plate located at $\eta = -1$ with enhancements in the parameters Ha, α, and λ_1. Conversely, it decreases at the plate positioned at $\eta = 1$ under the same conditions. However, the opposite trend is observed for the Hall current (m) and the channel inclination angle (γ). Skin friction falls with higher values of Sr and Rd. Additionally, Table 4.1 shows that the heat transfer rate magnifies at the left plate and subside at the right plate as the parameters m, Sr, α, and λ_1 increases, while the opposite tendency is seen for the magnetic parameter (Ha) and inclination angle (γ). The higher the value of radiation parameter (Rd), there is fall in temperature for both plates. Moreover, the mass transfer rate rises with increasing values of Sr, α, and λ_1 as indicated in Table 4.1, while it exhibits a reverse trend with Rd and γ. The rate of mass transfer amplifies at the left plate and diminishes at the right plate with an amplification in the hall parameter (m). Conversely, the magnetic parameter (Ha) has the opposite effect.

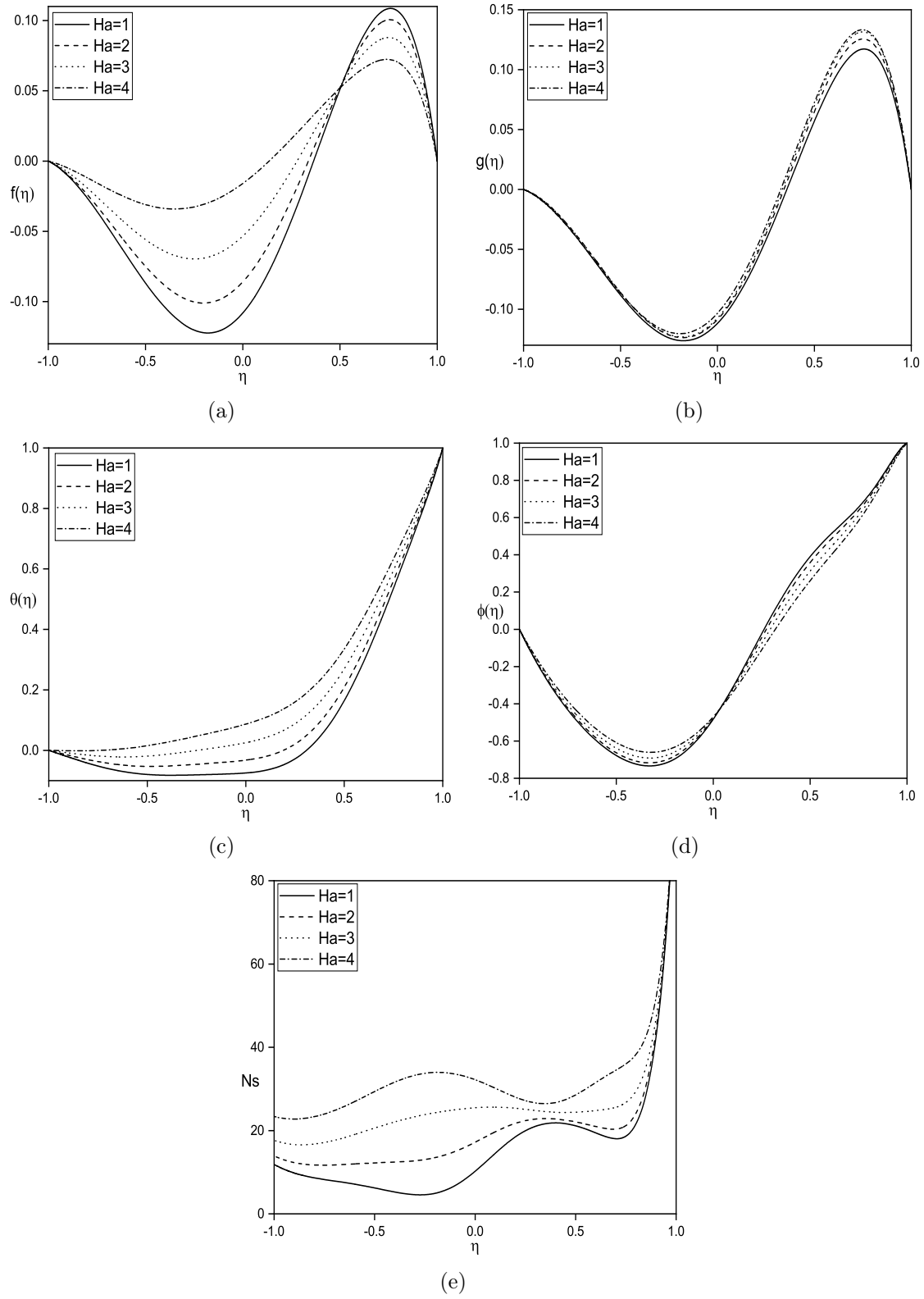

Figure 4.2: *Impact of magnetic parameter (Ha) on (a) $f(\eta)$, (b) $g(\eta)$, (c) $\theta(\eta)$, (d) $\phi(\eta)$, and (e) Ns.*

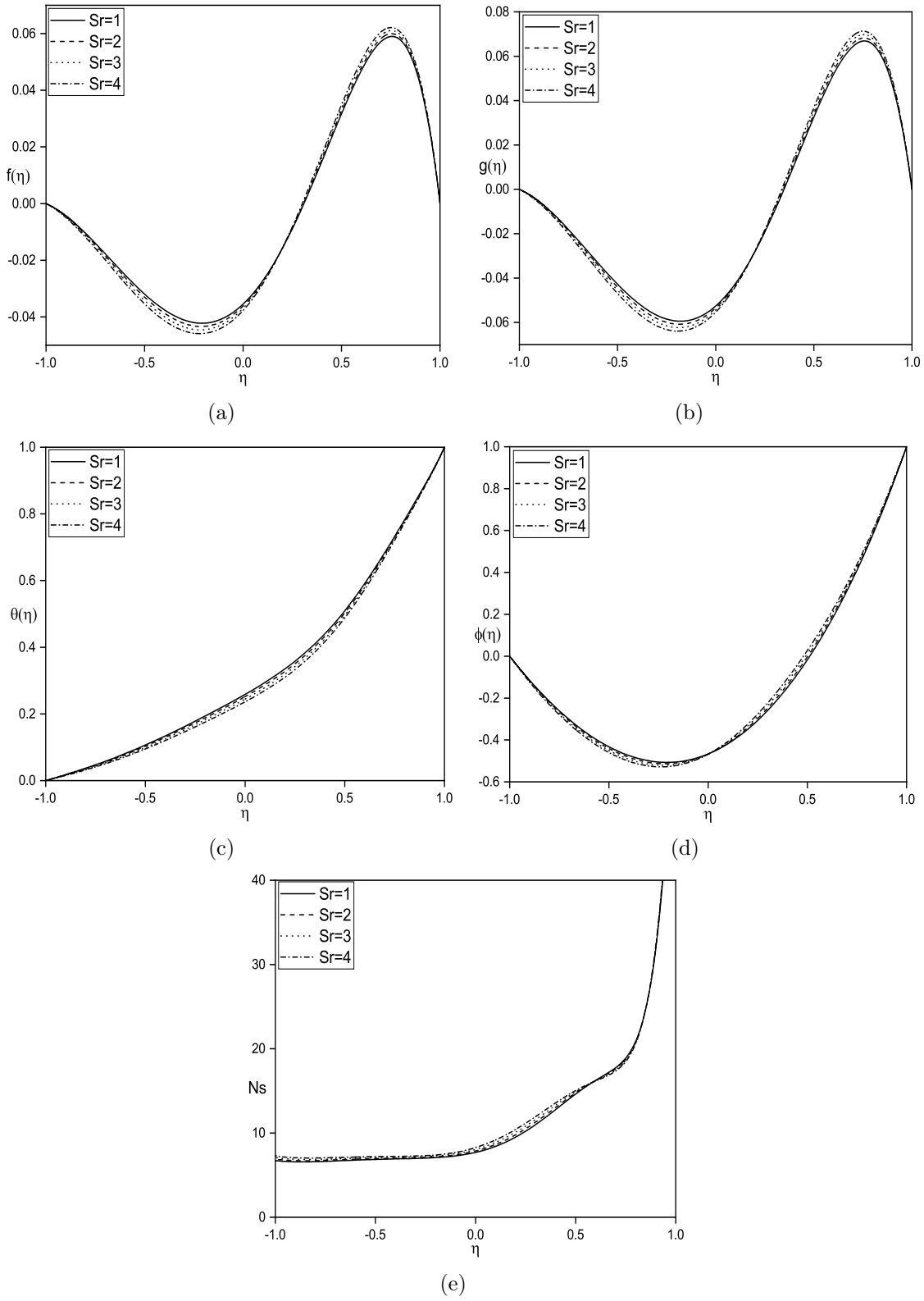

Figure 4.3: *Impact of Soret number (Sr) on (a) $f(\eta)$, (b) $g(\eta)$, (c) $\theta(\eta)$, (d) $\phi(\eta)$, and (e) Ns.*

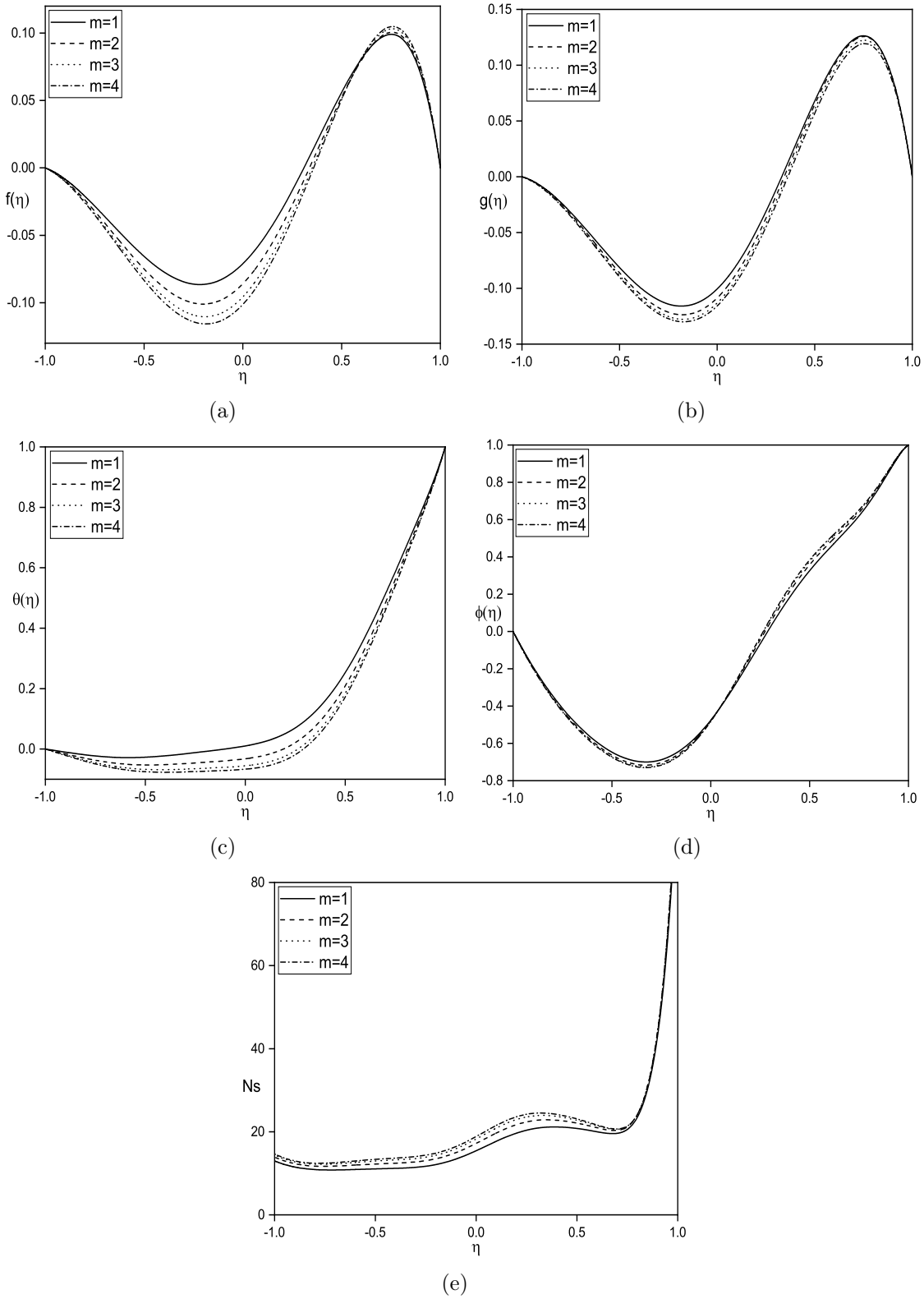

Figure 4.4: *Impact of hall current (m) on (a) $f(\eta)$, (b) $g(\eta)$, (c) $\theta(\eta)$, (d) $\phi(\eta)$, and (e) Ns.*

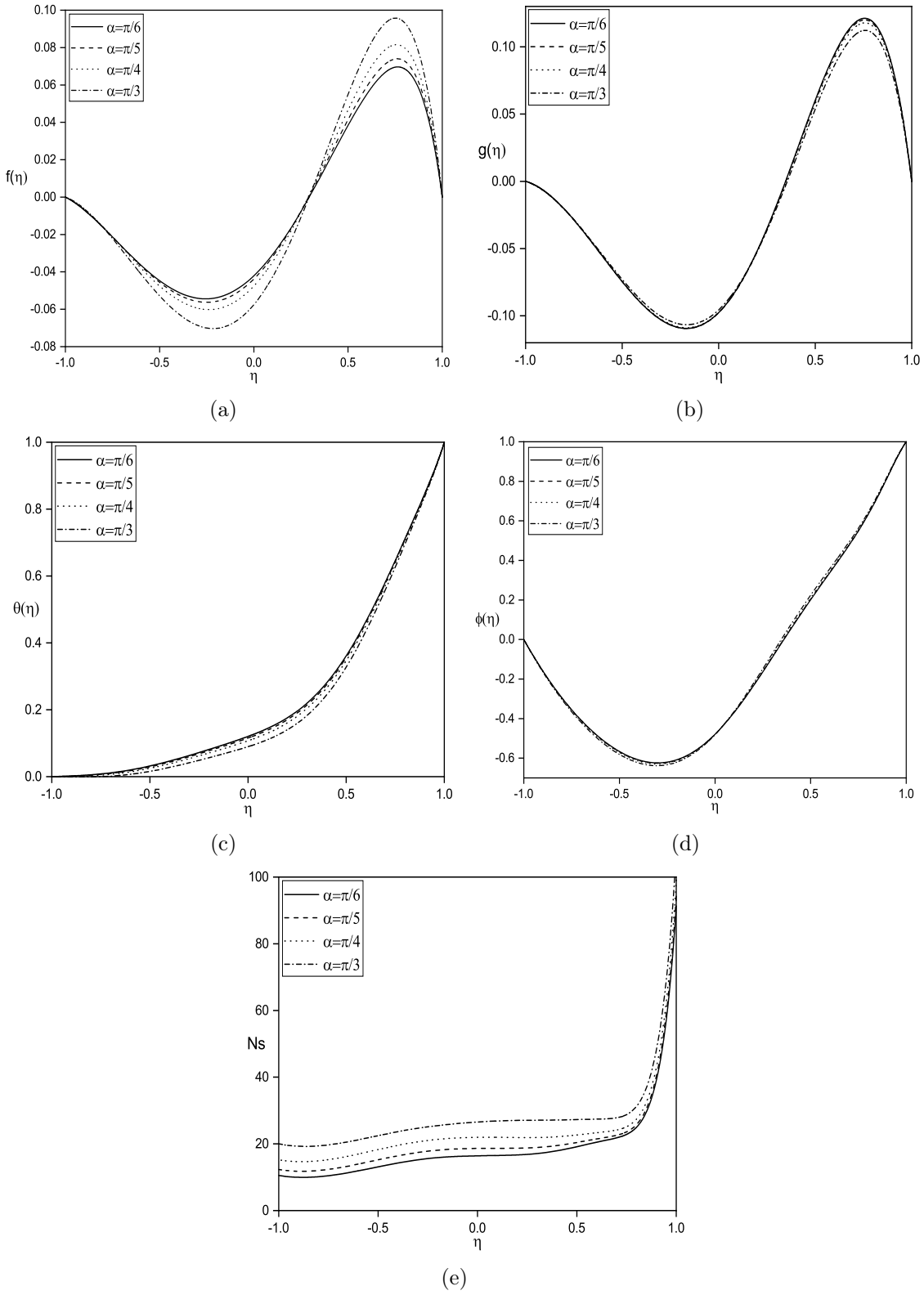

Figure 4.5: *Impact of inclination angle (α) on (a) $f(\eta)$, (b) $g(\eta)$, (c) $\theta(\eta)$, (d) $\phi(\eta)$, and (e) Ns.*

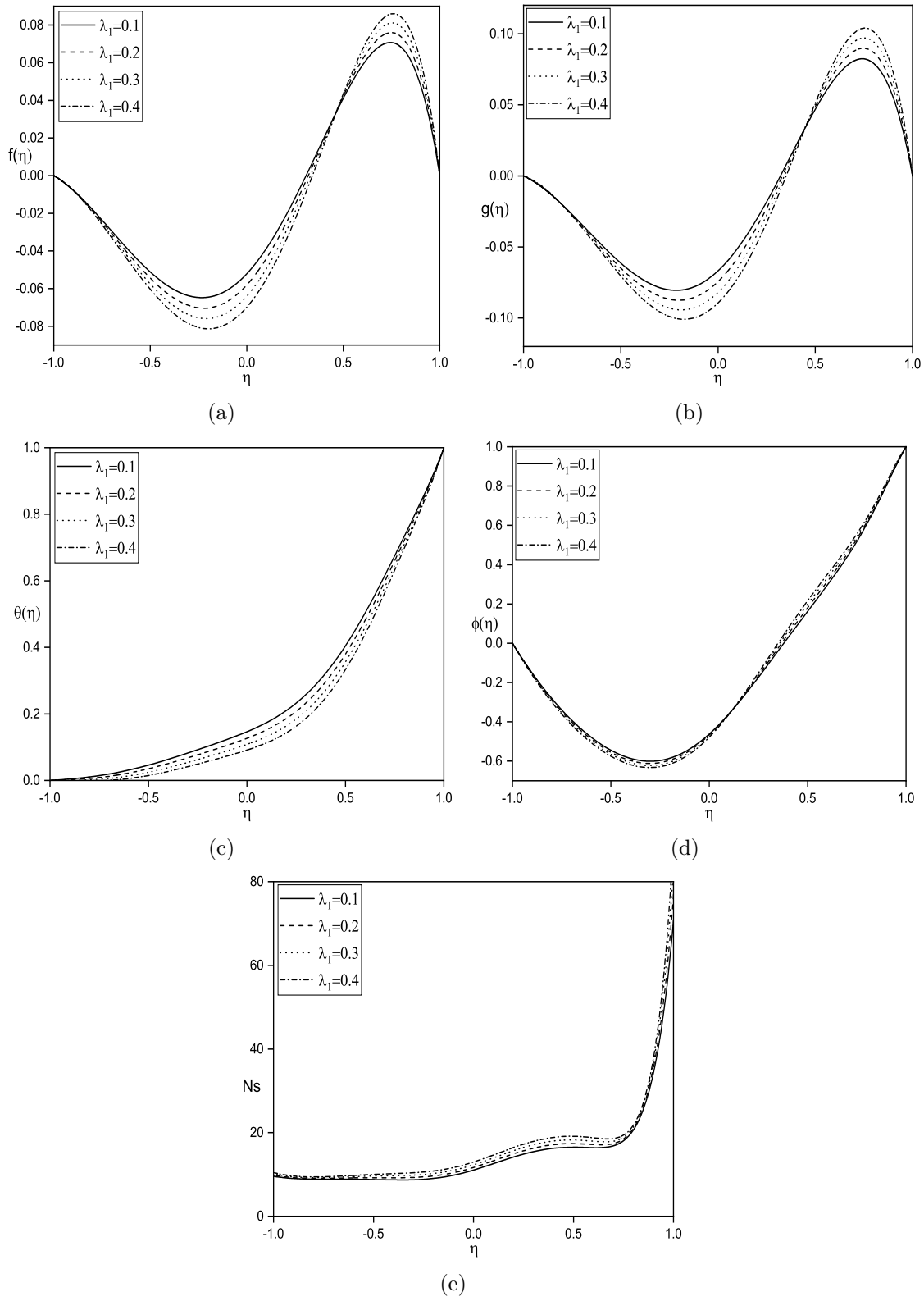

Figure 4.6: *Impact of Jeffrey fluid parameter (λ_1) on (a) $f(\eta)$, (b) $g(\eta)$, (c) $\theta(\eta)$, (d) $\phi(\eta)$, and (e) Ns.*

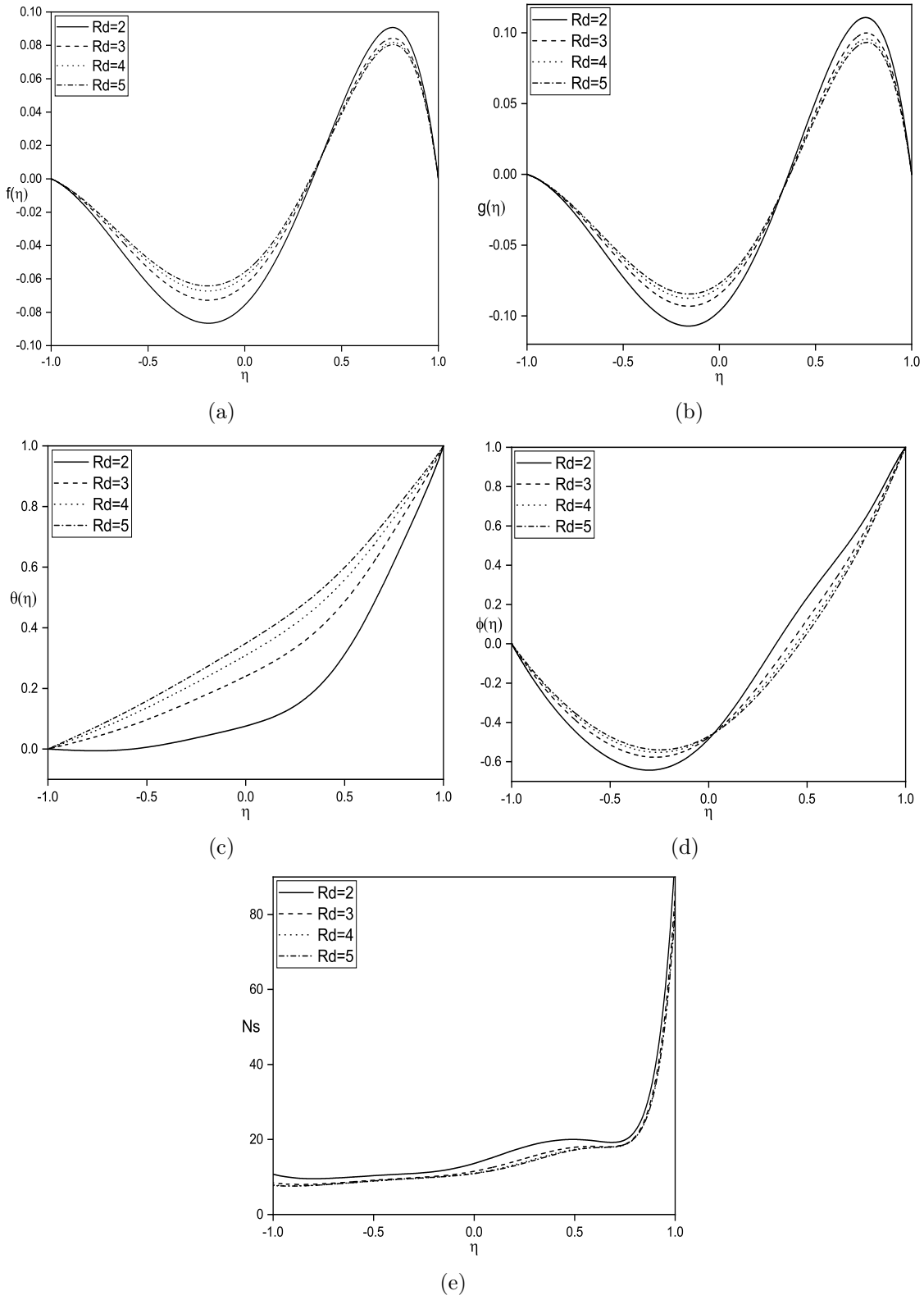

Figure 4.7: *Impact of radiation parameter (Rd) on (a) $f(\eta)$, (b) $g(\eta)$, (c) $\theta(\eta)$, (d) $\phi(\eta)$, and (e) Ns.*

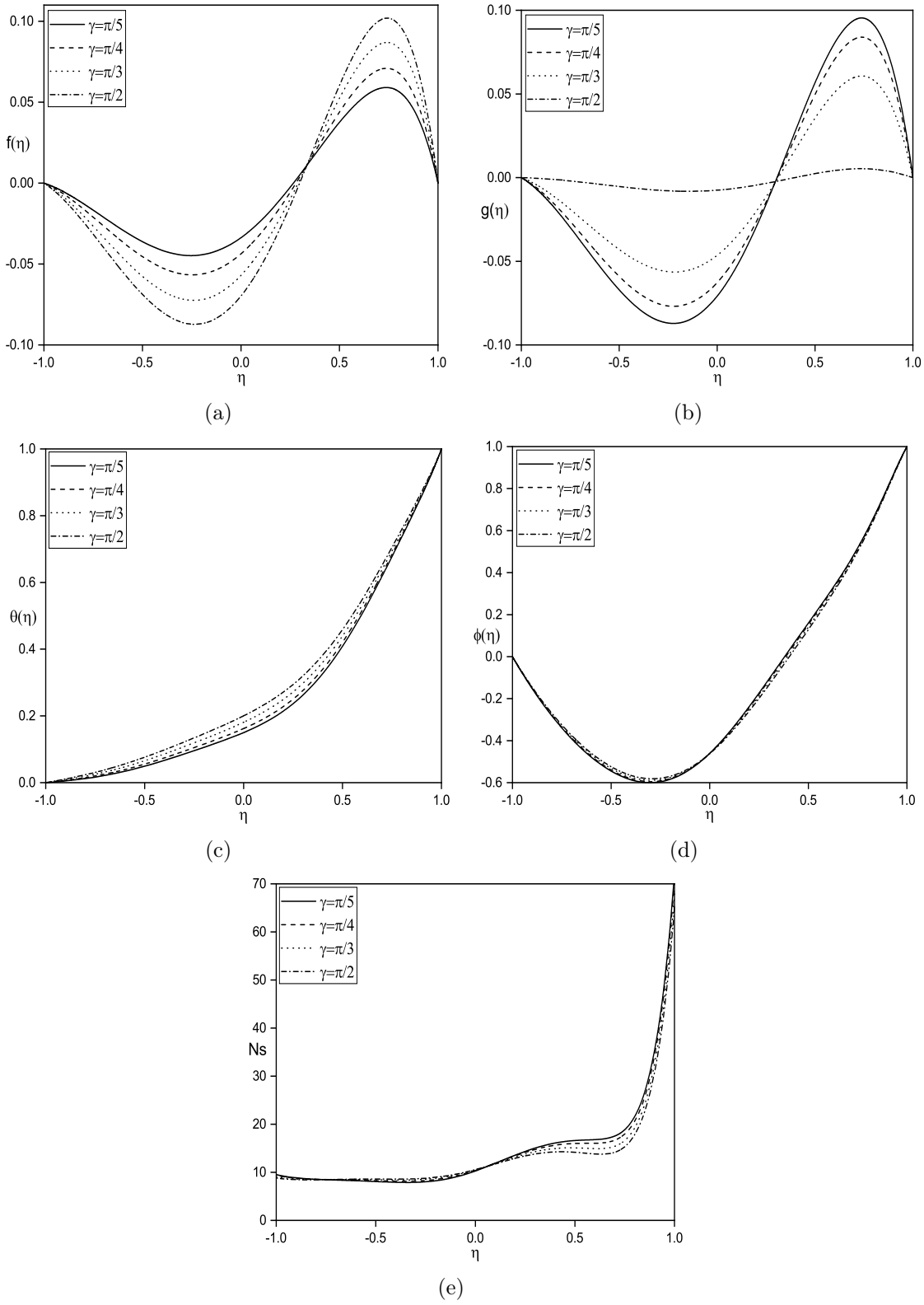

Figure 4.8: *Impact of channel angle of inclination (γ) on (a) $f(\eta)$, (b) $g(\eta)$, (c) $\theta(\eta)$, (d) $\phi(\eta)$, and (e) Ns.*

Table 4.1: Overview of the impact of different values of α, Sr, Ha, m, Rd, γ and λ_1 on skin friction ($Cf_{1,2}$), rate of heat transfer ($Nu_{1,2}$) and mass transfer ($Sh_{1,2}$).

Ha	Sr	m	α	Rd	λ_1	γ	Cf_1	Cf_2	Nu_1	Nu_2	Sh_1	Sh_2
1	2	2	$\pi/3$	2	0.2	$\pi/3$	-0.0549	-0.5938	-0.7214	-4.4908	1.2307	-2.6120
2	2	2	$\pi/3$	2	0.2	$\pi/3$	-0.0482	-0.5955	-0.7393	-4.4699	1.2301	-2.6117
3	2	2	$\pi/3$	2	0.2	$\pi/3$	-0.0356	-0.5978	-0.7627	-4.4485	1.2292	-2.6106
2	1	2	$\pi/3$	2	0.2	$\pi/3$	-0.0472	-0.5912	-0.7548	-4.4273	1.2043	-2.6812
2	2	2	$\pi/3$	2	0.2	$\pi/3$	-0.0482	-0.5955	-0.7393	-4.4699	1.2301	-2.6117
2	3	2	$\pi/3$	2	0.2	$\pi/3$	-0.0493	-0.6000	-0.7227	-4.5149	1.2571	-2.5399
2	2	1	$\pi/3$	2	0.2	$\pi/3$	-0.0426	-0.6085	-0.7563	-4.4695	1.2300	-2.6096
2	2	2	$\pi/3$	2	0.2	$\pi/3$	-0.0482	-0.5955	-0.7393	-4.4699	1.2301	-2.6117
2	2	3	$\pi/3$	2	0.2	$\pi/3$	-0.0517	-0.5902	-0.7281	-4.4721	1.2302	-2.6129
2	2	2	0	2	0.2	$\pi/3$	-0.0549	-0.5217	-0.7500	-4.4086	1.2285	-2.6162
2	2	2	$\pi/4$	2	0.2	$\pi/3$	-0.0496	-0.5703	-0.7436	-4.4418	1.2293	-2.6138
2	2	2	$\pi/3$	2	0.2	$\pi/3$	-0.0482	-0.5955	-0.7393	-4.4699	1.2301	-2.6117
2	2	2	$\pi/3$	1	0.2	$\pi/3$	-0.0372	-0.5872	-0.1899	-3.8916	1.2706	-2.5068
2	2	2	$\pi/3$	2	0.2	$\pi/3$	-0.0482	-0.5955	-0.7393	-4.4699	1.2301	-2.6117
2	2	2	$\pi/3$	3	0.2	$\pi/3$	-0.0535	-0.5989	-1.3482	-5.0895	1.2136	-2.6542
2	2	2	$\pi/3$	2	0.1	$\pi/3$	-0.0494	-0.5442	-0.7508	-4.3616	1.2276	-2.6208
2	2	2	$\pi/3$	2	0.2	$\pi/3$	-0.0482	-0.5955	-0.7393	-4.4699	1.2301	-2.6117
2	2	2	$\pi/3$	2	0.3	$\pi/3$	-0.0468	-0.6467	-0.7308	-4.5695	1.2323	-2.6030
2	2	2	$\pi/3$	2	0.2	$\pi/4$	-0.0334	-0.6695	-0.5420	-5.1401	1.2479	-2.5723
2	2	2	$\pi/3$	2	0.2	$\pi/3$	-0.0482	-0.5955	-0.7393	-4.4699	1.2301	-2.6117
2	2	2	$\pi/3$	2	0.2	$\pi/2$	-0.0702	-0.3527	-1.0321	-3.2162	1.1976	-2.6952

4.2.2 Case (b): Mixed Convection

Consider a mixed convection flow occurring with both natural (buoyancy-driven) and forced (externally-driven) convection mechanisms.

similarity transformations for this given problem is given as

$$\eta = \frac{y}{d},\ u = u_0 f,\ w = u_0 g,\ \phi = \frac{C - C_1}{C_2 - C_1},\ \theta = \frac{T - T_1}{T_2 - T_1} \tag{4.15}$$

In equations (4.2) – (4.5), Non-dimensional equations are obtained as

$$\begin{aligned} f'' - Re(1+\lambda_1)f' - \frac{Ha^2(1+\lambda_1)\cos\alpha}{1+m^2\cos^2\alpha}\left[mg\cos^2\alpha + f\cos\alpha - \lambda\sin\alpha\right] \\ + \frac{Gr}{Re}(1+\lambda_1)(\theta + N\phi)sin\gamma - \frac{f}{Da} - A(1+\lambda_1) = 0 \end{aligned} \tag{4.16}$$

$$\begin{aligned} g'' - Re(1+\lambda_1)g' - \frac{g}{Da} - \frac{Gr}{Re}(1+\lambda_1)(\theta + N\phi)cos\gamma \\ + \frac{Ha^2(1+\lambda_1)\cos^2\alpha}{1+m^2\cos^2\alpha}\left[mf\cos\alpha - m\lambda\sin\alpha - g\right] = 0 \end{aligned} \tag{4.17}$$

$$\frac{Br}{(1+\lambda_1)}((f')^2 + (g')^2) + (1 + \frac{4Rd}{3})\theta'' - RePr\theta' = 0 \tag{4.18}$$

$$ScSr\theta'' + \phi'' - ReSc\phi' - QSc\phi = 0 \tag{4.19}$$

where $Re = \rho v_0 d/\mu$ represents Reynolds number, $Da = k/d^2$ represents the Darcy number, $Rd = 4\sigma T_0^3/k_f k^*$ denotes the Radiation parameter, $Pr = \mu c_p/k_f$ is Prandtl number, $\lambda = Re/Gr$, $Br = \mu v^2/k_f d^2(T_2 - T_1)$ is Brinkman number, $Ha = dB_0\sqrt{\sigma/\mu}$ represents the magnetic parameter, $Sc = \nu/D$ stands for Schmidt number, $Q = k_1 d/\nu$ represents the chemical reaction parameter, $Gr = g^*\beta_T(T_2 - T_1)d^3/v^2$ indicates the Grashof number, $N = \beta_C(C_2 - C_1)/\beta_T(T_2 - T_1)$ indicates the buoyancy parameter, and $Sr = DK_T(T_2 - T_1)/\nu T_m(C_2 - C_1)$ represents soret parameter.

Boundary conditions (4.6) become

$$\begin{aligned} f = g = \theta = \phi = 0, \quad when\ \eta = -1 \\ f = g = 0, \quad \theta = \phi = 1, \quad when\ \eta = 1 \end{aligned} \tag{4.20}$$

The shear stress, heat transfer, and mass flows can be obtained from.

$$\tau_w = \left[\mu \frac{du}{dy}\right] |_{y=\pm d}; \quad q_w = \left[-k_f \frac{dT}{dy} + q_r\right] |_{y=\pm d}; \quad q_m = -D\frac{dC}{dy} |_{y=\pm d}$$

The dimensionless shear stress $C_f = \dfrac{\tau_w}{\rho u_0^2}$ is given by $ReC_{f_{1,2}} = f'(\eta) |_{\eta=-1,1}$.
The Sherwood number defined as $Sh = q_m d/D(C_2 - C_1)$ and Nusselt number defined as $Nu = q_w d/k_f(T_2 - T_1)$ for this problem are given by

$$Sh_{1,2} = -\left[\phi'(\eta)\right] |_{\eta=-1,1}; \quad Nu_{1,2} = -\left[1 + \frac{4}{3}Rd\right] \theta'(\eta) |_{\eta=-1,1}\ .$$

Entropy Generation

The expression for the volumetric entropy generation rate is expressed as:

$$\begin{aligned} S_{gen} = \frac{k_f}{T_0^2}\left[1 + \frac{16\sigma T_0^3}{3k_f k^*}\right]\left[\frac{dT}{dy}\right]^2 + \frac{\mu}{T_0(1+\lambda_1)}\left[\left(\frac{du}{dy}\right)^2 + \left(\frac{dw}{dy}\right)^2\right] + \frac{RD}{C_0}\left(\frac{dC}{dy}\right)^2 \\ + \frac{RD}{T_0}\left(\frac{dT}{dy}\right)\left(\frac{dC}{dy}\right) + \frac{\mu}{kT_0}(u^2 + w^2) + \frac{\sigma B_0^2}{T_0}\left[w^2 + (ucos\alpha - v_0 sin\alpha)^2\right] \end{aligned} \tag{4.21}$$

The initial term of the right hand side of equation (4.21) is because of heat transfer, the subsequent term is due to energy dissipation by fluid viscosity, the third and fourth terms represent mass transfer, the fifth term is connected to porosity effects, and the sixth term is due to applied magnetic field. The definition of entropy

generation rate is formally defined as:

$$(S_{gen})_0 = \frac{k_f(T_2 - T_1)^2}{T_0^2 d^2} \tag{4.22}$$

By using equations (4.21) and (4.22), the formation of dimensionless entropy is given as:

$$Ns = \frac{S_{gen}}{(S_{gen})_0}$$

$$Ns = \left[1 + \frac{4}{3}Rd\right](\theta')^2 + \frac{Br}{(1+\lambda_1)A_1}(f'^2 + g'^2) + \frac{\varepsilon B_1^2}{A_1^2}(\phi')^2 + \frac{\varepsilon B_1}{A_1}\theta'\phi' + \frac{Br}{DaA_1}(f^2 + g^2) + \frac{BrHa^2}{A_1}\left(g^2 + (fcos\alpha - \lambda sin\alpha)^2\right)$$

where A_1, Br, B_1, Ha, Rd, Da, and ε are dimensionless temperature difference, brinkman number, dimensionless concentration difference, magnetic parameter, thermal radiation, darcy number, and dimensionless constant parameter, which are given as

$$Br = \frac{\mu v^2}{k_f d^2(T_2 - T_1)}, \quad Ha = dB_0\sqrt{\frac{\sigma}{\mu}}, \quad Rd = \frac{4\sigma T_0^3}{k_f k^*}, \quad Da = \frac{k}{d^2},$$
$$A_1 = \frac{T_2 - T_1}{T_0}, \quad B_1 = \frac{C_2 - C_1}{C_0}, \quad \varepsilon = \frac{RDC_0}{k_f},$$

In engineering applications and entropy minimization studies, it's important to consider the contribution of various factors including heat transfer, mass transfer, porous medium, viscous dissipation, and magnetic force to the overall entropy generation rate. This helps us to gain insight into thermal optimization. To calculate the distribution of irreversibility, we use the Bejan number, which is the ratio of irreversibility due to heat transfer (N_h) to the total irreversibility (Ns).

$$Be = \frac{N_h}{Ns}$$

The table labeled as 4.2 presents the values for irreversibility caused by heat transfer (N_h), total irreversibility in the system (Ns), and the Bejan number across different angles of inclination in the channel (γ).

Results and discussion

The nonlinear and coupled flow eqns. (4.16) - (4.19) with respect to boundary conditions (4.20) are numerically solved by SQLM (as explained in chapter-2).

Figures 4.9 to 4.15 show the behavior of $f(\eta)$, $g(\eta)$, $\theta(\eta)$, $\phi(\eta)$, Ns, and Be for distinct values of Ha, α, m, Rd, Sr, λ_1, and γ with fixed values of Pr, K, Re, Br, N, $Da\ Sc$ at 21, 2, 2, 0.5, 2, 2, 0.22, respectively.

In Figure 4.9, we show how the variables f, g, θ, ϕ, Ns, and Be change with varying magnetic parameter (Ha). As seen in Figure 4.9(a), the flow velocity goes up as the value of Ha increases. The detected inclination angle of the applied magnetic field is $\alpha > 0$, meaning that no drag force can be produced. Figure 4.9(b) shows that the cross-flow velocity goes down as Ha increases. The fluid temperature rise and concentration fall with a rise in Ha as shown in figures 4.9(c) and 4.9(d). It is seen in figures 4.9(e) and 4.9(f) that entropy generation and bejan number magnifies as Ha magnify. This is happen due to a magnetic field creates a resistive force perpendicular to the direction of the magnetic field. This generates electric charges, leading to an increase in temperature.

Figure 4.10 displays the behavior of f, g, θ, ϕ, Ns, and Be for different values of Soret parameter (Sr). As seen in figures 4.10(a) and 4.10(b), flow velocity and cross-flow velocity magnify as Sr rise. This is due to the fact that increasing the Soret parameter raises the temperature gradient, which in turn causes greater velocities. Figures 4.10(c) and 4.10(d) illustrate that there is a fall in temperature and a rise in concentration as the Soret parameter increases. A higher Sr indicates a stronger thermophoretic effect, causes a redistribution of temperature and

concentration within the fluid. This leads to a fall in temperature and a rise in concentration. The Soret effect plays a crucial role in understanding heat and mass transfer phenomena in complex fluid flows. It is noted in figure 4.10(e) that the entropy increases and decreases as η approaches 1 as Sr increases. Figure 4.10(f) shows that increasing the Soret number leads to a decrease in the Bejan number. The Soret parameter plays a role in mass transfer in multicomponent fluid systems and can significantly impact flow behavior, particularly in situations involving heat and mass transfer.

Figure 4.11 demonstrates the impact of m on the variables f, g, θ, ϕ, Ns, and Be. Figures 4.11(a) and 4.11(b) demonstrate that as the parameter m increases, the flow velocity decreases while the cross-flow velocity increases. This is caused by the inclined magnetic field's influence. When a magnetic field is applied at an angle of $\alpha = \pi/4$, the Hall current is generated perpendicular to the x direction. This current acts as a drag on the flow velocity. Meanwhile, Figures 4.11(c) and 4.11(d) indicate a decrease in fluid temperature and an increase in fluid concentration as m is raised. Additionally, Figures 4.11(e) and 4.11(f) show that increasing m leads to higher entropy generation and lower Bejan number. The hall current plays a crucial role in magnetohydrodynamic flows, as it introduces additional complexity in fluid motion and magnetic field distribution. Magnetohydrodynamics is relevant in plasma physics, astrophysics, and engineering applications such as magnetohydrodynamics power generation and magnetohydrodynamics propulsion systems.

Figure 4.12 shows the behavior of f, g, θ, ϕ, Ns, and Be for distinct value of α. Figure 4.12(a) reveals that velocity rises with a rise in α. This is because the decrease in drag force will improve the net flow as the applied magnetic field's inclination angle changes (angle of inclination increases). Figures 4.12(b) and 4.12(c) illustrate the rise in cross-flow velocity and fall in temperature with increasing α. Figure 4.12(d) and 4.12(e) reveal that the concentration and entropy both rise with a rise in α.

As α increases, the Bejan number decreases, but it increases near $\eta = 1$, as shown in Figure 4.12(f). An inclined magnetic field is used in magnetohydrodynamics generators to convert the kinetic energy of hot, electrically conducting fluid into electrical energy.

Figure 4.13 showcases the influence of λ_1 on the variables f, g, θ, ϕ, Ns, and Be. As shown in 4.13(a) and 4.13(b), increasing λ_1 causes an increase in flow and cross-flow velocity. An increased Jeffrey fluid parameter enhances the fluid's elasticity, resistance to deformation, and quicker recovery from shearing forces. This results in higher flow and cross-flow velocities. Figure 4.13(c) shows that temperature decreases as λ_1 increases. As λ_1 increases, less heat is generated or absorbed during flow due to the increased elasticity of the Jeffrey fluid, resulting in a lower temperature profile. Figures 4.13(d) and 4.13(e) suggest that an increase in λ_1 corresponds to an increase in concentration and entropy generation. Higher Jeffrey fluid parameter means more elastic effects, viscous dissipation, shear-thinning behavior, and complex flow patterns, which lead to increased entropy generation. Figure 4.13(f) shows that the Bejan number decreases with an increasing value of the Jeffrey fluid parameter.

In Figure 4.14, we present the changes in the variables f, g, θ, ϕ, Ns, and Be for various values of Rd. Figures 4.14(a) and 4.14(b) reveal that as the parameter Rd increases, both the flow velocity and cross-flow velocity decrease. An increase in the radiation parameter lead to changes in temperature distribution, influencing the viscosity of the Jeffrey fluid. Higher viscosity results in reduced flow velocities. The results in figures 4.14(c) and 4.14(d) show that the fluid temperature rises and the concentration decreases as the radiation parameter increases. Higher radiation parameter leads to increased thermal radiation impact on fluid, elevating its temperature via associated heat transfer processes. This results in the fluid's energy being amplified by the radiation. Figures 4.14(e) and 4.14(f) indicate that a rise in

Rd leads to a rise in entropy generation and bejan number. This is due to thermal radiation, which adds sources of irreversibility and heat dissipation in the system.

Figure 4.15 displays the behavior of f, g, θ, ϕ, Ns, and Be for varying values of γ. As depicted in figure 4.15(a) and 4.15(b), an increase in flow and decrease in cross-flow velocity is observed as γ increases. When inclined plates are present, gravity can assist in the flow of fluid in a channel. This additional driving force results in an increase in flow velocity and a decrease in cross-flow velocity. Figure 4.15(c) reveals that the temperature of fluid rise with a rise in γ. Increasing channel angle leads to higher fluid shear rates and greater energy dissipation, resulting in a temperature rise due to viscous heating. Figures 4.15(d), and 4.15(e) demonstrate that as γ increases, there is subside in concentration and entropy generation. Figure 4.15(f) illustrates the variation of the Bejan number with respect to η. It increases to the left of $\eta = 0$ and decreases to the right. This is because the plates become vertical as $gamma$ increases to $90circ$, which causes the drag force to be generated along the y-axis by the applied magnetic field.

Table 4.3 presents the variations in the magnetic parameter (Ha), radiation parameter (Rd), Hall number (m), Soret number (Sr), inclination angle (α), Jeffrey fluid parameter (λ_1), and channel angle of inclination (γ) while keeping other parameters at $Q = 2$, $Re = 2$, $Gr = 10$, $Pr = 21$, $N = 2$, $Br = 0.5$, $Sc = 0.22$, and $Da = 2$. According to the table, an increase in both γ and λ_1 results in an increase in skin friction at the plate located at $\eta = -1$, while there is a reduction in skin friction at the plate located at $\eta = 1$. Skin friction falls with higher values of Sr, m, and Rd, while the opposite effect is noted for the Ha and α. Additionally, Table 4.3 demonstrates that when m, Sr, α, and λ_1 rise, the heat transfer rate magnifies at the left plate and subside at the right plate, while the opposite tendency is seen for the magnetic parameter (Ha) and channel inclination angle (γ). The higher the value of the radiation parameter (Rd), there is fall in the heat transfer rate for

both plates. Moreover, According to Table 4.3, the mass transfer rate increases with higher values of Sr, m, α, and λ_1, while it exhibits a reverse trend with Ha, Rd and γ.

4.3 Conclusions

In this chapter, the effects of the Soret number and chemical reactions on entropy of the system in the steady natural/mixed convection of Jeffrey fluid flow between inclined parallel plates are investigated. The original complex equations describing the system are changed into dimensionless equations using similarity transformations. SQLM is used to solve these dimensionless equations. According to the findings of this study, the velocity of fluid flow and its cross-flow velocity increase with an increase in the Soret number and Jeffrey fluid parameter. Conversely, the opposite effect is observed with an increase in the radiation parameter and channel angle of inclination. The temperature of the fluid decreases while the concentration rises with an increase in the Soret parameter, Hall parameter, inclination angle, and Jeffrey fluid parameter. However, the reverse tendency is noted in magnetic parameter, Radiation parameter, and channel inclination angle. Entropy generation in the system increases as the Soret parameter, Hall parameter, inclination angle, and Jeffrey fluid parameter increase, while it decreases as the channel angle of inclination increases.

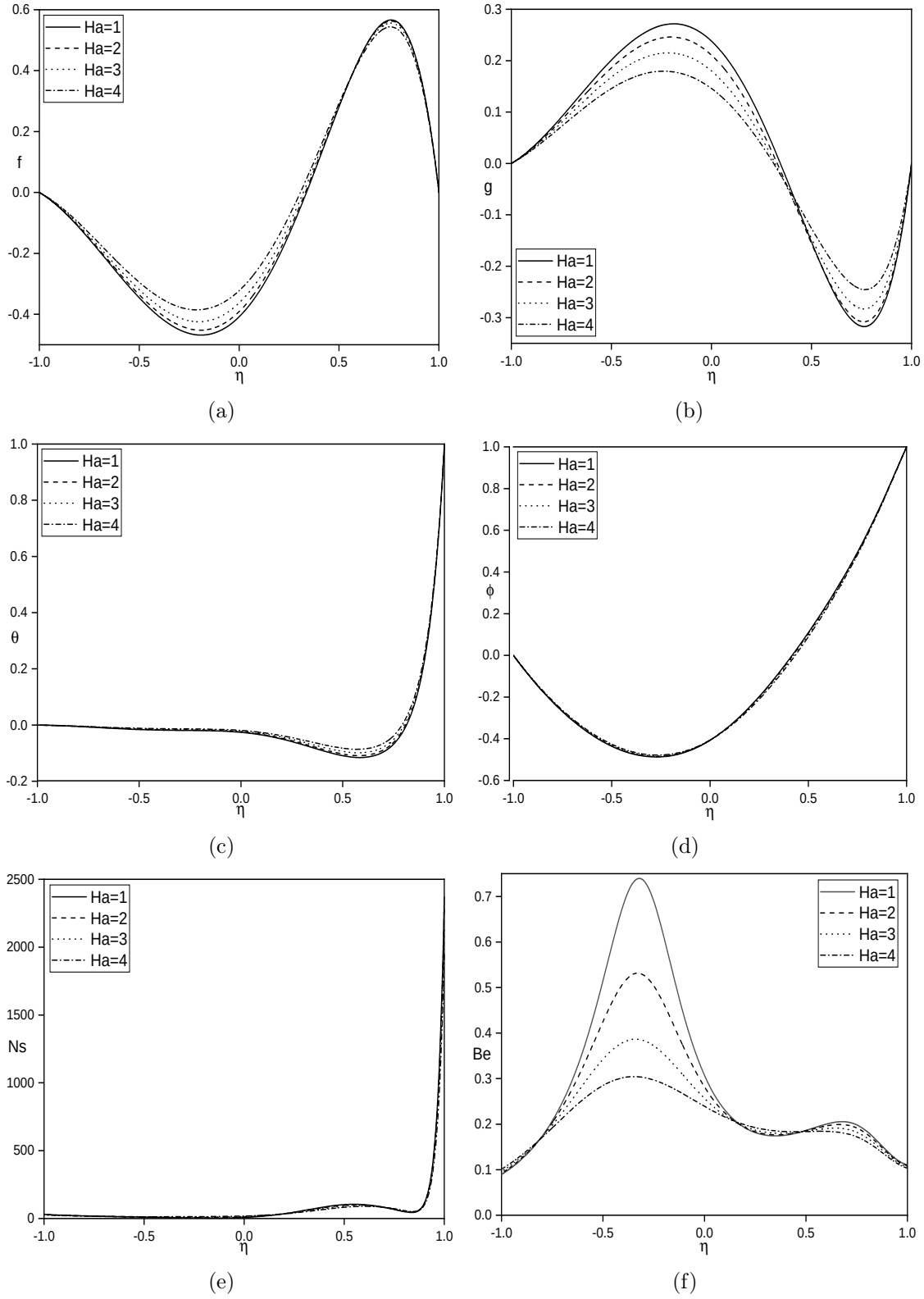

Figure 4.9: *Impact of magnetic parameter (Ha) on (a) $f(\eta)$, (b) $g(\eta)$, (c) $\theta(\eta)$, (d) $\phi(\eta)$, (e) Ns, and (f) Be.*

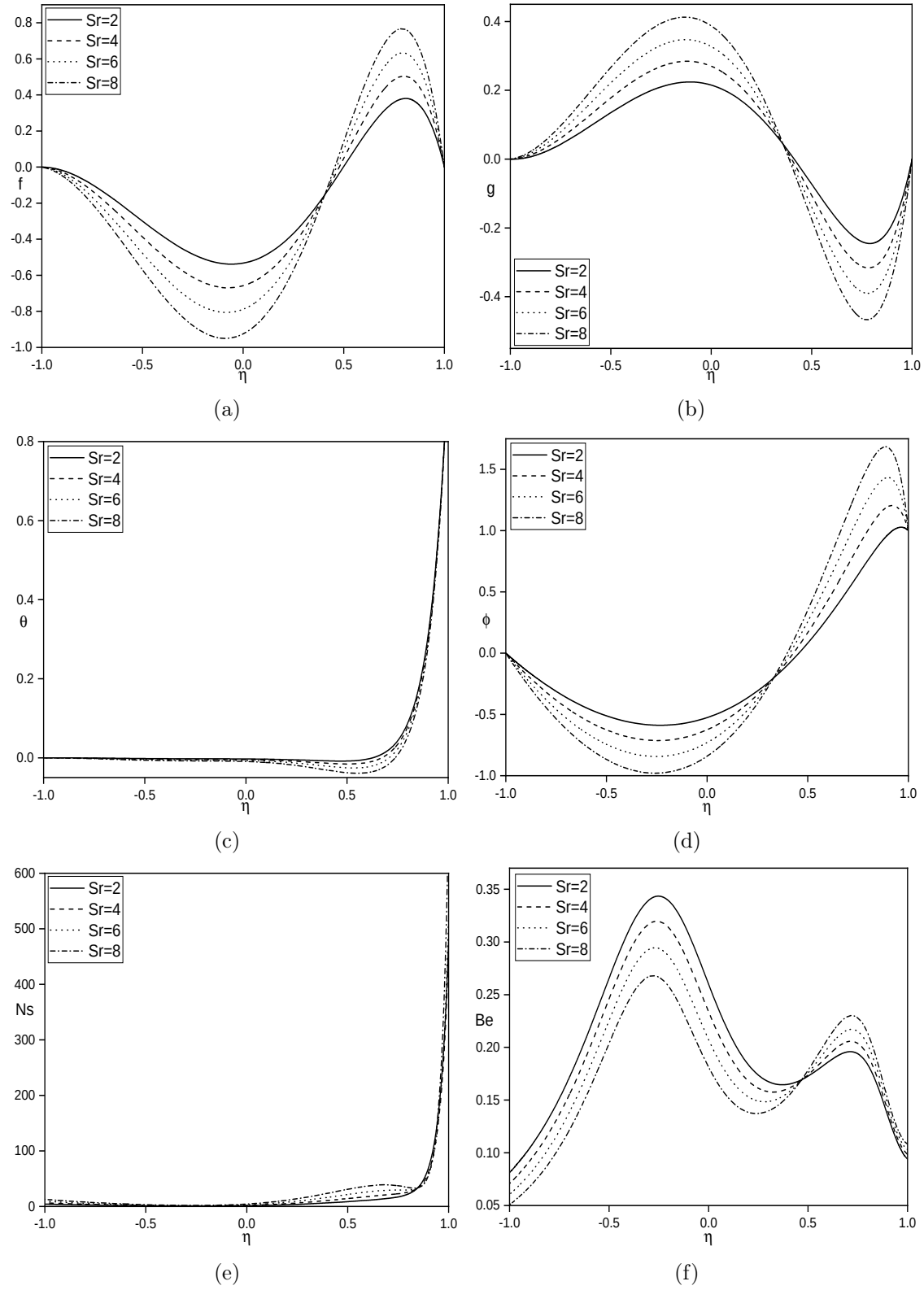

Figure 4.10: *Impact of Soret number (Sr) on (a) $f(\eta)$, (b) $g(\eta)$, (c) $\theta(\eta)$, (d) $\phi(\eta)$, (e) Ns, and (f) Be.*

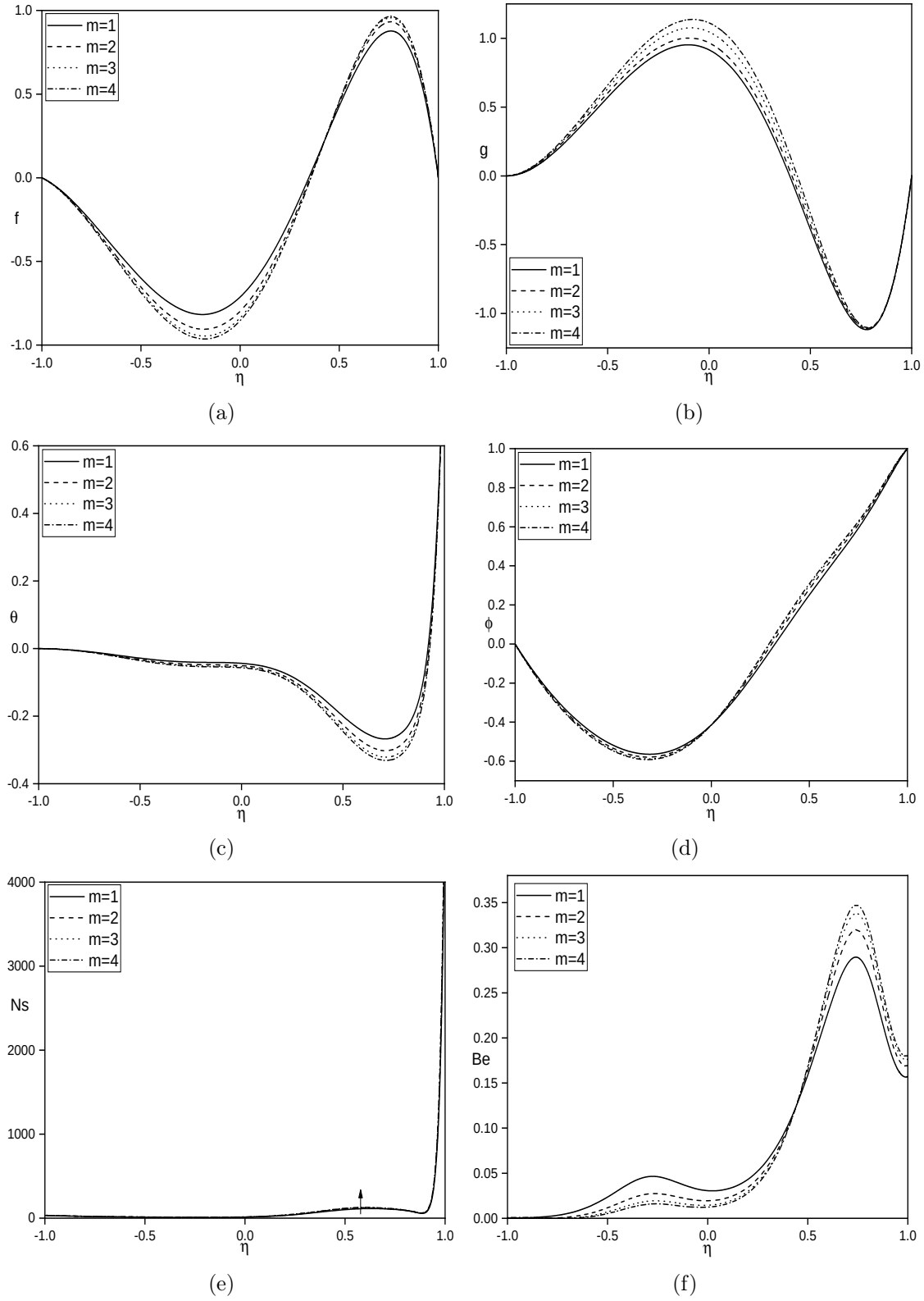

Figure 4.11: *Impact of hall current (m) on (a) $f(\eta)$, (b) $g(\eta)$, (c) $\theta(\eta)$, (d) $\phi(\eta)$, (e) Ns, and (f) Be.*

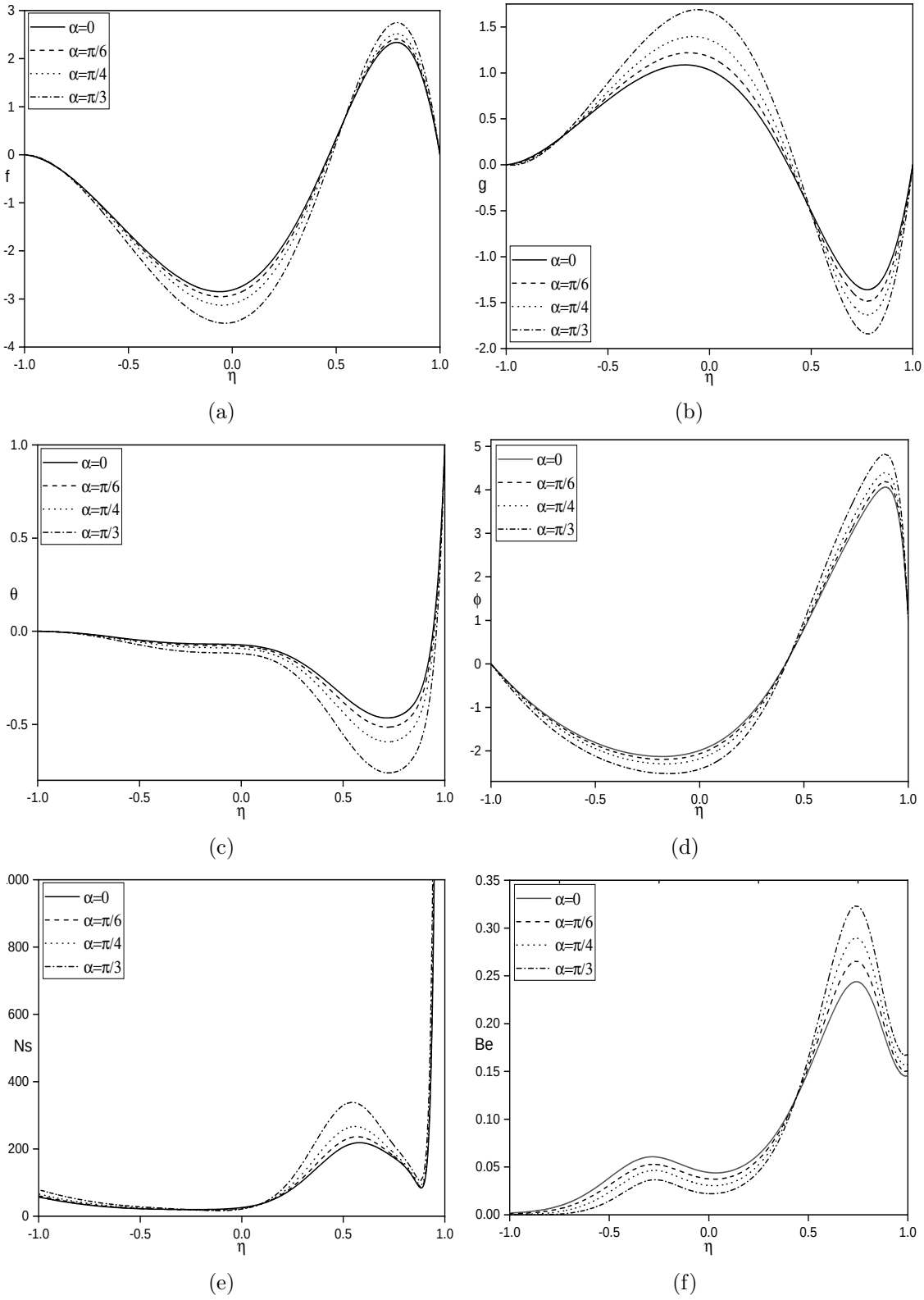

Figure 4.12: *Impact of inclination angle (α) on (a) $f(\eta)$, (b) $g(\eta)$, (c) $\theta(\eta)$, (d) $\phi(\eta)$, (e) Ns, and (f) Be.*

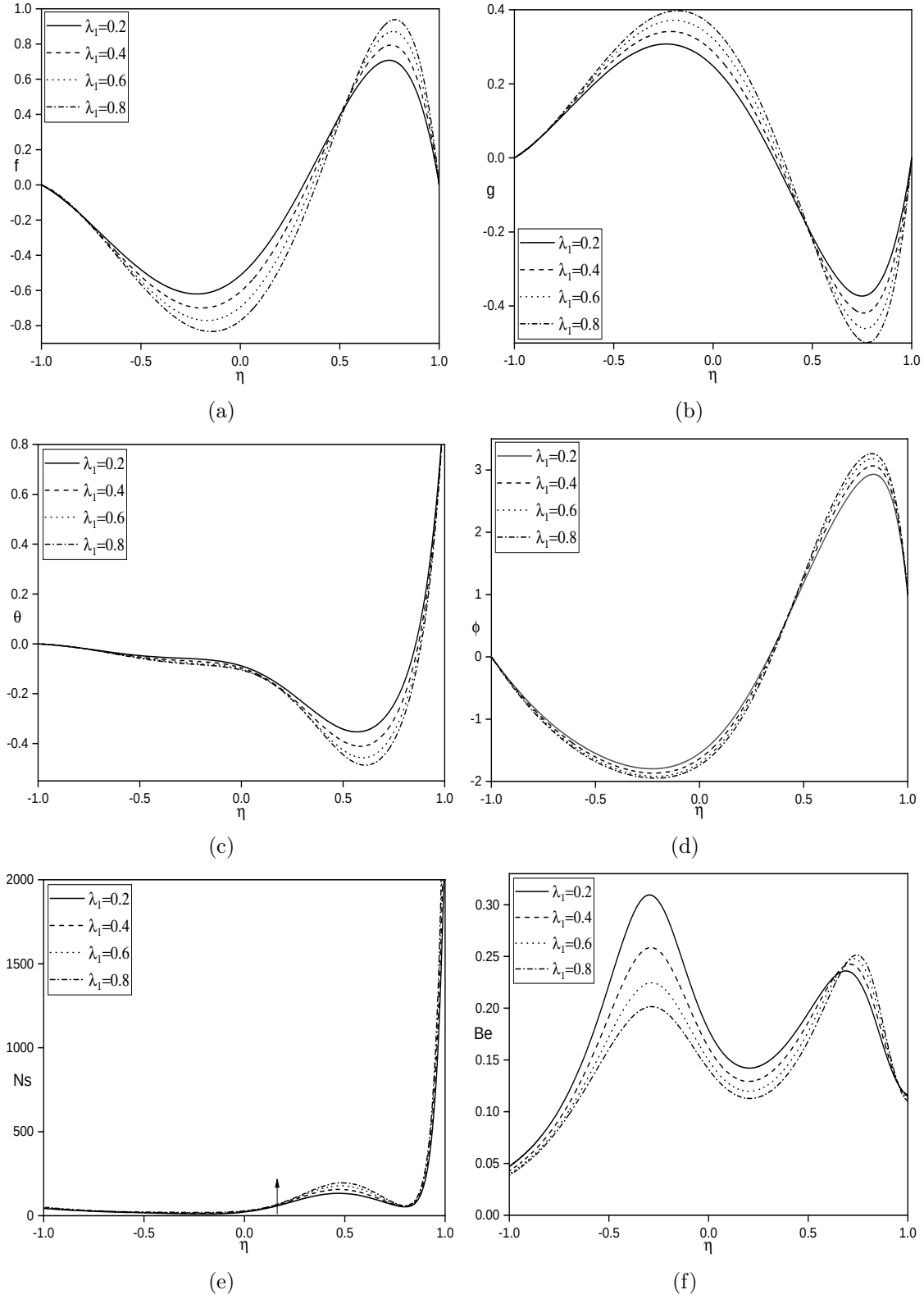

Figure 4.13: *Impact of Jeffrey fluid parameter (λ_1) on (a) $f(\eta)$, (b) $g(\eta)$, (c) $\theta(\eta)$, (d) $\phi(\eta)$, (e) Ns, and (f) Be.*

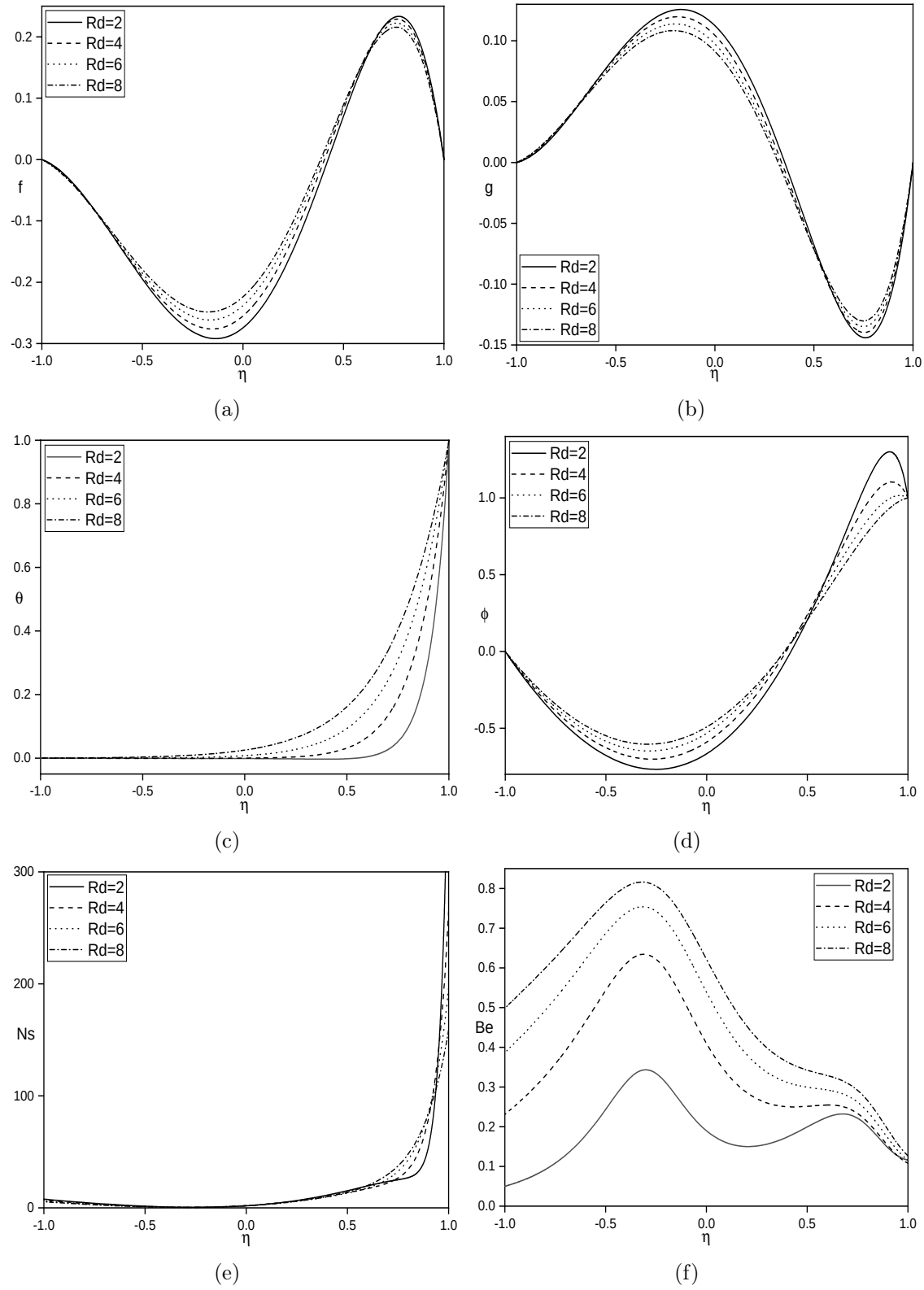

Figure 4.14: *Impact of radiation parameter (Rd) on (a) $f(\eta)$, (b) $g(\eta)$, (c) $\theta(\eta)$, (d) $\phi(\eta)$, (e) Ns, and (f) Be.*

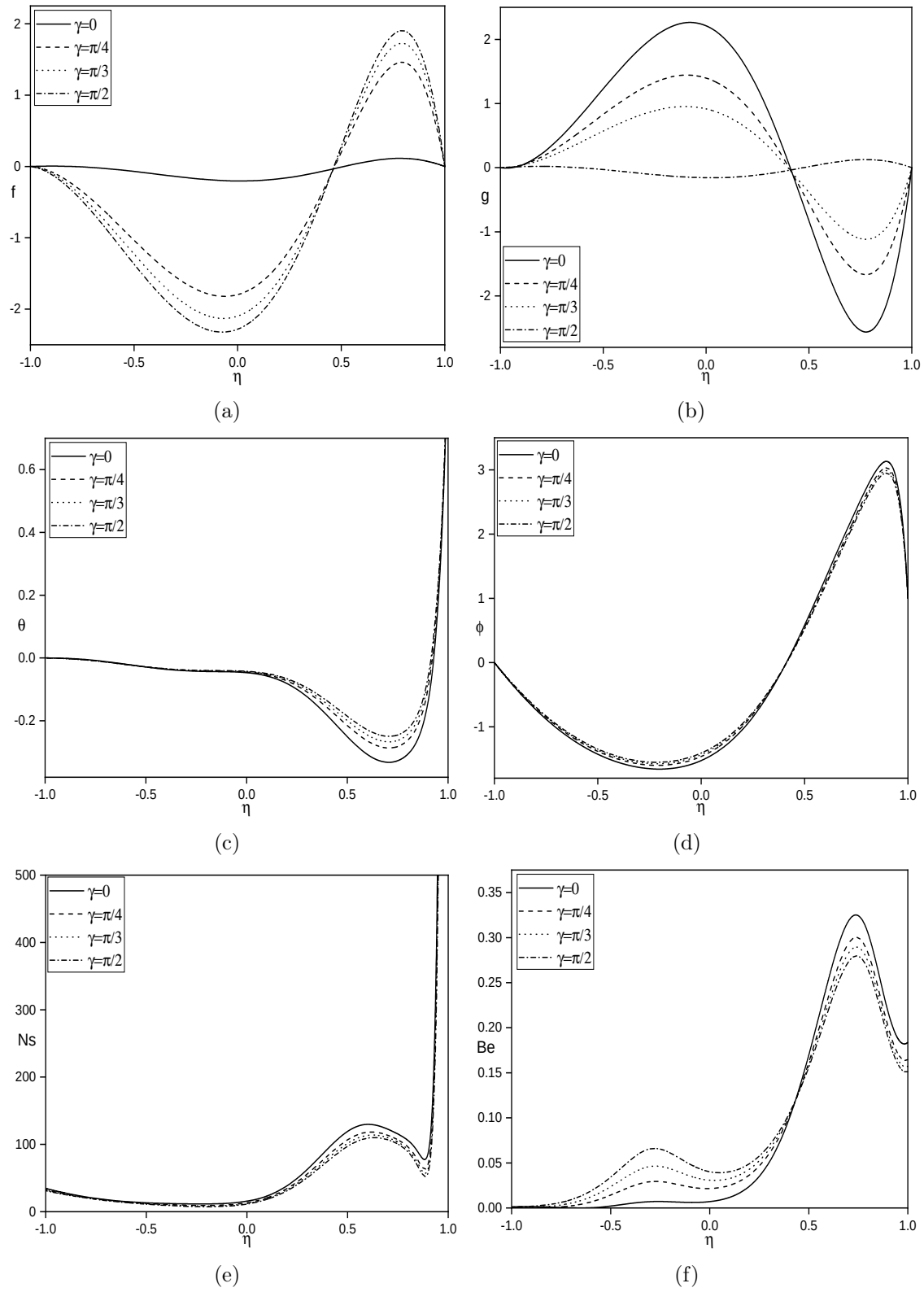

Figure 4.15: *Impact of channel angle of inclination (γ) on (a) $f(\eta)$, (b) $g(\eta)$, (c) $\theta(\eta)$, (d) $\phi(\eta)$, (e) Ns, and (f) Be.*

Table 4.2: Bejan Number variations for different values of η and γ.

η	γ	N_h	Ns	$Be = \frac{N_h}{Ns}$
-1	$\pi/4$	$9.19e^{-6}$	5.5792	$1.648e^{-6}$
-0.5	$\pi/4$	0.0284	2.1110	0.0135
0	$\pi/4$	0.0958	4.4841	0.0214
0.5	$\pi/4$	2.0497	12.2062	0.1679
1	$\pi/4$	8.7595	53.2090	0.1646
-1	$\pi/3$	0.0016	5.1928	0.0003
-0.5	$\pi/3$	0.0423	1.8857	0.0224
0	$\pi/3$	0.1233	4.0291	0.0306
0.5	$\pi/3$	1.9075	11.5990	0.1645
1	$\pi/3$	7.8556	49.9653	0.1572

Table 4.3: Overview of the impact of various values of α, Ha, Sr, m, Rd, γ, and λ_1 on skin friction ($Cf_{1,2}$), rate of heat transfer ($Nu_{1,2}$) and mass transfer ($Sh_{1,2}$).

Ha	Sr	m	α	Rd	λ_1	γ	Cf_1	Cf_2	Nu_1	Nu_2	Sh_1	Sh_2
1	2	2	$\pi/3$	2	0.2	$\pi/3$	-0.3227	-4.2297	-1.0495	-3.2551	1.1339	-2.6021
2	2	2	$\pi/3$	2	0.2	$\pi/3$	-0.3196	-4.2196	-1.0608	-3.2231	1.1331	-2.6039
3	2	2	$\pi/3$	2	0.2	$\pi/3$	-0.3136	-4.1777	-1.0789	-3.1662	1.1317	-2.6072
2	1	2	$\pi/3$	2	0.2	$\pi/3$	-0.3132	-4.2014	-1.0632	-3.2165	1.1249	-2.6343
2	2	2	$\pi/3$	2	0.2	$\pi/3$	-0.3196	-4.2196	-1.0608	-3.2231	1.1331	-2.6039
2	3	2	$\pi/3$	2	0.2	$\pi/3$	-0.3260	-4.2381	-1.0583	-3.2299	1.1416	-2.5731
2	2	1	$\pi/3$	2	0.2	$\pi/3$	-0.3095	-4.1176	-1.0729	-3.1872	1.1323	-2.6059
2	2	2	$\pi/3$	2	0.2	$\pi/3$	-0.3196	-4.2196	-1.0608	-3.2231	1.1331	-2.6039
2	2	3	$\pi/3$	2	0.2	$\pi/3$	-0.3225	-4.2528	-1.0544	-3.2419	1.1336	-2.6028
2	2	2	0	2	0.2	$\pi/3$	-0.3287	-4.2226	-1.0638	-3.2065	1.1327	-2.6051
2	2	2	$\pi/4$	2	0.2	$\pi/3$	-0.3196	-4.2196	-1.0608	-3.2231	1.1331	-2.6039
2	2	2	$\pi/3$	2	0.2	$\pi/3$	-0.3162	-4.2167	-1.0572	-3.2365	1.1335	-2.6030
2	2	2	$\pi/3$	1	0.2	$\pi/3$	-0.2886	-4.2112	-0.4615	-2.6315	1.1515	-2.5517
2	2	2	$\pi/3$	2	0.2	$\pi/3$	-0.3196	-4.2196	-1.0608	-3.2231	1.1331	-2.6039
2	2	2	$\pi/3$	3	0.2	$\pi/3$	-0.3342	-4.2231	-1.6950	-3.8536	1.1266	-2.6238
2	2	2	$\pi/3$	2	0.1	$\pi/3$	-0.3301	-3.8547	-1.0647	-3.1895	1.1324	-2.6067
2	2	2	$\pi/3$	2	0.2	$\pi/3$	-0.3196	-4.2196	-1.0608	-3.2231	1.1331	-2.6039
2	2	2	$\pi/3$	2	0.3	$\pi/3$	-0.3068	-4.5834	-1.0578	-3.2540	1.1338	-2.6012
2	2	2	$\pi/3$	2	0.2	$\pi/4$	-0.2566	-3.5300	-1.0570	-3.2380	1.1335	-2.6029
2	2	2	$\pi/3$	2	0.2	$\pi/3$	-0.3196	-4.2196	-1.0608	-3.2231	1.1331	-2.6039
2	2	2	$\pi/3$	2	0.2	$\pi/2$	-0.3709	-4.7310	-1.0640	-3.2096	1.1328	-2.6048

Chapter 5

Analysis of irreversibility in Jeffrey fluid flow through an inclined channel under Navier-slip condition with the effects of Hall current, Soret number, and Inclined magnetic field. [1]

5.1 Introduction

The Soret phenomenon, a thermal gradient-induced mass flow, holds a significant position in diverse domains, including geosciences and chemical engineering. Sardar et al. [78] studied the combined convective motion of Carreau nanofluid along a wedge in the existence of Soret and Dufour phenomena. Deepika et al. [79] examined the influence of the Soret and Dufour phenomena on the magnetohydrodynamic

[1] Case(a): Published in "**East Asian Journal of Applied Mathematics**", (2024). DOI:https://10.4208/eajam.2023-227.221023
Case(b):Published in "**Journal of Applied Mathematics and Mechanics (ZAMM)**", 104, e202300700 (1-15), (2024).

mixed convective motion of a Casson hybrid nanofluid over a stretching surface. Hayat et al. [80] explored how Dufour and Soret phenomena affect the entropy production in a mixed convective flow system.

Fluid flows with slip at boundaries indeed have significant implications in various micro and macroscopic devices. As early as 1823, A slip boundary condition was first presented by Navier [81], wherein the slip velocity at the solid-fluid interface is influenced by the shear stress linearly. Building upon Navier's work, Das et al. [82] presented the findings of their research, which focused on slip flow through sloping porous channels, accounting for joule heating and energy dissipation due to viscosity effects. Asghar et al. [83] examined magnetized mixed convection involving a hybrid nanofluid, accounting for heat generation effect and velocity slip conditions effect on fluid flow. Zainodin et al. [84] investigated the combined impact of slip boundary condition and chemical reaction on forced convection flow of a hybrid ferrofluid within a porous medium modeled by Darcy's law.

In this chapter, we study the Soret number, Hall current, and angled magnetic field effects on entropy of the system of steady convective flow between inclined parallel plates in Jeffrey fluid fluid with navier-slip condition. SQLM is used to solve the dimensionless flow equations. The impact of various relevant flow parameters on entropy, velocity, temperature, and concentration is examined.

5.2 Mathematical formulation

The physical configuration illustrated in Figure 5.1 of this research involves a configuration of inclined parallel plates. These plates are inclined at an angle γ relative to the reference base and are separated by a distance of $2d$. The occurrence of slip phenomena is acknowledged on both of these plates. The concentrations and temperatures at the plates are denoted as C_1, T_1, C_2, and T_2 respectively. An external magnetic field denoted as B_0, positioned at an angle α about the base, exerts an

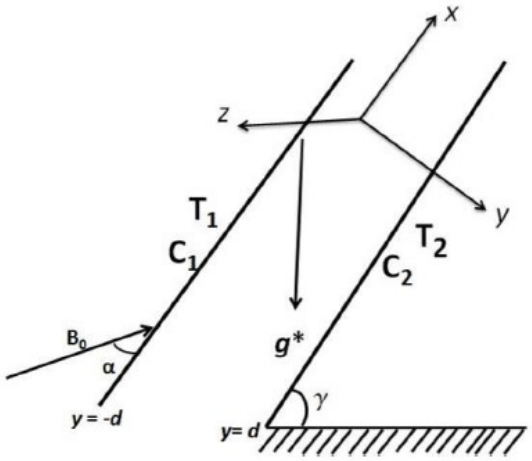

Figure 5.1: Physical interpretation.

impact on the plates. The present inquiry focuses on investigating the behavior of a Jeffrey fluid, which exhibits steady and incompressible. With the assumption that the boundaries extend infinitely along the x-axis, the parameters governing the flow are treated as functions solely dependent on the y coordinate. The properties of fluid are taken as constant, except for the change in density that affects the term in the buoyancy force. As such, these assumptions align with natural principles and are relevant in practical applications.

The governing equations are derived as follows:

$$\frac{\partial v}{\partial y} = 0 \tag{5.1}$$

$$\begin{aligned}\rho v_0 \frac{\partial u}{\partial y} = \frac{\mu}{1+\lambda_1}\frac{\partial^2 u}{\partial y^2} + \rho g^* sin\gamma\left(\beta_C(C-C_1)+\beta_T(T-T_1)\right) \\ -\frac{\sigma B_0^2 cos\alpha}{1+m^2cos^2\alpha}\left(ucos\alpha - v_0 sin\alpha + mwcos^2\alpha\right) - \frac{\partial p}{\partial x}\end{aligned} \tag{5.2}$$

$$\begin{aligned}\rho v_0 \frac{\partial w}{\partial y} = \frac{\mu}{1+\lambda_1}\frac{\partial^2 w}{\partial y^2} - \rho g^* cos\gamma\left(\beta_C(C-C_1)+\beta_T(T-T_1)\right) \\ +\frac{\sigma B_0^2 cos^2\alpha}{1+m^2cos^2\alpha}\left(mucos\alpha - w - mv_0 sin\alpha\right)\end{aligned} \tag{5.3}$$

$$\rho c_p v_0 \frac{\partial T}{dy} = k_f \frac{\partial^2 T}{\partial y^2} + \frac{\mu}{1+\lambda_1}\left(\left(\frac{\partial u}{\partial y}\right)^2 + \left(\frac{\partial w}{\partial y}\right)^2\right) \tag{5.4}$$

$$v_0 \frac{\partial C}{\partial y} = D \frac{\partial^2 C}{\partial y^2} + \frac{D K_T}{T_m} \frac{\partial^2 T}{\partial y^2} \tag{5.5}$$

in which λ_1 is the Jeffrey fluid parameter, K_T denotes the thermal diffusion ratio, c_p stands for the specific heat, k_f signifies thermal conductivity, μ embodies the viscosity coefficient, $m = \eta_1 \sigma B_0$ embodies the Hall parameter, ρ embodies the density, σ represents the electrical conductivity, β_T, and β_C are the thermal and solutal expansion respectively, D signifies the mass dissipation, T_m represents the mean temperature, gravitational acceleration is denoted by the symbol g^*, and γ_1 and γ_2 are coefficients associated with slip conditions.

From equation (5.1), we get $v = v_0 = constant$.

Boundary conditions are provided by

$$\begin{aligned} u &= \gamma_1 \frac{\partial u}{\partial y},\ w = 0,\ C = C_1,\ T = T_1,\ when\ y = -d. \\ u &= \gamma_2 \frac{\partial u}{\partial y},\ w = 0,\ C = C_2,\ T = T_2,\ when\ y = d. \end{aligned} \tag{5.6}$$

5.2.1 Case (a): Natural Convection

Natural convection flow is due to buoyancy forces, with the assumption that there is no external pressure gradient ($\frac{\partial p}{\partial x} = 0$).

similarity transformations for this given problem is given as

$$\eta = \frac{y}{d},\quad u = \frac{\nu Grf}{d},\quad w = \frac{\nu Grg}{d},\quad \phi = \frac{C - C_1}{C_2 - C_1},\ \theta = \frac{T - T_1}{T_2 - T_1} \tag{5.7}$$

By applying the similarity transformations to the equations (5.2) through (5.5), we yield the resulting transformed equations as follows:

$$\begin{aligned} f'' - Re(1 + \lambda_1) f' + (1 + \lambda_1)(\theta + N\phi) sin\gamma \\ - \frac{Ha^2 cos\alpha (1 + \lambda_1)}{1 + m^2 cos^2\alpha} \left(f cos\alpha - \lambda sin\alpha + mg cos^2\alpha \right) = 0 \end{aligned} \tag{5.8}$$

$$\begin{aligned} g'' - Re(1+\lambda_1)g' + (1+\lambda_1)(\theta + N\phi)cos\gamma \\ + \frac{Ha^2 cos^2\alpha(1+\lambda_1)}{1+m^2cos^2\alpha}\left(mfcos\alpha - g - m\lambda sin\alpha\right) = 0 \end{aligned} \tag{5.9}$$

$$\frac{BrGr^2}{(1+\lambda_1)}\left(f'^2 + g'^2\right) + \theta'' - RePr\theta' = 0 \tag{5.10}$$

$$ScSr\theta'' + \phi'' - ReSc\phi' = 0 \tag{5.11}$$

Where $Br = \mu\nu^2/k_f d^2(T_2 - T_1)$ pertains to the Brinkman number, $Re = \rho u_0 d/\mu$ indicates the Reynolds number, $Sr = DK_T(T_2 - T_1)/\nu T_m(C_2 - C_1)$ represents the Soret number, $Sc = \nu/D$ signifies the Schmidth number, $Gr = g^*\beta_T(T_2 - T_1)d^3/\nu^2$ corresponds to the Grashof number, $N = \beta_C(C_2 - C_1)/\beta_T(T_2 - T_1)$ indicate the buoyancy parameter, $Pr = \mu c_p/k_f$ pertains to Prandtl number, $Ha = dB_0\sqrt{\sigma/\mu}$ stands for magnetic parameter, $\lambda = Re/Gr$, $\beta_1 = \gamma_1/d$ and $\beta_2 = \gamma_2 d$ are defined as the slip parameters.

Boundary conditions (5.6) become

$$\begin{aligned} f = \beta_1 f',\ g = \phi = \theta = 0, \quad when\ \eta = -1 \\ f = \beta_2 f',\ g = 0,\ \phi = \theta = 1, \quad when\ \eta = 1 \end{aligned} \tag{5.12}$$

The shear stress, heat and mass transfer flows are given by

$$\tau_w = \left[\mu\frac{du}{dy}\right]|_{y=\pm d};\quad q_w = \left[-k_f\frac{dT}{dy}\right]|_{y=\pm d};\quad q_m = \left[-D\frac{dC}{dy}\right]|_{y=\pm d}$$

The dimensionless shear stress $C_f = \tau_w/\rho u_0^2$ is given by $ReC_{f_{1,2}} = f'(\eta)\,|_{\eta=-1,1}$.
The Sherwood number defined as $Sh = q_m d/D(C_2 - C_1)$ and the Nusselt number defined as $Nu = q_w d/k_f(T_2 - T_1)$ for this problem are given by

$$Sh_{1,2} = [-\phi'(\eta)]\,|_{\eta=-1,1};\quad Nu_{1,2} = [-\theta'(\eta)]\,|_{\eta=-1,1}\ .$$

Entropy Generation

The expression for the volumetric entropy generation rate is given as

$$S_{gen} = \frac{k_f}{T_0^2}\left[\frac{dT}{dy}\right]^2 + \frac{\mu}{T_0(1+\lambda_1)}\left[\left(\frac{du}{dy}\right)^2 + \left(\frac{dw}{dy}\right)^2\right] + \frac{RD}{C_0}\left(\frac{dC}{dy}\right)^2 + \frac{RD}{T_0}\left(\frac{dT}{dy}\right)\left(\frac{dC}{dy}\right) + \frac{\sigma B_0^2}{T_0}\left[w^2 + (ucos\alpha - v_0 sin\alpha)^2\right] \tag{5.13}$$

The initial expression on the right-hand side of equation (5.13) is linked to heat transfer; the subsequent term is indicative of viscous dissipation; the third and fourth terms represent mass transfer; the fifth term is because of magnetic field.

$$(S_{gen})_0 = \frac{k_f(T_2 - T_1)^2}{T_0^2 d^2} \tag{5.14}$$

By using equations (5.13) and (5.14), the formation of dimensionless entropy can be expressed as:

$$N_s = \frac{S_{gen}}{(S_{gen})_0}$$

$$N_s = (\theta')^2 + \frac{BrGr^2}{(1+\lambda_1)A_1}(f'^2 + g'^2) + \frac{\varepsilon B_1^2}{A_1^2}(\phi')^2 + \frac{\varepsilon B_1}{A_1}\theta'\phi' + \frac{BrGr^2Ha^2}{A_1}\left(g^2 + (fcos\alpha - \lambda sin\alpha)^2\right)$$

Here, Br, ε, B_1, Gr, Ha, and A_1 correspond to the brinkman number, dimensionless constant parameter, dimensionless concentration difference, grashof number, magnetic parameter, and dimensionless temperature difference, respectively, which are represented as

$$Br = \frac{\mu v^2}{k_f d^2(T_2 - T_1)},\ Gr = \frac{g^*\beta_T(T_2 - T_1)d^3}{v^2},\ \varepsilon = \frac{RDC_0}{k_f},$$
$$A_1 = \frac{T_2 - T_1}{T_0},\quad B_1 = \frac{C_2 - C_1}{C_0},\quad Ha = dB_0\sqrt{\frac{\sigma}{\mu}}$$

Result and Disscussion

The nonlinear and coupled flow eqns. (5.8) - (5.11) with respect to boundary conditions (5.12) are numerically solved by SQLM (as explained in chapter-2).

Figures 5.2 to 5.9 show the behaviour of $f(\eta)$, $g(\eta)$, $\theta(\eta)$, $\phi(\eta)$, and Ns for distinct values of Ha, α, m, Sr, λ_1, γ, β_1, and β_2 by taking Gr, N, Sc, Pr, Br, Re, A_1, B_1, ε, β_1, β_2 at 2, 2, 0.22, 0.71, 0.5, 2, 1, 1, 2, 0.1, 0.1, respectively.

In figure 5.2, the variations in f, g, θ, ϕ, and Ns are depicted across different values of magnetic parameter (Ha), while $Sr = 2$, $\alpha = \pi/4$, $m = 2$, $\lambda_1 = 0.5$, and $\gamma = \pi/3$ are held constant. Figures 5.2(a) and 5.2(b) exhibit the discernible augmentation of both flow velocity and cross-flow velocity with the progressive elevation of the magnetic parameter (Ha). It's noteworthy to highlight that the magnetic field is inclined at an angle $\alpha > 0$, leading to the absence of drag force generation. Figures 5.2(c) and 5.2(d) demonstrate the concurrent behavior of subsidence in fluid temperature and magnifies in concentration with elevated values of Ha. It is seen in figure 5.2(e) that entropy magnifies near the plates as Ha magnifies. Fluid dynamics can be influenced by a magnetic field owing to the magneto-hydrodynamic (MHD) phenomenon, which holds particular importance in the context of fluids that exhibit electrical conductivity. Magnetic parameters play a crucial role in power generation systems where a conducting fluid interacts with a magnetic field to generate electric power, high-speed trains, magnetic resonance imaging, paleomagnetism, metal sorting, etc.

In figure 5.3, the depictions illustrate the response of parameters f, g, θ, ϕ, and Ns regarding discrete orientations of the inclination angle (α), while keeping $Ha = 2$, $m = 2$, $\lambda_1 = 0.1$, $Sr = 2$, and $\gamma = \pi/3$ constant. Figures 5.3(a) and 5.3(b) elucidate a discernible decrease in both flow velocity and cross-flow velocity as the angle of inclination (α) experiences elevation. The behavior of temperature is depicted in Figure 5.3(c). Here, an observable reduction in fluid temperature is

noted with a rise in inclination angle (α). It is noted in figures 5.3(d) and 5.3(e) that as α rises, both fluid concentration and entropy generation exhibit augmentation. This is because, when the applied magnetic field's inclination angle decreases, the reduction in drag force on the net flow will also decrease. An inclined magnetic field is used in MHD generators to convert the kinetic energy of hot, electrically conducting fluid into electrical energy.

In figure 5.4, the graphical representation elucidates the effect of the parameter γ on the variables f, g, θ, ϕ, and Ns, while maintaining constant values for other parameters: $\alpha = \pi/4$, $Sr = 2$, $Ha = 2$, $\lambda_1 = 0.5$, and $m = 2$. Figures 5.4(a) and 5.4(b) exhibit contrasting trends. Specifically, the flow velocity demonstrates an ascending pattern, whereas the cross-flow velocity exhibits a descending trend as the parameter γ increases. This is because when the channel is inclined, a component of gravity acts along the channel direction. This component induces flow in an inclined direction due to the buoyancy force. The velocity increases as the inclined angle increases, leading to a higher flow rate in the direction of inclination. It is discerned that an elevation in the parameter γ leads to a fall in temperature and a simultaneous increase in fluid concentration, as depicted in figures 5.4(c) and 5.4(d). Entropy generation rises near $\eta = 1$ as γ rises, as shown in figure 5.4(e). This phenomenon arises from the observation that as the angle γ increases towards 90°, the plates transition to a vertical orientation. Consequently, the magnetic field applied in this scenario induces a drag force in alignment with the y-axis direction.

Figure 5.5 exemplifies the response of parameters f, g, θ, ϕ, and Ns to varying values of the Hall parameter (m), while maintaining constants for other parameters: $Sr = 2$, $Ha = 2$, $\lambda_1 = 0.5$, $\alpha = \pi/4$, and $\gamma = \pi/3$. As depicted in figure 5.5(a), a discernible reduction in flow velocity is observed with an escalation in m. It is seen from figures 5.5(b) and 5.5(c) that the cross-flow velocity and temperature both rise as m rises. A drag on flow velocity results from the generation of Hall

current perpendicular to both directions when a magnetic field acting at an angle $\alpha = \pi/4$. The fluid's temperature rises as a result of the extra charge produced by Hall current. The behaviors of fluid concentration and entropy generation near $\eta = 1$ are illustrated in figures 5.5(d) and 5.5(e), respectively. The concentration of fluid exhibits a rising trend, whereas entropy generation decreases with an increase in the Hall parameter (m). Hall current induces mixing in the fluid flow. Mixing can lead to better dispersion of solute particles, influencing concentration gradients. Enhanced mixing due to the Hall parameter effect results in more uniform concentration profiles in the flow. The hall current plays a crucial role in MHD flows, introducing supplementary intricacy to both fluid dynamics and magnetic field dispersion. The realm of magneto-hydrodynamics (MHD) holds significance within plasma physics, astrophysics, and engineering domains, such as MHD power generation and propulsion systems, where the interplay of magnetic fields and fluid behavior is paramount.

The influence of λ_1 on f, g, θ, ϕ, and Ns is displayed in figure 5.6, while keeping other parameters at $Sr = 5$, $m = 2$, $\alpha = \pi/4$, $Ha = 2$, and $\gamma = \pi/3$. As delineated in figures 5.6(a) and 5.6(b), as the parameter λ_1 increases, both velocity in the main flow direction and cross-flow velocity experience elevation. Higher values of the Jeffrey fluid parameter indicate more significant shear-thinning behavior. The shear-thinning behavior affects the flow profiles. As the fluid moves near the solid boundaries, where the shear rate is higher, a higher Jeffrey fluid parameter results in lower viscosity, allowing for faster flow. Figure 5.6(c) shows that as the parameter λ_1 increases, the dimensionless temperature decreases. The behaviors of fluid concentration and entropy generation are portrayed in figures 5.6(d) and 5.6(e), respectively. Both parameters exhibit a positive trend with increasing λ_1. This implies that higher values of λ_1 contribute to elevated fluid concentration and a slight increase in entropy generation near $\eta = 1$. This is because the shear thinning

behavior due to the Jeffrey fluid parameter affects the thickness of the concentration boundary layer. A thinner boundary layer facilitates faster diffusion of solute particles, leading to an increase in the concentration profile.

In figure 5.7, the graphical depictions showcase the fluctuations in parameters f, g, θ, ϕ, and Ns in response to varying values of the Soret number (Sr), while Ha=2, m=2, α=$\pi/4$, λ_1=0.5, and $\gamma = \pi/3$ are held constant. Figures 5.7(a) and 5.7(b) illustrate that as the Soret number (Sr) escalates, both the flow velocity and cross-flow velocity exhibit an increase. The result in figure 5.7(c) indicates that the higher Soret numbers lead to lower fluid temperatures within the system. This phenomenon is attributed to the fact that an augmentation in the Soret parameter induces an escalation in the temperature gradient, consequently resulting in heightened velocities. Figures 5.7(d) and 5.7(e) indicate that higher values of Sr contribute to elevated fluid concentration and entropy generation within the system. This happens because as the Soret parameter increases, the thermophoretic effect strengthens. Consequently, there is a greater mass flux of particles in response to a given temperature gradient. This effect can enhance mass transfer rates, leading to more rapid changes in concentration. This increased mass transfer results in higher entropy generation due to additional irreversibilities in the system.

In figure 5.8, the visualizations portray the responses of parameters f, g, θ, ϕ, and Ns to varying values of the parameter β_1, while keeping Ha=2, m=2, α=$\pi/4$, λ_1=0.5, Sr=2, and $\gamma = \pi/3$ constant. Figures 5.8(a) and 5.8(b) demonstrate a noticeable pattern. Increasing the parameter β_1 is associated with higher values of both flow velocity and cross-flow velocity. This is because the fluid particles at the solid boundary are not anchored, allowing for easier movement and, consequently, higher velocity. Figure 5.8(c) reveals that the temperature of the fluid rises with a rise in β_1. A higher slip leads to increased dissipation, affecting the overall temperature distribution in the flow. Figures 5.8(d), and 5.8(e) demonstrate that higher

values of β_1 contribute to reduced fluid concentration and entropy production within the system.

In figure 5.9, the graphical depictions present the variations in parameters f, g, θ, ϕ, and Ns corresponding to different values of the parameter β_2, while keeping Ha=2, m=2, α=$\pi/3$, λ_1=0.5, Sr=2, and $\gamma = \pi/3$ constant. Figure 5.9(a) illustrates that an augmentation in the parameter β_2 is correlated with a decrease in the flow velocity. Figure 5.9(b) shows that the cross-flow velocity increases as the value of the parameter β_2 rises. Figure 5.9(c) reveals that the fluid temperature decreases as the parameter β_2 rises. An elevated slip results in greater dissipation, impacting the overall temperature distribution within the flow. The elevated value of the parameter β_2 corresponds to an increase in fluid concentration and a slight elevation in entropy production near $\eta = 1$, as depicted in figures 5.9(d) and 5.9(e). This occurs because when the fluid slips along the solid boundaries at $\eta = 1$, it can lead to heightened friction and shear within the boundary layer. These added dissipative effects result in increased entropy generation near $\eta = 1$.

Table 5.1 comprehensively depicts the fluctuations in various parameters such as the Jeffrey fluid parameter (λ_1), magnetic parameter (Ha), Soret number (Sr), Hall number (m), inclination angle (α), and channel angle of inclination (γ), while keeping other variables at Re=2, Gr=2, Pr=0.71, Br=0.5, Sc=0.22, $N = 2$, $\beta_1 =$ 0.1, and β_2=0.1. The data in the table reveals that skin friction increases on the $\eta = -1$ plate and decreases on the $\eta = 1$ plate in sync with higher values of Ha, Sr, α, and channel inclination angle (γ), but decreases with increasing values of the Hall number (m). Conversely, skin friction reduces with higher values of the Jeffrey fluid parameter (λ_1). Table 5.1 also shows that as Ha, Sr, α, and γ increase, the heat transfer rate decreases for both plates. However, the Hall parameter (m) exhibits an opposite trend. Moreover, the rate of heat transfer increases on the left plate and decreases on the right plate with higher values of the Jeffrey fluid parameter

(λ_1). Additionally, mass transfer rate increases with higher values of Ha, Sr, α, and γ, while exhibiting the opposite trend for m. The mass transfer rate decreases on the left plate and increases on the right plate with an increase in the Jeffrey fluid parameter (λ_1), as shown in Table 5.1.

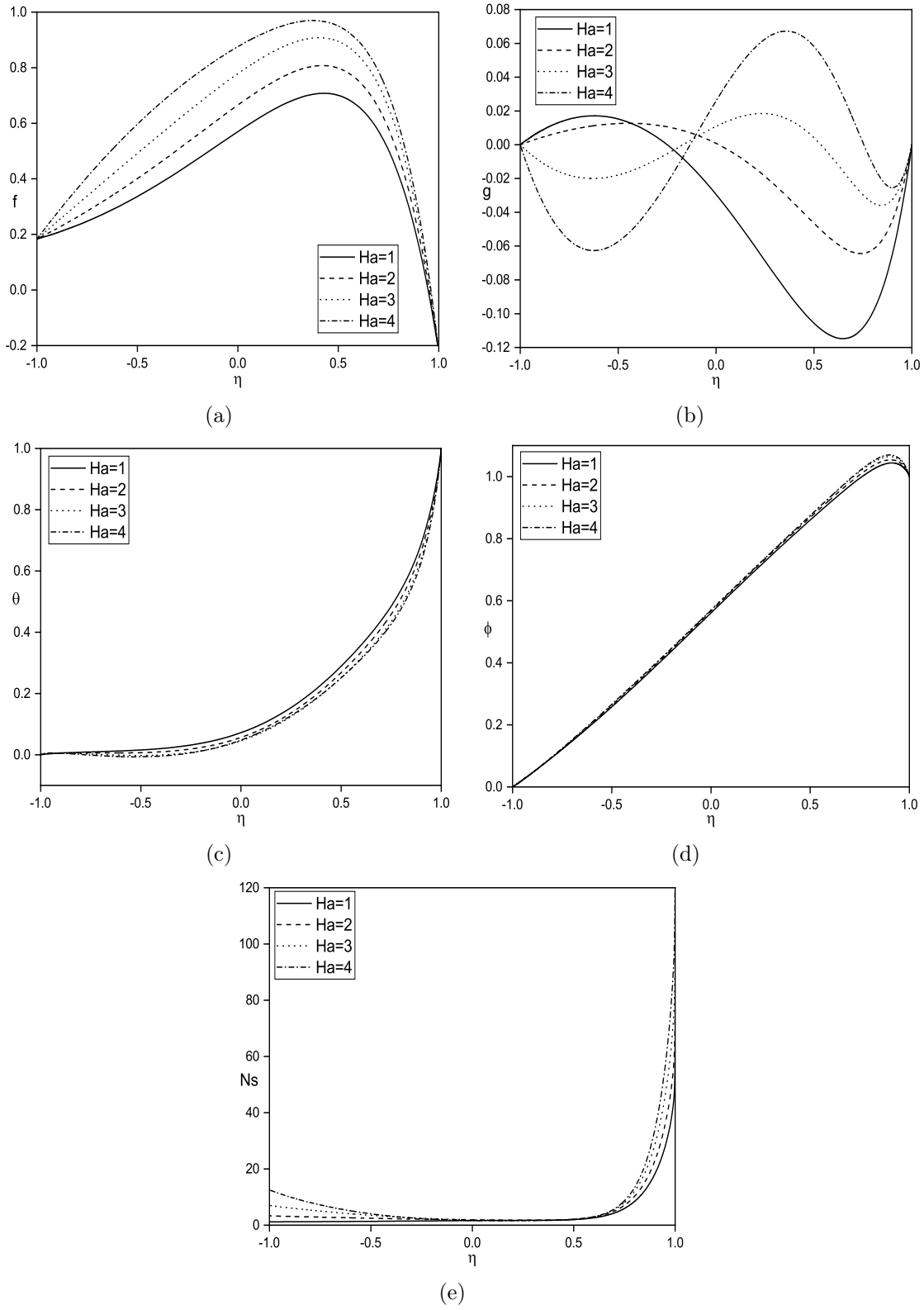

Figure 5.2: *Influence of magnetic parameter (Ha) on (a) $f(\eta)$, (b) $g(\eta)$, (c) $\theta(\eta)$, (d) $\phi(\eta)$, and (e) Ns.*

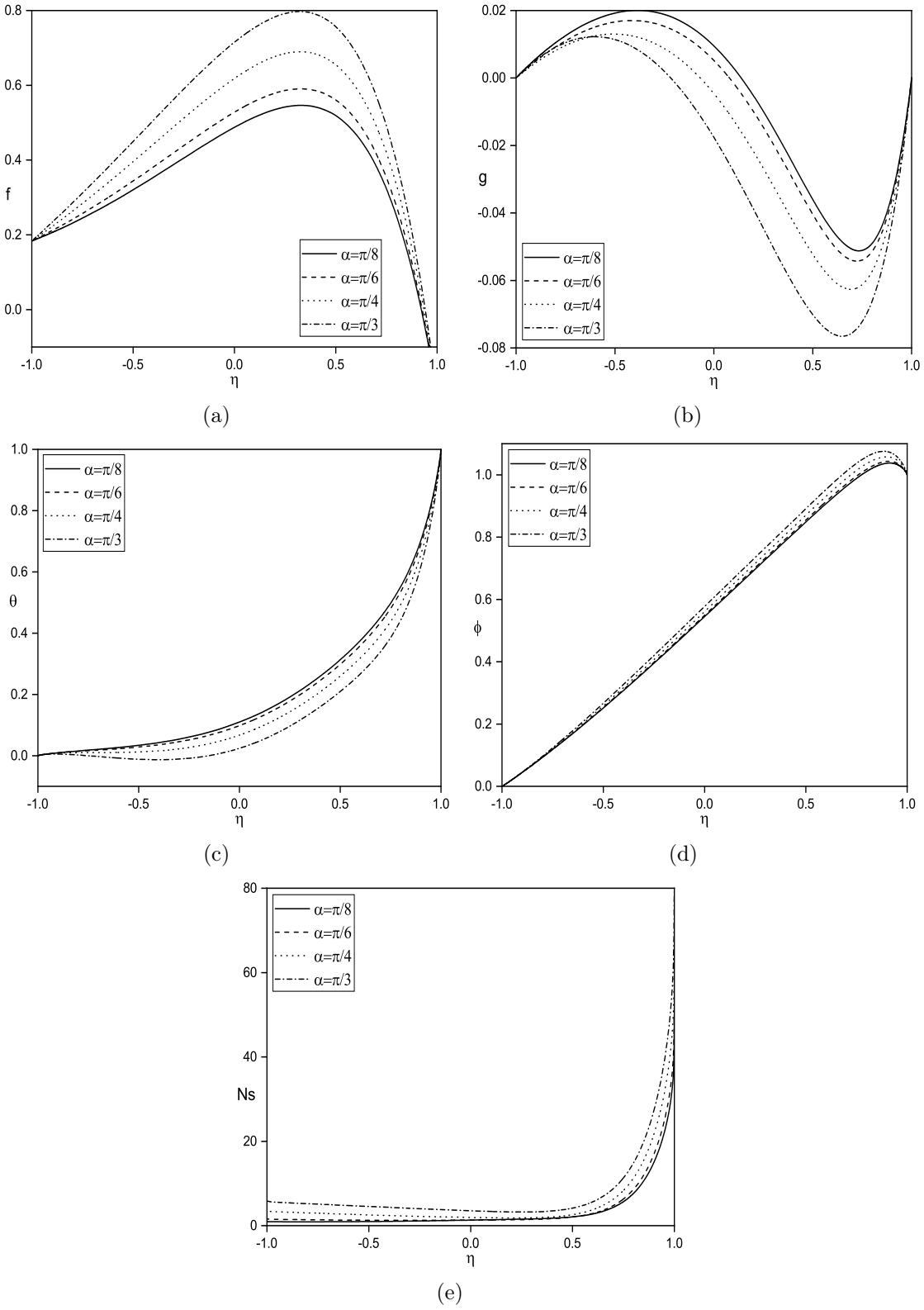

Figure 5.3: *Influence of inclination angle (α) on (a) $f(\eta)$, (b) $g(\eta)$, (c) $\theta(\eta)$, (d) $\phi(\eta)$, and (e) Ns.*

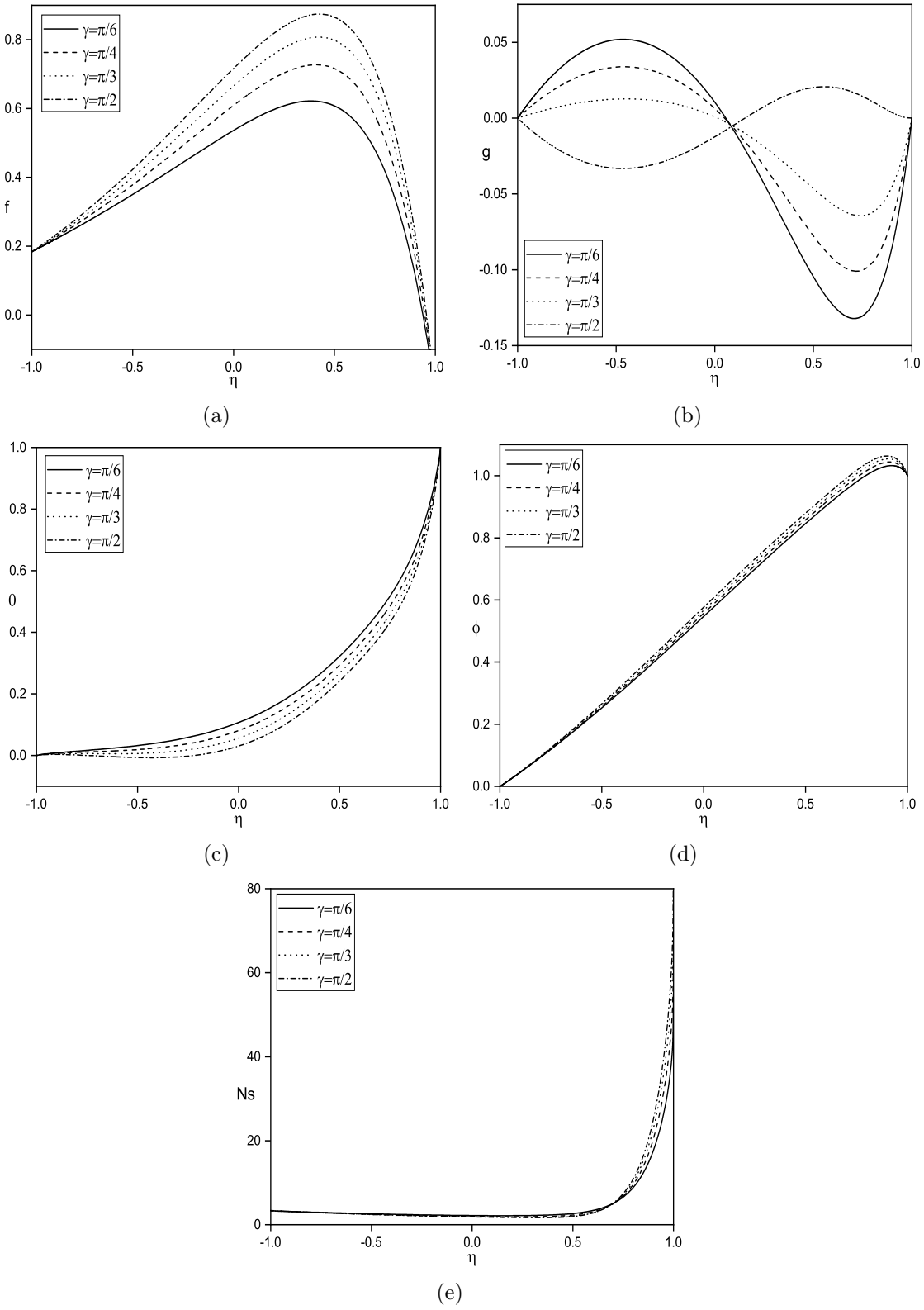

Figure 5.4: *Influence of channel angle of inclination (γ) on (a) $f(\eta)$, (b) $g(\eta)$, (c) $\theta(\eta)$, (d) $\phi(\eta)$, and (e) Ns.*

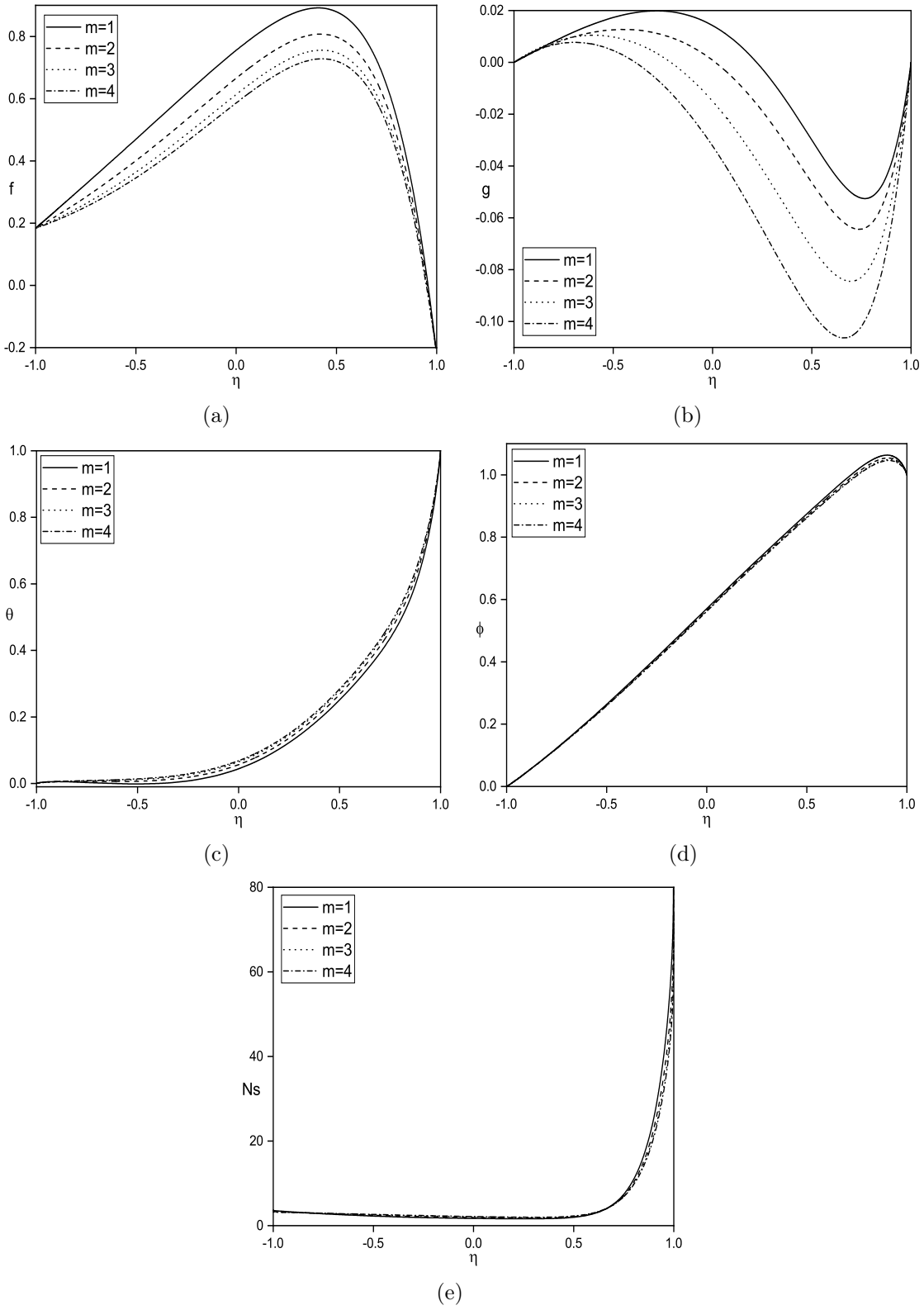

Figure 5.5: *Influence of hall current (m) on (a) $f(\eta)$, (b) $g(\eta)$, (c) $\theta(\eta)$, (d) $\phi(\eta)$, and (e) Ns.*

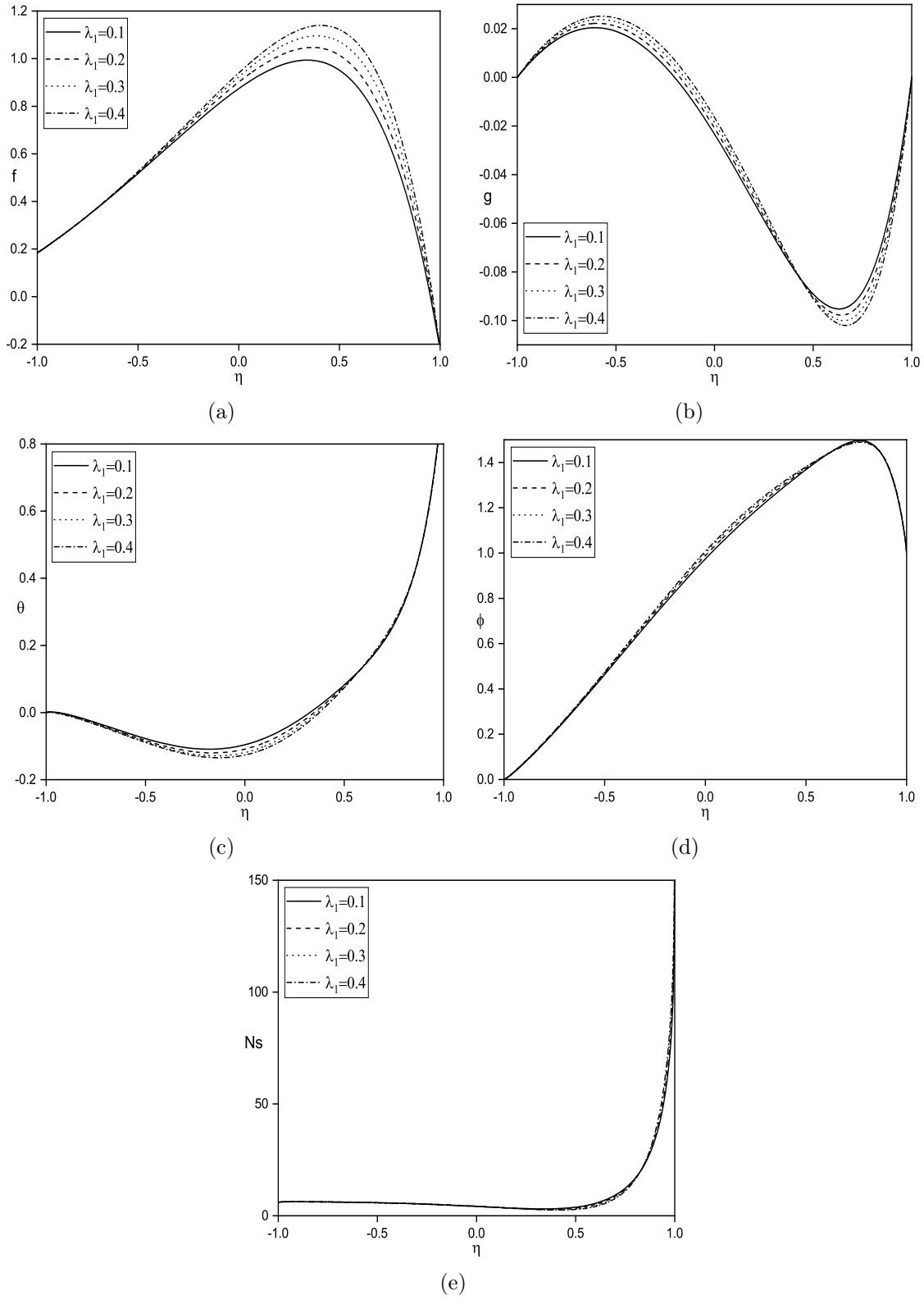

Figure 5.6: *Influence of Jeffrey fluid parameter (λ_1) on (a) $f(\eta)$, (b) $g(\eta)$, (c) $\theta(\eta)$, (d) $\phi(\eta)$, and (e) Ns.*

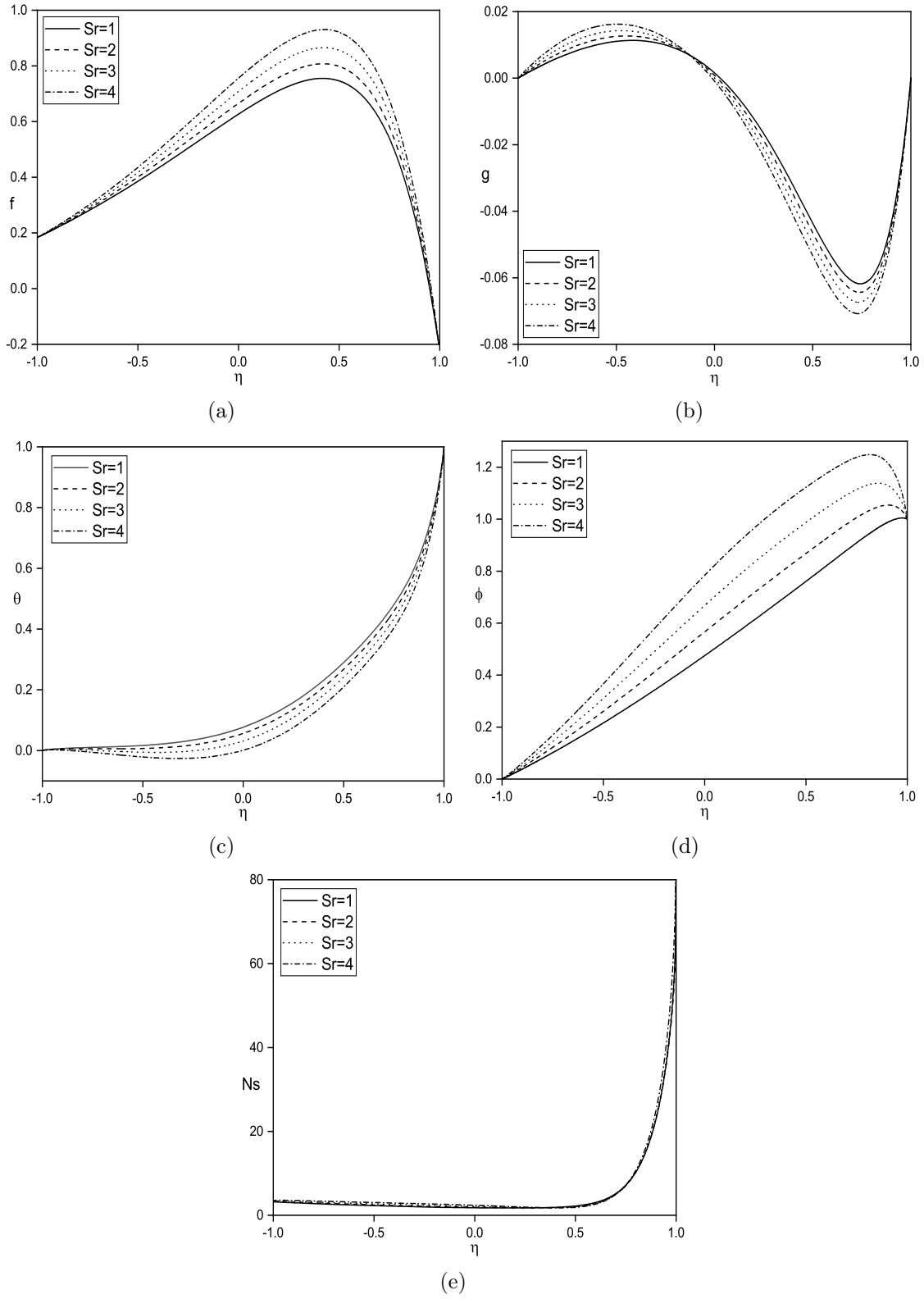

Figure 5.7: *Influence of Soret number (Sr) on (a) $f(\eta)$, (b) $g(\eta)$, (c) $\theta(\eta)$, (d) $\phi(\eta)$, and (e) Ns.*

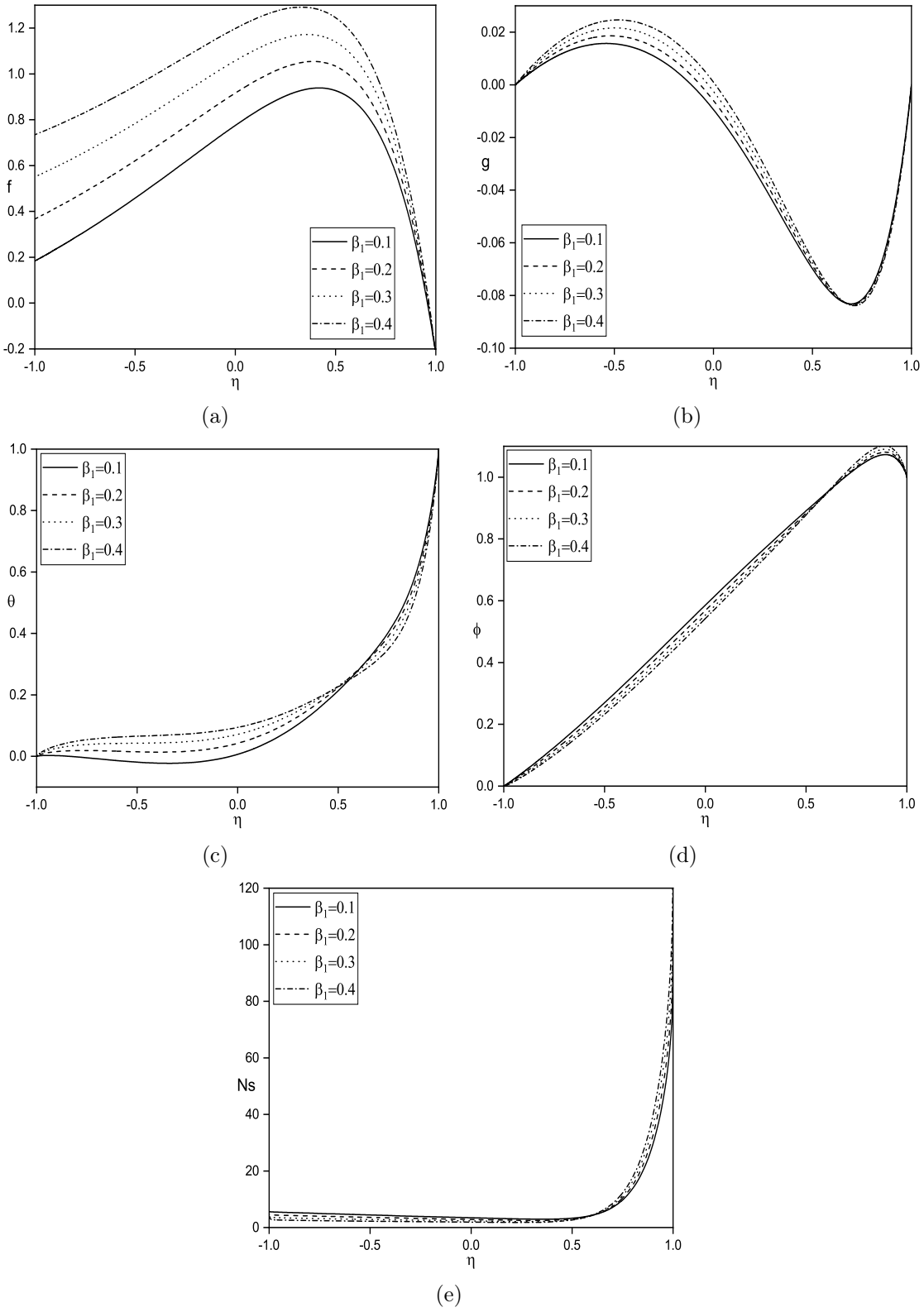

Figure 5.8: *Influence of slip condition (β_1) on (a) $f(\eta)$, (b) $g(\eta)$, (c) $\theta(\eta)$, (d) $\phi(\eta)$, and (e) Ns.*

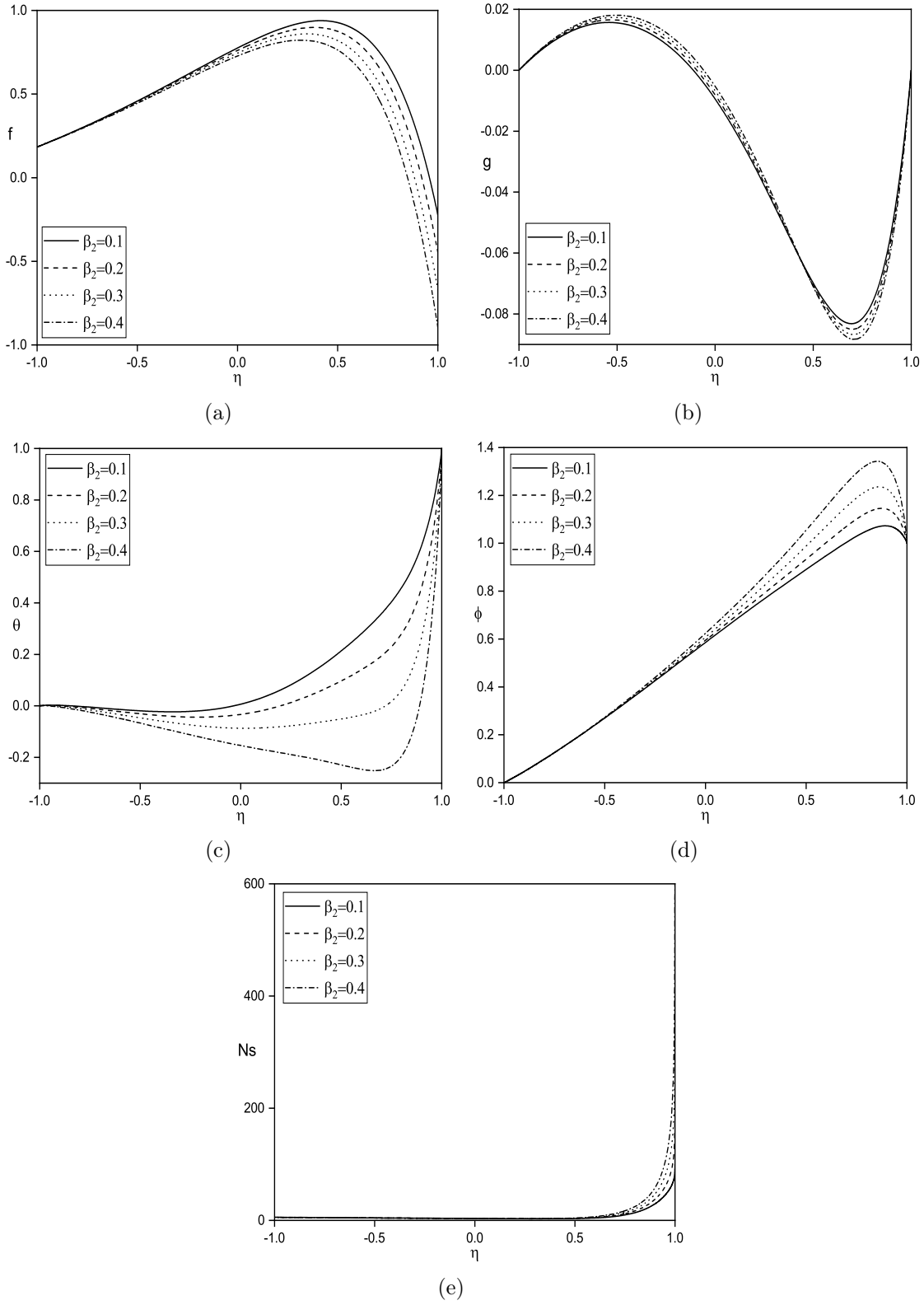

Figure 5.9: *Influence of slip condition (β_2) on (a) $f(\eta)$, (b) $g(\eta)$, (c) $\theta(\eta)$, (d) $\phi(\eta)$, and (e) Ns.*

Table 5.1: Overview of the impact of various values of α, Sr, Ha, m, γ and λ_1 on skin friction ($Cf_{1,2}$), rate of heat transfer ($Nu_{1,2}$) and mass transfer ($Sh_{1,2}$).

Ha	Sr	m	α	λ_1	γ	Cf_1	Cf_2	Nu_1	Nu_2	Sh_1	Sh_2
1	2	2	$\pi/3$	0.2	$\pi/3$	0.22678	-3.38201	-0.29039	-7.67815	-0.34881	2.46179
2	2	2	$\pi/3$	0.2	$\pi/3$	0.37472	-3.81323	-0.42761	-8.58568	-0.28540	2.86414
3	2	2	$\pi/3$	0.2	$\pi/3$	0.59747	-4.32660	-0.62654	-9.67099	-0.19451	3.34504
2	1	2	$\pi/3$	0.2	$\pi/3$	0.35478	-3.63391	-0.42096	-8.15135	-0.30135	0.95933
2	2	2	$\pi/3$	0.2	$\pi/3$	0.37472	-3.81323	-0.42761	-8.58568	-0.28540	2.86414
2	3	2	$\pi/3$	0.2	$\pi/3$	0.39636	-4.01036	-0.43264	-9.07484	-0.26435	4.99950
2	2	1	$\pi/3$	0.2	$\pi/3$	0.55038	-4.22350	-0.58366	-9.45923	-0.21377	3.25147
2	2	2	$\pi/3$	0.2	$\pi/3$	0.37472	-3.81323	-0.42761	-8.58568	-0.28540	2.86414
2	2	3	$\pi/3$	0.2	$\pi/3$	0.28778	-3.58438	-0.34749	-8.10287	-0.32229	2.65006
2	2	2	0	0.2	$\pi/3$	0.06925	-2.80344	-0.14782	-6.33032	-0.41812	1.86217
2	2	2	$\pi/4$	0.2	$\pi/3$	0.37472	-3.81323	-0.42761	-8.58568	-0.28540	2.86414
2	2	2	$\pi/3$	0.2	$\pi/3$	0.48631	-4.21221	-0.50397	-9.58565	-0.24584	3.31009
2	2	2	$\pi/3$	0.2	$\pi/3$	0.48683	-4.61141	-0.45622	-9.64363	-0.26638	3.33607
2	2	2	$\pi/3$	0.3	$\pi/3$	0.48553	-5.01154	-0.41514	-9.69241	-0.28413	3.35786
2	2	2	$\pi/3$	0.4	$\pi/3$	0.48307	-5.41226	-0.37985	-9.73289	-0.29947	3.37586
2	2	2	$\pi/3$	0.2	$\pi/4$	0.43757	-3.91268	-0.44750	-8.23809	-0.27666	2.7111
2	2	2	$\pi/3$	0.2	$\pi/3$	0.45864	-4.21439	-0.45248	-8.83504	-0.27186	2.97646
2	2	2	$\pi/3$	0.2	$\pi/2$	0.48683	-4.61141	-0.45622	-9.64363	-0.26638	3.33607

5.2.2 Case (b): Mixed Convection

Consider a mixed convection flow occurring with both natural (buoyancy-driven) and forced (externally-driven) convection mechanisms.

similarity transformations for this given problem is given as

$$\eta = \frac{y}{d},\ u = u_0 f,\ w = u_0 g,\ \phi = \frac{C - C_1}{C_2 - C_1},\ \theta = \frac{T - T_1}{T_2 - T_1} \tag{5.15}$$

Upon employing dimensionless transformations to equations (5.2) to (5.5), the resulting transformed equations are obtained as follows:

$$\begin{aligned} f'' - Re(1+\lambda_1)f' + \frac{Gr}{Re}(1+\lambda_1)(\theta + N\phi)sin\gamma \\ -\frac{Ha^2 cos\alpha(1+\lambda_1)}{1+m^2cos^2\alpha}\left(fcos\alpha - \lambda sin\alpha + mgcos^2\alpha\right) - A(1+\lambda_1) = 0 \end{aligned} \tag{5.16}$$

$$\begin{aligned} g'' - Re(1+\lambda_1)g' - \frac{Gr}{Re}(1+\lambda_1)(\theta + N\phi)cos\gamma \\ +\frac{Ha^2 cos^2\alpha(1+\lambda_1)}{1+m^2cos^2\alpha}\left(mfcos\alpha - g - m\lambda sin\alpha\right) = 0 \end{aligned} \tag{5.17}$$

$$\frac{Br}{(1+\lambda_1)}\left(f'^2 + g'^2\right) + \theta'' - RePr\theta' = 0 \tag{5.18}$$

$$ScSr\theta'' + \phi'' - ReSc\phi' = 0 \tag{5.19}$$

Where $Br = \mu\nu^2/k_f d^2(T_2 - T_1)$ pertains the Brinkman number, $Re = \rho u_0 d/\mu$ indicates Reynolds number, $Sr = DK_T(T_2 - T_1)/\nu T_m(C_2 - C_1)$ represents the Soret number, $A = d^2\partial p/\partial x u_0\mu$, $Sc = \nu/D$ signifies the Schmidth number, $\beta_1 = \gamma_1/d$, $\beta_2 = \gamma_2/d$ are defined as the slip parameters, $Gr = g^*\beta_T(T_2 - T_1)d^3/\nu^2$ corresponds to the Grashof number, $Pr = \mu c_p/k_f$ pertains to Prandtl number, $Ha = dB_0\sqrt{\sigma/\mu}$ stands for magnetic parameter, $\lambda = Re/Gr$, and $N = \beta_C(C_2 - C_1)/\beta_T(T_2 - T_1)$ indicates the buoyancy parameter.

Boundary conditions (5.6) become

$$\begin{aligned} \eta = -1: \quad & f = \beta_1 f', \ g = \phi = \theta = 0 \\ \eta = -1: \quad & f = \beta_2 f', \ g = 0, \ \phi = \theta = 1 \end{aligned} \tag{5.20}$$

The shear stress, heat and mass transfer flows for this problem are given by

$$\tau_w = \left[\mu \frac{du}{dy}\right] |_{y=\pm d}; \quad q_w = \left[-k_f \frac{dT}{dy}\right] |_{y=\pm d}; \quad q_m = \left[-D \frac{dC}{dy}\right] |_{y=\pm d}$$

The dimensionless shear stress $C_f = \tau_w/\rho u_0^2$ is given by $ReC_{f_{1,2}} = f'(\eta) \mid_{\eta=-1,1}$. The Sherwood number defined as $Sh = q_m d/D(C_2 - C_1)$ and the Nusselt number defined as $Nu = q_w d/k_f(T_2 - T_1)$ for this problem are given by

$$Sh_{1,2} = [-\phi'(\eta)] \mid_{\eta=-1,1}; \quad Nu_{1,2} = [-\theta'(\eta)] \mid_{\eta=-1,1} .$$

Entropy Generation

The expression for the volumetric entropy generation rate is given as

$$\begin{aligned} S_{gen} = & \frac{k_f}{T_0^2}\left[\frac{dT}{dy}\right]^2 + \frac{\mu}{T_0(1+\lambda_1)}\left[\left(\frac{du}{dy}\right)^2 + \left(\frac{dw}{dy}\right)^2\right] + \frac{RD}{C_0}\left(\frac{dC}{dy}\right)^2 \\ & + \frac{RD}{T_0}\left(\frac{dT}{dy}\right)\left(\frac{dC}{dy}\right) + \frac{\sigma B_0^2}{T_0}\left[w^2 + (ucos\alpha - v_0 sin\alpha)^2\right] \end{aligned} \tag{5.21}$$

The initial expression on the right-hand side of equation (5.21) is linked to heat transfer, the subsequent term is because of energy dissipation due to fluid viscosity, the third and fourth terms represent mass transfer, and the fifth term is because of magnetic field.

The definition of characteristic rate of entropy generation denoted by $(S_{gen})_0$ is defined as

$$(S_{gen})_0 = \frac{k_f(T_2 - T_1)^2}{T_0^2 d^2} \tag{5.22}$$

By using equations (5.21) and (5.22), the formation of dimensionless entropy can be expressed as:

$$N_s = \frac{S_{gen}}{(S_{gen})_0}$$

$$N_s = (\theta')^2 + \frac{Br}{(1+\lambda_1)A_1}(f'^2 + g'^2) + \frac{\varepsilon B_1^2}{A_1^2}(\phi')^2 + \frac{\varepsilon B_1}{A_1}\theta'\phi' + \frac{BrHa^2}{A_1}\left(g^2 + (fcos\alpha - \lambda sin\alpha)^2\right)$$

Here A_1, Br, B_1, Ha, and ε correspond to dimensionless temperature difference, Brinkman number, dimensionless concentration difference, magnetic parameter, and dimensionless constant parameter, respectively, which are represented as

$$Br = \frac{\mu v^2}{k_f d^2 (T_2 - T_1)},\ \varepsilon = \frac{RDC_0}{k_f},\ A_1 = \frac{T_2 - T_1}{T_0},\ B_1 = \frac{C_2 - C_1}{C_0},\ Ha = dB_0\sqrt{\frac{\sigma}{\mu}}$$

Results and discussion

The nonlinear and coupled flow Eqs. (5.16)-(5.19) with boundary conditions (5.20) are numerically solved using SQLM (as explained in chapter-2).

Figures 5.10 to 5.17 show the behavior of $f(\eta)$, $g(\eta)$, $\theta(\eta)$, $\phi(\eta)$, and Ns for distinct values of Ha, α, m, Sr, λ_1, γ, β_1, and β_2 by taking A, Pr, Br, Re, Gr, N, Sc, A_1, B_1, ε, β_1, β_2 at 1, 0.71, 0.5, 2, 0.5, 2, 0.22, 1, 1, 2, 0.1, 0.1 respectively.

In figure 5.10, the variations in f, g, θ, ϕ, and Ns are displayed for different values of Ha, while $Sr = 2$, $\alpha = \pi/4$, $m = 2$, $\lambda_1 = 0.5$, and $\gamma = \pi/3$ are held constant. Figures 5.10(a) and 5.10(b) demonstrate a clear trend of increasing flow velocity and cross-flow velocity with rising Hartmann number (Ha). It's noteworthy to highlight that the magnetic field is inclined at an angle $\alpha > 0$, leading to the absence of drag force generation. Figures 5.10(c) and 5.10(d) demonstrate the concurrent behavior of subside in fluid temperature and magnifies in concentration with elevated values of Ha. It is seen in figure 5.10(e) that entropy magnifies as Ha magnifies. The fluid dynamics can be influenced by a magnetic field owing to the magneto-hydrodynamic

phenomenon, which holds particular importance in the context of fluids that exhibit electrical conductivity.

In figure 5.11, the depictions illustrate the response of parameters f, g, θ, ϕ, and Ns concerning distinct values of the angle of inclination (α), while keeping $Ha = 2$, $m = 2$, $\lambda_1 = 0.5$, $Sr = 2$, and $\gamma = \pi/3$ constant. Figures 5.11(a) and 5.11(b) show that the flow velocity increase and cross-flow velocity decrease as the angle of inclination (α) experiences elevation. The behavior of temperature is depicted in figure 5.11(c). Here, an observable reduction in fluid temperature is noted with a rise in inclination angle (α). This behavior is caused by an increase in the inclination angle of the applied magnetic field, which reduces drag force and hence increases net flow in the fluid. It is noted in figures 5.11(d) and 5.11(e) that as α rises, both fluid concentration and entropy generation exhibit augmentation. An inclined magnetic field is used in MHD generators to convert the kinetic energy of hot, electrically conducting fluid into electrical energy.

In figure 5.12, the graphical representation elucidates the effect of the parameter γ on the variables f, g, θ, ϕ, and Ns, while maintaining constant values for other parameters: $\alpha = \pi/4$, $Sr = 10$, $Ha = 2$, $\lambda_1 = 0.5$, and $m = 2$. The two figures, 5.12(a) and 5.12(b), the flow velocity and cross-flow velocity shows an upward trend with increasing value of γ. This change in trend occurs as the value of the parameter γ increases. It is discerned that an elevation in the parameter γ leads to a fall in temperature and a simultaneous increase in fluid concentration, as depicted in figures 5.12(c) and 5.12(d). Entropy generation slightly rises near $\eta = 1$ as γ rises as shown in figure 5.12(e). This phenomenon arises from the observation that as the angle γ increases towards 90°, the plates transition to a vertical orientation. Consequently, the magnetic field applied in this scenario induces a drag force in alignment with the y-axis direction.

Figure 5.13 exemplifies the response of parameters f, g, θ, ϕ, and Ns to varying

values of the Hall parameter (m), while maintaining constants for other parameters: $Sr = 2$, $Ha = 2$, $\lambda_1 = 0.1$, $\alpha = \pi/4$, and $\gamma = \pi/3$. As depicted in figure 5.13(a), a discernible reduction in flow velocity is observed with an escalation in m. It is seen from figures 5.13(b) and 5.13(c) that the cross-flow velocity and temperature both rise as m rises. This is because the magnetic field is inclined at an angle of $\alpha = \pi/4$, which causes the hall effect to generate charge in the direction of inclined plates, thereby making it unable to act as a drag on the fluid. As mentioned earlier, the fluid's temperature rises as a result of the extra charge that the hall current generates. The behaviors of fluid concentration and entropy generation are illustrated in figures 5.13(d) and 5.13(e), respectively. Both parameters exhibit a rising trend with an increase in the Hall parameter (m). The Hall current plays a crucial role in MHD flows, introducing supplementary intricacy to both fluid dynamics and magnetic field dispersion. The realm of magneto-hydrodynamics (MHD) holds significance within plasma physics, astrophysics, and engineering domains, such as MHD power generation and propulsion systems, where the interplay of magnetic fields and fluid behavior is paramount.

The influence of Jeffrey fluid parameter (λ_1) on f, g, θ, ϕ, and Ns are displayed in figure 5.14, while keeping other parameters at $Sr = 2$, $Ha = 4$, $m = 2$, $\alpha = \pi/4$, and $\gamma = \pi/3$. As shown in figures 5.14(a) and 5.14(b), an increase in parameter λ_1 leads to a rise in both the flow velocity and cross-flow velocity. The dimensionless temperature is observed to increase as the parameter λ_1 increases as shown in figure 5.14(c). This is because higher values of the Jeffrey fluid parameter indicate a more elastic and less viscous fluid. Therefore, increasing the Jeffrey fluid parameter tends to enhance the fluid's elasticity, which increases the fluid's net flow and temperature profile. The behaviors of fluid concentration and entropy generation are portrayed in figures 5.14(d) and 5.14(e), respectively. Both parameters show that higher values of λ_1 contribute to a decrease in fluid concentration and entropy generation.

In figure 5.15, the graphical depictions showcase the fluctuations in parameters f, g, θ, ϕ, and Ns in response to varying values of the Soret number (Sr), while Ha=2, m=2, α=$\pi/4$, λ_1=0.5, and $\gamma = \pi/3$ are held constant. Figures 5.15(a) and 5.15(b) illustrate that as the Soret number (Sr) escalates, both the flow velocity and cross-flow velocity exhibit an increase. The result in figure 5.15(c) indicates that the higher Soret numbers lead to lower fluid temperatures within the system. This phenomenon is attributed to the fact that an augmentation in the Soret parameter induces an escalation in the temperature gradient, consequently resulting in heightened velocities. Figures 5.15(d) and 5.15(e) indicate that higher values of Sr contribute to elevated fluid concentration and entropy generation within the system. The Soret parameter plays a role in mass transfer in multi-component fluid systems and can significantly impact flow behavior, particularly in situations involving heat and mass transfer.

In figure 5.16, the visualizations portray the responses of parameters f, g, θ, ϕ, and Ns to varying values of the parameter β_1, while keeping Ha=2, m=2, α=$\pi/4$, λ_1=0.5, Sr=2, and $\gamma = \pi/3$ constant. Figures 5.16(a) and 5.16(b) show that increasing the parameter β_1 is associated with an increase in flow velocity and a decrease in cross-flow velocity. Figure 5.16(c) reveals that the temperature of fluid rises with a rise in β_1. Figures 5.16(d) and 5.16(e) demonstrate that higher values of β_1 contribute to reduced fluid concentration and entropy production within the system.

In figure 5.17, the graphical depictions present the variations in parameters f, g, θ, ϕ, and Ns corresponding to different values of the parameter β_2, while keeping Ha=2, m=2, α=$\pi/4$, λ_1=0.5, Sr=2, and $\gamma = \pi/3$ constant. Figures 5.17(a) and 5.17(b) illustrate that an augmentation in the parameter β_2 is correlated with a decrease in both flow velocity and cross-flow velocity. Figure 5.17(c) reveals that the fluid temperature decreases as the parameter β_2 rises. The elevated value of the

parameter β_2 corresponds to an increase in fluid concentration and a slight elevation in entropy production near $\eta = 1$, as depicted in figures 5.17(d) and 5.17(e). Slip conditions are commonly used when modeling fluid flow over surfaces with high slip characteristics, such as superhydrophobic surfaces.

Table 5.2 presents the variations in magnetic parameter (Ha), Hall number (m), Soret number (Sr), inclination angle (α), Jeffrey fluid parameter (λ_1), and channel angle of inclination (γ) while keeping other parameters at Re=2, Gr=0.5, Pr=0.71, Br=0.5, Sc=0.22, $N = 2$, $A = 1$, $\beta_1 = 0.1$, and β_2=0.1. The table indicates that the skin friction increases at the $\eta = -1$ plate and decreases at the $\eta = 1$ plate with an enhancement in Ha, Sr, α, γ, and λ_1. Conversely, the Hall parameter (m) has the opposite effect. Additionally, Table 5.2 demonstrates that as m, Sr, α, λ_1, and γ increase, the heat transfer rate increases at the left plate and decreases at the right plate, while the opposite tendency is seen for the Hall parameter (m). Moreover, the rate of mass transfer diminishes at the left plate and amplifies at the right plate with an amplification in the hall parameter Ha, Sr, α, λ_1, and γ, While the Hall parameter shows the opposite tendency.

5.3 Conclusions

The present investigation aims to analyze the entropy generation of a steady inclined magnetohydrodynamic Jeffrey flow occurring between inclined parallel plates. This investigation considers the influence of both the Soret number and Hall current. The original complex equations describing the system are transformed into dimensionless equations through the use of similarity transformations. The non-dimensional equations are solved with SQLM. Based on the findings of our study, we have observed that the flow velocity and cross-flow velocity increase as the Soret parameter, magnetic parameter, and Jeffrey fluid parameter increase. Conversely, both velocities decrease with an increase in the Hall parameter. Additionally, we have found

that fluid temperature decreases while concentration rises with a rise in the Soret parameter, magnetic parameter, inclination angle, and channel angle of inclination. Moreover, we have discovered that the entropy of the system increases with the augmentation of the magnetic parameter and inclination angle. However, it diminishes as the β_1 parameter increases.

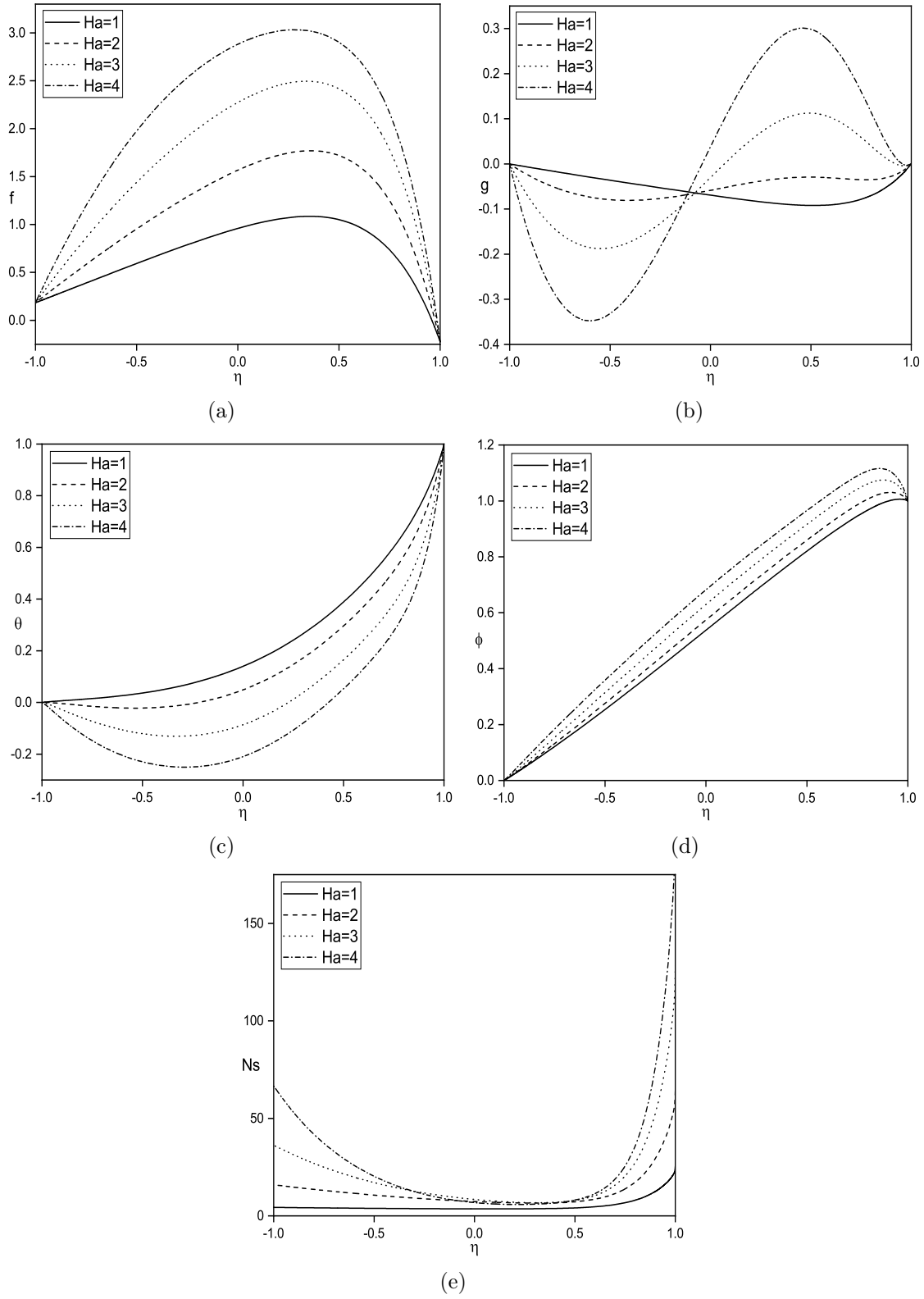

Figure 5.10: *Impact of magnetic parameter (Ha) on (a) $f(\eta)$, (b) $g(\eta)$, (c) $\theta(\eta)$, (d) $\phi(\eta)$, and (e) Ns.*

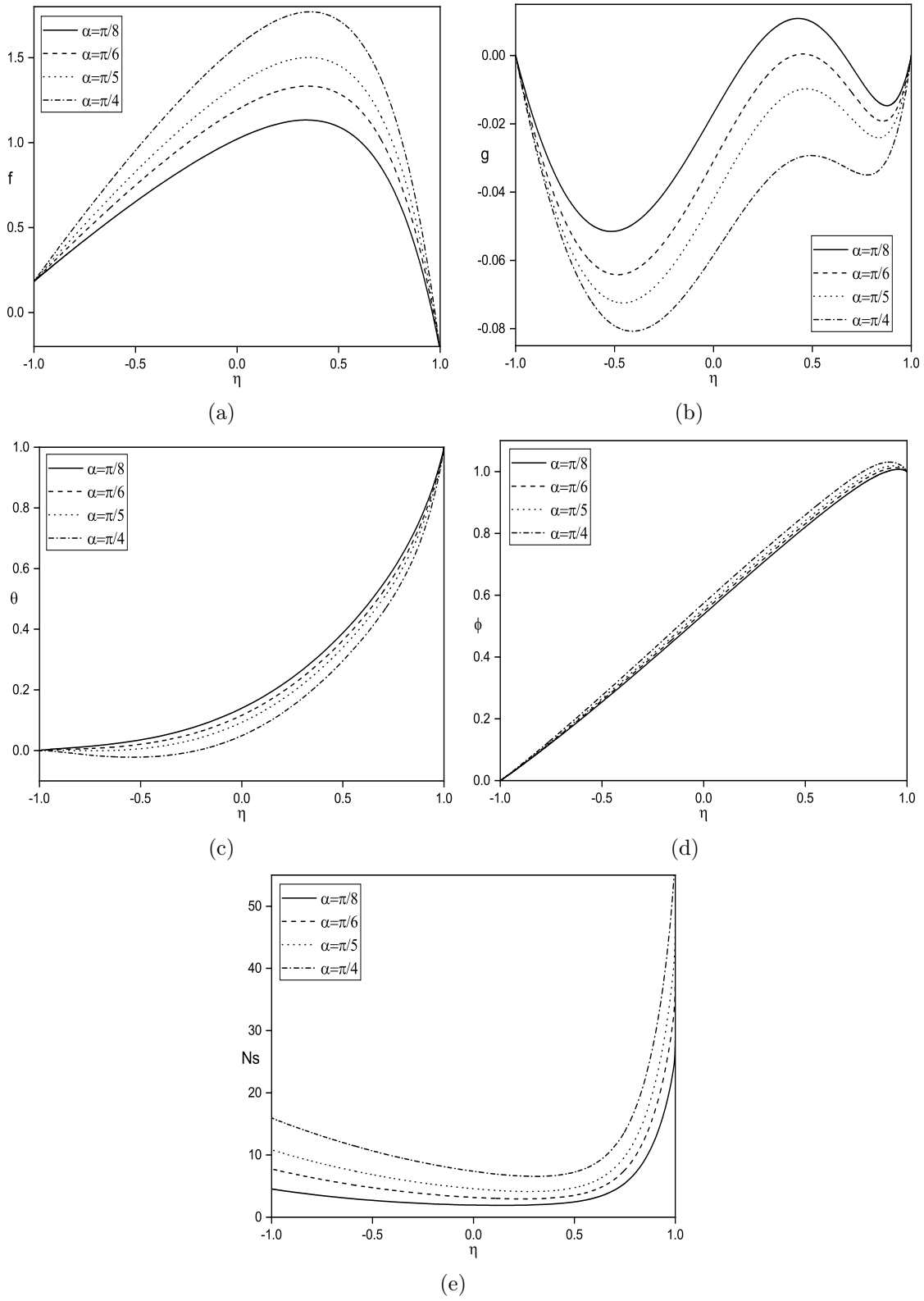

Figure 5.11: *Impact of inclination angle (α) on (a) $f(\eta)$, (b) $g(\eta)$, (c) $\theta(\eta)$, (d) $\phi(\eta)$, and (e) Ns.*

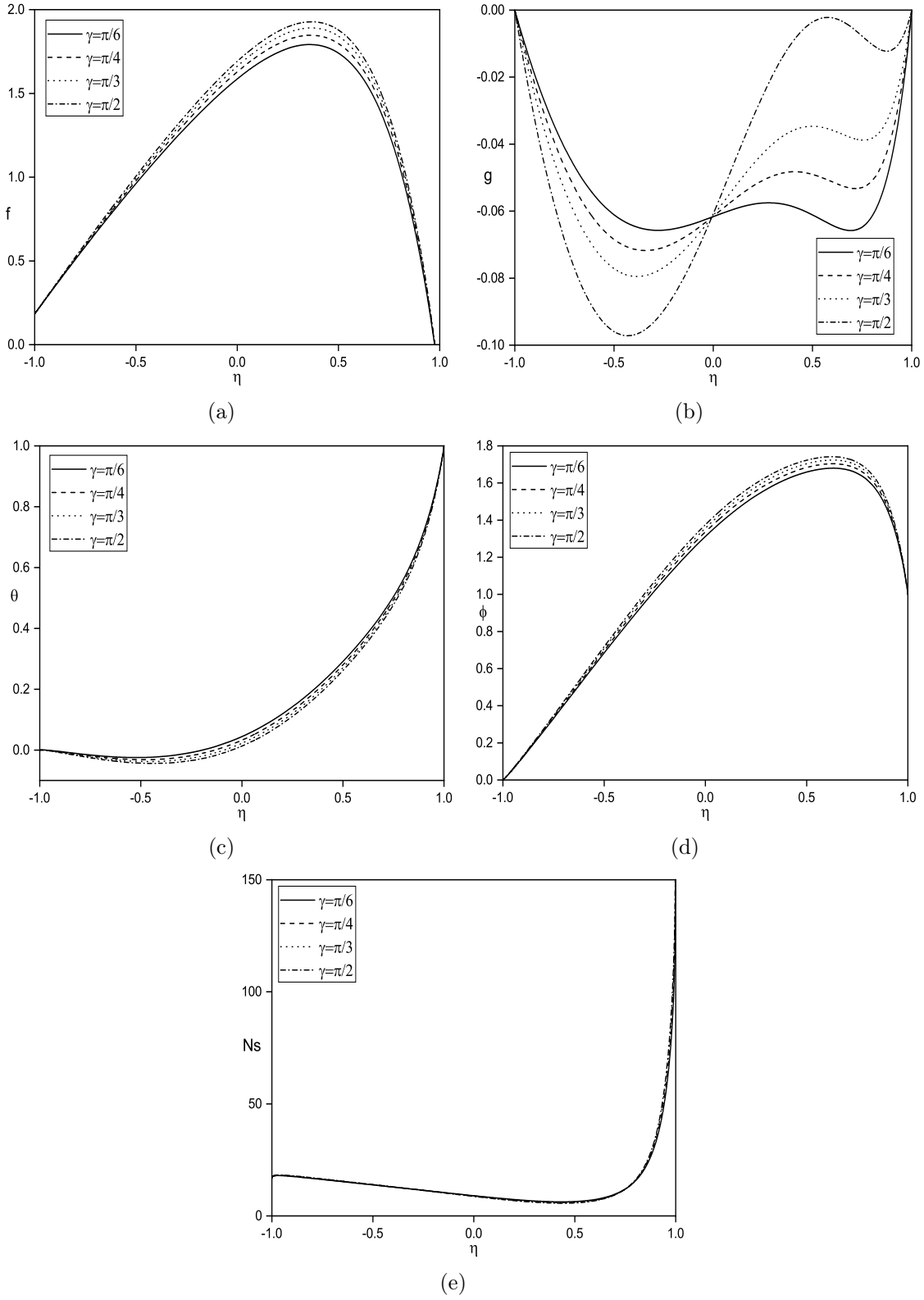

Figure 5.12: *Impact of channel angle of inclination (γ) on (a) $f(\eta)$, (b) $g(\eta)$, (c) $\theta(\eta)$, (d) $\phi(\eta)$, and (e) Ns.*

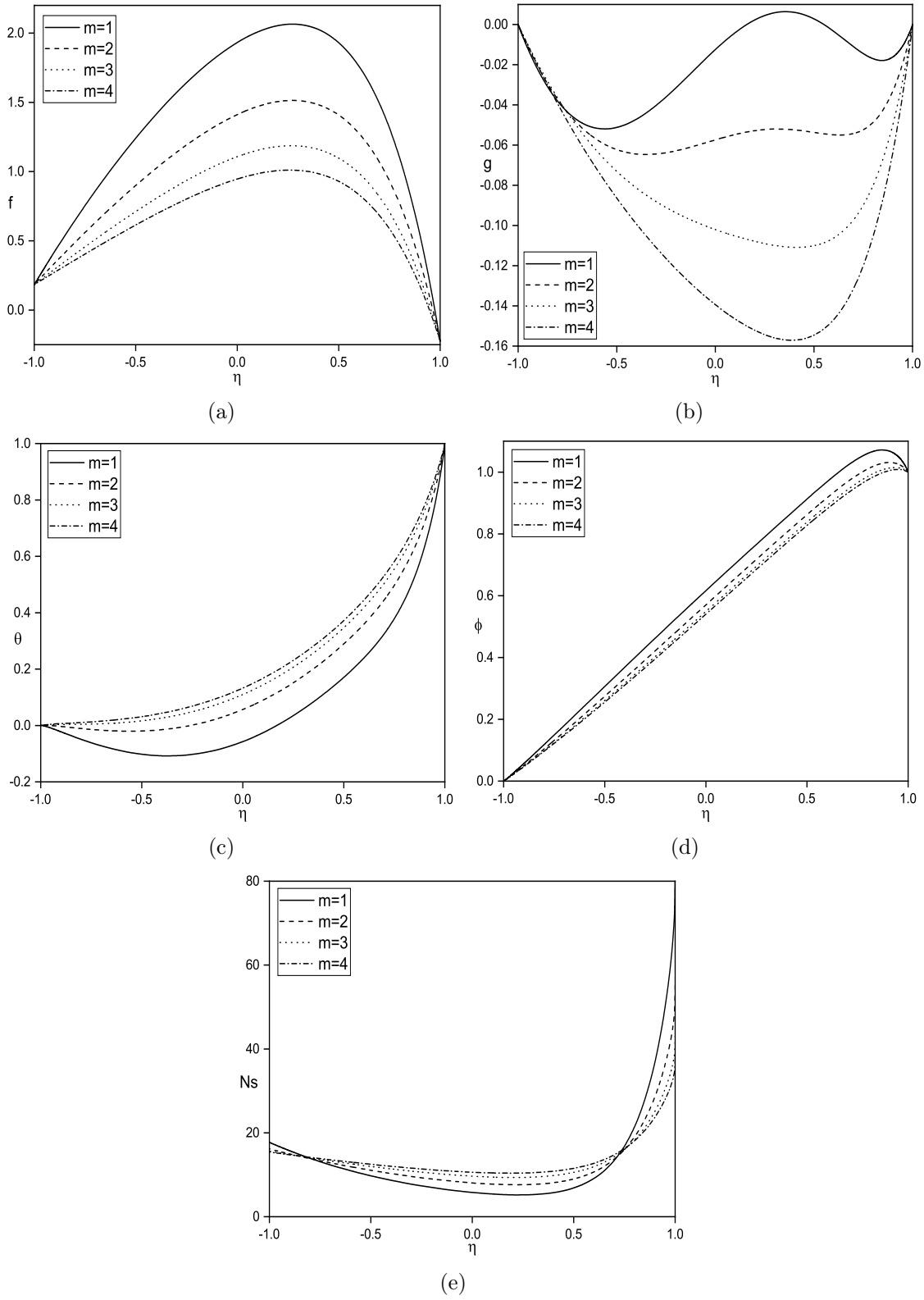

Figure 5.13: *Impact of hall current (m) on (a) $f(\eta)$, (b) $g(\eta)$, (c) $\theta(\eta)$, (d) $\phi(\eta)$, and (e) Ns.*

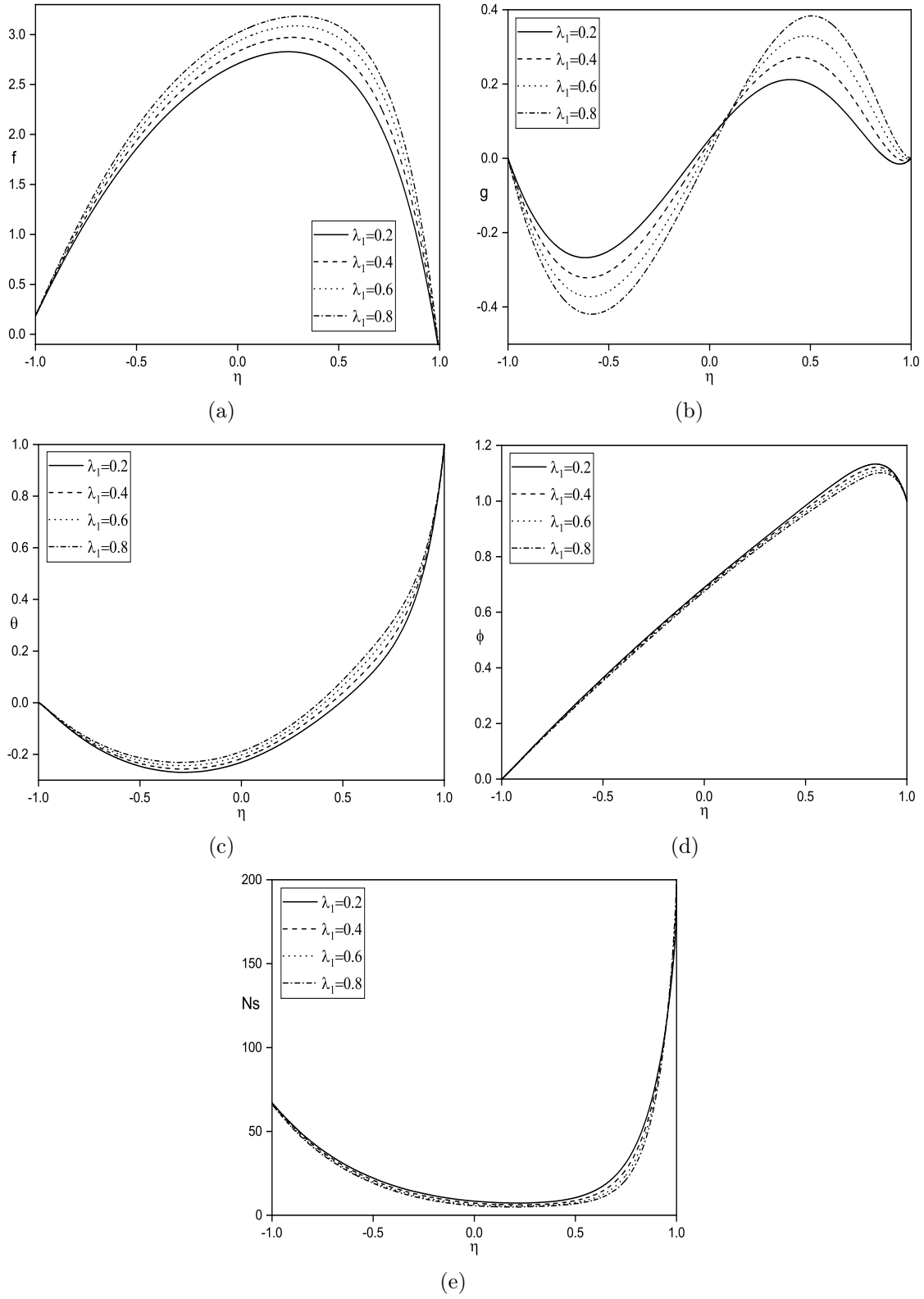

Figure 5.14: *Impact of Jeffrey fluid parameter (λ_1) on (a) $f(\eta)$, (b) $g(\eta)$, (c) $\theta(\eta)$, (d) $\phi(\eta)$, and (e) Ns.*

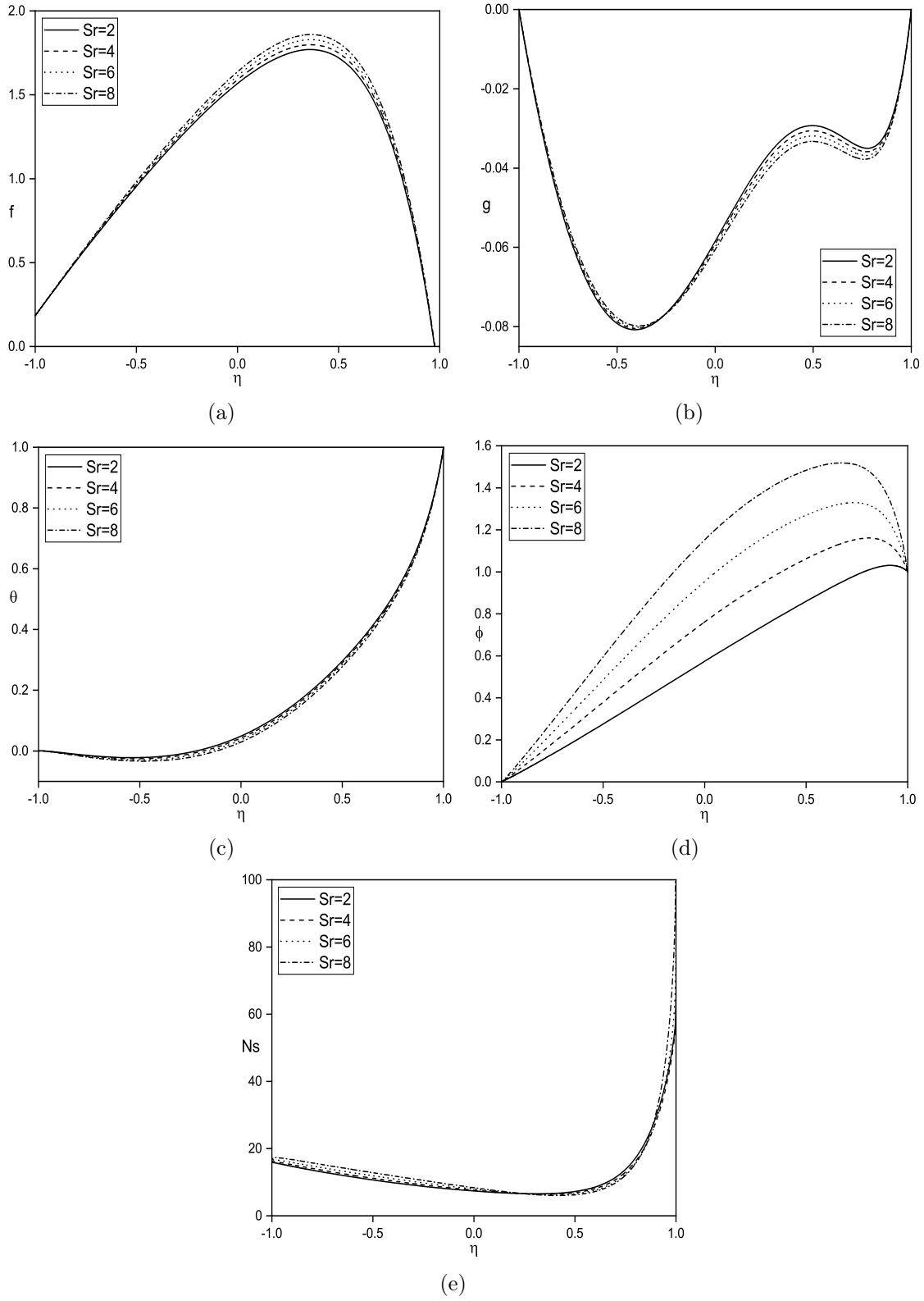

Figure 5.15: *Impact of Soret number (Sr) on (a) $f(\eta)$, (b) $g(\eta)$, (c) $\theta(\eta)$, (d) $\phi(\eta)$, and (e) Ns.*

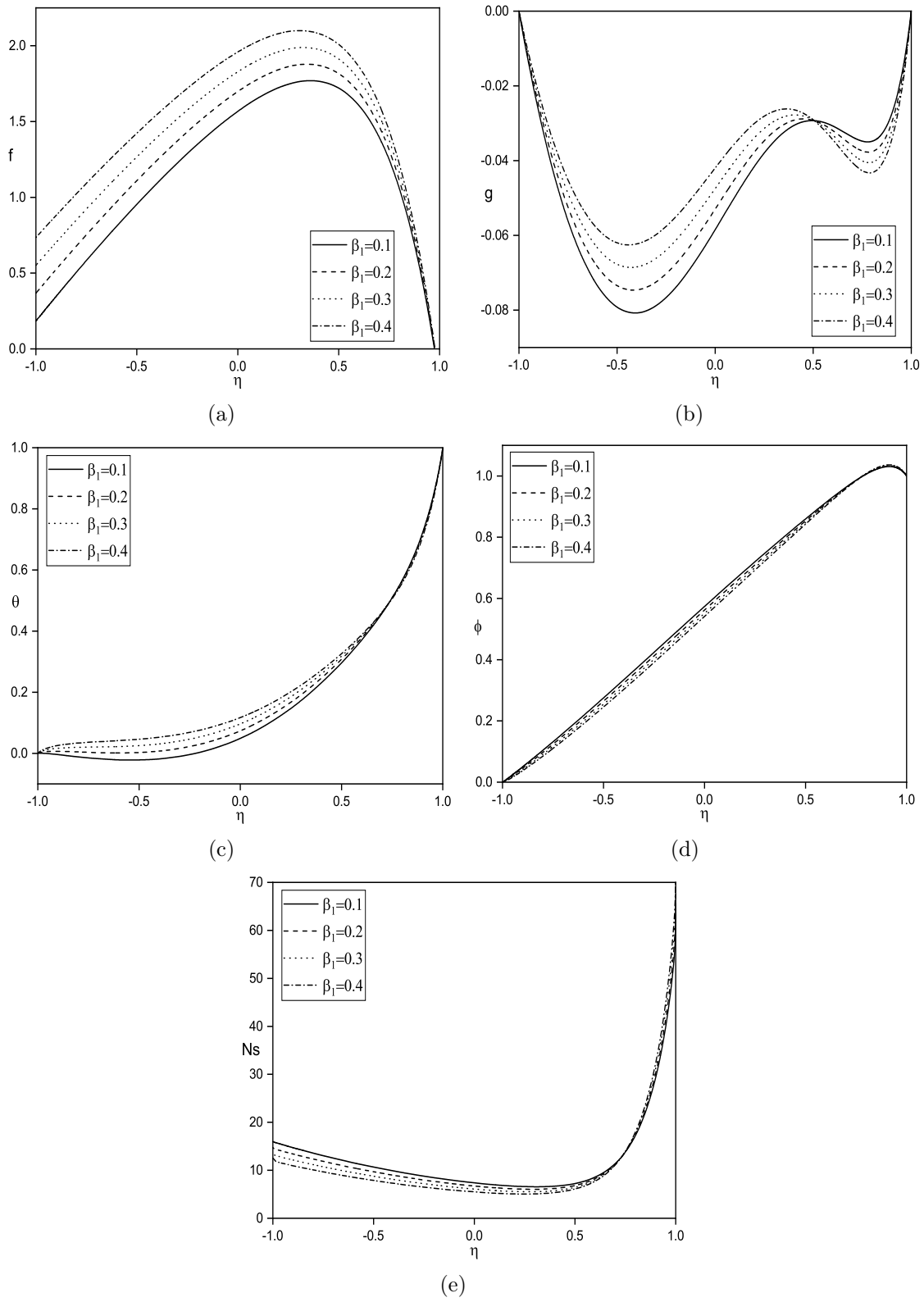

Figure 5.16: *Impact of slip condition (β_1) on (a) $f(\eta)$, (b) $g(\eta)$, (c) $\theta(\eta)$, (d) $\phi(\eta)$, and (e) Ns.*

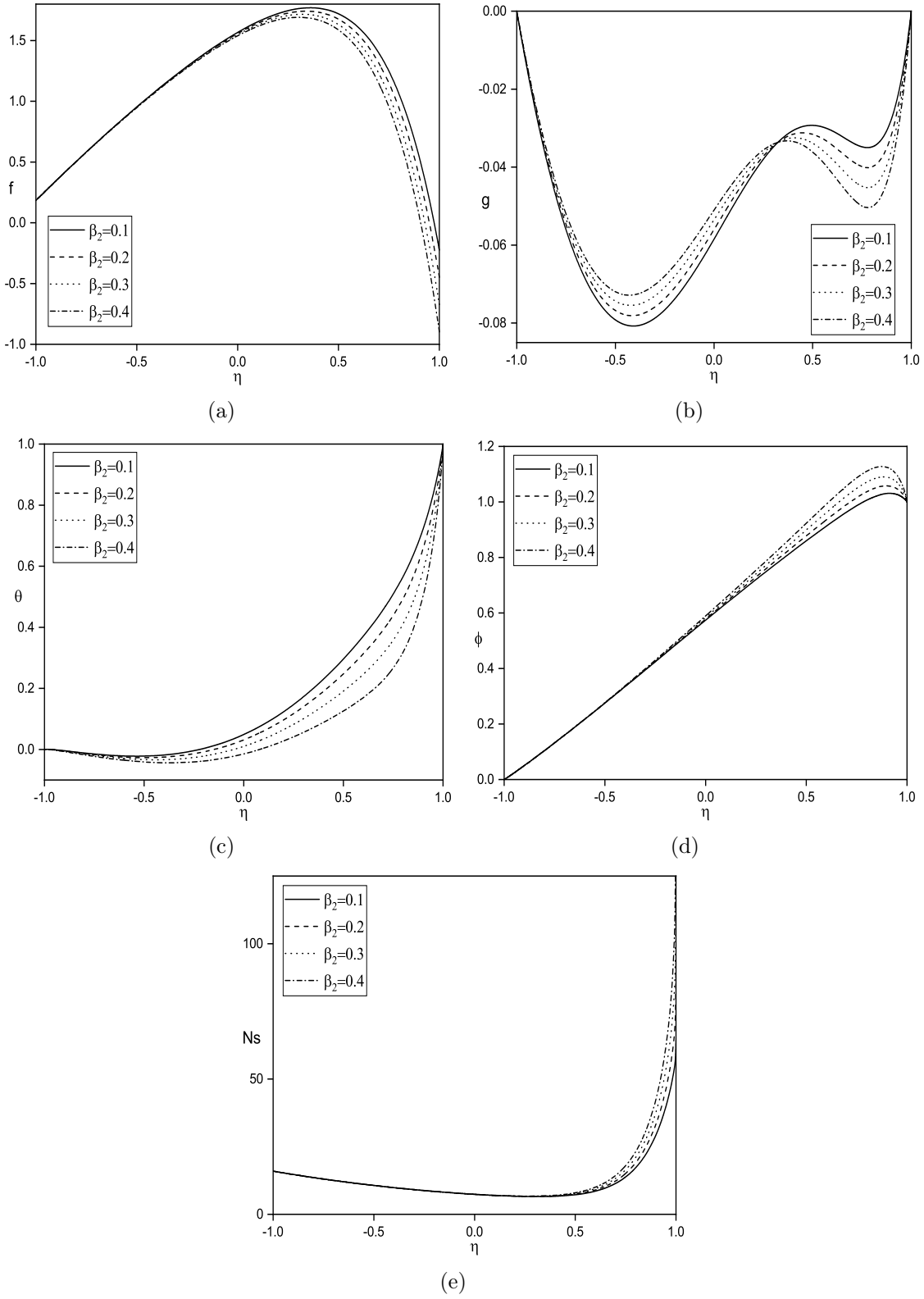

Figure 5.17: *Impact of slip condition (β_2) on (a) $f(\eta)$, (b) $g(\eta)$, (c) $\theta(\eta)$, (d) $\phi(\eta)$, and (e) Ns.*

Table 5.2: Overview of the impact of various values of α, Sr, Ha, m, γ and λ_1 on skin friction ($Cf_{1,2}$), rate of heat transfer ($Nu_{1,2}$) and mass transfer ($Sh_{1,2}$).

Ha	Sr	m	α	λ_1	γ	Cf_1	Cf_2	Nu_1	Nu_2	Sh_1	Sh_2
1	2	2	$\pi/3$	0.2	$\pi/3$	0.90447	-5.04259	-0.24585	-3.88913	-0.37556	0.78747
2	2	2	$\pi/3$	0.2	$\pi/3$	1.98903	-8.88627	-0.24218	-6.67250	-0.38363	2.03570
3	2	2	$\pi/3$	0.2	$\pi/3$	3.60053	-13.70138	0.02524	-11.21032	-0.42436	4.07928
2	1	2	$\pi/3$	0.2	$\pi/3$	1.98141	-8.82120	-0.24608	-6.61423	-0.33220	0.62879
2	2	2	$\pi/3$	0.2	$\pi/3$	1.98903	-8.88627	-0.24218	-6.67250	-0.35363	2.03570
2	3	2	$\pi/3$	0.2	$\pi/3$	1.99678	-8.95250	-0.23815	-6.73213	-0.37621	3.46980
2	2	1	$\pi/3$	0.2	$\pi/3$	2.77267	-11.34876	-0.14888	-8.85188	-0.37304	3.01627
2	2	2	$\pi/3$	0.2	$\pi/3$	1.98903	-8.88627	-0.24218	-6.67250	-0.35363	2.03570
2	2	3	$\pi/3$	0.2	$\pi/3$	1.45354	-7.07590	-0.26307	-5.26972	-0.35211	1.40581
2	2	2	$\pi/5$	0.2	$\pi/3$	1.33392	-6.31130	-0.28670	-4.66617	-0.35250	1.13446
2	2	2	$\pi/4$	0.2	$\pi/3$	1.59240	-7.28590	-0.28339	-5.37036	-0.35301	1.45025
2	2	2	$\pi/3$	0.2	$\pi/3$	1.98903	-8.88627	-0.24218	-6.67250	-0.35363	2.03570
2	2	2	$\pi/3$	0.2	$\pi/3$	1.98903	-8.88627	-0.24218	-6.67250	-0.35363	2.03570
2	2	2	$\pi/3$	0.3	$\pi/3$	2.01486	-9.69870	-0.21425	-6.75141	-0.36566	2.07068
2	2	2	$\pi/3$	0.4	$\pi/3$	2.03504	-10.51405	-0.19128	-6.81910	-0.37569	2.10054
2	2	2	$\pi/3$	0.2	$\pi/4$	1.98186	-8.78563	-0.24659	-6.59584	-0.35238	2.00128
2	2	2	$\pi/3$	0.2	$\pi/3$	1.98903	-8.88627	-0.24218	-6.67250	-0.35363	2.03570
2	2	2	$\pi/3$	0.2	$\pi/2$	1.99570	-8.96843	-0.23814	-6.73484	-0.35482	2.06372

Part IV

Conclusions and Scope for Future Work

Chapter 6

Conclusions and Scope for Future Work

The study of entropy generation in Jeffrey fluid is valuable both theoretically and practically. Exploring the complex dynamics of non-Newtonian fluids provides deeper insights into thermodynamic processes, leading to practical advancements in various engineering and industrial applications. It gives an idea of power consumption by the thermodynamic losses. Entropy generation helps in determine the irreversibility of system by various factors. The primary contributors to entropy generation and energy loss in a thermodynamic system are fluid viscosity, diffusion processes, frictional forces, and chemical reactions between solid surfaces.

In this thesis, We analyzed the entropy generation of Jeffrey fluid flow model with different physical parameters. According to the references already in existence, the current investigation covers a adequate results.

The main results indicate the following findings

Conclusions from Part-II

The steady, convective incompressible electrically conducting Jeffrey fluid flow under the influence of angled magnetic field, thermal radiation, chemical reaction,

through vertical parallel plates is studied in part II. This part explores how factors like hall current, angled magnetic field, thermal radiation, Jeffrey fluid parameter, and chemical reaction influence the generation of entropy, velocity, temperature, and concentration components. The original complex equations of the system are changed into dimensionless equations using similarity transformations. These dimensionless governing equations are solved with the help of SQLM.

The following are some of the important observations.

- The increase in magnetic parameter, radiation parameter, and inclination angle results in the increase of flow velocity. The Hall parameter, on the other hand, is showing the opposite trend. Cross-flow velocity is brought down by an increase in Soret number and the Hall parameter.

- The temperature of the fluid rises while the concentration decreases with an increasing value of inclination angle, Soret number, thermal radiation, and Jeffrey fluid parameter.

- Increasing the magnetic parameter, Hall parameter, inclination angle, and Soret number all lead to a rise in entropy generation within the system.

Conclusions from Part-III

In part III, we will examine the behavior of a steady, convective, incompressible, electrically conducting Jeffrey fluid that flows through inclined parallel plates. We will investigate the impact of various parameters, including inclined magnetic field, Hall effect, thermal radiation, chemical reaction, and Jeffrey fluid characteristics, on the generation of entropy, as well as on the flow velocity, temperature, and concentration components of the fluid.

The following are some of the important observations.

- Entropy generation within the system increases with an increase in the magnetic parameter, Soret number, inclination angle, and Hall parameter.

- The flow velocity increases with the increasing value of the magnetic parameter, radiation parameter, inclination angle, and Soret number. With the Hall parameter, however, a contrary tendency is noted. In contrast, the cross-flow velocity falls as the Soret number, inclination angle, and Hall parameter increase.

- The fluid temperature seems to decrease and concentration exhibits an increase as the inclination angle, Soret number, slip parameter, and Jeffrey fluid parameter increase.

Future Scope:

The thesis work can be further extended to study the influence of various factors such as viscosity variation, wall channeling, joule effects, stratification, double diffusion, conjugate convection, etc. These factors can be studied independently and then their combined effects can be examined over the complex structure. Although this study can be challenging and time-consuming, it can be a rewarding experience. The SQLM has been successfully applied in various fields, including biomedical functions, biotechnology, power transformers, and cooling processes. Spectral methods have also been successfully used in numerical simulations in many areas, such as heat conduction, fluid dynamics, and quantum mechanics.

List of Papers Published/Accepted/Communicated

List of Publications

1. K. Kaladhar, Ravi Mahla, "Entropy analysis of natural convection Jeffrey fluid flow through a vertical channel with an inclined magnetic field effect under Navier-slip conditions", The European Physical Journal Plus., Vol. 138, pp. 1–14 (2023).
   DOI: https://doi.org/10.1140/epjp/s13360-023-04357-8

2. Kaladhar Kolla, Ravi Mahla,"Irreversibility mixed convection Jeffrey fluid flow analysis in a vertical channel with an inclined magnetic field and Soret effects under slip conditions", Proceedings of the Institution of Mechanical Engineers, Part E: Journal of Process Mechanical Engineering, pp. 09544089231218977(1-12) (2023).
   DOI: https://doi.org/10.1177/09544089231218977

3. Ravi Mahla, Kolla Kaladhar, "Effect of Hall current, Soret number, and inclined magnetic field on entropy generation of mixed convection Jeffrey fluid flow through sloping channel under Navier-slip condition", ZAMM-Journal of Applied Mathematics and Mechanics, Vol. 104, pp. e202300700(1-15) (2024).
   DOI: https://doi.org/10.1002/zamm.202300700

4. K. Kaladhar, Ravi Mahla, "Entropy Analysis of the Natural Convection Jeffrey Fluid Flow Through a Vertical Porous Channel in an Inclined Magnetic Field", Special Topics and Reviews in Porous Media — An International Journal, (2024).
   DOI: https://10.1615/SpecialTopicsRevPorousMedia.2024048949

5. K. Kaladhar, Ravi Mahla, "Irreversibility Analysis of Jeffrey Fluid Flow on Mixed Convection between Vertical Parallel Plates with an Inclined Magnetic Field", Special Topics and Reviews in Porous Media — An International Journal, (2024).
   DOI: https://10.1615/SpecialTopicsRevPorousMedia.2024048872

6. Ravi Mahla, K. Kaladhar, "Analysis of Irreversibility in the Flow of Jeffrey Fluid Through an Inclined Channel Considering Navier-Slip", East Asian Journal on Applied Mathematics, (2024).
   DOI: https://10.4208/eajam.2023-227.221023

List of Papers Accepted for Publication

1. Ravi Mahla, K. Kaladhar, “Entropy-Based Investigation of Jeffrey Fluid Flow in a Sloping Channel with Hall Current, Thermal Radiation, and Inclined Magnetic Field Effects", *Journal of Thermal Analysis and Calorimetry.*

2. Ravi Mahla, K. Kaladhar, “Irreversibility Analysis of Jeffrey fluid mixed convection flow through a sloping channel under the influence of angled magnetic field", *Thermophysics and Aeromechanics.*

Bibliography

[1] R Ellahi, SU Rahman, and S Nadeem. Blood flow of jeffrey fluid in a catherized tapered artery with the suspension of nanoparticles. *Physics Letters A*, 378(40):2973–2980, 2014.

[2] M Kothandapani and S Srinivas. Peristaltic transport of a jeffrey fluid under the effect of magnetic field in an asymmetric channel. *International Journal of Non-Linear Mechanics*, 43(9):915–924, 2008.

[3] G.W. Sutton and A. Sherman. *Engineering Magnetohydrodynamics*. McGraw-Hill, New Yark, 1965.

[4] C. Soret. Influence de la temperature sur la distribution des sels dans leurs solutions. *C.R. Acad. Sci., Paris*, 91:289–291, 1880.

[5] D. A. Nield and A. Bejan. *Convection in Porous Media, 3rd Edition*. Springer-Verlag, New York, 2006.

[6] J. Qi and R. F. Savinell. Analysis of flow-through porous electrode cell with homogeneous chemical reactions: application to bromide oxidation in brine solutions. *J. Applied Electrochemistry.*, 23:873–886, 1993.

[7] Y. A. Guloyan. Chemical reactions between components in the production of glass-forming melt. *Glass and Ceramics.*, 60:233–235, 2003.

[8] P. Ducrocq, S. Duquesne, S. Magnet, S. Bourbigot, and R. Delobel. Interactions between chlorinated paraffins and melamine in intumescent paint- investing a way to suppress chlorinated paraffins from the formulations. *Progress in Organic Coatings.*, 57:430–438, 2006.

[9] D Srinivasacharya, Sandile S Motsa, and O Surender. Numerical study of free convection in a doubly stratified non-darcy porous medium using spectral

quasilinearization method. *International Journal of Nonlinear Sciences and Numerical Simulation*, 16(3-4):173–183, 2015.

[10] K Kaladhar, K Madhusudhan Reddy, and D Srinivasacharya. Inclined magnetic field, thermal radiation, and hall current effects on mixed convection flow between vertical parallel plates. *Journal of Heat Transfer*, 141(10):102501 (7 pages), 2019.

[11] K Madhusudhan Reddy, K Kaladhar, D Srinivasacharya, et al. Influence of inclined magnetic field, radiation, and hall current on mixed convection flow through an inclined channel with navier-slip condition. *Journal of Applied Nonlinear Dynamics*, 11(2):271–282, 2022.

[12] Farideh Zare, Mohammad Heydari, and Ghasem Barid Loghmani. Spectral quasilinearization method for the numerical solution of the non-standard volterra integral equations. *Iranian Journal of Science*, 47(1):229–247, 2023.

[13] W. Elenbaas. Heat dissipation of parallel plates by free convection. *Physica.*, 9(1):1–278, 1942.

[14] A Bar-Cohen and WM Rohsenow. Thermally optimum spacing of vertical, natural convection cooled, parallel plates. 106(1):116–123, 1984.

[15] Ahmad Hajizadeh, Nehad Ali Shah, FD Zaman, and IL Animasaun. Analysis of natural convection bionanofluid between two vertical parallel plates. *Bio-NanoScience*, 9:930–936, 2019.

[16] Muhammad Tanveer, Saif Ullah, and Nehad Ali Shah. Thermal analysis of free convection flows of viscous carbon nanotubes nanofluids with generalized thermal transport: A prabhakar fractional model. *Journal of Thermal Analysis and Calorimetry*, 144:2327–2336, 2021.

[17] Gohar Ali, Farhad Ali, Arshad Khan, Abdul Hamid Ganie, and Ilyas Khan. A generalized magnetohydrodynamic two-phase free convection flow of dusty casson fluid between parallel plates. *Case Studies in Thermal Engineering*, 29:101657, 2022.

[18] Ponnan Bako and Abiodun O Ajibade. G-jitter effects on transient natural convection couetteflow in a vertical channel. *International Journal of Advanced Networking and Applications*, 14(5):5632–5644, 2023.

[19] C. H. Cheng, H. S. Kou, and W. H. Huang. Flow reversal and heat transfer of fully developed mixed convection in vertical channels. *J. Thermophys Heat Transfer*, 4:375–383, 1990.

[20] Youssef Azizi, Brahim Benhamou, Nicolas Galanis, and Mohammed El-Ganaoui. Buoyancy effects on upward and downward laminar mixed convection heat and mass transfer in a vertical channel. *International Journal of Numerical Methods for Heat & Fluid Flow*, 17(3):333–353, 2007.

[21] Hasan Celik, Moghtada Mobedi, Oronzio Manca, and Bernardo Buonomo. Enhancement of heat transfer in partially heated vertical channel under mixed convection by using al2o3 nanoparticles. *Heat Transfer Engineering*, 39(3):229–240, 2018.

[22] Hang Xu. Mixed convective flow of a hybrid nanofluid between two parallel inclined plates under wall-slip condition. *Applied Mathematics and Mechanics*, 43(1):113–126, 2022.

[23] Zia Ullah and Mohammed Alkinidri. Effect of variable viscosity on oscillatory heat and mass transfer in mixed convective flow with chemical reaction along inclined heated plate under reduced gravity. *Alexandria Engineering Journal*, 77:539–552, 2023.

[24] Canghu Yang, Carlos A Grattoni, Ann H Muggeridge, and Robert W Zimmerman. Flow of water through channels filled with deformable polymer gels. *Journal of colloid and interface science*, 250(2):466–470, 2002.

[25] T Hayat and Z Abbas. Heat transfer analysis on the mhd flow of a second grade fluid in a channel with porous medium. *Chaos, Solitons & Fractals*, 38(2):556–567, 2008.

[26] R Ellahi and S Afzal. Effects of variable viscosity in a third grade fluid with porous medium: an analytic solution. *Communications in Nonlinear Science and Numerical Simulation*, 14(5):2056–2072, 2009.

[27] M Fiza, Hakeem Ullah, and S Islam. Three-dimensional mhd rotating flow of viscoelastic nanofluid in porous medium between parallel plates. *Journal of Porous Media*, 23(7), 2020.

[28] Mohamed Y Abou-zeid and Mahmoud E Ouaf. Hall currents effect on squeezing flow of non-newtonian nanofluid through a porous medium between two parallel plates. *Case Studies in Thermal Engineering*, 28:101362, 2021.

[29] K Sudarmozhi, D Iranian, and Ilyas Khan. A steady flow of mhd maxwell viscoelastic fluid on a flat porous plate with the outcome of radiation and heat generation. *Frontiers in Physics*, 11:1126662, 2023.

[30] J. Hartmann and F. Lazarus. Hg-dynamics i. theory of the laminar flow of an electrically conductive liquid in a homogeneous magnetic field. *Kgl. Danske Videnskab. Selskab. Mat-Fys Medd.*, 15(6):1–28, 1937.

[31] WIt Axford. The magnetohydrodynamic jeffrey-hamel problem for a weakly conducting fluid. *The Quarterly Journal of Mechanics and Applied Mathematics*, 14(3):335–351, 1961.

[32] L. Jahanshah and S. Vireshwar. Magnetohydrodynamic heat transfer in two-phase flow between parallel plates. *App. Sci. Res.*, 45:53–66, 1988.

[33] A.J. Chamkha. Unsteady laminar hydromagnetic fluid-particle flow and heat transfer in channels and circular pipes. *Int. J. Heat Fluid Flow.*, 21:740–746, 2000.

[34] C. Kurtcebe and M.Z. Erim. Heat transfer of a viscoelastic fluid in a porous channel. *Int. J. Heat and Mass Trans.*, 48:5072–5077, 2005.

[35] Hillal M Elshehabey, FM Hady, Sameh E Ahmed, and RA Mohamed. Numerical investigation for natural convection of a nanofluid in an inclined l-shaped cavity in the presence of an inclined magnetic field. *International Communications in Heat and Mass Transfer*, 57:228–238, 2014.

[36] N.S. Bondareva and M.A. Sheremet. Natural convection heat transfer combined with melting process in a cubical cavity under the effects of uniform inclined magnetic field and local heat source. *International Journal of Heat and Mass Transfer*, 108:1057–1067, 2017.

[37] M. Hussain and M. Sheremet. Convection analysis of the radiative nanofluid flow through porous media over a stretching surface with inclined magnetic field. *International Communications in Heat and Mass Transfer*, 140:106559, 2023.

[38] Z. Dursunkaya and W.M.. Worek. Diffusion-thermo and thermal diffusion effects in transient and steady natural convection from a vertical surface. *Int. J. Heat Mass Transfer.*, 35:2060–2065, 1992.

[39] Siva Reddy Sheri and R Srinivasa Raju. Soret effect on unsteady mhd free convective flow past a semi–infinite vertical plate in the presence of viscous dissipation. *International Journal for computational methods in engineering Science and Mechanics*, 16(2):132–141, 2015.

[40] B. Mandal, K. Bhattacharyya, A. Banerjee, A.K. Verma, and A.K. Gautam. Mhd mixed convection on an inclined stretching plate in darcy porous medium with soret effect and variable surface conditions. *Nonlinear Engineering*, 9(1):457–469, 2020.

[41] M. Mishra and J.P. Panda. Soret effect for unsteady mhd mixed convective flow in porous medium with viscous dissipation. *International Journal of Ambient Energy*, 43(1):5605–5615, 2022.

[42] MO Durojaye, JA Kazeem, FO Ogunfiditimi, and IJ Ajie. Method of lines analysis of soret and dufour effects on an unsteady heat and mass transfer mhd natural convection couette flow. *Physical Science International Journal*, 27(2):10–18, 2023.

[43] Syeda Humaira Tasnim, Mahmud Shohel, and Mohammad Arif Hasan Mamun. Entropy generation in a porous channel with hydromagnetic effect. *Exergy, An International Journal*, 2(4):300–308, 2002.

[44] M.Q. Al-Odat, R.A. Damseh, M. Al-Nimr, et al. Effect of magnetic field on entropy generation due to laminar forced convection past a horizontal flat plate. *Entropy*, 6(3):293–303, 2004.

[45] G. Ibanez, S. Cuevas, and M. de Haro. Optimization of a magnetohydrodynamic flow based on the entropy generation minimization method. *International communications in heat and mass transfer*, 33(3):295–301, 2006.

[46] Atef El Jery, Nejib Hidouri, Mourad Magherbi, and Ammar Ben Brahim. Effect of an external oriented magnetic field on entropy generation in natural convection. *Entropy*, 12(6):1391–1417, 2010.

[47] Z. Abbas, M. Naveed, M. Hussain, and N. Salamat. Analysis of entropy generation for mhd flow of viscous fluid embedded in a vertical porous channel with thermal radiation. *Alexandria Engineering Journal*, 59(5):3395–3405, 2020.

[48] M.C. Jayaprakash and M.B. Patil. Entropy generation analysis for mixed convective flow of casson fluid in a vertical microchannel with the influence of nonlinear radiation by maintaining inconstant viscosity. *Heat Transfer*, 51(7):6915–6936, 2022.

[49] B. Iftikhar, T. Javed, and M.A. Siddiqu. Entropy generation analysis during mhd mixed convection flow of non-newtonian fluid saturated inside the square cavity. *Journal of Computational Science*, 66:101907, 2023.

[50] I. Pop, T. Grosan, and R. Cornelia. Effect of heat generated by an exothermic reaction on the fully developed mixed convection flow in a vertical channel. *Comm. in Nonlinear Sci. and Num. Sim.*, 15:471–474, 2010.

[51] AK Dash, SR Mishra, and BP Acharya. Chemical reaction effect of mhd micropolar fluid flow between two parallel plates in the presence of heat source/sink. *Model Measurement Control B*, 86(3):593–608, 2017.

[52] H. Mondal and S. Bharti. Spectral quasi-linearization for mhd nanofluid stagnation boundary layer flow due to a stretching/shrinking surface. *Journal of Applied and Computational Mechanics*, 6(4):1058–1068, 2020.

[53] P. Humane, V.S. Patil, and A.B. Patil. Chemical reaction and thermal radiation effects on magnetohydrodynamics flow of casson–williamson nanofluid over a porous stretching surface. *Proceedings of the Institution of Mechanical Engineers, Part E: Journal of Process Mechanical Engineering*, 235(6):2008–2018, 2021.

[54] M. Awais and T. Salahuddin. Variable thermophysical properties of magnetohydrodynamic cross fluid model with effect of energy dissipation and chemical reaction. *International Journal of Modern Physics B*, 38(16):2450197, 2023.

[55] M. Hatami and D.D. Ganji. Natural convection of sodium alginate (sa) non-newtonian nanofluid flow between two vertical flat plates by analytical and numerical methods. *Case Studies in Thermal Engineering*, 2:14–22, 2014.

[56] M.A. Sheremet, I. Pop, and O. Mahian. Natural convection in an inclined cavity with time-periodic temperature boundary conditions using nanofluids:

application in solar collectors. *International Journal of Heat and Mass Transfer*, 116:751–761, 2018.

[57] N.A. Bakar, R. Roslan, A. Karimipour, and I. Hashim. Mixed convection in lid-driven cavity with inclined magnetic field. *Sains Malaysiana*, 48(2):451–471, 2019.

[58] D. Kumar and B. Premachandran. Investigation of transition in a natural convection flow in an inclined parallel plate channel. *International Communications in Heat and Mass Transfer*, 130:105768, 2022.

[59] Shobha Kenkere Channappa, Kavitha Linganna, and Patil Mallikarjun Basavaraj. Mixed convection of jeffrey nanofluid in a vertical porous channel with the significance of hall and ion slip effect, suction/injection and variable thermal conductivity: Entropy analysis. In *AIP Conference Proceedings*, volume 2649. AIP Publishing, 2023.

[60] R. Bellman, H. Kagiwada, and R. Kalaba. Quasilinearization, system identification and prediction. *International Journal of Engineering Science*, 3(3):327–334, 1965.

[61] Hiranmoy Mondal, Mohammed Almakki, and Precious Sibanda. Dual solutions for three-dimensional magnetohydrodynamic nanofluid flow with entropy generation. *Journal of Computational Design and Engineering*, 6(4):657–665, 2019.

[62] Dulal Pal, Sagar Mondal, and Hiranmoy Mondal. Entropy generation on mhd jeffrey nanofluid over a stretching sheet with nonlinear thermal radiation using spectral quasilinearisation method. *International Journal of Ambient Energy*, 42(15):1712–1726, 2021.

[63] T.A. Ameel, X. Wang, R.F. Barron, and R.O. Warrington. Laminar forced convection in a circular tube with constant heat flux and slip flow. *Microscale Thermophysical Engineering*, 1(4):303–320, 1997.

[64] A Raisi, B Ghasemi, and SM Aminossadati. A numerical study on the forced convection of laminar nanofluid in a microchannel with both slip and no-slip conditions. *Numerical Heat Transfer, Part A: Applications*, 59(2):114–129, 2011.

[65] J.H. Merkin, A.M. Rohni, S. Ahmad, and I. Pop. On the temperature slip boundary condition in a mixed convection boundary-layer flow in a porous medium. *Transport in porous media*, 94(1):133–147, 2012.

[66] G.M. Gie and J.P. Whitehead. Boundary layer analysis for navier-slip rayleigh–bénard convection: The non-existence of an ultimate state. *Journal of Mathematical Fluid Mechanics*, 21:1–25, 2019.

[67] R. Zhang and Qiaolin He. The least–square/fictitious domain method based on navier slip boundary condition for simulation of flow–particle interaction. *Applied Mathematics and Computation*, 415:126687, 2022.

[68] A.J. Badday and Akil J Harfash. The effects of the soret and slip boundary conditions on thermosolutal convection with a navier–stokes–voigt fluid. *Physics of Fluids*, 35(1), 2023.

[69] Kostas D Housiadas and Christos Tsangaris. Channel flow with variable geometry and navier slip at the walls using high-order lubrication theory. *European Journal of Mechanics-B/Fluids*, 98:194–207, 2023.

[70] A.S. Dogonchi, M.A. Sheremet, D.D. Ganji, and I. Pop. Free convection of copper–water nanofluid in a porous gap between hot rectangular cylinder and cold circular cylinder under the effect of inclined magnetic field. *Journal of Thermal Analysis and Calorimetry*, 135:1171–1184, 2019.

[71] Mrinmoy Goswami, Krishna Gopal Singha, Biju Kr Dutta, and Amarjyoti Goswami. The unsteady magnetohydrodynamtc flow and heat transfer between two non-conducting infinite vertical parallel plates with inclined magnetic field. *Mathematical Statistician and Engineering Applications*, 72(1):413–431, 2023.

[72] H. Vaidya, C Rajashekhar, G Manjunatha, A Wakif, KV Prasad, IL Animasaun, and K Shivaraya. Analysis of entropy generation and biomechanical investigation of mhd jeffery fluid through a vertical non-uniform channel. *Case Studies in Thermal Engineering*, 28:101538, 2021.

[73] Adrian Bejan. A study of entropy generation in fundamental convective heat transfer. 1979.

[74] R Biswas, M Mondal, Kazi Shanchia, Rubel Ahmed, SK Abdus Samad, and SF Ahmmed. Explicit finite difference analysis of an unsteady magnetohydrodynamics heat and mass transfer micropolar fluid flow in the presence of radiation

and chemical reaction through a vertical porous plate. *Journal of nanofluids*, 8(7):1583–1591, 2019.

[75] D Iranian, S Karthik, and A Seethalakshmy. Heat generation effects on magnetohydrodynamic powell-eyring fluid flow along a vertical surface with a chemical reaction. *Forces in Mechanics*, 12:100212, 2023.

[76] A. Rauf, Fiaz Hussain, Aqsa Mushtaq, Nehad Ali Shah, and Mohamed R Ali. Mhd mixed convection flow for maxwell hybrid nanofluid with soret, dufour and morphology effects. *Arabian Journal of Chemistry*, 16(8):104965, 2023.

[77] Utpal Jyoti Das and Nayan Mani Majumdar. A study of magnetohydrodynamic flow on a channel with induced magnetic field, soret effect and heat radiation. *ZAMM-Journal of Applied Mathematics and Mechanics/Zeitschrift für Angewandte Mathematik und Mechanik*, 103(12):e202200624, 2023.

[78] H. Sardar, Latif Ahmad, Masood Khan, and Ali Saleh Alshomrani. Investigation of mixed convection flow of carreau nanofluid over a wedge in the presence of soret and dufour effects. *International Journal of Heat and Mass Transfer*, 137:809–822, 2019.

[79] AR Deepika, Kamatam Govardhan, Amalendu Rana, and Motahar Reza. Soret and dufour effects on mhd mixed convection flow of casson hybrid nanofluid over a permeable stretching sheet. *International Journal of Ambient Energy*, 44(1):2115–27, 2023.

[80] Tasawar Hayat, Aneeta Razaq, Sohail A Khan, and Shaher Momani. Soret and dufour impacts in entropy optimized mixed convective flow. *International Communications in Heat and Mass Transfer*, 141:106575, 2023.

[81] Claude Navier. *Mémoire sur les lois du mouvement des fluides*. éditeur inconnu, 1822.

[82] S Das, RN Jana, and OD Makinde. Magnetohydrodynamic mixed convective slip flow over an inclined porous plate with viscous dissipation and joule heating. *Alexandria Engineering Journal*, 54(2):251–261, 2015.

[83] Adnan Asghar, Abdul Fattah Chandio, Zahir Shah, Narcisa Vrinceanu, Wejdan Deebani, Meshal Shutaywi, and Liaquat Ali Lund. Magnetized mixed convection hybrid nanofluid with effect of heat generation/absorption and velocity slip condition. *Heliyon*, 9(2):e13189, 2023.

[84] S. Zainodin, A. Jamaludin, R. Nazar, and I. Pop. Effects of higher order chemical reaction and slip conditions on mixed convection hybrid ferrofluid flow in a darcy porous medium. *Alexandria Engineering Journal*, 68:111–126, 2023.